Use of systems biology in deciphering mode of action and predicting potentially adverse health outcomes of nanoparticle exposure, using carbon black as a model

Julie Andrée Bourdon

Thesis submitted to the
Faculty of Graduate and Postdoctoral Studies
In partial fulfilment of the requirements for the
Ph.D. degree in Biology, Specialization in Chemical and Environmental Toxicology

Department of Biology
Faculty of Science
University of Ottawa

May 11th, 2012

ABSTRACT

Nanoparticles (NPs) are particles that are less than 100 nm in at least one dimension. These particles exhibit chemical properties that differ from their bulk counterparts and therefore, regulatory assays alone may not always be appropriate for evaluation of their full spectrum of toxicity. NPs reach the alveolar space upon inhalation, where they can potentially mediate systemic effects via molecular signalling cascades and/or translocation. Systems biology (e.g., the study of molecular processes to describe a system as a whole) has emerged as a powerful platform proposed to provide insight in potential hazard, mode of action and human disease relevance. Toxicogenomics evaluates global gene expression in response to toxicant exposure and can serve as a basis for exploring cross-talk between tissues and systems biology responses. The overarching objectives of this thesis were to employ toxicogenomics and a systems biology approach in mice exposed to carbon black NPs (Printex 90) to: 1) examine NP mode of action; 2) examine molecular cross-talk and exposure impact on extra-pulmonary tissues; and 3) query relevance to human diseases and potential utility in human health risk assessment. C57BL/6 female mice were exposed to vehicle, 0.018, 0.054 and 0.162 mg Printex 90 and sacrificed 1, 3, and 28 days after a single intratracheal instillation. Analysis of Printex 90-induced phenotypes revealed persistent pulmonary inflammation, sustained DNA strand breaks in lung, liver and bronchoalveolar lavage cells, and formamidopyrimidine DNA glycosylase sensitive sites in lung, all of which occurred even at the lowest exposure dose. Transcriptional changes within lungs revealed overwhelming

inflammatory and acute phase responses. Acute phase response was confirmed by increased plasma serum amyloid A and was associated with reduced plasma high density lipoprotein, up-regulation of hepatic cholesterol biosynthetic pathways and modest increases in plasma low-density lipoprotein. Analysis of responsive microRNAs revealed increased pulmonary expression of miR-135b over time in two mouse models. MiR-135b was hypothesized to contribute to resolution of inflammation, however, specific mRNA targets could not be identified. Heart gene and microRNA expression was unperturbed; however, increases in cell adhesion molecules persisted to day 28, and immediate decreases in apolipoproteins were measured in plasma. Bioinformatics analyses, data mining and modeling of all data to produce benchmark doses revealed that lung gene expression profiles effectively predicted observed phenotypes (e.g., genotoxicity and inflammation) at relevant threshold doses. Comparison of Printex 90 profiles with those of inflammatory lung disease models identified lung injury and fibrosis as the primary predicted adverse health effect of Printex 90 exposure, and revealed that pathways leading to these outcomes were highly similar in mice and humans. In conclusion, this work demonstrates the power of systems biology approaches in establishing mode of action, systemic toxicities and relevance of an exposure to potential human disease outcomes. In general, the work provides an example of how toxicogenomics can be used to support human health risk assessment.

RÉSUMÉ

Une nanoparticule (NP) est définie comme étant une particule dont le diamètre nominal est inférieur à 100 nm. Puisque les propriétés des matières changent considérablement à l'échelle nanométrique, les essaies biologiques typiques ne sont pas toujours convenables à l'évaluation de la toxicité des NPs. Lors d'exposition par voie pulmonaire, les NPs atteignent la région alvéolaire, où ces dernières peuvent potentiellement causer des effets néfastes hors-poumons par initiation de réactions biomoléculaires ou par translocation directe. La biologie des systèmes (p. ex., la modélisation moléculaire d'un système en entier) offre de nouvelles approches toxicologiques permettant l'identification de risques potentiels et de modes d'action qui sont pertinents au développent de maladies chez les humains. L'ensemble des changements au niveau d'expression génétiques lors d'une exposition chimique (p. ex. la toxicogénomique) peut être utilisé pour interpréter les messages moléculaires entre tissus ainsi que la biologie du système en entier. Les objectifs de cette thèse étaient d'appliquer ces concepts à des souris exposées au noir de carbone (Printex 90) pour 1) évaluer les modes d'actions des NPs; 2) déterminer la communication moléculaire entre tissus et les impacts toxicologiques sur ces derniers; et 3) examiner l'utilité de ces approches pour l'évaluation de risques à la santé humaine. Des souris femelles C57BL/6 furent exposées par installation intratrachéale (véhicule seulement ou 0.018, 0.054 et 0.162 mg de Printex 90), et euthanasiées aux jours 1, 3 et 28. Les analyses phénotypiques ont démontrées de l'inflammation pulmonaire et de la génotoxicité persistante ainsi que de la génotoxicité reliée au stress oxydatif même

à la plus petite dose d'exposition. L'inflammation et la réponse à phase aigüe pulmonaire furent les plus perturbées au niveau de l'expression de gènes. La réponse à phase aigüe fut confirmée par la présence de serum amyloïde A dans le plasma et associée à une baisse en lipoprotéines de haute densité, à une expression reliée à la biosynthèse de cholesterol dans le foie et à une hausse de lipoprotéines de basse densité. L'expression de miR-135b fut démontrée dans deux modèles expérimentaux. Cependant, les cibles moléculaires spécifiques de miR-135b n'ont pu êtres identifiées. Aucuns changements en matière d'expression de gènes ou de microARNs ne furent observés dans le cœur. Malgré ceci, des protéines en circulation impliquées dans l'adhésion cellulaire et la coagulation étaient à la hausse et persistantes, alors que les apolipoprotéines étaient à la baisse tôt, suivant l'exposition. Il fut démontré par l'analyse complète des gènes régulés à la hausse ou à la baisse, et par la modélisation de doses repères pour l'ensemble des données, que les profiles toxicogénomiques pouvaient efficacement prédire les phénotypes pulmonaire observés (p. ex., génotoxicité et inflammation) à de doses comparables. L'analyse de maladies pulmonaires potentielles suite à l'exposition aux NPs suggère la fibrose comme condition la plus probable. En somme, l'application d'une approche « biologie des systèmes » a permis l'identification de modes d'actions, de toxicité systémiques et de maladies potentielles chez l'humain suite à une exposition au Printex 90. Ce travail fournit un exemple de l'utilité de la toxicogénomique pour supporter l'évaluation des risques à la santé.

ACKNOWLEDGMENTS

Words cannot express how grateful I am to the many people who have made my goal of completing my Ph.D. within three years a reality.

My deepest gratitude goes to my parents, Jacques and Jacqueline Bourdon, for their unconditional love and unending support which have given me the courage and ambition to take on such a challenge. Big thanks to my little sister, Joanne Bourdon, for the great company, and for the countless hours spent editing so many of my documents when I first started writing in English. I cannot thank my soon to be husband, Pascal Lacombe, enough for his help, understanding and support throughout these very hectic times. His warm, calm and optimistic nature has helped me tremendously in the successful completion of this work. I also thank my long-time friends (especially Marie-Eve Daigneault, Marie-France Martel and Lisanne McCullough), the new friends I have made at Health Canada, (especially Jennifer McAllister, Mélanie Charlebois, Caroline Rose and Sarah Labib) and even my fury little friend (Milou) for the great times spent together which have allowed me to stay centered throughout my doctoral studies.

Special thanks go out to collaborators at the Danish National Institute for the Working Environment (especially Ulla Vogel, Håkan Wallin, Anne Saber, Nicklas Jacobsen and Petra Jackson) for sharing their tremendous knowledge of particle toxicology with me and for their contagious enthusiasm for research (not to mention

all of the work that went into providing me with samples). I also thank collaborators at the University of Copenhagen (especially Peter Møller, Steffen Loft, and Mille Løhr) for showing me the ropes on the comet assay and for help in data analysis. *Tak til jer alle* for the warm welcome (also Wojciech Ruminski) during my stay abroad.

Very many thanks to the kind people at Health Canada's Environmental Health Centre (and many apologies for the loudness of my shoes over the years). In particular, thanks to Andrew Williams and Byron Kuo for their invaluable expertise in bioinformatics. I thank Sabina Halapanavar for sharing her immense knowledge of nano-toxicogenomics with me. For technical guidance and troubleshooting advice, I thank Andrea Rowan-Caroll, Julie Buick, Dongmei Wu, Amal Malik and Martin Paquette. Also, thanks to Azam Tayabali for critical review of much of this work and Karen Leingartner for plasma analyses. I am extremely grateful to Ivy Moffat, not only for sharing her immense knowledge of the chemical regulatory decision making process, but also for taking me under her "risk assessment" wing so that I can put my Ph.D. skills into practice. I also want to thank everyone at the Water Air and Climate Change Bureau (especially Richard Carrier and Michèle Giddings) for being so understanding and supportive throughout the final sprint of my thesis submission.

I thank my committee members, Renaud Vincent and Iain Lambert for their expert advice and for being involved in my graduate work since the very beginning.

Special thanks to Iain Lambert who was very helpful in my transfer to the Ph.D. I am also very thankful to my co-advisor, Paul White for his encouragement and guidance, especially on the concluding chapters of this thesis.

Above all, I would like to thank my primary advisor, Carole Yauk. Carole's impressive wealth of knowledge and dedication to her students, work and family has truly been a source of inspiration to me. I greatly admire her not only as a scientist but as a woman. Thank you for your endless support and patience and for trusting my judgment in the various directions we have taken this project. Surely, I would not have come this far without you.

Finally, this work would not have been possible without the financial assistance of the National Sciences and Engineering Research Council of Canada, Health Canada and the Chemical's Management plan. I humbly thank you for selecting me out of many talented candidates and can only hope that this thesis will be worthy of the trust you have placed in me.

Un très grand MERCI à toutes et tous!

TABLE OF CONTENTS

LIST OF TABLES

LIST OF FIGURES

LIST OF ABBREVIATIONS

3′UTR	3′ Untranslated Region
8-oxo-dG	8-oxo-7, 8-dihydro-2′-deoxyguanosine
Abca1	ATP-Binding Cassette Subfamily A Member 1
Abcg1	ATP-Binding Cassette Subfamily G Member 1
ACGIH	American Conference of Governmental Hygienists
Adamts	A Disintegrin and Metalloproteinase with Thrombospondin Motifs
Adcy7	Adenylate Cyclase Type 7
AIC	Akaike's Information Criterion
Apo	Apoliporotein
AOP	Adverse Outcome Pathway
APR	Acute Phase Response
B[a]P	Benzo[a]Pyrene
BAL	Bronchoalveolar Lavage
BET	Brunauer Emmett and Teller
BMD	Benchmark Dose
BMDL	Lower Confidence Limit Benchmark Dose
BMDS	Benchmark Dose Software
BMR	Benchmark Factor
CAM	Cell Adhesion Molecule
CB	Carbon Black
CBNP	Carbon Black Nanoparticles
Ccl	Chemokine (C-C) Motif Ligand
cDNA	Complementary DNA
Cp	Ceruloplasmin
CRP	C-Reactive Protein
CXCL	C-X-C Motif Chemokine
CVD	Cardiovascular Disease
DEP	Diesel Exhaust Particles
Dhcr7	7-Dehydrocholesterol Reductase
DLS	Dynamic Light Scattering
DMA	Dimethylarsinic acid
EPA	U.S. Environmental Protection Agency
EU	Endotoxin Unit
E-Selectin	Endothelial Selectin
Fbn1	Fibrillin-1
Fdps	Farnesyl-Diphosphate Synthase
FDR	False Discovery Rate
FEV_1	Forced Expiratory Volume in One Second
FPG	Formamidopyrimidine DNA Glycosylase
FVC	Forced Vital Capacity
GDP1	Glycerol-3-phosphate dehydrogenase

GSH	Glutathione
HDL	High Density Lipoprotein
HESI	Health and Environmental Sciences Institute
HHRA	Human Health Risk Assessment
HMG-CoA	3-hydroxy-3-methylglutaryl-CoA
HRP	Horseradish Peroxidase
IARC	International Agency for Research on Cancer
ICAM	Intercellular Adhesion Molecule
ICBA	International Carbon Black Association
ICRP	International Commission on Radiological Protection
Idi	Isopentyl-Diphosphate Synthase
ILSI	International Life Sciences Institute
IPA	Ingenuity Pathway Analysis
KEGG	Kyoto Encyclopedia of Genes and Genomes
Klf	Krueppel-Like Factor
LDH	Lactate Dehydrogenase
LDL	Low Density Lipoprotein
LOWESS	Locally Weighted Scatterplot Smoothing
LPS	Lipopolysaccharide
LXR/RXR	Liver X Receptor/Retinoid X Receptor
MAC	Maximal Allowable Concentration
MAANOVA	Microarray Analysis of Variance
miRNA	MicroRNA
mRNA	Messenger RNA
Mt	Metallothionein
Mvd	Mevalonate Kinase
NADPH	Nicotinamide Adenine Dinucleotide Phosphate
NCBI	National Center for Biotechnology Information
NF-κB	Nuclear Factor Kappa B
NIEHS	National Institute of Environmental Health Sciences
NIOSH	National Institute for Occupational Safety and Health
NM	Nanomaterial
NP	Nanoparticle
OECD	Organisation for Economic Co-Operation and Development
Orm	Orosomucoid
OSHA	Occupational Safety and Health Administration
PAI-1	Plasminogen Activator Inhibitor 1
PAH	Polycyclic Aromatic Hydrocarbon
PAM	Prediction Analysis for Microarray
PDI	Polydispersity Index
PEL	Permissible Exposure Limit
PM	Particulate Matter
PMN	Polymorphonuclear Cells

Rbp	Ribosome Binding Protein
ROS	Reactive Oxygen Species
RT-PCR	Real-Time Polymerase Chain Reaction
SAA	Serum Amyloid A
SB	DNA Strand Breaks
SMR	Standard Mortality Ratio
SOD	Superoxide Dismutase
SPP1	Secreted Phosphoprotein 11
Sqle	Squalene Epoxidase
STEL	Short-Term Exposure Limit (15 min unless otherwise specified)
TEM	Transmission Electron Microscopy
TGF-β	Transforming Growth Factor Beta
TLV	Threshold Limit Value
TNF	Tumor Necrosis Factor
TRGS	Technical Rules for Hazardous Substances
TWA	Time Weighted Average (8 h unless otherwise specified)
VCAM	Vascular Cell Adhesion Molecule
VLDL	Very Low Density Lipoprotein

STATEMENT OF CONTRIBUTION

Chapter 2

Overall Data Interpretation and Manuscript Writing…..….	*Julie Bourdon*
Experimental Design and Manuscript Preparation……..	*Julie Bourdon* *Anne Saber* *Nicklas Jacobsen* *Keld Jensen* *Anne Madsen* *Jacob Lamson* *Håkan Wallin* *Peter Møller* *Steffen Loft* *Carole Yauk* *Ulla Vogel*
Animal Handling, Exposure and Tissue Collection……..	*Ulla Vogel* *Håkan Wallin* *Anne Saber* *Nicklas Jacobsen*
Particle Characterization……...	*Keld Jensen* *Anne Madsen*
Lung Comet and FPG Comet……...	*Julie Bourdon*
BAL Cell Count, Liver and BAL Comet……..	*Anne Saber* *Nicklas Jacobsen*
Statistical Analysis…….	*Peter Møller*
Real-Time PCR……	*Jacob Lamson*

Chapter 3

Overall Data interpretation and Manuscript Writing…..….	*Julie Bourdon*
Experimental Design and Manuscript Preparation……..	*Julie Bourdon* *Sabina Halappanavar* *Anne Saber* *Nicklas Jacobsen* *Andrew Williams* *Håkan Wallin*

	Ulla Vogel *Carole Yauk*
Animal Handling, Exposure and Tissue/Plasma Collection…….	*Ulla Vogel* *Håkan Wallin* *Anne Saber* *Nicklas Jacobsen*
Lung and Liver RNA Extraction and DNA Microarray Hybridization……..	*Julie Bourdon*
Microarray Normalization and MANOVA……	*Andrew Williams*
Pathway Analysis……...	*Julie Bourdon*
Real-time PCR and PCR Arrays……...	*Julie Bourdon*
Liver Total Cholesterol……..	*Julie Bourdon*
Plasma HDL, LDL/VLDL, Total Cholesterol and SAA…...	*Karen Leingartner*
Chapter 4	
Overall Data Interpretation and Manuscript Writing…….	*Julie Bourdon*
Experimental Design and Manuscript Preparation……...	*Julie Bourdon* *Anne Saber* *Sabina Halappanavar* *Petra Jackson* *Dongmei Wu* *Karin Hougaard* *Nicklas Jacobsen* *Andrew Williams* *Ulla Vogel* *Håkan Wallin* *Carole Yauk*
Animal Handling, Exposure and Tissue Collection…….	*Ulla Vogel* *Håkan Wallin* *Anne Saber* *Nicklas Jacobsen* *Petra Jackson* *Karin Hougaard*

Heart Total Cholesterol…….. *Julie Bourdon*

Plasma CVD Markers……. *Karen Leingartner*

Chapter 6

Overall Data Interpretation and Manuscript Writing……. *Julie Bourdon*

Experimental Design and Manuscript Preparation……..... *Julie Bourdon*
Andrew Williams
Byron Kuo
Ivy Moffat
Paul White
Sabina Halappanavar
Ulla Vogel
Håkan Wallin
Carole Yauk

Rank-Based Pathway Analysis and Prediction Analysis for Microarray…….. *Andrew Williams*

BMD/BMDL Modeling…… *Julie Bourdon*

BMD Express…….. *Byron Kuo*

Ingenuity Pathway, Functional and Disease Prediction Analyses…….. *Julie Bourdon*

CHAPTER 1: INTRODUCTION

1.1 General Introduction to Nanotoxicology

An abundant amount of evidence implicates fine and ultrafine particulate matter (PM) in increased morbidity and mortality (Dockery et al. 1993; Pope et al. 1995; Pope III et al. 2002). Particle toxicity generally increases with decreasing particle size and increasing surface area (Nel et al. 2006). Therefore, the growing use of nanoparticles (NPs) (defined as particles smaller than 100 nm in at least one dimension) in a variety of consumer products and the ensuing increase in occupational exposures to NPs is creating widespread health and safety concerns (Stern and McNeil 2008). Although adverse health impacts associated with NP exposure and mechanisms of toxicity remain to be elucidated, the increased manufacturing of NP-based products is of concern. The estimated value of NP-based products was $254 billion in 2009 and is expected to reach $2.5 trillion by 2015 (Bradley et al. 2009). Thus, thorough scientific investigations are required to assess the possible repercussions of exposure to NPs.

1.2 Principles of Nanotoxicology

1.2.1 Properties of NPs versus Bulk Particles

Particles smaller than 100 nm in diameter are generally more reactive than larger particles and can exhibit physical and chemical properties that differ greatly from their bulk counterparts. The primary reason for this is the increased fraction of atoms at the surface of NPs in comparison to larger particles. The

larger surface area and high particle number per unit of mass in NPs enable more surface space onto which chemical reactions can take place (Buzea et al. 2007). In addition, atoms situated on the surface of smaller particles have fewer neighbouring atoms, resulting in lower binding energy and thus decreased melting points (Roduner 2006). Very small NPs (typically < 10 nm) can exhibit quantum confinement, resulting in substantial changes in optical, electric and magnetic properties not observed in bulk materials of the same substance (Buzea et al. 2007; Roduner 2006). Due to these unique properties, nanomaterials (NMs) can potentially exert toxic effects that are vastly different from their larger counterparts.

1.2.2 Deposition and Clearance of Inhaled NPs

NPs can form readily respirable dusts, and thus inhalation is a frequent means of exposure. Deposition of NPs is discernible in all sites of the human respiratory system, including the extrathoracic region (e.g., mouth and nose), the bronchotracheal region, as well as in the alveolar region (Borm et al. 2006). Deposition of particles in alveoli increases substantially for particles in the nano-size range (ICRP 1994). Particles retained in the extrathoracic and bronchotracheal regions are primarily entrapped in a layer of mucus produced by secretory epithelial cells (e.g., goblet cells) and cleared from the airways via cilium, hair-like structures attached to epithelium that propel particle-containing mucus upwards and out of the lungs. Clearance of PM in the alveolar region is

mediated via uptake by phagocytes (e.g., primarily macrophages) which are then cleared from alveoli via lymphatic drainage or migration to the bronchotracheal region. However, removal of NPs from alveoli can be problematic as the process is very slow (Moller et al. 2004b) and macrophage activation and functioning can be impaired in the case of NPs (Green et al. 1998; Renwick et al. 2001). As such, inhaled NPs can accumulate in the alveolar region of lung thus potentially increasing their toxicity.

1.2.3 Proposed Mechanisms of NP-Mediated Pulmonary Toxicity

The increased reactivity of NPs can enhance their potential for extra-cellular interaction and cellular uptake (e.g., via endocytosis, passive diffusion and phagocytosis), as reviewed in (Unfried et al. 2007), thus increasing the likelihood of disturbing biological processes. NPs have been shown to cross the cellular membrane *in vivo* and *in vitro*, resulting in potential contact or damage of essential molecules and organelles within the cell (Geiser et al. 2005). Deposition of various NPs in the lung is primarily associated with substantive inflammation that can persist considerably after initial exposure, presumably due to slow clearance of NPs in the alveolar space and activation of alveolar macrophages (Oberdorster 2001; Zhou and Kobzik 2007). Inefficacy of NP clearance can result in production of a spectrum of pro-inflammatory mediators that recruit leukocytes (Fujii et al. 2002; Fujii et al. 2001). Prolonged presence of NPs can also lead to granulomatous lesion formation (Li et al. 2003). Thus, NPs can potentially

mediate toxic outcomes via cellular internalization and substantive recruitment of inflammatory mediators to the lung.

Most NPs can elicit genotoxicity, as reviewed in (Ng et al. 2010; Singh et al. 2009). NPs have been shown to cause DNA damage in fibroblasts across a placental cell line barrier (Bhabra et al. 2009) and NPs of relatively low toxicity have been demonstrated to induce substantive DNA damage (Jacobsen et al. 2009; Trouiller et al. 2009). This suggests that NPs most likely mediate genotoxic responses via secondary effects, such as oxidative stress.

Although essential to a variety of biological processes, reactive oxygen species (ROS) when produced excessively can exceed cellular antioxidant defence mechanisms causing cellular oxidative damage. Many NPs have been shown to induce oxidative stress *in vitro* and *in vivo* (Oberdorster et al. 2005; Yang et al. 2009). The exact reasons for NP-mediated oxidative stress remain unclear. Various NPs have been shown to induce ROS in acelular systems, suggesting that NP-bound radicals may be the source of excessive ROS. However, NPs also trigger biological processes involved in ROS generation, including NADPH oxidase-mediated respiratory burst upon nanoparticle phagocytosis (Fernandez-Urrusuno et al. 1997), leakage from the electron transport chain as suggested by NP-induced mitochondrial damage (Li et al. 2003), and inflammation-related degranulation of neutrophils (Papatheofanis

and Barmada 1991). Overall, toxicological investigations of various NPs strongly suggest inflammation and oxidative stress as important mediators of NP-mediated toxic responses that may be associated with adverse health outcomes including pulmonary fibrosis, pneumoconiosis, exacerbation of asthma and carcinogenicity when exposed chronically (Li et al. 2010).

1.2.4 Potential for NP-Mediated Systemic Toxicity

Accumulation of NPs within the lung can potentially cause toxicities in extra-pulmonary tissues via translocation and/or molecular signalling mechanisms. Although very few NPs (less than 1%) are hypothesized to translocate directly from lungs to the systemic circulation (Kreyling et al. 2002), there remain concerns over particle translocation due to the various pathways by which this may be possible. For example, translocation of inhaled NPs can occur directly from the alveolus to systemic circulation (Geiser and Kreyling 2010), by ingestion of NP-containing mucus cleared from the airways (Geiser and Kreyling 2010), by clearance of macrophages containing NPs to draining lymph nodes (Videira et al. 2002), and by travelling along the olfactory nerve to the central nervous system during nasal inhalation of NPs (Elder et al. 2006). Thus, because of their small size and the likelihood that NPs will remain within the lung for a longer period of time than larger particles, the probability of NP translocation is increased in comparison to larger particles (Figure 1.1). To date, several studies conducted in rats have reported minor translocation of NPs to the liver, kidney

and lymph nodes (Choi et al. 2010; Oberdorster et al. 2002), confirming that these effects are possible.

In addition to particle translocation, substantial inflammation and pulmonary molecular responses can elicit important systemic effects. For example, the release of inflammatory mediators in systemic circulation leads to recruitment of leukocytes to lung for most NMs (Goncalves et al. 2011) (Figure 1.1). Inhalation of particles is also associated with abrupt changes in signalling within the nervous system, possibly resulting in onset of cardiac arrhythmia (Magari et al. 2001) and changes in blood pressure (Cheng et al. 2003). As such, it is important to expand research on NP toxicity to non-contact organs (i.e., beyond the lung), in order to fully understand their effects.

1.3 Carbon Black (CB)

1.3.1 Physical and Chemical Properties of CB

CB consists of finely dispersed almost pure elemental carbon (> 97%, (Watson and Valberg 2001)) produced by the incomplete combustion of gaseous or vaporized liquid hydrocarbons under controlled conditions. Its appearance is that of a black pellet or fluffy powder. Very minimal amounts of other elements and chemical compounds can be found on the surface of CB, making these particles very different from soot, which is generally composed of < 60% carbon (ICBA 2006). Impurities on CB include organic compounds such as polycyclic

aromatic hydrocarbons (PAHs) and nitro-PAHs (< 1%), inorganic matter such as metals (< 1%) and other elements including hydrogen, oxygen and sulphur (Watson and Valberg 2001). Additional organic and inorganic compounds that can be extracted from CB are described in (IARC 2010). Primary CB particles are typically 10-500 nm in size, spherical in shape and generally rapidly agglomerate into open-chain structures upon contact. CB with a high degree of agglomeration is referred to as having a high "structure". The size, structure, surface area, conductivity and color of CB are the primary properties used to determine commercial application and value of CB. Over 40 grades of CB are currently used in the rubber industry alone (primary use of CB) with many others marketed for non-rubber applications (ASTM International 2005). Although most CB used for commercial applications is under 100 nm in size (thus in the NP size range), some CBs exceed 100 nm (Auchter 2005). For this reason, they are collectively referred to as CB and not as carbon black nanoparticles (CBNPs).

1.3.2 Commercial Applications of CB

CB is among the top 50 manufactured chemicals worldwide with a total production estimate of 8,100,00 metric tons in 2006 (ICBA 2006). The demand for small CB particles make CBNPs the most widely used NM (IARC 2010). Approximately 70% of CB is consumed for tire production, with most of the CB employed in the nano-range (Auchter 2005). CBNPs reinforce rubber and conduct heat away from the tread and belt area of tires, thus reducing damage

and increasing tire longevity. Approximately 20% of CB is used in other rubber goods within the automotive industry (e.g., for belts, hoses, O-rings) and for non-automotive purposes (e.g., for tubing, conveyor belts, footwear, floormats, toys) (Auchter 2005). The remaining CB is used as a pigment in inks, printer toner, coatings, plastics, and food, as well as for production of carbon paper (Auchter 2005).

1.3.3 Production of CB

Production of CB dates back over 3,500 years, when it was produced by the Chinese by collection from oil lamps. Today, nearly all CB (> 95%) is produced using the oil-furnace process (Voll and Kleinschmit 2002). This process employs heavy aromatic oils (e.g., petroleum or coal oil) introduced into a hot gas stream, where the oils are vaporized then pyrolyzed directly in the vapour phase to form CBNPs and other small CB particles (ICBA 2006). The process takes place in a closed reactor under carefully monitored temperature and pressure conditions, in order to control for specific chemical properties of the CB produced. CB is then cooled and collected in bag filters.

The remaining portion of CB is primarily manufactured through the thermal process. This process employs natural gas injected into a furnace in the absence of air, decomposing the natural gas into CB and hydrogen (ICBA 2006). Other seldom used methods of CB production include the acetylene process

(thermal decomposition of acetylene gas), the channel process (contact of partially combusted fuel with channel steel) and the lampblack process (collection of soot from burning oils or wood) (Mitsubishi Chemical Corporation 2006). CB is often referred to by the process by which it was manufactured (e.g., furnace blacks, lampblacks, thermal blacks, acetylene blacks and channel blacks).

1.3.3 Printex 90

Printex® grade CB particles (e.g., Printex U, V, 140U, 140V, 95, 90, 85, 80, 75, 55, 45, alpha, P, 60, 60-A, L6, L, 300, 30, 3, 35, 25, 200, A, G, 12, XE2-B, HV, F 85, F80, F alpha, F P, L6 SQ, L SQ and alpha SQ) are furnace blacks manufactured by Evonik-Degussa (Germany) and typically employed in the automotive industry in the application of high-tech windshield adhesives. Because most CB particles contain negligible amounts of trace contaminants, they are not considered to be highly toxic. In the mid 1980's, CB particles were used as a benchmark control for diesel exhaust particles (DEP) studies revealing CB-induced genotoxicity (Kawabata et al. 1986; Medalia et al. 1983) and approximately one decade later, both CB and DEP were shown to cause lung tumours in chronically exposed rats (presumably due to particle overload mechanisms) (Heinrich et al. 1995; Mauderly et al. 1994; Nikula et al. 1995). These unexpected findings sparked CB-related toxicological research in which Printex 90 became widely utilized. Since then, Printex 90 has become the most widely used CBNP for evaluation of CB safety.

1.4 Toxicology of CBNPs

1.4.1 Toxicity in vitro

CBNPs cause substantive cytotoxicity in lung tumour and fibroblast cell lines with exposures resulting in increased cell death, reduced proliferation and LDH leakage (Magrez et al. 2006; Yang et al. 2008). Genotoxic properties of CBNPs include induction of DNA strand breaks (Don Porto Carero et al. 2001; Mroz et al. 2007; Mroz et al. 2008), DNA base oxidation (Jacobsen et al. 2007), mutation (Jacobsen et al. 2011; Jacobsen et al. 2007) and micronuclei (Totsuka et al. 2009) in lung epithelial cells, as well as DNA strand breaks in cultured fibroblasts (Yang et al. 2009) and monocytes (Don Porto Carero et al. 2001). CBNPs also cause oxidative stress in fibroblasts as shown by depletion of intracellular glutathione (GSH) and superoxide dismutase (SOD) (Yang et al. 2009) and in monocytes as shown by induction of lipid peroxidation products and depletion of GSH (Foucaud et al. 2010). Cytokine and chemokine expression in human bronchial epithelial cells exposed to CBNPs is substantially altered (> 10-fold) for four inflammatory genes (i.e., *Ccl20*, *Cxcl8*, *Cxcl10* and *Cxcl14*) (Ovrevik et al. 2009). Lastly, global gene expression analyses in human vascular endothelial cells suggest that inflammatory responses are the primary molecular pathways perturbed by CBNP exposure (Yamawaki and Iwai 2006). Thus, *in vitro* studies demonstrate CBNP-induced cytotoxicity, genotoxicity, oxidative stress and inflammatory responses.

1.4.2 Pulmonary Exposure and Toxicity in Mammals

Chronic exposure to CBNPs causes lung tumours in male and female rats (Heinrich et al. 1995; Mauderly et al. 1994; Nikula et al. 1995b), although frequency was lower in males (Heinrich et al. 1995). Subchronic exposures cause increased mutation frequency in isolated rat alveolar epithelial cells (Driscoll et al. 1996). However, tumours do not occur in mice despite similar lung burdens (Elder et al. 2005; Heinrich et al. 1995). DNA strand breaks (SB) are manifested in bronchoalveolar lavage (BAL) cells of exposed mice (Jacobsen et al. 2009; Saber et al. 2005). However, only one study has investigated SB in lung tissue and demonstrates the occurrence of SBs only at a relatively high exposure dose (0.2 mg instillation) (Totsuka et al. 2009). Work in rats demonstrates that exposures causes 8-oxo-7, 8-dihydro-2′-deoxyguanosine (8-oxo-dG) that persist considerably after exposure (up to 44 weeks) (Gallagher et al. 2003). These data collectively demonstrate CBNP-mediated genotoxicity and potential for lung neoplasmic outcomes.

Other pulmonary effects of CBNP exposure include acute inflammation, as suggested by infiltration of polymorphonuclear cells (PMN) in lung of rodents upon pulmonary exposure (Brown et al. 2000; Driscoll et al. 1996; Elder et al. 2005; Li et al. 1999; Sager and Castranova 2009; Tong et al. 2009). In some cases, inflammation persists for a considerable time after the exposure (Driscoll et al.

1996; Elder et al. 2005; Sager and Castranova 2009). Moreover, CBNPs have adjuvant activity, which can play a role in allergic airway inflammation (de Haar et al. 2005). Analysis of gene expression supports inflammation as a mode of action of CBNPs in lung (Jackson et al. 2011b; Jacobsen et al. 2009) as well as in olfactory bulb of mice (Schwe et al. 2006) in mice.

In addition to effects at the point of contact (i.e., lung), a limited number of studies demonstrate toxicities in extra-pulmonary organs of exposed mice and in offspring exposed *in utero*. Pregnant mice exposed by inhalation exhibit sustained SB in liver and in liver of their offspring (Jackson et al. 2011a). Global gene expression analysis in the livers of the same offspring revealed significant changes in several genes (Jackson et al. 2011b). A separate CBNP inhalation study showed very subtle changes in hepatic global gene expression profiles of exposed mice (Saber et al. 2009). These data suggest the potential for CBNP-mediated systemic toxicities.

1.4.3 Morbidity and Mortality

Epidemiological investigations of CB associated mortality were conducted in studies within the UK, Germany and the USA. Workers from five major UK plants (n=1147, employed between 1947-1974 and mortality assessed 1951-1996) revealed a standard mortality ratio (SMR) of 1.73 for lung cancer ((Sorohan et al. 2001) updated from (Hodgson and Jones 1985)). Although no firm conclusions

were established due to confounding factors, an in-depth analysis revealed that CB exposure may have an effect on later stage lung carcinogenesis, as suggested by the trend between lung cancer mortality and cumulative CB exposure in the last fifteen years (Sorohan and Harrington 2007). An additional mortality study of German CB manufacturing workers (n=1535, employed > 1 year between 1960-1976 and alive in 1976, mortality assessed 1976-1998) revealed an SMR of 1.2 for all causes, 2.18 for lung cancer, 1.26 for heart disease and 1.58 for COPD (Wellmann et al. 2006). However, no apparent dose-response relationship between lung cancer mortality and occupational exposure (years of employment or CB exposure) was observed. Further examination of the data by (Buchte et al. 2006; Morfeld et al. 2006) revealed no excess risk of death from CB exposure. Six major studies have investigated mortality in employees of major CB production facilities within the USA (Dell et al. 2006; Ingalls 1950; Ingalls and Risquez-Iribarren 1961; Robertson and Ingalls 1980; Robertson and Ingalls 1989; Robertson and Inman 1996). The most complete and recent study reported no excess risk of death from all causes, nor from lung cancer in comparison to the general population (Dell et al. 2006). These data suggest the possibility that working within the CB manufacturing industry increases risk of lung cancer related death. However, impact of CB exposure on mortality is unclear due to the lack of consensus between studies.

Mortality in downstream CB industries (e.g., rubber and tire production) was examined in a limited number of studies. German rubber industry workers exhibit CB-associated excess risk of lung, larynx and stomach cancer (Straif et al. 2000), however, these correlations were not significant when nitrosamine, asbestos and talc exposures were taken into consideration. Excess risk of bladder cancer was found in Italian dockyard workers responsible for shipping and handling of CB (Puntoni et al. 2001; Puntoni et al. 2004). In Canada, investigations applying interviews of lifetime job history to approximate exposure to CB suggest an association with cancers of the lung, oesophagus and kidney (Parent et al. 2000; Parent et al. 1996). Thus, mortality outcomes within downstream industries were similar to those of CB manufacturing itself.

Epidemiological studies of morbidity reveal an array of adverse respiratory symptoms associated to CB exposure. These include chronic cough and sputum production as well as decrements in forced vital capacity (FVC) and forced expiratory volume in one second (FEV_1) (Crosbie 1986; Gardiner et al. 1993; Gardiner et al. 2001; Harber et al. 2003b). Decrements in FEV_1 were shown to correspond to a loss of 27-48 mL over a 40 year working lifetime, taking aging into consideration (Harber et al. 2003b). However, chest films indicative of pneumoconiotic abnormalities were not significant (van Tongeren et al. 2002). These studies demonstrate the probable impacts of CB on human lung function.

1.4.4 Exposure Information

Exposure to CB through consumer materials in which CB is bound within material is not thought to occur. However, substantive CB levels (measured as dust according to methods described in (Kuhlbusch et al. 2004)) have been detected in occupational settings. Very elevated occupational exposure levels of CB have been reported prior to the 1970s, but have been greatly reduced since. By the late 1970s, studies of facilities within the United States of America and Western Europe revealed personal geometric mean exposures to inhalable dust to be less than 5 mg/m^3 (Harber et al. 2003a; Smith and Musch 1982; van Tongeren et al. 2000). By the late 1990s, exposure to inhalable dust was reduced to below 2 mg/m^3 (Harber et al. 2003a; Muranko et al. 2001; van Tongeren et al. 2000) with the fraction of respirable dust (in NP-size range) below 0.5 mg/m^3 (van Tongeren et al. 2000). However CB exposure in downstream user industries remains to be elucidated. Exposure to CB can vary significantly between and within production facilities and over time. As such, precise exposure levels are currently unknown and warrant further investigation.

1.4.5 Occupational Exposure Limits and Guidelines

Potential long-term risks associated with elevated exposure to CB have prompted several countries to establish occupational exposure limits (Table 1.1). Currently, the International Agency for Research on Cancer (IARC) has established CB as *possibly carcinogenic to humans* (Group 2B) because of sufficient

evidence of carcinogenicity in experimental animals (for CB and CB extracts) but inadequate evidence of carcinogenicity in humans (IARC 2010). CB carcinogenicity data has been employed to establish regulatory guidelines in several countries (Table 1.1). It is important to note that established occupational exposure limits are, for the most part, relevant to CB or inhalable dust and do not make a distinction for CBNPs.

1.5 Systems Biology, Toxicogenomics and Hazard Identification

The evaluation of potentially toxic substances and human health hazard is currently carried out using established assays on animals that screen for various endpoints of toxicity including acute systemic toxicity, carcinogenicity, mutagenicity and reproductive and developmental toxicity. The existing guidelines for comprehensive evaluation of toxicity apply methods that are extremely lengthy, costly and require a large number of animals. Consequently, the vast quantity of chemicals requiring evaluation has overwhelmed the system and hampered risk assessment (Firestone et al. 2010). Thus, many substances that are potentially toxic to humans currently have little to no information on which to base regulatory decisions.

Toxic stress and the resulting adverse responses can elicit important molecular changes that include widespread alterations in genes (including non-coding genes such as microRNAs) transcription and protein translation

(Auerbach et al. 2010; Gatzidou et al. 2007). Identification of perturbed molecules and the pathways in which they are involved can provide insight in potential hazard, mode of action and disease relevance of toxicant exposure and potentially predict adverse effects at lower doses and earlier time-points than established assays (Halligan and Lunec 2008). Systems biology makes use of molecular responses (e.g., at the transcript, protein and metabolite level) in describing a biological system (e.g., at the cell, tissue or organismal level) as a whole. Gene expression profiling (i.e., toxicogenomics), can serve as an important base for exploring molecular cross-talk between tissues and systems biology responses. Thus, integrated systems biology and toxicogenomics are promising approaches for effectively guiding and supporting risk assessment (Dix et al. 2007; Heijne et al. 2005; Pennie et al. 2004).

Although systems biology and toxicogenomic approaches are not currently implemented in risk assessment by regulators, there is growing recognition that such pathway-based methodologies could greatly strengthen and expedite human health risk assessment. This call for a shift in the way risk assessment is currently conducted is the general premise of such widely supported documents as Toxicity Testing in the 21st Century (National Academy of Sciences 2007). The general objective is to use systems biology and pathway-based screening tools to guide follow up experiments and to provide information on chemical mode of action, thus decreasing the number of animals, time and

cost associated with toxicity testing. The integration of systems biology into risk assessment is currently at the center of several international initiatives (e.g., by the International Life Sciences Institute/Health and Environmental Sciences Insititute (ILSI/HESI), the National Institute of Environmental Health Sciences (NIEHS) and the Environmental Protection Agency (U.S. EPA)) that will ultimately determine how the approach is used in regulatory toxicology.

1.6 Thesis Overview

1.6.1 Rationale

Inhalation of fine and ultrafine particulate air pollution has long been associated with elevated risks of adverse cardiovascular and pulmonary health effects (Dockery et al. 1993; Pope et al. 1995; Pope III et al. 2002). By extension, increasing commercialization of NM has raised concerns over their safety. The bulk of NP research has focused on individual endpoints of toxicity in cultured cells and in rodent pulmonary tissues. However, very little is known about the systemic effects and NP mode of action involved in the development of adverse effects. Systems biology offers a promising approach in understanding mechanistic toxicology. Since the emergence of toxicogenomics and systems biology, a limited number of studies have evaluated global gene expression profiles following exposure to NMs including CB, titanium dioxide, gold and silver NPs *in vitro* (Fujita et al. 2009; Kawata et al. 2009; Yamawaki and Iwai 2006) and *in vivo* (Chen et al. 2006; Cho et al. 2009; Halappanavar et al. 2011; Jackson et

al. 2011b; Saber et al. 2009; Yu et al. 2007). These studies have revealed important molecular pathways and novel mechanisms involved in NP toxicities. However, *in vivo* evaluations of multiple tissues, doses and time-points to provide insight into the systemic effects of NPs over dose and time remain a gap in knowledge.

The overarching objectives of this Ph.D. thesis are three-fold. First, the work aims to employ systems biology to examine NP mode of action and to determine the relationship between molecular endpoints and pathways elucidated using a systems biology approach and more conventional toxicity assessment endpoints. Second, this thesis employs systems biology to elucidate molecular signalling cascades and impacts on non-targeted tissues. Third, the systems biology data produced are used to query the biological relevance of the observed responses to human diseases, and to determine the utility of systems biology endpoints in qualitative and quantitative human health risk assessment. The work employs CBNPs as a model NP; CBNPs have a rich database of traditional toxicity endpoints on which systems biology approaches can be anchored. The systems biology response in the exposed mice is evaluated over multiple doses and time-points. The work provides important insight into NP mode of action, systemic effects of exposure and the potential utility of systems biology in determining the health risks of NP exposure.

1.6.2 Specific Research Objectives and Hypotheses

Experiments were designed to investigate genomic response, specific systemic toxicities, and mode of action of NPs by pulmonary CBNP exposure in mice. The specific objectives and hypotheses for the five experimental chapters are as follows.

Chapter 2

Hypothesis: Intratracheal instillation of CBNPs causes *in vivo* pulmonary inflammation and genotoxicity that is associated with oxidative stress. Genotoxicity extends to hepatic tissue.

Objectives: To investigate pulmonary inflammation by influx of inflammatory cells collected in BAL and to determine genotoxicity using the comet assay in lung and liver of CBNP exposed mice.

Chapter 3

Hypotheses: CBNP-induced transcriptional changes occurring in the lung initiate signalling cascades that regulate molecular pathways in the liver.

Objectives: To investigate global gene expression profiles in the lungs and livers of exposed mice, and to determine the molecular pathways, molecules and signalling cascades linking the tissue responses over time.

Chapter 4

Hypotheses: Changes in miRNA expression occur upon CBNP exposure. These miRNAs mediate transcriptional responses in the lungs of exposed mice.

Objectives: To examine perturbations in miRNA expression in the lungs of mice exposed to CBNP and to investigate changes in the mRNA levels of their predicted targets.

Chapter 5

Hypotheses: Intratracheal installation of CBNPs causes transcriptional changes in cardiac tissue and systemic inflammation related changes associated with adverse cardiovascular effects in plasma.

Objectives: To investigate cardiac global gene and miRNA expression profiles in CBNP exposed mice and to measure plasma markers of endothelial inflammation and proteins involved in lipid transport.

Chapter 6

Hypotheses: Global gene expression profiles can be used in human health risk assessment of nanoparticles to identify modes of action and to predict biological outcomes of exposure. Expression profiling can also be used to quantitatively assess dose-responses (i.e., by deriving benchmark doses) and to identify potential disease outcomes of relevance to humans.

Objectives: To model BMDs in relevant and sensitive pathways and in apical endpoint and to compare systems biology critical doses to those of apical endpoints. To query relevance of gene expression profiles to rodent and human diseases.

1.7 Tables and Figures

Table 1.1. International occupational exposure limits and guidelines for carcinogenicity. Data are summarized from (IARC 2010; ICBA 2006).

Country	Exposure Limit (mg/m^3)	Regulated Substance	Interpretation	Carcinogenicity
Australia	3	CB	TWA	n/a
Belgium	3.6	CB	TWA	n/a
Brazil	3.5	CB	TWA	n/a
China	4	Total Dust	TWA	n/a
	8	CB	STEL	n/a
Canada	3.5	CB	TWA	n/a
Czech Republic	2	CB	TWA	n/a
Denmark	3.5	CB	TWA	carcinogen
Finland	3.5	CB	TWA	n/a
	7	CB	STEL	
France	3.5	CB	TWA	n/a
Germany	1	CB Respirable	TWA-MAC	*in vitro*/*in vivo* carcinogenicity with insufficient evidence of human carcinogenicity
	4	CB Inhalable	TWA-MAC	
	6	CB Respirable	TWA-TRGS	
	10	CB Inhalable	TWA-TRGS	
Hong Kong	3.5	CB	TWA	not classifiable as human carcinogen
Ireland	3.7	CB	TWA	n/a
Italy	3.5	CB	TWA	n/a
Japan	1	Respirable Dust, < 10% free silica	TWA	possibly carcinogenic to humans
	4	Total Dust, < 10% free silica	TWA	

Malaysia	3.5	CB	TWA	n/a
Mexico	3.5	CB	TWA	not classifiable as human carcinogen
	7	CB	STEL	
Netherlands	3.5	CB	TWA	n/a
New Zealand	3	CB	TWA	n/a
Norway	3.5	CB	TWA	n/a
Poland	4	Total Inhalable, < 35 mg B[a]P/kg	TWA	n/a
Republic of Korea	3.5	CB	TWA	n/a
Russia	4	CB	TWA	n/a
South Africa	3.5	CB	TWA	n/a
	7	CB	STEL	
Spain	3.5	CB	TWA	n/a
Sweden	3	Total Dust	TWA	n/a
United Kingdom	3.5	Inhalable Dust	TWA	n/a
United States (ACGIH)	3.5	CB	TWA-TLV	not classifiable as human carcinogen
United States (NIOSH)	3.5	CB	TWA (10 h)	n/a
United States (OSHA)	3.5	CB	TWA-PEL	carcinogen

ACGIH, American Conferance of Governmental Industrial Hygienists; B[a]P, Benzo[a]Pyrene; MAC, maximal allowable concentration; NIOSH, National Institute for Occupational Safety and Health; OSHA, Occupational Safety and Health Administration; PEL, permissible exposure limit; STEL, short-term exposure limit (15 min unless otherwise specified); TLV, threshold limit value; TRGS, Technische Regeln für Gefahrstoffe (Technical Rules for Hazardous Substances); TWA, time-weighted average (8 h unless otherwise specified).

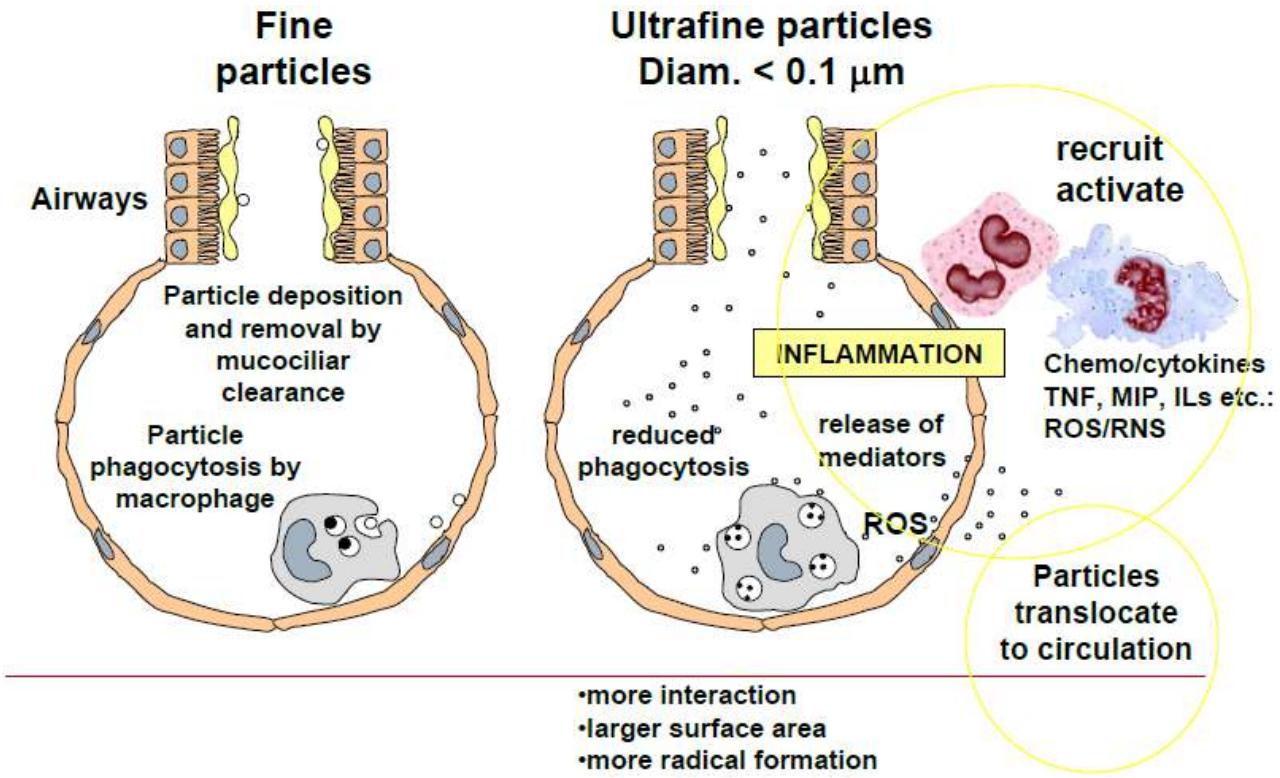

Figure 1.1. Deposition of fine particles (> 100 nm) and ultrafine particles or NPs (< 100 nm) in lung alveolus and potential for systemic toxicity by translocation of NPs to systemic circulation or secretion of inflammatory mediators. Figure was created by Marianne Dybdal (2008) (permission for reproduction granted).

CHAPTER 2: CARBON BLACK NANOPARTICLE INSTILLATION INDUCES SUSTAINED INFLAMMATION AND GENOTOXICITY IN MOUSE LUNG AND LIVER

Modified from: Bourdon, JA, Saber, AT, Jacobsen, NR, Jensen, KA, Madsen, AM, Lamson, JS, Wallin, H, Møller, P, Loft, S, Yauk, CL and Vogel, UB. (2012) *Particle and Fibre Toxicology*, 9(5), 1-14.

2.1 Abstract

Widespread occupational exposure to carbon black nanoparticles (CBNPs) raises concerns over their safety. CBNPs are genotoxic *in vitro* but less is known about their genotoxicity in various organs *in vivo*. We investigated inflammatory and acute phase responses, DNA strand breaks (SB) and oxidatively damaged DNA in C57BL/6 mice 1, 3 and 28 days after a single instillation of 0.018, 0.054 or 0.162 mg Printex 90 CBNPs, alongside sham controls. Bronchoalveolar lavage (BAL) fluid was analyzed for cellular composition. SB in BAL cells, whole lung and liver were assessed using the alkaline comet assay. Formamidopyrimidine DNA glycosylase (FPG) sensitive sites were assessed as an indicator of oxidatively damaged DNA. Pulmonary and hepatic acute phase response was evaluated by *Saa3* mRNA real-time quantitative PCR. Inflammation was strongest 1 and 3 days post-exposure, and remained elevated for the two highest doses (i.e., 0.054 and 0.162 mg) 28 days post-exposure ($P < 0.001$). SB were detected in lung at all doses on post-exposure day 1 ($P < 0.001$) and remained

elevated at the two highest doses until day 28 ($P < 0.05$). BAL cell DNA SB were elevated relative to controls at least at the highest dose on all post-exposure days ($P < 0.05$). The level of FPG sensitive sites in lung was increased throughout with significant increases occurring on post-exposure days 1 and 3, in comparison to controls ($P < 0.001$-0.05). SB in liver were detected on post-exposure days 1 ($P < 0.001$) and 28 ($P < 0.001$). Polymorphonuclear (PMN) cell counts in BAL correlated strongly with FPG sensitive sites in lung ($r=0.88$, $P < 0.001$), whereas no such correlation was observed with SB ($r = 0.52$, $P = 0.08$). CBNP increased the expression of *Saa3* mRNA in lung tissue on day 1 (all doses), 3 (all doses) and 28 (0.054 and 0.162 mg), but not in liver. Deposition of CBNPs in lung induces inflammatory and genotoxic effects in mouse lung that persist considerably after the initial exposure. Our results demonstrate that CBNPs may cause genotoxicity both in the primary exposed tissue, lung and BAL cells, and in a secondary tissue, the liver.

2.2 Introduction

The use of nanoparticles (NPs) in consumer products and applications continues to rise (Rocco 2005). In parallel, the potential for NP mediated toxicity is a growing public concern. Many of the unique properties exhibited by NPs increase the likelihood of deleterious biological interactions and subsequently, the risk of adverse health outcomes (Borm et al. 2006; Seaton et al. 2010; Vishwakarma et al. 2010). Understanding the repercussions of inhaling NPs is

particularly important because NPs penetrate deeper regions of the lung (e.g., alveoli and pulmonary interstitium) (Ferin et al. 1992; ICRP 1994), are translocated from lung to systemic circulation more readily (Choi et al. 2010; Oberdorster et al. 2002), and are cleared from the lungs less effectively (Renwick et al. 2001) than their larger counterparts. As such, there is a great probability of cellular interactions, necessitating investigations of NP-mediated toxicity and risk of health consequences.

Carbon black (CB) has been widely investigated since its use as a benchmark control for *in vivo* toxicological evaluation of diesel exhaust particles and as a model of urban air pollution particulate matter almost three decades ago (Kawabata et al. 1986; Medalia et al. 1983). Since then, CB has become the focus of numerous toxicity studies as well as an important reference material (i.e., Printex 90) (Heinrich et al. 1995; Nikula et al. 1995). CBNPs are reactive oxygen species (ROS) generators as shown in cellular (Hussain et al. 2009; Kroll et al. 2011) and acellular systems (Jacobsen et al. 2008). Moreover, inhalation or intratracheal instillation exposures to CBNPs result in large pulmonary inflammatory responses in rodents (Brown et al. 2000; Driscoll et al. 1996; Elder et al. 2005; Li et al. 1999; Sager and Castranova 2009; Tong et al. 2009; Wolff et al. 1990), which can greatly exacerbate ROS generation via activation of polymorphonuclear (PMN) granulocytes (Knaapen et al. 2004). As such, it is expected that CBNPs can mediate secondary genotoxicity by means of

inflammation and oxidative stress. CBNPs are genotoxic *in vitro*, as shown by increases in DNA base oxidation (Jacobsen et al. 2007), mutation frequency (Jacobsen et al. 2011; Jacobsen et al. 2007), strand breaks (Mroz et al. 2007; Mroz et al. 2008) and micronucleus frequency in lung epithelial cells (Totsuka et al. 2009) as well as increases in strand breaks in fibroblasts (Yang et al. 2008). However, less is known about the genotoxicity of CBNPs *in vivo*. A few studies in rats have demonstrated CBNP-induced DNA base oxidation (Gallagher et al. 2003) and increased mutation frequency (Driscoll et al. 1996). However, rats may not be the most suitable model for exposure to particulates due to their predisposition to particle overload. Studies in mice have demonstrated DNA strand breaks in BAL cells (Jacobsen et al. 2009; Saber et al. 2005) and one study has established CBNP-induced lung DNA strand breaks, but this was found using a high dose (i.e., 0.2 mg) immediately (3 hours) post instillation (Totsuka et al. 2009).

The growing demand for CBNPs for diverse commercial applications (e.g., rubber products and pigments) raises health concerns for the increasing number of individuals routinely exposed, especially in occupational settings where relatively high levels of exposure may occur. As such, it is critical to establish whether genotoxicity and oxidative stress arise *in vivo* at low doses of exposure and in extrapulmonary tissues, and to determine whether these effects are

associated with inflammation and/or persist for long periods of time following the initial exposure.

Here, we investigate the relationships between inflammation and genotoxic outcomes over time after a single exposure to Printex 90 CBNPs in BAL cells, lung and liver. Mice were exposed via intratracheal instillation using various doses (i.e., 0.018, 0.054 and 0.162 mg) and post-exposure recovery time-points (i.e., 1, 3 and 28 days), alongside sham controls. We report that instillation of CBNPs leads to prolonged generation of DNA damage in BAL cells, lung and liver of exposed mice as well as persistent pulmonary inflammation, acute phase response and oxidatively damaged DNA.

2.3 Materials and Methods

2.3.1 Animals

Female C57BL/6 mice aged 5-6 weeks were obtained from Taconic (Ry, Denmark). Mice were acclimatized for 2-3 weeks before the experiment and were 8 weeks of age at the start of the study. All mice were given food (Altromin no. 1324, Christian Petersen, Denmark) and water *ad libitum*. The mice were group housed in polypropylene cages with sawdust bedding at controlled temperature (21±1^{o}C) and humidity (50±10%) with a 12-h light:12-h dark cycle. The experiments were approved by the Danish "Animal Experiments Inspectorate" (permit 2010/561-1179) and carried out following their guidelines for ethical

conduct and care when using animals in research. All procedures complied with EC Directive 86/609/EEC and Danish laws regulating experiments on animals.

2.3.2 Preparation of Exposure Stock

Printex 90 was suspended by sonication in 0.9% NaCl MilliQ water containing 10% v/v acellular BAL from C57BL/6 mice. The BAL fluid was prepared by flushing unexposed mice twice with 0.6 ml 0.9% NaCl solution yielding approximately 1 ml of BAL fluid. Acellular BAL was prepared by centrifugation of BAL fluid at 400 g (10 min, 4°C). The particle suspensions (4.05 mg/ml) were sonicated using a 400 W Branson Sonifier S-450D (Branson Ultrasonics Corp., Danbury, CT, USA) equipped with a disruptor horn (Model number: 101-147-037). Total sonication time was 8 min, with alternating 10 s pulses and 10 s pauses at amplitude of 10%. Samples were continuously cooled on ice during the sonication procedure. This suspension was used for the high dose, diluted 1:3 for the medium dose (0.054 mg) and diluted further 1:3 for the low dose (0.018 mg). Vehicle control solutions were prepared containing 90% 0.9% NaCl MilliQ water and 10% acellular BAL fluid.

2.3.3 Characterization of Exposure

The hydrodynamic particle size distributions in the exposure media were determined by Dynamic Light Scattering (DLS) using a Malvern Zetasizer Nano ZS (Malvern Instruments Ltd, UK). Data were analyzed using the Dispersion

Technology Software (DTS) version 5.0 (Malvern Instruments Ltd). Samples were measured at 25°C in 1 mL Malvern disposable polystyrene cuvettes. For analysis of hydrodynamic size, we used the refractive (R_i) and absorption indices (R_{abs}) of 2.020 and 2.000, respectively, for Printex 90 and standard optical and viscosity properties for H_2O. For analysis of the instillation medium we used the Malvern standard conditions for both water and protein (R_i = 1.450; R_{abs}= 0.001). The nature of particles and level of agglomeration was also evaluated by TEM using a 200 kV Tecnai T20 G2 Transmission Electron Microscope at the DTU Center for Electron Nanoscopy, Technical University of Denmark, Lyngby. DLS analysis of exposure media was performed on the raw instillation dispersions and after filtration through 3 μm (Glass Micro Fiber;Whatmann, UK) and 0.2 μm (hydrophilic DISMIC®-25CS Cellulose Acetate; Toyo Roshi Kaisha Ltd, Japan) syringe filters. Zeta-potential measurements were completed using instillation mediums with a Printex 90 concentration of 0.3 mg/ml according to the Smoulowkowski model and using Malvern's folded capillary cuvettes DTS1060 in the general purpose mode using the Malvern Zetasizer above. All data were obtained based on six consecutively repeated analyses of the same sample with no pause. Acceptance of the size-distribution data was done after evaluation of the correlation spectra and size-distribution fit and standard quality reports in the software. The quality of the zeta-potential measurements was controlled by evaluation of counts, sample conductivity, phase-plots, as well as zeta- and

mobility data. In all cases, outliers identified following quality control were removed from the final average value.

2.3.4 Exposure of Mice

A total of 72 mice (6 per group) were given 0.018, 0.054 or 0.162 mg of Printex 90 CBNPs by a single intratracheal instillation. Before the intratracheal instillation, the mice were anesthetized using Hypnorm® (fentanyl citrate 0.315 mg/ml and fluanisone 10 mg/ml from Janssen Pharma) and Dormicum® (Midazolam 5 mg/mL from Roche). Both anaesthetics were mixed with equal volumes sterile water. A volume of 0.15 ml was injected subcutaneously in the neck of each mouse. The sedated mice were kept on 37 ^{o}C heating plates. During instillation the mice were placed on their backs on a 40 degree slope. The trachea was intubated using a 24 gauge BD Insyte catheter (Becton Dickinson, Denmark) with a shortened needle. The correct location of each intubation was tested using a highly sensitive pressure transducer (pneutachymeter) developed at the National Research Centre for the Working Environment in collaboration with John Frederiksen (FFE/P, Copenhagen, Denmark). A 40 µl suspension was instilled followed by 150 µl air with a 250 µl SGE glass syringe (250F-LT-GT, MicroLab, Aarhus, Denmark). Control animals received vehicle instillations. The intubation catheter was held head up until proper breathing was assured. The mice were then transferred to the 37 ^{o}C heating plate until they recovered from

anaesthesia. The animals did not show signs of respiratory distress, lethargy or other physical symptoms of exposure.

2.3.5 Preparation of Tissue and Cells

One, 3 and 28 days after the instillation, the mice were anaesthetised with Hypnorm/Dormicum as described above. Immediately after withdrawing the heart blood, a bronchoalveolar lavage (BAL) was performed four times with 0.8 mL of 0.9% sterile saline through the trachea. The BAL was immediately put on ice until BAL fluid and BAL cells were separated by centrifugation at 4°C and 400 g for 10 min. The BAL cells were resuspended in 100 µL medium (HAMF12 with 10% fetal bovine serum). The suspension (40 µL) was mixed with 160 µL medium containing 10% DMSO and stored at –80°C for later analysis in the comet assay. For differential count, cells from 50 µL were collected on microscope slides by centrifugation at 10,000 rpm for 4 min in a Cytofuge 2 (StatSpin, Bie and Berntsen, Rødovre, Denmark). The slides were fixed with 96% ethanol and stained with May–Grünwald–Giemsa stain. The cellular composition of BAL cells was determined on 200 cells. The total number of cells was determined by using the NucleoCounter (Chemometec, Allerød, Denmark) live/dead assay according to the manufacturer's instructions. The lungs and liver were snap frozen in cryotubes (NUNC) in liquid N_2 and stored at –80°C.

2.3.6 DNA Damage Measured by Comet Assay

Whole lung and liver were broken into specific pieces under liquid nitrogen, homogenized in Merchant's EDTA (0.14M NaCl, 1.47mM KH_2PO_4, 2.7mM KCl, 8.1mM Na_2HPO_4, 10mM EDTA) and filtered at 70 µm to yield individual cells. Two different comet methods were used to process the BAL cells/liver tissue and the lung tissue samples.

DNA SB in liver and BAL cells were analyzed using a high throughput protocol allowing 48 samples per GelBond® film, developed at the Norwegian Institute of Public Health (Gunnar Brunborg and Kristine Bjerve Gutzkow) within the COMICS EU Project as previously described (Jackson et al. 2011a). The BAL cells were quickly thawed in a 37°C waterbath before being mixed with agarose. The freezing and thawing of the cells was validated not to have any effect on experimental outcome in a cell line and in primary lymphocytes with correlation coefficients (r) of 0.96-0.99. In the present experiment, the cell/agarose suspension was applied onto a GelBond(R) film (7 µL per sample) with a multichannel pipette. Eight films were processed per electrophoresis, in two parallel electrophoresis tanks. Due to preparation time, the lysing procedure varied between 1-2 hours for samples in the present study (up to 3.5 hours). The high volume protocol allowed processing of all related samples on one film and reduced the variation caused by increased processing time and different electrophoreses.

The slides were inspected using a Leica LB fluorescence microscope at 400x magnification with a 450-490 nm emission filter and an LP515 excitation filter. DNA damage was measured as comet tail length (TL) using the Kinetics image analysing system (version 3.0). To eliminate day-to-day variation, the data were normalized to the level in A549 cells included on each electrophoresis gel. The mean TL±SEM (μm) for the 0 and 30 μM H_2O_2 exposed A549 cells were 45.85±4.49 and 73.27±3.14 for analysis of the liver samples and 45.13±2.59 and 71.92±3.13 for the analysis of the BAL cells.

DNA SB in whole lung were measured as the formation of SB and FPG sensitive sites as previously described (Folkmann et al. 2007). The level of FPG sensitive sites was calculated as the differences in DNA damage between slides that had been treated with the FPG enzyme and buffer. The FPG enzyme was a gift from Professor Andrew Collins (University of Oslo, Norway). Scoring was accomplished by visual inspection of 100 nuclei and categorized using a five class scoring system (ranging from 0-400). The five class scoring system shows excellent correlation with computerised image analysis of the DNA migration (Moller 2006). We used this calibration of the comet assay endpoint because this provides better inter-investigator accuracy (Forchhammer et al. 2008; Moller et al. 2004a) and reduces the inter-laboratory variation in reported values of DNA damage by the comet assay (Forchhammer et al. 2009; Johansson et al. 2010;

Moller et al. 2010b). The data were transformed into lesions/10^6 bp using a previously established gamma irradiation calibration curve (Forchhammer et al. 2009). All samples were coded prior to scoring and organized to block the effects of day of experiments. We used human lymphocytes, treated with 1 μM Ro19-8022 photosensitizer and UV-light as control samples as described previously (Jensen et al. 2012). This treatment generates predominantly FPG sensitive sites as compared to SB. The Ro19-8022 photosensitizer was a gift from F. Hoffman, La Roche, Basel, Switzerland. The mean lesion per bp ± SEM were in these reference control samples were 0.068 ± 0.002 SB/10^6 bp and 2.045 ± 0.002 FPG sensitive site/10^6 bp.

2.3.7 Saa3 mRNA Expression

RNA was prepared using the NucleoSpin 96 RNA kit (Macherey–Nagel, Germany). RNA from the entire left lung of each mouse or a piece of liver tissue was prepared by lysing the tissue in 2 ml RLT buffer, while vigorously disrupting the sample with a Tissuelyser (Qiagen, Denmark) with a 5 mm stainless steel bead for 2×60 seconds and run through a QIAshredder (Qiagen, USA). The rest of the purification was performed as described by the manufacturer. cDNA was prepared using TaqMan reverse transcription reagents (Applied Biosystems, USA) as described by manufacturer.
Saa3 mRNA expression levels were determined as described previously (Saber et al. 2009).

2.3.8 Statistics

The data on DNA damage, *Saa3* mRNA expression and total number of cells in BAL fluid were analysed using a two-factor ANOVA analysis with the day of sacrifice and dose as categorical variables. We assessed differences in the BAL fluid cell composition using a one-factor ANOVA for each day of sacrifice, as well as by non-parametric Kruskal-Wallis or Mann-Whitney tests. The same significant effects were found in both parametric and non-parametric tests. The results on the number of cellular subsets of the BAL fluid were analyzed as log-transformed for macrophages and epithelial cells. Some samples of BAL fluid did not contain neutrophils, lymphocytes and eosinophils; we added the mean level of cells from the control group to all results to avoid problems with log-transformation of zero. Associations between the level of PMN and FPG sensitive sites in lung tissue were assessed by linear regression analysis with or without adjustment for effect of dose and time point. In all tests, the level of significance was 5%. The analyses were performed in Statistica version 5.5 for Windows (StatSoft Inc. (1997), USA).

2.4 Results

2.4.1 Particle Characterization

Printex 90 CBNPs were a gift from Evonik/Degussa (Frankfurt, Germany). The manufacturer reported an average primary particle size of 14 nm

and an organic impurity content of less than 1%. The specific surface area was determined to be 295-338 m^2/g, corresponding to a theoretical average spherical particle size of 8.1-9.5 nm (Saber et al. 2011). The total carbon content measured was greater than 99 wt%, with 0.82 nitrogen and 0.01 hydrogen wt%. Very low levels of both total polycyclic aromatic hydrocarbon (PAH) (74.2 ng/g) (Jacobsen et al. 2011; Jacobsen et al. 2007) and total endotoxin (0.142 EU/mg Printex 90) were detected in the sample. The particle suspension (the 0.054 mg dose) was characterised by transmission electron microscopy (TEM) and dynamic light scattering (DLS) analysis as previously reported (Saber et al. 2011). The TEM analysis of the instillation suspension showed that the Printex 90 consisted of both free and open to partially open chain-agglomerates. The size of the primary carbon black spheres was wide, ranging from less than 10 nm to more than 500 nm, whereas the agglomerate sizes typically were on the order of 200 nm or larger. High-resolution analysis showed that the spheres consisted of concentric layers with graphitic spacing, resembling the nano-onions structure.

By DLS, the unfiltered Printex 90 instillation suspension (which was employed for intratracheal instillation), was shown to be highly agglomerated in the 10% BAL-saline instillation medium. The propensity towards agglomeration was in accordance with the low peak zeta-potential of -10.7 mV determined for Printex 90 at 0.3 mg/ml instillation medium (conductivity 13.6 mS/cm). The DLS size analysis of Printex 90 stock dispersion has been reported before (Saber et al.

2011). Here, we present the data in more detail. The Printex 90 stock-dispersion was highly agglomerated and had a very high polydispersity index (PDI = 1). The hydrodynamic number size-distribution analysis showed a major peak at approximately 2.6 µm (n=4), almost comparable to the peak-size (3.1 µm) in the volume-size-distribution. Filtration was performed through a 3.0 and 0.2 µm filter to investigate the possible presence of smaller particles, which may not be detected by DLS due to the high abundance of large agglomerates. Filtration through the 3.0 µm filter (n=5) revealed the presence of smaller particles with a number peak size of approximately 190 nm (220 nm by volume). Again the polydispersity index was relatively high (PDI = 0.558) indicating a broad size-distribution. This 190-220 nm size corresponds well with the typical smaller free particle and agglomerate sizes of the Printex 90 (Figure 2.1A). By filtration through a 0.2 µm filter most of the particles were removed resulting in low intensities and hence only a relatively weak, but consistent DLS signal was obtained on this final filtrate. Repeated analyses showed consistent results, but only one out of the first six analyses of the same sample had acceptable data-quality for sizing. The number size-distribution plot showed a highly dominant size-mode with a primary peak-size at 7 nm. By volume, a larger agglomerate mode was also found at 460 nm, which can explain the relatively high polydispersity index (PDI = 0.515) found in the 0.2 µm filtrate. The 7 nm size-mode obtained in the last filtrate could be due to proteins in the dispersion vehicle (BAL fluid). However, analysis of the pure instillation media did not

reveal any peak-sizes smaller than 20 nm (Figure 2.1B). Therefore, the small size material found in the instillation medium is ascribed to a minor fraction of very small Printex 90 particles, which were indeed observed by TEM (Figure 2.2). It should be noted that Printex 90 dispersed in MilliQ-filtered water results in much smaller peak sizes of approximatly 50 to 60 nm (Jackson et al. 2011a).

2.4.2 BAL Fluid Cell Composition

We collected BAL fluid from Printex 90 CBNP instilled mice using three doses (i.e., 0.018, 0.054 and 0.162 mg) and three post-exposure time-points (i.e., 1, 3 and 28 days). The inflammatory response was neutrophil dominated and persisted 28 days post-exposure. The largest cellular influxes were observed on post-exposure recovery days 1 and 3 (Table 2.1).

Increased total cell counts in BAL fluid were found for all doses and time-points, except for the lowest dose delivered at the 28 day recovery time-point. The net increase in the total number of cells relative to controls in the BAL fluid by the largest CBNP dose was 1.5×10^5 cells (95% CI: 0.9×10^5 - 2.1×10^5), 2.0×10^5 cells (95% CI: 1.3×10^5- 2.8×10^5) and 0.6×10^5 cells (95% CI: 0.3×10^5 - 1.1×10^5) in the mice sacrificed on days 1, 3 and 28, respectively.

The increase in total BAL fluid cell counts was primarily the result of large neutrophil influxes, which were observed at all doses and time-points (Table 2.1).

The net influx of neutrophils relative to controls in the BAL fluid following exposure to the highest dose of Printex 90 was 1.5 x 10^5 cells (95% CI: 0.7 x 10^5-3.2 x 10^5), 1.2 x 10^5 cells (95% CI: 0.8 x 10^5 - 1.9 x 10^5) and 0.5 x 10^5 cells (95% CI: 0.3 x 10^5 - 0.6 x 10^5) on post-exposure days 1, 3 and 28, respectively.

The number of macrophages decreased following exposure to the highest dose of Printex 90 on post-exposure day 1, but increased following low and high dose Printex 90 exposures on post-exposure day 3 (Table 2.1). The number of lymphocytes increased 3 days post-exposure for all three doses of Printex 90. Increased numbers of lymphocytes were also observed on post-exposure day 28 for both the medium and high doses of Printex 90, thus suggesting onset of allergic airway inflammation. On post-exposure day 3, increased eosinophils were observed for all doses, and an increased number of epithelial cells was found at the highest dose of Printex 90.

2.4.3 Acute Phase Response

Printex 90 increased the mRNA expression of *Saa3* in lung tissue on day 1 (all doses), 3 (all doses) and 28 (0.018 and 0.054 mg doses), whereas there were no effects on the *Saa3* mRNA expression in the liver (Table 2.2).

2.4.4 DNA Damage

We observed increased levels of SB in CBNP Printex 90 instilled mouse lung, liver and isolated BAL cells, relative to sham controls. SB in BAL cells were observed at the high dose (i.e., 0.162 mg) for each time-point, as well as at all doses 28 days post-exposure, relative to controls (Figure 2.3). DNA SB, even 28 days after exposure, were increased from 2.34 SB per 10^6 bp in the control group to between 2.65-2.68 per 10^6 bp in the exposed group (i.e., all doses). There was no apparent dose-response relationship.

Increased SB were also observed in lung for all doses relative to control, with the largest effects observed on day 1. Levels of DNA SB 24 hours after the exposure were greatly increased from 0.1 SB per 10^6 bp in the control group, to between 0.3-0.5 SB per 10^6 bp in the exposed group (i.e., all doses) (Figure 2.4A). Mice exposed to the higher doses (i.e., 0.054 and 0.162 mg) also exhibited elevated levels of SB 3 and 28 days post-exposure relative to control animals.

The number of formamidopyrimidine DNA glycosylase (FPG) sensitive sites in lungs (an indicator of oxidative damage to DNA) was significantly elevated in all dose groups of the CBNP exposed animals relative to controls on day 1, with FPG sensitive sites of 0.9-1.5 per 10^6 bp in the exposed animals, compared to 0.4 per 10^6 bp in the controls (Figure 2.4B). Statistically significant increases in FPG sensitive sites were also observed for the high dose exposure

(i.e., 0.162 mg) at the 3 day recovery time-point. Marginal increases were observed for the low dose groups on day 3 (i.e., 0.018 and 0.054 mg) and for the high dose groups on day 28 (i.e., 0.054 and 0.162 mg) in a dose-response trend.

DNA damage also occurred in liver of the CBNP exposed mice with significantly elevated levels of SB on days 1 and 28 (Figure 2.5), although not on day 3. Levels of SB were increased from 1.61 lesions per 10^6 bp in the control group, to 2.27-2.46 SB per 10^6 bp 24 hours post-exposure and from 1.93 lesions per 10^6 bp in the control group, to 2.10-2.34 SB per 10^6 bp 28 days post-exposure. No apparent dose-response relationships were observed in the liver.

In the lung, there was a strong correlation ($r = 0.88$, $P < 0.001$) between FPG sensitive sites and BAL cell numbers across the doses and time points, whereas no such correlations were observed between the number of BAL cells and SB ($r = 0.52$, $P = 0.08$). The correlation between the number of BAL cells and FPG sensitive sites in the lung was mainly driven by the differences related to the doses and time points because the statistically significant association between BAL cell influxes and FPG sensitive sites ($r = 0.61$, $P < 0.001$) vanished in regression models adjusted for the effect of dose and time-point.

2.5 Discussion

We investigated CBNP-mediated DNA damage and inflammatory responses in Printex 90 instilled mice using multiple doses (i.e., 0.018, 0.054 and 0.162 mg) and post-exposure time-points (i.e., 1, 3 and 28 days), alongside sham controls. These doses equal the pulmonary deposition after 1, 3 and 9 working days for a mouse at the occupational exposure limit of 3.5 mg/m^3 CB per 8 hour work shift (as established by the Occupational Safety and Health Administration (OSHA) and the National Institute for Occupational Safety and Health (NIOSH)). These calculations assume that 33.8% of the inhaled mass ends up in the pulmonary region (Jacobsen et al. 2009) with a volume of inhaled air per hour of 1.8 L/h (Dybing et al. 1997) and 8 h working days. CB exposure levels of up to 3.7 mg/m^3, 2.2 mg/m^3 and 4.2 mg/m^3 have been reported for workers implicated in packaging and in handling CB (Smith and Musch 1982; van Tongeren et al. 2000; Williams et al. 1980). BAL cell influxes revealed CBNP-induced inflammation that peaked 1 and 3 days post-exposure and persisted 28 days thereafter (Table 2.1). SB were detected in lung and liver tissues and isolated BAL cells relative to controls and persisted to day 28 (Figures 2.3, 2.4A and 2.5). FPG sensitive sites in lung were increased throughout with significant increases occurring on post-exposure days 1 and 3 in comparison to controls (Figure 2.4B). The expression of *Saa3* mRNA in lung tissue was increased at all time-points. This reflects a persistent acute phase response during the entire experiment (Table 2.2). The correlation between total BAL cells and FPG sensitive sites across all doses and time-points suggests an important role for BAL cell

influxes in generation of oxidative stress in the lungs. This study is the first to demonstrate *in vivo* low dose CBNP-induced SB in lung and liver, which persist 28 days after a single exposure.

Although the primary particle size of Printex 90 (as dry powder) was stated by the supplier to be 14 nm, CBNP suspensions were shown to be highly agglomerated by DLS. When analyzing the unfiltered suspension we were only able to detect particles with a peak size of 2.6 μm. However, this is an artefact of the DLS methodology in which larger agglomerated particles will overshadow smaller particles. Consequently, DLS on unfiltered samples can only detect the largest particles in the suspension. Therefore, we filtered the suspension to remove the largest particles in order to be able to detect the smaller particles. DLS on the filtered suspension confirmed the presence of smaller particles as well (peak size of 190 nm and range of 90-350 nm). This shows that some of the particles in the suspension used for instillation are nano-sized, but the DLS analysis is unable to quantify the proportion of nano-sized particles in the suspension.

As in other studies of NP toxicity, endotoxin present on the NPs can result in inflammatory responses. However, the very low level of endotoxin detected on the CBNPs (0.142 EU/mg CBNP) is not anticipated to result in any significant inflammatory response. In another study, the response of LPS instillation was

investigated in mice (Dong et al. 2009). Instillation of a high dose of LPS (100 μg = 1200 000 EU) resulted in a high inflammatory response, while a low dose of LPS (0.1 μg = 1200 EU) resulted in a low inflammatory response. We have instilled doses ranging from 0.003 EU (0.142 EU/mg x 0.018 mg) to 0.02 EU (0.142 EU/mg x 0.162 mg). The ensuing doses of endotoxin administered in our study are therefore several orders of magnitude below what is considered a low dose of LPS, and thus are expected to result in very little (if any) endotoxin induced inflammation.

SB in lung and BAL cells demonstrate CBNP-induced DNA damage at the site of exposure (Figures 2.3 and 2.4A). Although CBNP-induced DNA SB have been investigated *in vitro* (Jacobsen et al. 2009; Saber et al. 2011; Totsuka et al. 2009; Yang et al. 2008), only one study has investigated SB in mouse lung *in vivo*, and this work used a single high dose (i.e., 0.2 mg instillation) (Totsuka et al. 2009). In contrast, we demonstrate that SB in lung occur at much lower doses of exposure (e.g., as low as 0.018 mg). Our BAL findings corroborate two earlier studies demonstrating CBNP-induced SB in C57BL/6 and tumour necrosis factor (TNF) deficient mice exposed by inhalation (i.e., 20 mg/m^3, 90 min/day, 4 days) (Saber et al. 2005), and apolipoprotein E (ApoE) deficient and C57BL/6 mice exposed by instillation (i.e., 0.054 mg) (Jacobsen et al. 2009). Thus, our results indicate that SB result from exposure levels that are much lower than previously reported.

The aforementioned *in vivo* works investigated pulmonary and BAL SB shortly after CBNP exposure, using recovery time-points ranging from 1 to 24 hours (Jacobsen et al. 2009; Saber et al. 2005; Totsuka et al. 2009). Taking into consideration that SB are readily repaired within a few hours of induction (Risom et al. 2003), we aimed to establish whether *de novo* DNA SB could be induced at much later post-exposure time-points (e.g., 3 and 28 days). Interestingly, we observed SB at all post-exposure time-points for the mice exposed to the high dose relative to controls in both lung and BAL cells, and these effects often extended to lower dose groups (Figures 2.3 and 2.4A). As such, we demonstrate that CBNPs can generate pulmonary and BAL SB even 28 days after a single exposure. In addition, we demonstrate that assessing SB in cells may serve as a potential biomarker of pulmonary genotoxicity in human studies.

Several mechanisms are hypothesized to contribute to CBNP-induced genotoxicity. It has been suggested that CB may be genotoxic because of adsorbed surface compounds, primarily polycyclic aromatic hydrocarbons (PAHs). However, because of the low levels of PAHs found on the CBNP surface (e.g., 72.4 ng/g in the Printex 90 used in this work) and the high affinity of these compounds for the CB particle core, CBNP-induced toxicity is not likely mediated via PAH exposure (Borm et al. 2005; Jacobsen et al. 2011; Jacobsen et al. 2007). Alternatively, CBNPs have been identified as potent ROS generators

(Hussain et al. 2009; Jacobsen et al. 2008; Kroll et al. 2011) and are also associated with large inflammatory responses, as established by our BAL cell profiles and by the work of others (Brown et al. 2000; Driscoll et al. 1996; Elder et al. 2005; Li et al. 1999; Sager and Castranova 2009; Tong et al. 2009; Wolff et al. 1990). Pulmonary influxes in BAL cells induce ROS production at sites of acute inflammation as a result of degranulation and oxidative burst mechanisms (Babior 2000). More importantly, the mutation spectrum arising *in vitro* following CBNP exposure points to ROS as the primary mutagenic factor (Jacobsen et al. 2011), providing substantial evidence that ROS-induced DNA damage occurs upon CBNP exposure. As such, we speculate that oxidative stress could be an important parameter of toxicity requiring further investigation *in vivo*.

It has been established that oxidative damage to DNA leads to increased mutation frequencies, and there is increasing evidence for a direct association between levels of oxidatively damaged guanine lesions and increased risks of lung cancer in humans (Loft et al. 2006; Loft et al. 2011). In contrast to BAL cells that are generated from hematopoietic stem cells, mutations in lung can result in permanent genetic changes within tissue and therefore increased cancer risk. As such, we examined lung tissue directly for oxidative damage to DNA. FPG sensitive sites were quantified using the alkaline comet assay, by which oxidized purines, primarily 8-oxo-7,8-dihydro-2′-deoxyguanosine (8-oxodG) and 2,6-

diamino-4-hydroxy-5-formamidopyrimidine are recognized. 8-oxodG is the most commonly oxidized lesion and is pro-mutagenic due to its ability to base-pair with adenine, resulting in G to T transversions (Cheng et al. 1992). Previous *in vitro* work has revealed non-significant increases in the levels of FPG sensitive sites in human Caco-2 cells exposed to CB (20 μg/cm^2, 4 h exposure) (Gerloff et al. 2009), whereas significant increases in FPG sensitive sites were found in an immortalized Muta^{tm}Mouse lung epithelial cell line (11.3 μg/cm^2 or 75 μg/ml, 3 h exposure) (Jacobsen et al. 2007). Here, we demonstrate that CBNPs induce FPG sensitive sites *in vivo* in the lungs. This is consistent with a previous inhalation study in rats where an elevated dose of Printex 90 (i.e. more than 5 mg retained in the lungs) caused increased 8-oxodG, which persisted for 44 weeks (Gallagher et al. 2003). No effects were observed for lower doses. Considering differences between species (e.g., approximate weights of 20 and 200 g and pulmonary surface area of 82.2 and 300 cm^2 in mouse and rat respectively (Donaldson et al. 2008; Knust et al. 2009)) this 5 mg retained dose in our model would translate to instilled doses of 0.5 mg or 1.4 mg according to body weight and lung surface area, which is well above our highest exposure dose. However, levels of 8-oxodG can often be elevated by spurious oxidation (Moller and Loft 2010) and thus it is possible that effects may have been detected at lower dose levels with lower background levels. A high dose (i.e., 0.050 mg x 6) of Printex 90 repeated six times in six weeks also caused increased immunostaining for 8-oxodG in the lungs of mice (Inoue et al. 2005). Thus, in the present study we observed

increased FPG sensitive sites at much lower CBNP doses (i.e., 0.018 and 0.054 mg) and at later post-exposure recovery time-points relative to previous studies, with significant increases occurring on post-exposure days 1 and 3 (Figure 2.4B).

The increase in possible oxidatively damaged DNA observed in our study in comparison to controls was much higher than previous *in vitro* observations. For example, (Jacobsen et al. 2007) showed a less than two fold increase over controls in lung epithelial cells, following 3h of exposure to 75 µg/ml CBNPs (a dose of approximately 11.3 µg/cm^2 cells compared to 0.2-2.0 µg/cm^2 in the current work (Knust et al. 2009)). This might be because of the presence of ROS-producing granulocytes in the mouse lung, as indicated by the close correlation of PMN cells and FPG sensitive sites found. In keeping with this observation, rats exposed by intratracheal administration of 0.64 mg/kg body weight (i.e., our low dose is approximately 0.9 mg/kg body weight in mouse), developed neither inflammation in terms of PMN infiltration nor increased levels of 8-oxodG in lung parenchyma (Danielsen et al. 2010). We speculate that the pulmonary genotoxocity observed in our work is most likely related to oxidative stress mediated by inflammatory cells, which is in accordance with previous work that has shown CBNP-induced mutation frequency increases only after inflammation is established (Driscoll et al. 1996). On the other hand, we have previously found that SB and pro-inflammatory effects occurred independently of each other *in vi*tro (Bornholdt et al. 2007) and in BAL cells *in vivo* (Bornholdt et al. 2002;

Madsen et al. 2008; Saber et al. 2011; Saber et al. 2005). In the present study, inflammation and BAL cell SB were observed at all doses and time points, and thus, we are not able to determine if the observed SB are caused by inflammation or whether inflammation and genotoxicity occur independently of each other.

Large inflammatory responses, such as the ones observed in our work, are associated with systemic effects of exposure due to increases in circulating inflammatory cells (e.g., PMN) and molecular mediators of inflammation (e.g., pro-inflammatory cytokines and chemokines). Additionally, NPs themselves have been demonstrated to translocate into systemic circulation (Sadauskas et al. 2009a) and spark generated ultrafine carbon NPs have been shown to accumulate in liver of rats upon inhalation (Oberdorster et al. 2002). Likewise, individual exposure to traffic related air pollution at the home address and by occupation has been associated with an increased risk of hepatic cancer (Raaschou-Nielson et al. 2011; Soll-Johanning et al. 1998). In order to investigate the possibility of adverse effects in extra-pulmonary tissues, we used the alkaline comet assay to quantify SB in liver tissue of the same mice. We found that SB were elevated on post-exposure days 1 and 28 (Figure 2.5). The reason for the lack of damage on day 3 remains unclear. It is possible that two separate mechanisms may come into play at different times (e.g., direct instillation effects on day 1 vs. particle relocation to liver or persistent inflammation on day 28), thus not affecting this post-exposure time-point. The results on particle-induced hepatic DNA damage

are consistent with our recently published study on DNA damage in mice exposed to Printex 90 by inhalation (Jackson et al. 2011a). Two different mechanisms are hypothesized to be responsible for the observed hepatic DNA damage: 1) direct particle-mediated effect caused by particles translocated from the lungs to the systemic circulation, and 2) indirect effects related to systemic inflammation. To investigate if the hepatic DNA damage resulted from a systemic acute phase response, we measured the mRNA expression of *Saa3* in pulmonary and hepatic tissue. As we reported before with mice exposed to CB or diesel exhaust particles by inhalation (Saber et al. 2009), we did not detect a change in *Saa3* mRNA in the liver in the current study. In contrast, we found a large increase in pulmonary *Saa3* mRNA expression. SAA protein can be detected in circulation during pulmonary inflammation and may induce a systemic acute phase response (Erdely et al. 2011). We have recently reported that the acute phase response is also induced in the lungs of mice exposed to nanotitanium dioxide where increased levels of SAA protein was also detected in lung tissue (Halappanavar et al. 2011). We do not know whether the hepatic effects are caused by inflammation or direct effects of translocated particles, but since translocation of the CBNPs is expected to be low, and particles accumulate primarily in Kupffer cells in the liver (Sadauskas et al. 2009b), the observed hepatic effects are most likely caused by inflammation. To our knowledge, our work is the first to demonstrate that hepatic SB occur as a result of exposure to CBNPs via intratracheal instillation.

There is increasing evidence that both DNA SB and oxidative damage to DNA can lead to increased risk of tumorigenesis and carcinogenesis (Cooke et al. 2003; Federico et al. 2007; Loft and Poulsen 1996; Valko et al. 2004). Likewise, the relationship linking chronic inflammation to increase risk of carcinogenic outcome is increasingly well supported (Coussen and Werb 2002). As such, it is likely that regular exposure to CBNPs is involved in adverse health outcomes that include cancer. Although previous epidemiological data have linked CBNP exposures to pulmonary carcinogenesis (Parent et al. 1996; Sorohan et al. 2001; Wellmann et al. 2006), evidence to date is insufficient to classify these particles as human carcinogens (currently classified as possibly carcinogenic to humans under Group 2B) (IARC 2010). As such, further investigations should elucidate additional underlying mechanisms of toxicity induced by CBNPs and their relationship with disease development. This should include simultaneous investigations of oxidative stress, genotoxicicty and inflammation in lung and liver of exposed mice using multiple endpoints (e.g., micronucleus assay, mutation analysis and GSH levels) and in repeated chronic daily inhalation studies to more closely mimic human exposures. Furthermore, as effects were observed at lower doses of exposure, dose-response relationships should be examined to establish the lowest observable effects and no observable effects levels. In addition to mechanistic studies, future works should clearly establish

current human exposure levels in order to evaluate the risks of adverse health effects in individuals routinely exposed to CBNPs.

2.6 Tables and Figures

Table 2.1. BAL fluid cell counts and distribution of cells by type (%) in C57BL/6 mice 1, 3 and 28 days post-exposure to 0.018, 0.054 and 0.162 mg Printex 90 CBNPs and control mice. *, ** refers to a statistical significance of $P < 0.05$ and $P < 0.001$ respectively.

		Control	0.018 mg	0.054 mg	0.162 mg
24 h					
	Neutrophils x10³ (%)	7.7 ± 1.7 (9.8)	65.0 ± 20.0 (44.3) **	140.0 ± 28.0 (61.5) **	160.0 ± 18.0 (73.9) **
	Macrophages x10³ (%)	53.0 ± 2.5 (73.1)	53.0 ± 6.8 (47.2)	50.0 ± 6.3 (31.4)	37.0 ± 5.8 (16.9) **
	Eosinophils x10³ (%)	0.3 ± 0.4 (0.3)	1.1 ± 0.4 (0.8)	3.1 ± 2.1 (1.3)	4.2 ± 2.6 (1.6)
	Lymphocytes x10³ (%)	1.5 ± 0.2 (2.2)	1.4 ± 0.6 (0.9)	2.5 ± 0.7 (1.3)	1.7 ± 0.9 (0.8)
	Total BAL Cells x10³	74.0 ± 3.6	130.0 ± 16.7 **	200.0 ± 28.0 **	220.0 ± 24.0 **
3 days					
	Neutrophils x10³ (%)	3.0 ± 2.3 (2.4)	21.0 ± 5.9 (16.2) **	63.0 ± 4.8 (40.5) **	120.0 ± 13.0 (46.7) **
	Macrophages x10³ (%)	56.0 ± 4.2 (83.1)	86.0 ± 12.0 (65.8) *	63.0 ± 6.9 (40.3)	89.0 ± 12.0 (33.4) *
	Eosinophils x10³ (%)	0.4 ± 0.6 (0.6)	13.0 ± 5.8 (8.8) **	16.0 ± 4.3 (10.4) **	29.0 ± 9.9 (10.8) **
	Lymphocytes x10³ (%)	0.9 ± 0.2 (1.4)	3.8 ± 1.0 (2.9) **	4.3 ± 1.0 (2.8) **	8.4 ± 1.8 (3.3) **
	Total BAL Cells x10³	69.0 ± 6.4	130.0 ± 15.0 **	160.0 ± 22.0 **	270.0 ± 24.0 **
28 days					
	Neutrophils x10³ (%)	1.2 ± 0.2 (1.2)	3.1 ± 0.5 (3.4) *	15.0 ± 3.1 (10.9) **	50.0 ± 13.0 (29.3) **
	Macrophages x10³ (%)	82.0 ± 5.7 (85.6)	73.0 ± 9.4 (77.5)	99.0 ± 15.0 (73.3)	75.0 ± 4.3 (48.4)
	Eosinophils x10³ (%)	0.3 ± 0.0 (0.3)	3.4 ± 3.4 (2.8)	0.1 ± 0.1 (0.1)	0.1 ± 0.1 (0.1)
	Lymphocytes x10³ (%)	2.1 ± 0.4 (2.2)	3.5 ± 1.2 (4.1)	12.0 ± 2.7 (8.9) **	22.0 ± 6.1 (13.4) **
	Total BAL Cells x10³	96.0 ± 5.8	93.0 ± 10.0	140.0 ± 21.0 **	160.0 ± 16.0 **

Table 2.2. Expression of *Saa3* presented as fold-changes over matched control in C57BL/6 mice 1, 3 and 28 days post-exposure to 0.018, 0.054 and 0.162 mg Printex 90 CBNPs. *, ** refers to a statistical significance of $P < 0.05$ and $P < 0.001$ respectively.

		0.018 mg	**0.054 mg**	**0.162 mg**
Lung				
	24 h	63.7 ± 33.2 **	240.3 ± 75.4 **	298.2 ± 78.0 **
	3 days	8.2 ± 4.2 **	23.5 ± 6.7 **	50.5 ± 14.6 **
	28 days	1.1 ± 0.4	4.9 ± 2.2 **	21.8 ± 10.1 **
Liver				
	24 h	1.2 ± 0.5	1.6 ± 0.5	1.3 ± 0.3
	3 days	0.7 ± 0.2	0.7 ± 0.2	0.7 ± 0.2
	28 days	1.0 ± 0.2	1.5 ± 0.2	1.3 ± 0.2

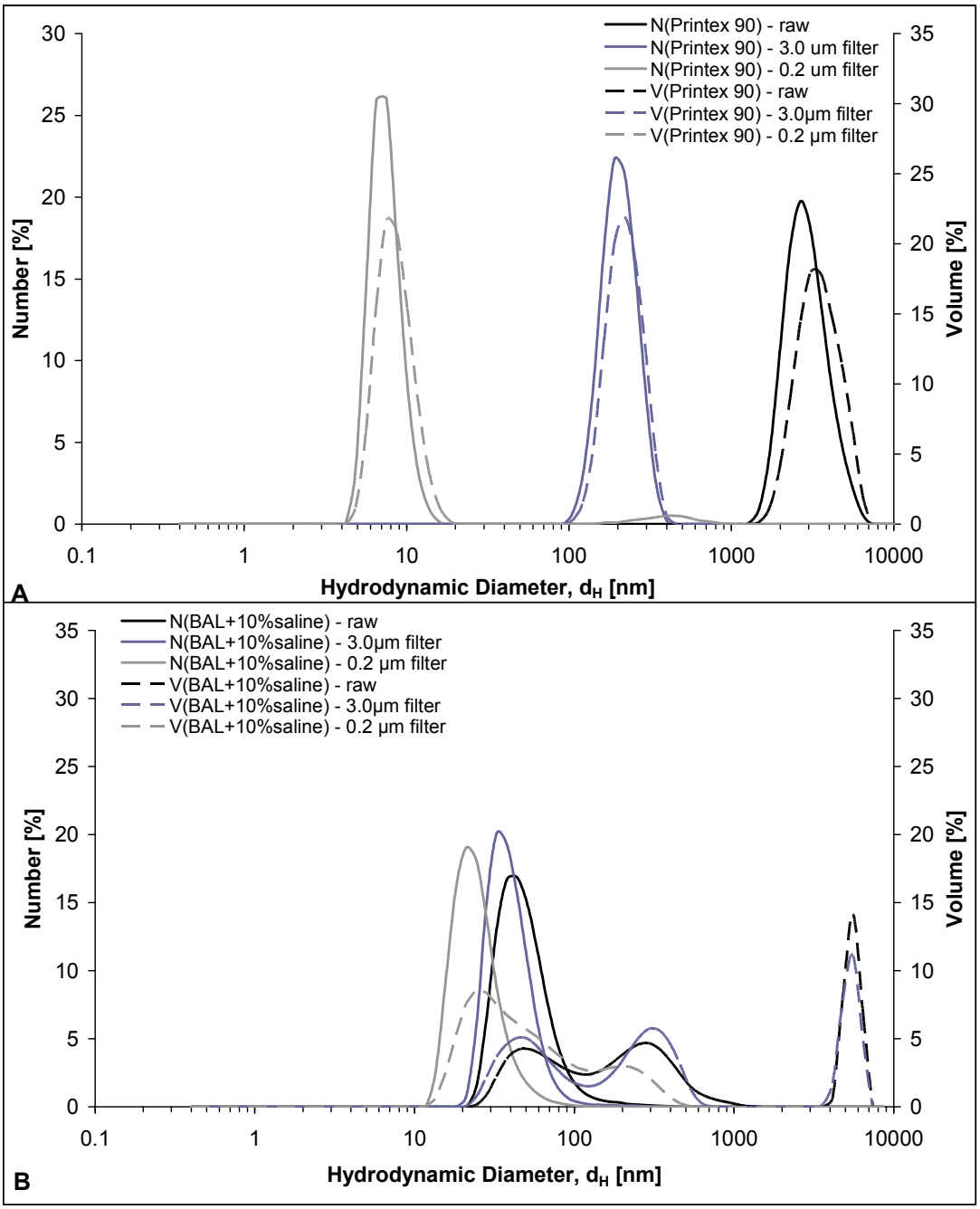

Figure 2.1. Dynamic light scattering analysis of instillation vehicle: A) with 0.054 mg dose of Printex 90 CBNPs and B) instillation vehicle alone (BAL + 10% saline).

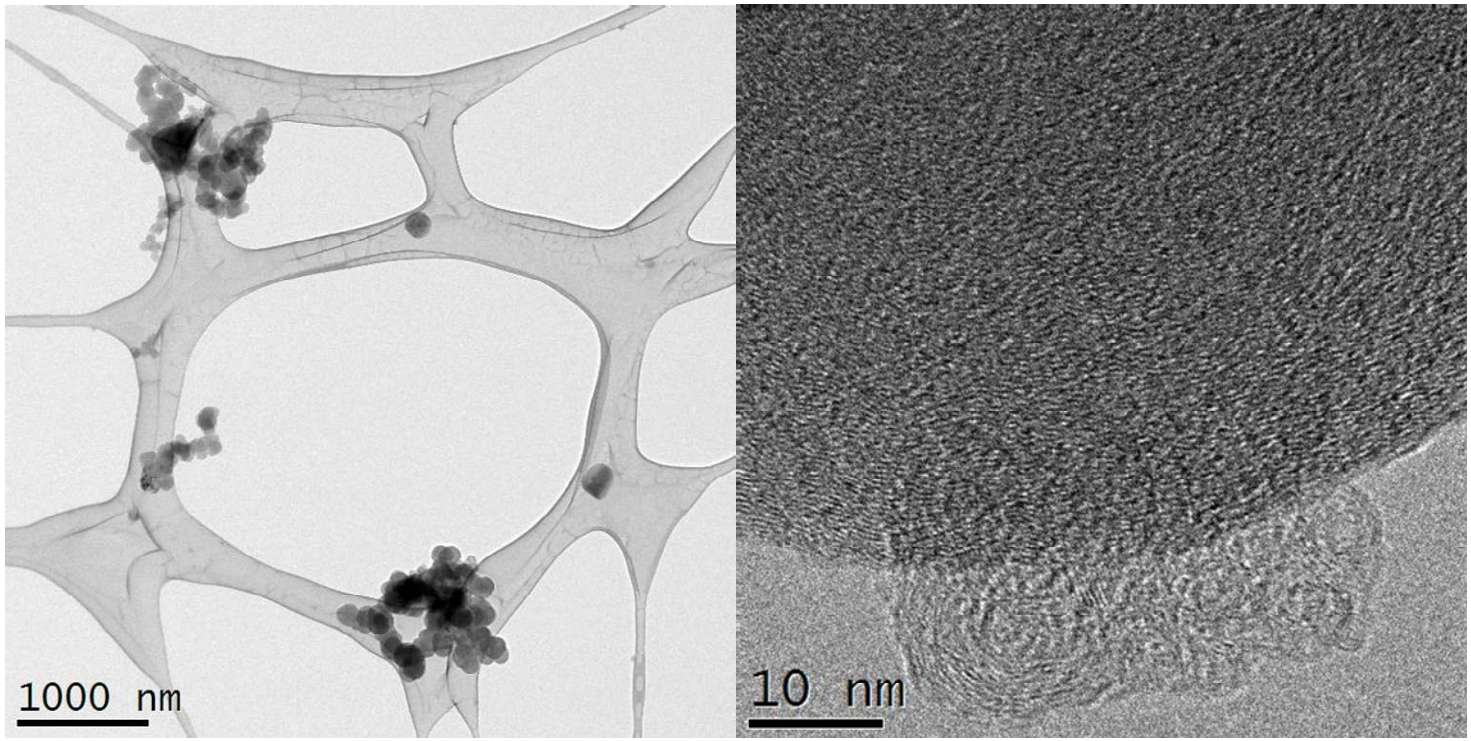

Figure 2.2. Transmission electron microscopy images of CBNP particles in the instillation vehicle. A) Example of free and agglomerated CBNP spheres of various sizes ranging from nano- to µm-size. Particles are caught on lacy-carbon Cu-grids. B) High-resolution image showing the presence of 10 nm-size CB particles at the rim of a larger CB particle with mottled concentric layers with graphitic structure.

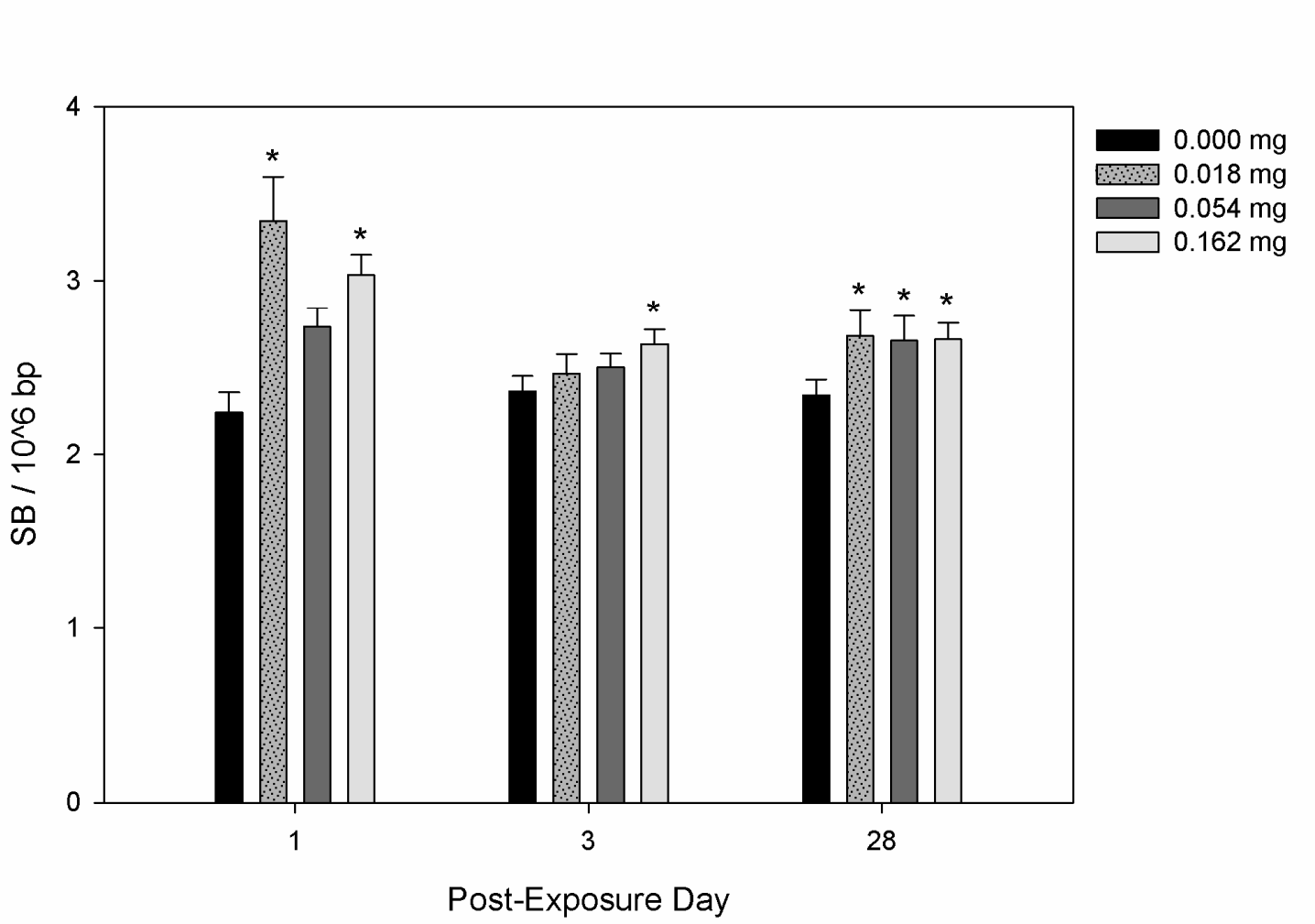

Figure 2.3. DNA strand breaks (SB) per 10^6 base pairs in C57BL/6 mouse BAL cells following exposure to 0.000, 0.018, 0.054 or 0.162 mg Printex 90 CBNPs and sacrificed 1, 3, and 28 days post-exposure. Error bars represent the standard error of the mean for 6 mice in each group. *, ** refers to a statistical significance of $P < 0.05$ and $P < 0.001$ respectively, when compared by two-factor ANOVA using the day of sacrifice and dose as categorical variables.

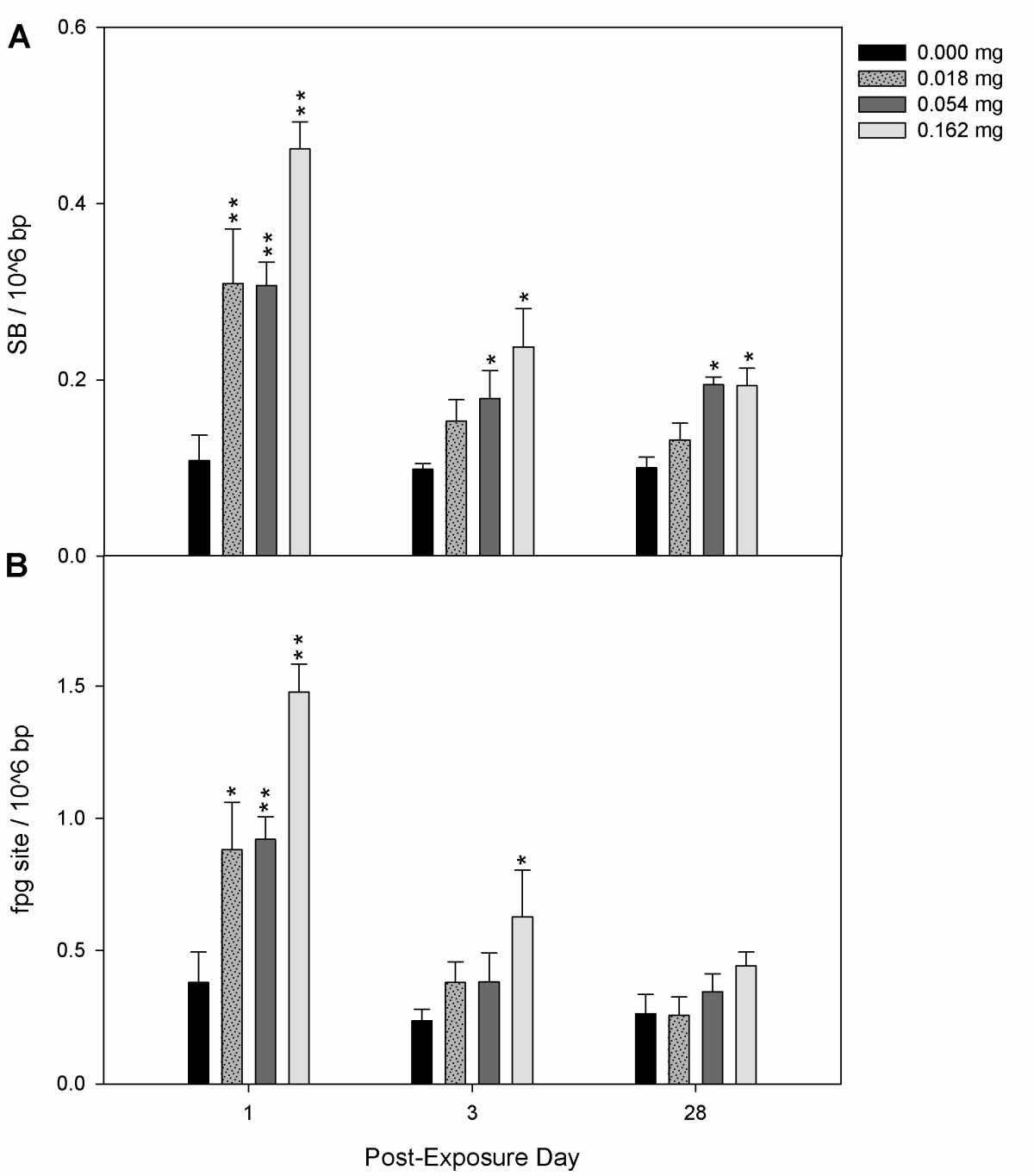

Figure 2.4. DNA strand breaks (SB) and formamidopyrimidine DNA glycosylase (FPG) sensitive sites in lung of CBNP exposed mice. SB (A) and FPG sensitive sites (B) per 10^6 base pairs in C57BL/6 mouse lung tissue following exposure to 0.000, 0.018, 0.054 or 0.162 mg Printex 90 CBNPs and sacrificed 1, 3, and 28 days post-exposure. Error bars represent the standard error of the mean for 6 mice in each group. *, ** refers to a statistical significance of $P < 0.05$ and $P < 0.001$ respectively, when compared by two-factor ANOVA using the day of sacrifice and dose as categorical variables.

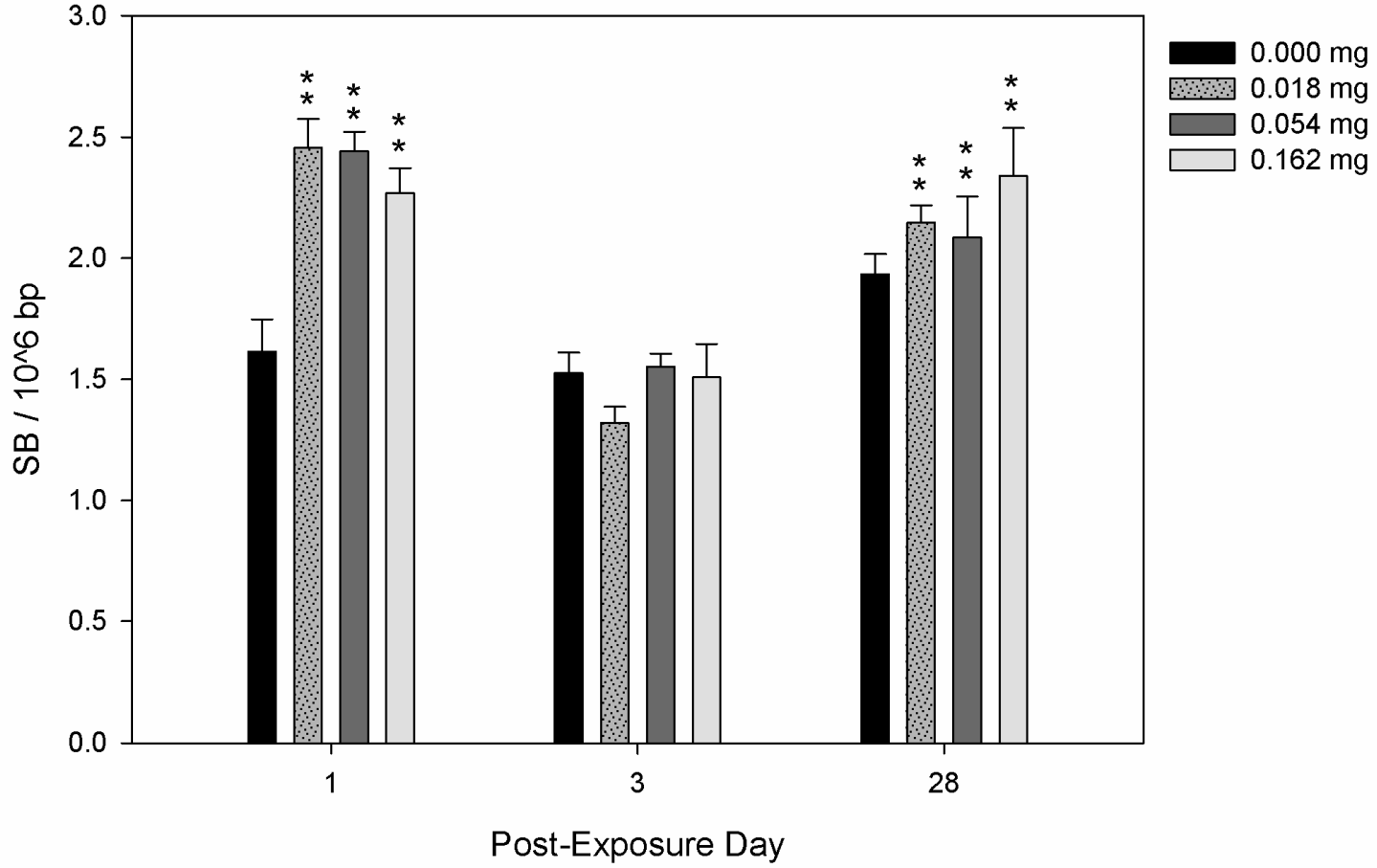

Figure 2.5. DNA strand breaks (SB) per 10^6 base pairs in C57BL/6 mouse liver following exposure to 0.000, 0.018, 0.054 or 0.162 mg Printex 90 CBNPs and sacrificed 1, 3, and 28 days post-exposure. Error bars represent the standard error of the mean for 6 mice in each group. *, ** refers to a statistical significance of $P < 0.05$ and $P < 0.001$ respectively, when compared by two-factor ANOVA using the day of sacrifice and dose as categorical variables.

CHAPTER 3: HEPATIC AND PULMONARY TOXICOGENOMIC PROFILES IN MICE INTRATRACHEALLY INSTILLED WITH CARBON BLACK NANOPARTICLES REVEAL PULMONARY INFLAMMATION, ACUTE PHASE RESPONSE AND ALTERATIONS IN LIPID HOMEOSTASIS

Modified from: Bourdon, JA, Halappanavar, S, Saber, AT, Jacobsen, NR, Williams, A, Wallin, H, Vogel, U and Yauk, C. (2012) *Toxicological Sciences*, doi: 10.1093/toxsci/kfs119.

3.1 Abstract

Global pulmonary and hepatic mRNA profiles in adult female C57BL/6 mice intratracheally instilled with carbon black nanoparticles (Printex 90) were analysed to identify biological perturbations underlying systemic responses to nanoparticle exposure. Tissue gene expression changes were profiled 1, 3 and 28 days following exposure to 0.018, 0.054 and 0.162 mg Printex 90 alongside controls. Pulmonary response was marked by increased expression of inflammatory markers and acute phase response genes that persisted to day 28 at the highest exposure dose. Genes in the 3-hydroxy-3-methylglutaryl-coenzyme A (HMG-CoA) pathway were increased and those involved in cholesterol efflux were decreased at least at the highest dose on days 1 and 3. Hepatic responses mainly consisted of the HMG-CoA reductase pathway on days 1 (high dose) and 28 (all doses). Protein analysis in tissues and plasma of 0.162 mg Printex 90 exposed mice relative to control revealed increase in plasma serum amyloid A

(SAA) on days 1 and 28 ($p < 0.05$), decreases in plasma high density lipoprotein on days 3 and 28, increase in plasma low density lipoprotein on day 28 ($p < 0.05$) and marginal increase in total hepatic cholesterol on day 28 ($p = 0.06$). The observed changes are linked to acute phase response. Although further research is needed to establish links between observations and the onset and progression of systemic disorders, the present study demonstrates the ability of nanoparticles to induce systemic effects.

3.2 Introduction

There is a growing number of commercial products containing nanoparticles (NPs, defined as particles between 1 and 100 nm in at least one dimension), which could lead to increased occupational exposures. NPs vary significantly in their size, surface area, shape, composition, charge and surface chemistry compared to their bulk counterparts. Studies suggest that NPs readily infiltrate deeper pulmonary regions, are capable of interacting with subcellular structures such as DNA, and are able to move readily across cellular and tissue barriers (Vishwakarma et al. 2010). Consequently, some NPs exhibit increased toxicity in comparison to larger particles. Upon inhalation, they have been associated with a variety of adverse biological and physiological responses including inflammation, fibrosis, genotoxicity and carcinogenicity (Hubbs *et al.* 2011).

As inhalation is a primary route of exposure for most NPs, the pulmonary effects of various nanomaterials have been well documented. It has also been established that NPs can induce systemic effects in organs remote from the primary site of exposure. For example, mice and rats exposed to carbon-based NPs via inhalation or intratracheal instillation exhibit oxidative stress, cardiovascular effects, and genotoxicity in various tissues (Moller et al. 2010a) including the systemic microvascular wall (Nurkiewicz et al. 2006) and liver (Jackson et al. 2011a; Nurkiewicz et al. 2006). One suggested mechanism for such distal effects is the physical translocation of NPs into the systemic circulation. However, it is estimated that very limited amounts of deposited NPs translocate into circulation (Sadauskas et al. 2009a) and systemic effects have been observed with negligible particle translocation (Jackson et al. 2011a). These distal effects may result from NP-induced molecular signaling cascades in lung tissue, which in turn initiate downstream toxic responses in secondary organs. For example, pulmonary inflammation and oxidative stress following NP exposure may result in the release of cytokines, chemokines and reactive oxygen species into systemic circulation. Furthermore, pulmonary exposure to NPs may activate receptors leading to imbalances in the autonomic nervous system and the development of cardiac arrhythmia, as suggested in epidemiological studies of humans exposed to fine and ultrafine particles (Magari et al. 2001). Although the mechanisms by which NPs may induce systemic effects have been inferred, the biological

processes and the underlying molecular pathways leading to such systemic toxicities remain unclear and warrant further investigation.

Carbon black NPs (CBNPs) are poorly soluble spherical particles of amorphous carbon. CBNPs, including Printex 90 (14 nm CBNP), are the dominating black pigment in printing inks, paints, and plastics, and large volumes are used as reinforcing agents in tires and other rubber goods. Concerns over CBNP safety arose in the mid 1990's, when it was demonstrated that chronic exposure of rats to carbon black had the potential to induce tumors similar to those observed with diesel exhaust particles (presumably via particle overload mechanisms) (Nikula et al. 1995). Occupational exposure to CBNPs is associated with decreased lung function (Gardiner et al. 2001), but it has not been conclusively demonstrated to be associated with lung cancer (IARC 1996). In animal models, chronic and subchronic exposure to poorly soluble NPs of low toxicity, including CBNPs, induce mutations (Driscoll et al. 1996) and lung tumors (Schins and Knaapen 2007) that are most likely associated with inflammation and oxidative stress. Printex 90 CBNPs have been very well characterized and are used extensively as a reference material for toxicological evaluations of NPs. Thus, they are an ideal model for exploring systemic effects of NP exposure.

We recently demonstrated that exposure to Printex 90 induces sustained pulmonary inflammation and persistent genotoxicity in the lungs and livers of adult female mice (Bourdon et al. 2012b). In the present study we establish global pulmonary and hepatic mRNA transcriptional profiles using tissues from the same animals. In addition, we quantify plasma and tissue proteins to determine if exposure to Printex 90 initiates systemic signaling cascades potentially leading to effects in the liver. This study provides insight into the molecular events associated with systemic perturbations of cholesterol homeostasis that are likely associated with CBNP-induced adverse cardiovascular outcomes.

3.3 Materials and Methods

3.3.1 Animal Handling, Exposure and Tissue Collection

Animal handling, exposure and tissue collection have been described previously (Bourdon et al. 2012b). Briefly, female C57BL/6 mice (Taconic, Denmark) were acquired at 5-6 weeks of age and given food (Altromin no 1324; Christian Petersen, Denmark) and water *ad libitum*. All procedure complied with EC Directive 86/609/EEC and Danish laws regulating experiments on animals (permit 2010/561-1179).

Mice were exposed to 0.018, 0.054 and 0.162 mg Printex 90 CBNPs alongside controls for each post-exposure day (1, 3 and 28 days). These doses equal the pulmonary deposition after 1, 3 and 9 working days for a mouse at the

occupational exposure limit of 3.5 mg/m^3 CB per 8 hour work shift (as established by the Occupational Safety and Health Administration (OSHA) and the National Institute for Occupational Safety and Health (NIOSH)). These calculations assume that 33.8% of the inhaled mass ends up in the pulmonary region with a volume of inhaled air per hour of 1.8 L/h and 8 h working days as described in (Jacobsen et al. 2009). The mice did not display any signs of respiratory distress, decreased locomotor activity, lethargy or any other physical symptoms of exposure.

Printex 90 was suspended by sonication in 0.9% NaCl MilliQ water containing 10% v/v acellular bronchial alveolar lavage fluid from C57BL/6 mice. A total of 72 mice (6 per group) were given 0.018, 0.054 or 0.162 mg of Printex 90 CBNPs by single intratracheal instillation. Before the intratracheal instillation, the mice were anesthetized using Hypnorm® (fentanyl citrate 0.315 mg/ml and fluanisone 10 mg/ml from Janssen Pharma) and Dormicum® (Midazolam 5 mg/ml from Roche).

The trachea of each mouse was intubated using a 24 gauge BD Incyte catheter (Becton Dickinson, Denmark) with a shortened needle. The proper location of the catheter was ensured using a highly sensitive pressure transducer developed at the National Research Centre for the Working Environment in collaboration with John Frederiksen (FFE/P, Denmark). A 40 µl suspension was

instilled followed by 150 µl air with a 250 µl SGE glass syringe (250F-LT-GT, MicroLab, Aarhus, Denmark). Control animals received 40 µl vehicle instillations (0.9% NaCl MilliQ water containing 10% v/v acellular BAL from C57BL/6 mice). Mice were placed on a 37°C heating pad to recover from anesthesia. One, 3 and 28 days after the instillation, the mice were anaesthetized with Hypnorm®/Dormicum® as described above. Heart blood (800-1000 µL) was stabilized in 72 µL 0.17 M K_2EDTA and kept on ice until plasma was isolated by centrifugation at 2000 g for 10 min (4°C). Bronchoalveolar lavage fluid, lung and liver were collected immediately after withdrawing the heart blood. Tissues were frozen in liquid nitrogen and stored at –80°C.

3.3.2 Particle Characterization

Printex 90 CBNPs were a gift from Evonik/Degussa (Frankfurt, Germany). The hydrodynamic particle size distributions in the exposure media were determined by Dynamic Light Scattering (DLS) using a Malvern Zetasizer Nano ZS, as described previously (Bourdon et al. 2012b). Agglomeration levels were also assessed by transmission electron microscopy (TEM). DLS analysis of the exposure media was performed on the raw instillation dispersions and after filtration through 3 µm (Glass Micro Fiber; Whatmann, UK) and 0.2 µm (hydrophilic DISMIC®-25CS Cellulose Acetate; Toyo Roshi Kaisha Ltd, Japan) syringe filters.

3.3.3 Total RNA Extraction

Total RNA was isolated from lung and liver tissue of 72 mice in total (n=6 mice per group). Isolations were done using TRIzol reagent (Invitrogen, Canada) and purified using the RNeasy MiniKit (Qiagen, Canada). An on-column DNase treatment was applied (Qiagen, Canada). RNA concentrations were determined using a NanoDrop 2000 spectrophotometer (Thermo Scientific, Canada). RNA quality was assessed using a BioAnalyzer (Agilent Technologies, Canada) and only RNA with RNA integrity numbers above 7.5 were used in the experiment. Total RNA was stored at -80°C until analysis.

3.3.4 Microarray Hybridization

Total RNA (200 ng) from each sample (n=6 per group), alongside Stratagene universal mouse reference RNA (Agilent, Canada) was used to synthesize double-stranded cDNA and cyanine labeled cRNA using the Agilent Linear Amplification kit (Agilent Technologies, Canada). Experimental samples were labeled with cyanine 5-CTP whereas reference RNA was labeled with cyanine 3-CTP (Perkin-Elmer Life Sciences, Canada). The cyanine-labeled cRNA was *in vitro* transcribed using T7 polymerase and purified using RNeasy mini kits (Qiagen, Canada). Sample and reference targets (825 ng) were combined and hybridized to Agilent 4 x 44K oligonucleotide microarrays (Agilent Technologies, Canada) for 17 hours at 60°C. The arrays were washed according to supplier

instructions and then scanned on an Agilent G2505B scanner at 5 µm resolution. Data were acquired using Agilent Feature Extraction software version 9.5.3.1.

3.3.5 Statistical Analysis of Microarray Data

A reference design was employed to determine global differential gene expression and randomized blocks were used to offset inter-array effects. Median signal intensities were normalized using LOWESS in R and differential gene expression was determined using the MAANOVA library (R Development Core Team 2010). The Fs statistic, a shrinkage estimator, was used to determine gene-specific treatment effects and the associated *p*-values were estimated using the permutation method (30,000 permutations with residual shuffling). Data were adjusted for multiple comparisons using the Benjamini and Hochberg false-discovery rate (FDR) approach to limit false-positive results. Fold-changes were based on least square means of each pairwise comparison. *P*-values and fold-changes for probes of the same target were averaged. Genes having an FDR-adjusted $p < 0.1$ and a fold-change > 1.5 were deemed differentially expressed.

Data quality was evaluated in GeneSpring GX version 11.5.1 (Agilent Technologies, Canada). Dye bias was determined by generating MA plots and scatter plots. Outliers were identified using hierarchal clustering and box plots. Mining of the pathways and processes represented among the significant genes was conducted in Ingenuity Pathway Analysis version 8.6. A right-tailed Fisher's

exact test was used to calculate *p*-values for each biological pathway. DAVID Bioinformatics Resources 6.7 was used to identify enriched biological functions from terms with similar genes and biological meaning (Huang et al. 2009a; Huang et al. 2009b). Biological functions with enrichment scores > 1.3 were considered significant, in accordance with DAVID recommendations (Huang et al. 2009b).

3.3.6 Real-Time Polymerase Chain Reaction

Primers were designed within the same exon as the Agilent microarray probe sequence using Beacon design 2.0 (Premier BioSoft International, USA). Primer specificity was assured by melting curve analysis and optimal annealing temperatures were determined by gradient PCR experiments. Total RNA (1 µg) from lung and liver was reverse transcribed to cDNA for each sample (n=4 per group), using the SuperScript III First-Strand Synthesis system (Invitrogen, Canada). RT-qPCR was performed on 10-fold cDNA dilutions in duplicate using a CFX96 real-time PCR detection system (Bio-Rad, Canada). Threshold cycle values were averaged. PCR efficiency for both the gene of interest and the reference gene was extrapolated from a standard curve, established by a 5-fold serial dilution of pooled cDNA. Fold-changes were calculated according to the $2^{-\Delta\Delta CT}$ method, using the CFX manager software (Bio-Rad, Canada). Statistical inference was established using the REST program version 2.0.13 (Pfaffl *et al.* 2002).

3.3.7 PCR Arrays

PCR arrays were employed for analysis of transcripts involved in inflammatory responses, oxidative stress and cholesterol efflux in lung. Total RNA (1 µg) from lung was reverse transcribed into cDNA using an RT^2 First Strand Kit (SABiosciences, USA). RT^2 SYBR green PCR master mix was employed for real-time PCR and experiments were carried out using a CFX96 real-time PCR detection system (Bio-Rad). Threshold cycles were averaged.

Using the delta CT values, differentially expressed genes were identified using a two-sample bootstrap test (t-Pivot method) assuming unequal variances using the R software (Higgins 2003). Standard errors for the fold-change for each comparison were estimated using the bootstrap method.

3.3.8 Total Lipid Extraction and Total Hepatic Cholesterol Analysis

Total lipids were extracted from liver tissue according to the Folch method. Briefly, liver tissue was homogenized in 500 µl equal volumes of methanol and water. A double volume of 5:1 chloroform/methanol was then added and phases were separated by centrifugation. The lower chloroform lipid containing layer was separated and chloroform removed under nitrogen gas flow. Lipids were re-suspended in 100 µl EnzyChrom™ assay buffer and stored at -20°C until analysis.

The EnzyChrom™ AF Cholesterol Assay Kit (BioAssay Systems, USA) was employed for quantitative colorimetric determination of hepatic cholesterol levels (n=6 per group; 0.162 mg dose group and controls), according to manufacturer recommendations. Briefly, lipid extracts from each sample and a serial dilution of a standard cholesterol reference supplied by the manufacturer were diluted 10-fold and 50 µl aliquots were placed in a clear 96 well plate, in duplicate. Fifty µl of a dye reagent-enzyme mix was added and the plate was incubated at room temperature for 30 min. The color intensity of the reaction product was spectrophotometrically measured at 570 nm and total cholesterol concentrations were determined by comparison to the standard curve, with normalization to extracted tissue weight. Statistical significance was determined using an unpaired one-tailed *t*-test assuming unequal variances.

3.3.9 Plasma High Density lipoprotein (HDL), Low density lipoprotein/Very low density lipoprotein (LDL/VLDL) and Total Cholesterol Analysis

Fluorimetric quantification of cholesterol was determined in plasma using the EnzyChrom™ AF HDL and LDL/VLDL assay kit (BioAssay Systems, USA) according to the manufacturer's instructions (n=6 per group; 0.162 mg dose group and controls). HDL isolation was performed by collection of the supernatant following centrifugation of a 1:1 plasma-precipitating reagent solution. The LDL/VLDL fraction was separated by dissolution of the collected

pellet in PBS. Plasma, HDL and LDL/VLDL isolations from each sample and a serial dilution of a standard cholesterol reference supplied by the manufacturer were diluted 10-fold and 50 µl aliquots were placed in a clear 96 well plate, in duplicate. Fifty µl of a dye reagent-enzyme mix were added and the plate was incubated at room temperature for 30 min. Fluorescence measurements were recorded on a SpectraMax M2 (Molecular Devices, USA) at 530 nm (excitation) and 585 nm (emission), and cholesterol concentrations were determined by comparison to a standard curve. Statistical inference was determined using an unpaired one-tailed *t*-test assuming unequal variances.

3.3.10 Plasma SAA Analysis

Total SAA was measured in plasma samples using the Phase™Range Mouse SAA ELISA kit (Tridelta Development Ltd, Ireland), according to manufacturer's instructions (n=6 per group; 0.162 mg dose group and controls). Briefly, plasma from each mouse and a serial dilution of a standard SAA reference supplied by the manufacturer were diluted 200-fold and mixed with an equal volume of anti-SAA HRP conjugate. One hundred µl of each plasma-antibody solution was loaded in duplicate in a 96-well plate pre-coated with SAA antibody, incubated for 1 hour at 37°C, and subjected to 4 wash cycles. A streptavidin-HRP enzyme was then added to each well and incubated for 15 min at room temperature. The reaction was quenched by the addition of 100 µl of stop solution. Absorbance measurements were read at 450 nm with a SpectraMax

M2 (Molecular Devices, USA) and SAA concentrations were determined by comparison to the standard curve. Statistical inference was determined by unpaired one-tailed *t*-test, assuming unequal variances.

3.4 Results

3.4.1 Particle Characterization

Printex 90 CBNPs have been characterized extensively in (Bourdon et al. 2012b). A summary of this particle characterization can be found in Table 3.1. Briefly, the manufacturer declares a primary particle size of 14 nm. The reported polycyclic aromatic hydrocarbon (PAH) and endotoxin content reported in Table 3.1 are not expected to cause biological effects, as described thoroughly in (Bourdon et al. 2012b; Jacobsen et al. 2007; Jacobsen et al. 2008). CBNPs within instillation vehicle displayed a high degree of agglomeration, which is in accordance with the low zeta-potential reported. DLS analysis of the raw instillation vehicle revealed that the suspension was highly polydisperse, with a peak size of approximately 2.6 µm. Size distribution of these agglomerates was broad, ranging from less then 100 nm but typically 200 nm or larger. The largest of the agglomerates were in the range of 20-30 µm. This wide distribution is in agreement with the very elevated polydispersity index (PDI) observed. Filtering (3.1 and 0.2 µm) of the raw dispersion vehicle revealed the presence of smaller particles.

3.4.2 Inflammatory Cell Influx in Bronchoalveolar Lavage (BAL)

The animals used in this study were from a previous experiment. Details of this study can be found in (Bourdon et al. 2012b). Briefly, characterization of the cell composition of bronchoalveolar lavage (BAL) revealed elevated total BAL cell counts 1 and 3 days post-exposure for all doses (0.018, 0.054 and 0.162 mg), and sustained increases for the medium and high doses up to the 28 day time-point. This response was primarily dominated by increases in neutrophils at all doses and time-points studied. Eosinophils and lymphocytes were also increased at all doses, but only at the 3 day time-point. BAL cell counts for neutrophils, eosinophils, macrophages, lymphocytes and total BAL cells are presented in Supplementary Figure SP1.

3.4.3 Global Pulmonary Differential Gene Expression

Gene expression microarray analysis was conducted on the left lung lobe (whole tissue) from a total of 72 mice (n=6/treatment group) exposed to vehicle (control), 0.018, 0.054 and 0.162 mg of Printex 90 CBNPs by a single intratracheal instillation and necropsied 1, 3 and 28 days post-exposure. MA plots, boxplots and cluster analyses of normalized signal intensities for all probes revealed that 5 of 72 microarrays produced sub-standard data quality (data not shown). These arrays were distributed across treatment conditions and were removed from the analysis. The MAANOVA analysis was thus conducted on a final sample size of at least 5 mice per treatment group to identify differentially expressed genes.

Genes with FDR adjusted $p < 0.1$ and fold changes > 1.5 in either direction were considered differentially expressed.

MAANOVA analysis revealed that 487 genes were significantly differentially expressed (up- or down-regulated relative to control samples) in at least one of the treatment conditions. The complete list is presented in Supplementary Table SP1. There were 2, 45 and 294 differentially expressed genes 1 day post-exposure and 0, 11 and 201differentially expressed genes 3 days post-exposure in the 0.018, 0.054 and 0.162, mg dose groups, respectively. At 28 days post-exposure, the high-dose group showed 123 altered genes, but no effects were observed for the two lower doses. Thus, the low-dose treatment groups had very little effect on the global expression profiles as measured on DNA microarrays. The number of genes that were in common between the 0.162 mg dose across time-points is shown in a venn diagram in Supplementary Figure SP2A. Cluster analysis revealed dose-response trends within time-points with similar pathways/functions affected at the high dose and the lower doses. The results demonstrate substantial changes over time in the subset of genes differentially affected by the Printex 90 exposure (evident within the 0.054 and 0.162 mg doses only as shown by heat maps in Supplementary Figure SP3A-B). The complete microarray dataset is available through the Gene Expression Omnibus at NCBI (http://www.ncbi.nlm.nih.gov/geo/, Superseries GSE35284, SubSeries GSE35193).

Data mining using DAVID functional annotation clustering to determine functional groups of similar genes and affected biological processes, revealed 40 annotations with enrichment scores > 1.3 (Supplementary Table SP2). These biological functions were mostly related to inflammatory, immune and acute phase responses, but also included changes in sterol biosynthesis, apoptosis signaling and cell cycle regulation. Ingenuity pathway analysis of the high dose group revealed the predominance of inflammatory and immune responses across all time-points (Supplementary Figure SP2C). Transcript changes for genes involved in inflammation (29 genes), cholesterol transport (2 genes), oxidative stress and antioxidant responses (8 genes) were validated using PCR arrays and showed a high correlation with the DNA microarray results (Supplementary Table SP3).

3.4.4 Global Hepatic Differential Gene Expression

Since major persistent effects were only observed in the lungs at the highest doses, hepatic microarray gene expression profiling was only conducted on mice exposed to 0.162 mg CBNPs and sacrificed 1, 3 and 28 days post-exposure. Six outliers were removed from the analysis based on quality control metrics (MA plots, box plots and cluster analysis of normalized signal intensities for reference RNA and biological samples). MAANOVA analysis was conducted on a final sample number of at least 4 per treatment group to identify

differentially expressed genes. Genes with FDR adjusted *p*-value < 0.1 and fold changes > 1.5 in either direction were considered significant (differentially expressed) and were analyzed in detail. The analysis revealed 81 differentially expressed genes (up- and down-regulated) overall (Supplementary Table SP4). Within time-points, 53, 2 and 26 changes in transcripts were found on days 1, 3 and 28, respectively. None of the genes identified overlapped across time-points as shown in the venn diagram in Supplementary Figure SP2B. Cluster analysis revealed clear exposure effects on day 1 and day 28, but not on day 3 as shown in the heat map in Supplementary Figure SP3C). Microarray data are available through the Gene Expression Omnibus at NCBI (http://www.ncbi.nlm.nih.gov/geo/, SuperSeries GSE35284, SubSeries 35192).

DAVID functional annotation clustering revealed four biological functions with an enrichment score > 1.3 (Supplementary Table SP5). These clusters were related to sterol and terpenoid biosynthesis biosynthesis, cytochrome p450 and cell movement. Ingenuity Pathway analysis of biological functions across time-points also revealed lipid metabolism as the primary process perturbed in liver by Printex 90 exposure (Supplementary Figure SP2D).

3.4.5 Inflammation and Acute Phase Response Signaling in Lung, Liver and Plasma

Mining of lung microarray data by Ingenuity Pathway Analysis showed that approximately 38% of the differentially expressed genes were directly

associated with inflammatory responses. In the high dose groups, up-regulated expression of several of these genes, including chemokine (C-C motif) ligands 2 (*Ccl2*), *Ccl3*, *Ccl8*, *Ccl9* and *Ccl12* was evident on day 1 and persisted up to 28 days post-exposure, with fold changes ranging from 1.5- to 5.0-fold above control animals. Twenty-nine genes involved in inflammation were validated using PCR arrays and correlated highly with the DNA microarray results (Supplementary Table SP3).

The highest fold-changes in the lungs of mice intra-tracheally instilled with CBNPs were attributed to serum amyloid A genes (*Saa1*, *Saa2* and *Saa3*) and other genes involved in acute phase response (APR) signaling, including metallothioneins and orosomucoids (Table 3.2). Quantitative real-time PCR analysis in lung revealed that *Saa1* and *Saa3* were also affected at lower doses of exposure (i.e., all doses on post-exposure day 3) and at later time-points (i.e., the 0.162 mg dose on post-exposure day 28) (Supplementary Table SP3). Our results correlate strongly with previous measurements of *Saa3* in the same tissue (Bourdon et al. 2012b). However, we could not validate the up-regulation of *Saa3* in liver by quantitative-real time PCR (Bourdon et al. 2012b).

To confirm the presence of SAA protein, we measured total SAA levels in plasma of an additional set of mice exposed to 0.162 mg CBNPs using identical exposure procedures. Total SAA levels were increased by 15.3% on post-

exposure day 1 (from 1.2 to 1.4 mg/dL; $p < 0.05$), by 15.6% on day 3 (from 1.1 to 1.3 mg/dL; $p = 0.0789$) and by 11.8% on day 28 (from 1.0 to 1.1 mg.dL; $p < 0.05$) (Figure 3.1A).

3.4.6 Alterations in Cholesterol Homeostasis

Pulmonary and hepatic gene expression profiling in parallel with plasma analysis strongly suggested systemic alterations in cholesterol homeostasis. Pulmonary gene expression profiles of the high dose group revealed significant up-regulation of genes involved in cholesterol synthesis, on post-exposure days 1 and 3 relative to control mice (Table 3.3). DAVID functional annotation clustering revealed this subset of genes to be involved directly in sterol and terpenoid biosynthesis (enrichment score = 3.4) (Supplementary Table SP2). These biological functions collectively form the 3-hydroxy-3-methylglutaryl-coenzyme A (HMG-CoA) reductase pathway and the rate limiting-reactions of cholesterol synthesis. Two genes of this pathway (*Sqle* and *Fdps*) were confirmed by quantitative real-time PCR in lung (Supplementary Table SP6).

Microarray analysis of pulmonary profiles also demonstrated substantial down-regulation of cholesterol efflux gene ATP-binding cassette subfamily G member 1 (*Abcg1*, -1.7 fold) at the highest exposure dose on day 1. Quantitative real-time PCR of *Abcg1* and associated ATP-binding cassette subfamily A member 1 (*Abca1*) showed 2.3 and 2.6 fold down-regulation of *Abcg1*and *Abca1*

on day 1, and 1.8 fold down-regulation of *Abcg1* on day 3 (Supplementary Table SP3).

Substantial up-regulation of the HMG-CoA reductase pathway was also found in liver, as demonstrated by the highly enriched sterol and terpenoid biosynthesis cluster using DAVID functional annotation clustering (enrichment score = 9.5) (Supplementary Table SP5). The pathway was perturbed on post-exposure day 1 in the high dose mice, relative to controls. Expression changes were fairly consistent across these genes, ranging from a 1.6 to a 2.6 fold increase in treated over control mice (Table 3.3). In order to clarify whether the HMG-CoA reductase pathway activity is also affected at later time-points and lower doses of exposure, we measured *Hmgcr*, *Dhcr7*, *Fdps*, *Mvd* and *Sqle* transcript levels using quantitative real-time PCR. Our microarray findings were confirmed for post-exposure day 1. However, many genes were also found to be differentially expressed on day 28 at all exposure doses (Supplementary Table SP6).

In order to substantiate changes in cholesterol synthesis, we measured cholesterol levels in plasma and livers of the mice. Plasma analysis in the additional mice exposed according to the same exposure regimen (high dose and controls only) revealed no effects of CBNP exposure on total plasma cholesterol (data not shown). However, HDL levels were decreased on post-exposure days 3

and 28 ($p < 0.05$) by 21.8 and 25.7 % (Figure 3.1B). LDL levels were also increased by 18.8 % on post-exposure day 28 (Figure 3.1C). The changes corresponded to LDL/HDL ratios of 0.4, 0.4 and 0.5 for exposed mice and 0.4, 0.3 and 0.3 for control mice, on days 1, 3 and 28, respectively. Total cholesterol levels in hepatic tissues were marginally elevated in the 0.162 mg exposed mice groups on day 28 ($p = 0.06$) compared to sham controls. Overall, total hepatic cholesterol was increased by 22.2, 12.1 and 22.6 % in the high dose group on days 1, 3 and 28, respectively (Figure 3.1D). We note that our cholesterol analyses resulted in some variability between post-exposure day controls. The reason for this effect is unknown, but may be related to the intratracheal instillation procedure.

3.5 Discussion

We investigated pulmonary and hepatic gene expression in mice instilled with vehicle control, 0.018, 0.054 and 0.162 mg Printex 90 CBNPs and sacrificed 1, 3 and 28 days after this single exposure. Gene expression profiles in lungs revealed large-scale CBNP-induced perturbations of inflammatory cytokine and chemokine transcripts, supported by concomitant changes in BAL cell counts. Large changes in acute phase serum amyloids A transcripts (*Saa1*, *Saa2* and *Saa3*) were measured in the lungs up to 28 days post-exposure for the highest dose group and up to 3 days post-exposure in the lower dose groups relative to controls. Elevated SAA protein was confirmed in the plasma of mice exposed to 0.162 mg Printex 90 on post-exposure days 1 and 28. Genes in the HMG-CoA

reductase pathway were perturbed in both lung and liver. In the lung, these changes were observed at the two higher doses on post-exposure days 1 and 3, whereas more substantial changes in liver were detected on days 1 (0.162 mg dose) and 28 (all doses). In parallel, HDL cholesterol was decreased relative to controls 3 and 28 days post-exposure, whereas LDL cholesterol was increased at 28 days (i.e., 0.162 mg dose group). Thus, our genomic profiling demonstrates the cascade of events initiated through inflammation and acute phase response in the lungs leading to liver transcriptional changes and impacting lipid homeostasis following nanoparticle exposure.

Inhalation of CBNPs can cause direct pulmonary injury, thus instigating an inflammatory response. Indeed, the inflammatory response was the overwhelming biological effect observed in our transcript profiles, supporting the observed phenotype. The pro-inflammatory genes identified were primarily involved in recruitment and activation of various inflammatory markers including neutrophils (*Cxcl5*, *Ccl3*, *Cxcl1*), eosinophils, (*Ccl11*, *Ccl12*, *Ccl8*), monocytes (*Ccl7*, *Ccl2*, *Ccl4*, *Cc12*, *Ccl8*) and lymphocytes (*Ccl20*, *Ccl24*, *Ccl12*) with large, persisting increases in *Cxcl5* that may explain the predominance of neutrophils in our BAL cell profiles (Bourdon et al. 2012b).

Inflammatory signaling molecules, including IL-6 and TNF (both up-regulated by CBNP exposure), have been suggested to trigger the APR. APR is

characterized by rapid induction of positive acute phase proteins (e.g., c-reactive protein, SAA and serum amyloid P), decreases in negative acute phase proteins (e.g., albumin and transferrin), and physiological changes (e.g., altered metabolism and fever). Generally, the APR is a transient response initiated to prevent further injury and to activate repair processes. Prolonged APR is linked to aortic inflammation and accelerated atherosclerosis, as observed in individuals with chronic inflammatory diseases including rheumatoid arthritis and systemic lupus erythematosus (Hollan *et al.* 2007). It has also been shown that increased levels of SAA in plasma directly accelerate progression of atherosclerosis in ApoE$^{-/-}$ mice (Dong *et al.* 2011). For such reasons, positive acute phase proteins (e.g., c-reactive protein, phospholipase A2 and SAA) are proposed biomarkers of potential cardiovascular disease (Ballantyne *et al.* 2004). Inhalation of nano-sized nickel and titanium dioxide has been shown to initiate an APR in mouse (Halappanavar et al. 2011; Kang et al. 2011). Here, we demonstrate that a single installation of relatively low doses of CBNPs induces inflammation with an associated APR that persists for 28 days. As such, we speculate that exposure to CBNPs and possibly other nanoparticulates may be associated with chronic inflammation-mediated APR, which in turn may increase susceptibility to cardiovascular disease.

One of the mechanisms by which inflammation-triggered APR may elicit adverse cardiovascular outcomes is through interruption of cholesterol transport

(Feingold and Grunfeld 2010). APR is implicated in disrupting reverse cholesterol transport at many levels, including reduced levels and altered functions of HDL, as well as reduced efficacy of cholesterol efflux and bile acid synthesis. HDL, which facilitates reverse cholesterol transport and inhibits the oxidation of LDL in healthy individuals, is greatly reduced in humans (Annema *et al.* 2010) and in mice (McGillicuddy *et al.* 2009) during the APR and in our study. Increased plasma levels of SAA observed in our study may lead to interruption of reverse cholesterol transport by displacement of apolipoproteins, and replacement of cholesterol esters and phospholipids by triglycerides, unestrified cholesterol and ceramides (Feingold and Grunfeld 2010). Such modifications in HDL are suggested to inhibit both cholesterol efflux from macrophages and protection against LDL oxidation (Annema *et al.* 2010; Feingold and Grunfeld 2010; McGillicuddy *et al.* 2009). These alterations may even allow HDL to participate in inflammatory responses and to deliver cholesterol to macrophages (Feingold and Grunfeld 2010). In addition, APR also affects lipid transport by down-regulating cholesterol efflux genes in peripheral tissues and by reducing hepatic cholesterol uptake and synthesis of bile acids (McGillicuddy *et al.* 2009). Although we did not detect any alterations in hepatic cholesterol uptake or bile synthesis, we observed down-regulation of cholesterol efflux genes *Abca1* and *Abcg1* in pulmonary tissue. Our results suggest that a single instillation of Printex 90 leads to inflammation and APR, which markedly alters

systemic cholesterol transport and metabolism over a prolonged time scale. These processes can lead to adverse health outcomes when induced chronically.

Alterations in lipid transport (such as those described above) can trigger sterol sensitive pathways in extra-pulmonary tissues. As a central site of metabolism, the liver plays an important role in regulating lipid homeostasis. The mice in the present study exhibited significant changes in hepatic expression of *Hmgcr*, which is rate limiting in the HMG-CoA reductase pathway and in *de novo* cholesterol production. HMG-CoA is exclusively activated under low sterol conditions in a negative feedback loop, and fulfills two important biological functions: (1) production of terpenoid intermediates to serve in the prenylation of small GTPases (e.g., Ras, Rac and Rho) and activation of a variety of cellular processes (e.g., actin cytoskeleton remodeling, cellular proliferation, generation of reactive oxygen species and inflammatory responses) (Liao 2002); and (2) cholesterol production. Exposure to CBNP in the present study caused a fairly uniform up-regulation of genes across this entire pathway (*Hmgcr*, *Mvd*, *Fdps*, *Sqle*, *Dhcr7*). Up-regulation of genes downstream of *Sqle* suggests that CBNP exposure tips this pathway towards cholesterol production. Cholesterol is critical for maintaining cellular membrane integrity (e.g., lipid rafts, signal transduction and molecular exchanges). It has been established that severe inflammation, infection and APR activate the HMG-CoA reductase pathway in the liver of rodents, as demonstrated in models of LPS treatment (Feingold *et al.* 1993;

Feingold *et al.* 1995; Memon *et al.* 1993). Here, we demonstrate that Printex 90 intratracheal instillation leads to up-regulation of the HMG-CoA reductase pathway in liver and lung, with concomitant modest changes in plasma LDL and marginal increases in hepatic cholesterol. The results suggest that pulmonary CBNP responses trigger molecular signaling cascades affecting the liver, and that these responses may drive excess production of cholesterol. It is possible that perturbations of cholesterol homeostasis observed in our work may be further exacerbated by the protein corona created around CBNPs. A recent study using *N*-isopropylacrylamide and *N*-*t*-butylacrylamide copolymers of varying size and composition demonstrates that nanoparticles bind cholesterol, triglycerides and phospholipids (with preference to HDL), and that binding reaches saturation (Hellstrand *et al.* 2009). This effect is strongest with increased hydrophobicity and surface area of the particle, and thus relevant to the chemical properties of Printex 90 CBNPs. Therefore, this may be an additional mechanism by which the HMG-CoA reductase pathway is up-regulated in the present study.

Exposure to fine and ultrafine particles is associated with increased incidences of cardiovascular events and long-term risk of heart disease (PopeIII et al. 2004). Prominent mechanisms of particle-induced cardiovascular disease include alterations in the autonomic nervous system resulting in cardiac arrhythmia, chronic systemic oxidative stress and inflammation leading to atherosclerotic plaque formation, endothelial dysfunction and acute phase

response induced thrombosis (Brook 2008). Here, we propose that nanoparticle-induced APR triggers changes in lipid transport and metabolism, thus activating the atherogenic HMG-CoA reductase pathway (Figure 3.2). The implication of the HMG-CoA reductase pathway in cardiovascular disease extend beyond excess cholesterol synthesis, to endothelial nitric oxide (eNos) expression and activation-mediated endothelial dysfunction (Rikitake and Liao 2005), systemic oxidative stress induced oxidation of LDL and activation of macrophages (Ilker-Yilmaz *et al.* 2003), and release of pro-inflammatory factors that participate in leukocyte adhesion and progression of atherosclerotic lesions (Yoshida 2003). In parallel, it has been suggested that HMG-CoA reductase inhibitors (i.e., statins) may be effective in preventing ambient particulate matter-induced coronary artery disease in individuals with elevated c-reactive protein levels, regardless of lipid profiles (Sandhu *et al.* 2005). Further investigations are required to decipher the role of nanoparticles in the disruption of cholesterol synthesis and metabolism and possible implications to metabolic and cardiovascular disease. At this time, it is unclear whether intratracheal instillations of NPs are expected to induce more substantive effects than exposure by inhalation. Although intratracheal instillation of Printex 90 CBNPs has been shown to cause more inflammation in terms of neutrophil influx in comparison to inhalation of the same dose (Jackson et al. 2011a; Jacobsen et al. 2009), it has been shown that daily inhalation exposure to nano-titanium dioxide over eleven days and at doses well bellow the current occupational exposure limit resulted in pulmonary APR that

persisted at least 5 days after the last exposure (Halappanavar et al. 2011). This study is the first to simultaneously assess global lung and liver gene expression responses to CBNPs across various doses and extended to late time-points to explore sustained molecular effects. The results provide important insights into nanoparticle-mediated systemic changes in acute phase response, inflammation and cholesterol homeostasis. The data indicate the power of a global systems-biology approach to identify perturbed processes and identify candidate biological pathways supporting observed phenotypes.

3.6 Tables and Figures

Table 3.1. Physical-chemical properties of Printex 90 as a raw material and in vehicle (0.9% NaCl MilliQ water containing 10% vol/vol accellular BAL).

Particle Characterization	
Manufacturer Declared Size	14 nm
Surface Area (BET)	295-338 m^2/g
Pycnometric Particle Density	2.1 g/cm^3
Chemical Composition	99% C, 0.8% N and 0.01% H_2
PAH Content	74.2 ng/g
Endotoxin	142 EU/g
Particle Properties in Exposure Vehicle	
Morphology	Free and open chain-aggregates with minor amounts of free single primary spheres.
Polydispersity Index (PDI)	1
Zeta Potential	-10.7 mV
Peak Hydrodynamic Number	2.6 um
Peak Volume-Size-Distribution	3.1 um

Table 3.2. Expression over control of acute phase response signaling genes measured by Agilent 4 x 44K microarray analysis in C57BL/6 mice exposed to 0.162 Printex 90 CBNPs and sacrificed 1, 3 and 28 days post-exposure. Fold-changes over matched controls and *p*-value are presented. Data in bold are FDR significant (< 0.1).

	Day 1		**Day 3**		**Day 28**	
Gene Name	fold-change	*p*-value	fold-change	*p*-value	fold-change	*p*-value
Lung						
Serum amyloid A3 (*Saa3*)	**65.3**	**0.00**	**8.3**	**0.00**	6.8	0.00
Metallothionein 2 (*Mt2*)	**5.7**	**0.00**	**2.1**	**0.00**	1.3	0.30
Ceruloplasmin (*Cp*)	**3.5**	**0.00**	**2.2**	**0.00**	1.1	0.55
Metallothionein 1 (*Mt1*)	**2.1**	**0.00**	**1.7**	**0.00**	1.2	0.06
Serum amyloid A1 (*Saa1*)	**11.3**	**0.00**	1.7	0.02	1.5	0.07
Serum amyloid A2 (*Saa2*)	**6.9**	**0.00**	1.4	0.11	1.3	0.23
Orosomucoid 2 (*Orm2*)	**3.6**	**0.00**	1.3	0.19	1.4	0.12
Orosomucoid 1 (*Orm1*)	**2.6**	**0.00**	1.1	0.42	1.2	0.15
Complement component 3 (*C3*)	**2.0**	**0.00**	1.4	0.00	1.5	0.01
Liver						
Serum amyloid A3 (*Saa3*)	**4.2**	**0.00**	1.0	0.91	0.5	0.96
Orosomucoid 3 (*Orm3*)	2.2	0.02	0.5	0.98	1.0	0.92
Serum amyloid A1 (*Saa1*)	1.5	0.03	0.6	0.77	0.6	0.27
C-reactive protein (*Crp*)	1.0	0.92	1.5	0.10	1.7	0.03

Table 3.3. Expression of genes part of the HMG-CoA reductase pathway measured by Agilent 4 x 44K microarray analysis in C57BL/6 mice exposed to 0.162 Printex 90 CBNPs and sacrificed 1, 3 and 28 days post-exposure. Fold-changes over matched controls and *p*-value are presented. Data in bold are FDR significant(<0.1).

	Day 1		**Day 3**		**Day 28**	
Gene Name	fold-change	*p*-value	fold-change	*p*-value	fold-change	*p*-value
Lung						
Squalene epoxidase (*Sqle*)	**1.6**	**0.00**	**1.8**	**0.00**	1.2	0.04
Isopentyl-diphosphate delta isomerase (*Idi*)	**1.4**	**0.00**	**1.7**	**0.00**	1.2	0.11
Farnesyl-diphosphate synthase (*Fdps*)	1.3	0.02	**1.6**	**0.00**	1.3	0.02
Diphosphomevalonate decarboxylase (*Mvd*)	1.4	0.01	**1.5**	**0.00**	1.3	0.03
Liver						
3-hydroxy-3-methylgluatyl-CoA reductase (*Hmgcr*)	**2.8**	**0.00**	0.5	0.67	2.4	0.00
Lanosterol synthase (*Lss*)	**2.6**	**0.00**	1.2	0.34	1.3	0.08
Isopentyl-diphosphate delta isomerase (*Idi*)	**2.3**	**0.00**	1.2	0.10	1.5	0.03
HMG-CoA synthase (*Hmgcs1)*	**2.0**	**0.00**	1.2	0.28	1.4	0.13
Squalene epoxidase (*Sqle*)	**1.9**	**0.00**	1.2	0.33	1.2	0.25
Mevalonate kinase (*Mvk*)	**1.9**	**0.00**	1.2	0.12	1.2	0.12
Farnesyl-diphosphate synthase (*Fdps*)	**1.8**	**0.00**	1.1	0.30	1.2	0.08
7-dehydrocholesterol reductase (*Dhcr7*)	**1.6**	**0.00**	1.1	0.48	1.2	0.24
Diphosphomevalonate decarboxylase (*Mvd*)	1.9	0.00	0.5	0.79	1.1	0.98

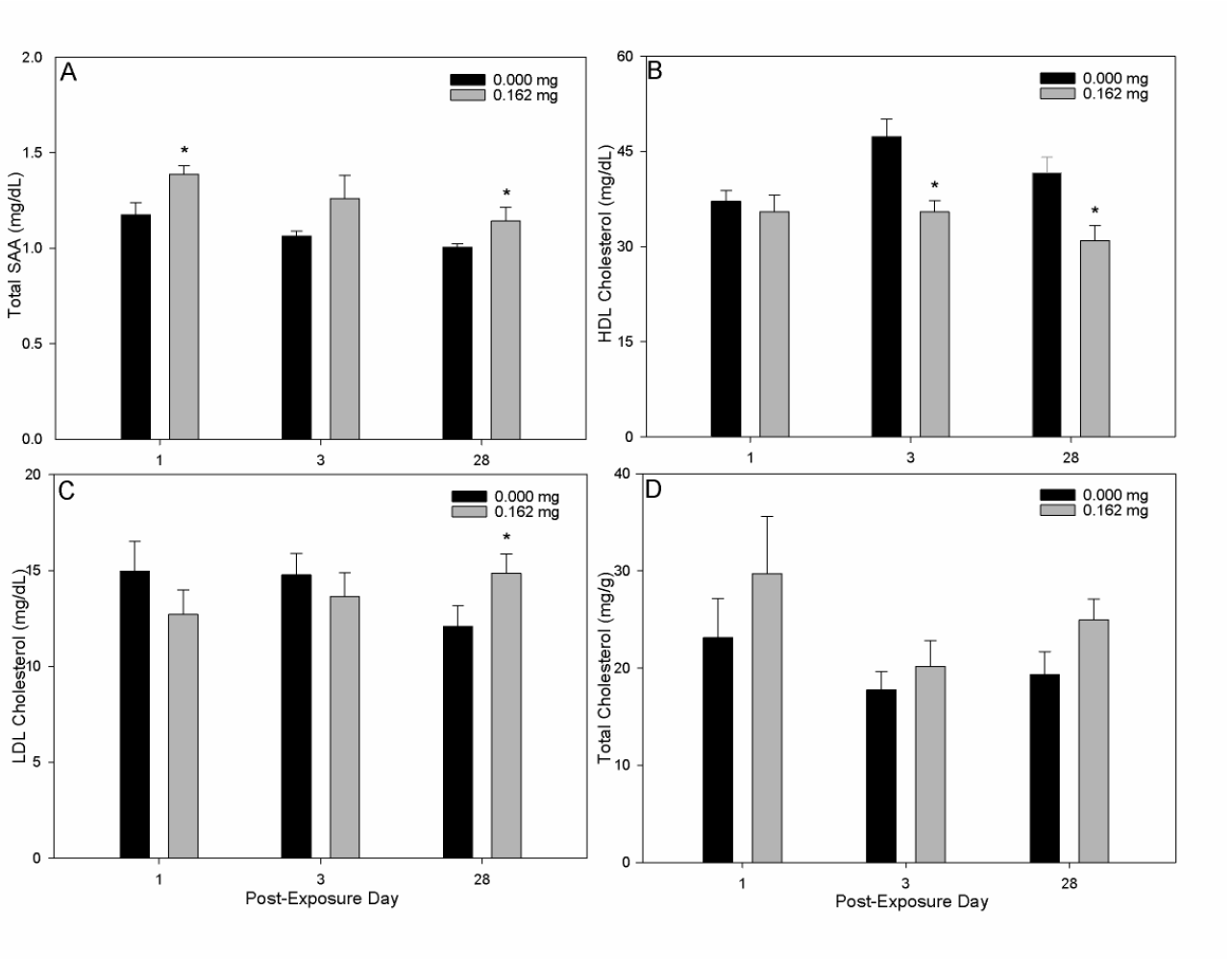

Figure 3.1. Changes in A) plasma total SAA; B) plasma high-density lipoprotein; C) plasma low-density lipoprotein; and D) hepatic total cholesterol in C57BL/6 mice exposed to vehicle and 0.162 mg Printex 90 CBNPs and sacrificed 1, 3 and 28 days post-exposure. Significance was calculated by comparison to matched control and * indicates $p < 0.05$.

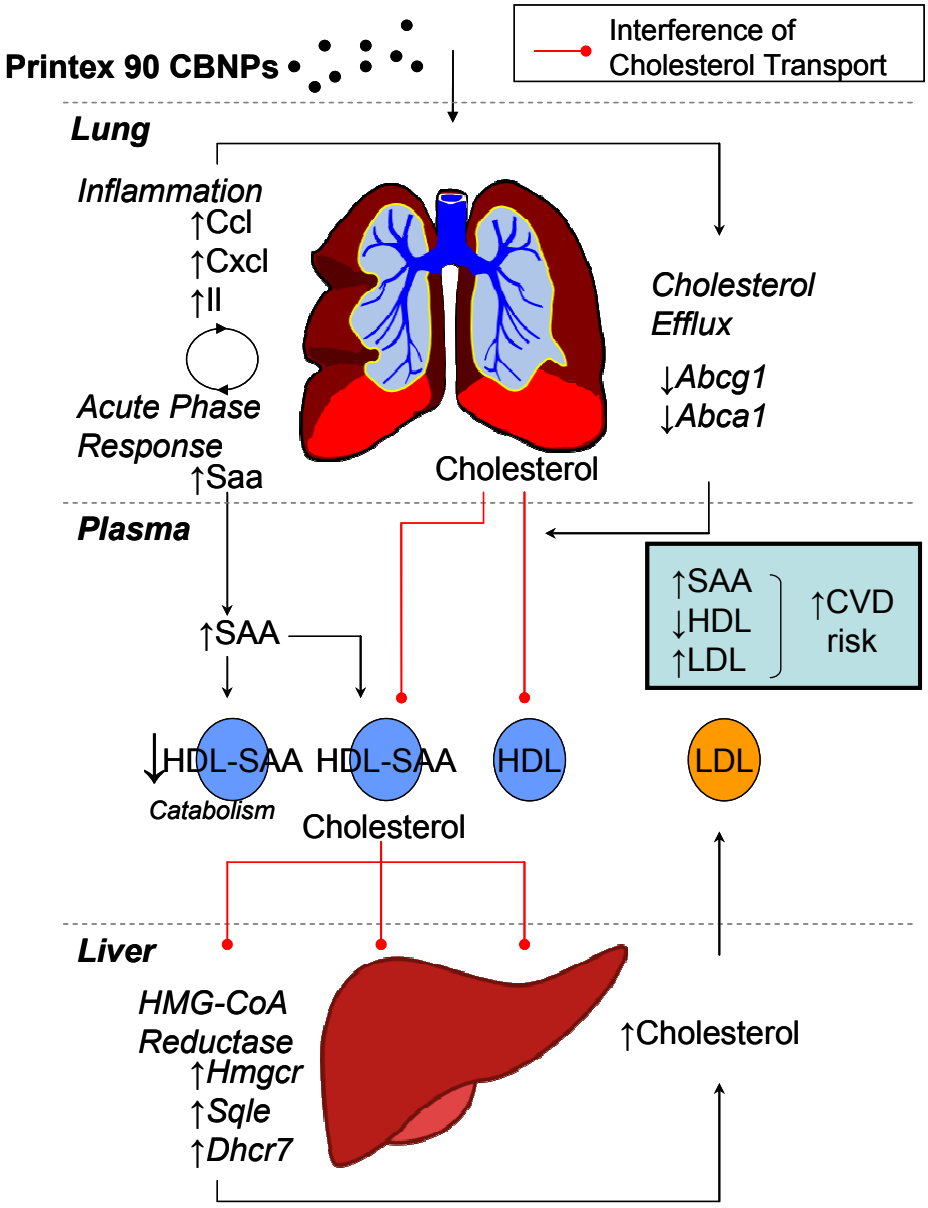

Figure 3.2. Suggested mechanisms by which nanoparticles may induce molecular signaling cascades leading to up-regulation of the HMG-CoA reductase pathway in the liver of exposed C57BL/6 mice. We demonstrate that inflammation is induced by pulmonary deposition of nanomaterials, resulting in activation of APR. Secretion of APR reactants such as SAA into plasma is suggested to induce structural changes of HDL that may increase its catabolism and inhibit its capacity to associate with cholesterol, thus potentially inhibiting reverse cholesterol transport. Inflammation may also down-regulate cholesterol efflux genes in lung (for example, *Abcg1* and *Abca1*), thus inhibiting cholesterol from reaching HDL. Such molecular changes inhibiting transport of excess cholesterol to liver for secretion into bile may lead to activation of the sterol sensitive HMG-CoA reductase pathway in liver, leading to increased terpenoid and cholesterol synthesis. Increased SAA and LDL and decreased HDL are associated with cardiovascular disease risk.

CHAPTER 4. CARBON BLACK NANOPARTICLE INTRATRACHEAL INSTALLATION RESULTS IN LARGE AND SUSTAINED CHANGES IN THE EXPRESSION OF MIR-135B IN MOUSE LUNG

Modified from: Bourdon, JA, Saber, AT, Halappanavar, S, Jackson, PA, Wu, D, Hougaard, KS, Jacobsen, NR, Williams, A, Vogel, U, Wallin, H and Yauk, CL. (2012) *Environmental and Molecular Mutagenesis*, in press.

4.1 Abstract

MicroRNAs (miRNA) are important non-coding regulatory molecules that bind target messenger RNA (mRNA), primarily affecting their translation into protein. Because miRNAs can simultaneously target hundreds of mRNAs, subtle changes in their expression can elicit important cellular effects. Little is known about the role of miRNAs in pulmonary responses to inhaled particulate matter. We studied pulmonary global miRNA responses to Printex 90 carbon black nanoparticles in 1) non-pregnant C57BL/6 female mice instilled with vehicle or a single dose of 0.162 mg and euthanized 1, 3 and 28 days post-exposure, and 2) C57BL/6Bom Tac dams instilled with vehicle or a cumulative dose of 0.268 mg (4 separate instillations of vehicle or 0.067 mg Printex 90 during pregnancy) and euthanized at weaning (26-27 days post-exposure). We measured similar expression profiles in both exposure scenarios, with marked increases in miR-135b and subtle changes in miR-21 and miR-146b. All three miRNAs were confirmed in non-pregnant females by RT-PCR, whereas only miR-135b was

confirmed in the dams. Target analysis revealed no concomitant changes in established and predicted targets of miR-135b, miR-21 or miR-146b. Analysis of potentially perturbed pathways did not reveal changes that would suggest down-stream miRNA effects. The reasons for the lack of association between miRNA and transcript profiles may be related to the complexity of miRNA function and fate, or to the possibility that targets may differ from those already established or predicted *in silico*. We hypothesize that changes in the expression of these miRNAs may be associated with resolution of pulmonary inflammation, but future work will be necessary to precisely identify specific targets of these miRNAs in lungs.

4.2 Introduction

MicroRNAs (miRNA) are small (20-25 nucleotide long), phylogenetically well-conserved, non-coding RNA molecules that function as important regulators of at least one third of the transcriptome. MiRNAs mediate gene expression through binding to 3' untranslated regions of mRNA sequences to cause mRNA degradation or translational repression (Lewis et al. 2005). MiRNA deregulation is involved in the pathogenesis of various diseases (Farazi et al. 2011; Maes et al. 2009). It has also become apparent that miRNAs play pivotal roles in mediating toxic responses to chemicals (Lema and Cunningham 2010). Thus, interest in the utility of miRNAs as exposure biomarkers and for understanding chemical mode of action is increasing.

Concerns have arisen over exposure to engineered nanomaterials in consumer products and occupational settings. Several *in vitro* studies have shown that nanoparticle exposure leads to perturbations of miRNA responses (Li et al. 2011a; Li et al. 2011b; Mahmood et al. 2011; Ng et al. 2011). Pulmonary exposure to nano-titanium dioxide in mice elicits changes in miRNA expression in lung (e.g., miR-21, miR-135b, miR-1 and miR-449a) (Halappanavar et al. 2011). However, the effects of other nanoparticles and the implications of altered miRNA expression in response to nanoparticulates remain to be elucidated.

In this study, we investigate pulmonary miRNA expression following intratracheal-instillation with Printex 90 carbon black nanoparticles (CBNPs). CBNPs, including Printex 90, are used extensively in tires and other rubber products, as well as in printing inks, paints, and plastics. Two exposure scenarios (non-pregnant females exposed to a single dose and dams exposed to four small doses during pregnancy) were applied to identify consistently perturbed miRNAs. Pulmonary inflammation, DNA damage and global gene expression for the mice used in this experiment were published previously (Bourdon et al. 2012a; Bourdon et al. 2012b; Jackson et al. 2011a; Jackson et al. 2011b). These studies revealed substantial inflammation in the mice from both experiments, and significant DNA strand breaks in non-pregnant females. Gene expression profiles were similar in both studies, reflecting Printex 90-induced inflammatory

and acute phase-responses, as well as alterations in lipid metabolism and transport. It has been demonstrated that mammalian miRNAs primarily regulate the transcriptome by decreasing mRNA target levels as opposed to translational suppression (Guo et al. 2010). In the present study we mine previously published global gene expression profiles (Bourdon et al. 2012a; Jackson et al. 2011b) to identify potential mRNA targets of the miRNAs that were disregulated by Printex 90 exposure.

4.3 Materials and Methods

4.3.1 Particle Characterization

Printex 90 CBNPs were a gift from Evonik/Degussa (Frankfurt, Germany) and have been extensively characterized (Bourdon et al. 2012b; Jacobsen et al. 2007; Saber et al. 2011). Hydrodynamic particle size distributions in the exposure media were determined by Dynamic Light Scattering (DLS) using a Malvern Zetasizer Nano ZS (Malvern, UK). Aggregation levels were determined by transmission electron microscopy (TEM) and scanning electron microscopy (SEM) as described previously(Bourdon et al. 2012b; Jacobsen et al. 2007; Saber et al. 2011).

4.3.2 Experimental Design and Animal Exposure

Two sets of Printex 90 instilled mice were studied alongside their respective controls: 1) C57BL/6 female mice (Taconic, Denmark) exposed to a

single dose of 0.162 mg Printex 90 and euthanized 1, 3 and 28 days post-exposure (6 mice per group; 36 samples in total); and 2) time-mated nulliparous C57BL/6Bom Tac mice (Taconic, Denmark) exposed to a cumulative dose of 0.268 mg Printex 90 (delivered as 0.067 mg instillations on gestational days 7, 10, 15 and 18) during pregnancy and euthanized at weaning 26-27 days post-exposure (5 mice per group; 10 samples in total). These two groups are referred to as non-pregnant females and dams throughout. Exposure metrics have been described extensively for both groups (Bourdon et al. 2012a; Bourdon et al. 2012b; Jackson et al. 2011a; Jackson et al. 2011b). Mice were selected as an exposure model as they are less prone to particle overload compared to rats, and there is a large body of studies to support their use in particle exposure investigations. Moreover, the use of both non-pregnant mice and dams allowed us to identify miRNAs that are consistently perturbed in various biological states. All experiments were approved by the Danish "Animal Experiments Inspectorate" (permit 2010/561-1179 and 2006/561-1123). Procedures complied with EC Directive 86/609/EEC and Danish laws regulating experiments on animals. Briefly, mice were anesthetised and instilled with their respective doses of Printex 90 in 40 µl instillation vehicle (0.9% NaCl MilliQ water containing 10% v/v acellular BAL or nanopure water), followed by 150-160 µl air. Control mice received 40 µl of the instillation vehicle alone. The animals were closely monitored following exposure and did not exhibit any signs of respiratory distress, lethargy or any other physical symptoms. On the day of euthanasia,

mice were anesthetised, bronchoalveolar lavage (BAL) was obtained by flushing lungs 4 times with 0.8 mL 0.9% sterile saline, and lungs were removed and snap frozen in liquid N_2.

Doses were selected on the basis of relevant occupational exposure levels. The 0.162 mg dose for non-pregnant females is representative of pulmonary deposition in a mouse after 9 working days at the occupational exposure limit of 3.5 mg/m^3 carbon black per 8 hour work shift, as established by the Occupational Safety and Health Administration (OSHA) and the National Institute for Occupational Safety and Health (NIOSH) (assuming 33.8% of particles reach lung, 1.8 L/h inhaled air and 8h working day). The 0.268 mg dose (4 x 0.067 mg) for the dams corresponds to 16.5 working days at the occupational exposure level stated above. Although this dose is relatively high, it is comparable to the expected inhaled pulmonary dose from a previous Printex 90 inhalation study (Jackson et al. 2011a) in which mice were exposed to 42 mg/m^3 of CBNPs for 1h/day on gestation days 8 through 18 by a whole-body inhalation, resulting in a total inhaled mass of 0.826 mg per animal. Based on deposition estimates (Jacobsen et al. 2009), the pulmonary dose would be 0.287 mg per animal. Thus, the exposure models are physiologically relevant.

4.3.3 MiRNA Microarrays

Total RNA enriched with small RNA was isolated from the left lung lobe (a random section of the whole tissue) from non-pregnant females and dams using the mirVana miRNA isolation kit (Ambion, Canada). RNA quality was confirmed by UV spectrophotometry (Nanodrop 2000, Thermo Scientific, Canada) and using an Agilent BioAnalyzer (Agilent Technologies, Canada). Total RNA was labelled using the Agilent miRNA Complete Labelling and Hybridization kit (Agilent Technologies, Canada). Labelled RNA samples were hybridized on 8 X 15K Agilent mouse miRNA array slides (Agilent Technologies, Canada). Arrays were scanned using an Agilent G2505B scanner (5 µm resolution). Data were acquired using Agilent Feature Extraction software version 9.5.3.1.

4.3.4 MiRNA Microarray Statistical Analysis

The quality of the miRNA microarrays was examined using Agilent Feature Extraction quality control metrics, MA plots, boxplots and cluster analyses. Microarrays from three non-pregnant females produced sub-standard data quality and were left out of the analysis. No microarrays were eliminated for the dams. MAANOVA analysis was conducted on a final sample size of at least 4 mice per treatment group.

Non-background subtracted raw data were cyclic lowess normalized using R (R Development Core Team 2010). Technical replicates for each miRNA were averaged using the median signal intensity. The MAANOVA model (Wu et al. 2003) included the slide as a block effect as each slide could accommodate 8 samples, and the Fs statistic was used to test for differences between the controls and treated samples. Permutation *P*-values, obtained using residual shuffling, were estimated and false-discovery rate (FDR) adjusted (Benjamini and Hochberg 1995). Least-square means were used to estimate the fold-change for each comparison. MiRNAs were considered differentially expressed when FDR *P*-values were ≤ 0.05 and fold-changes ≥ 1.4.

4.3.5 Real-Time Quantitative PCR (RT-PCR) of miRNAs

Microarray results were verified in non-pregnant females (1, 3 and 28 days post-exposure, n=4/group) and dams (at weaning 26-27 days post-exposure, n=4/group) using the Qiagen miScript PCR system (Qiagen, Canada). Briefly, 1 µg of total RNA was used for polyadenylation of mature miRNAs by poly(A) polymerase and reverse transcribed into cDNA using oligodT primers with a universal tag (Qiagen, Canada). RT-PCR was performed in duplicate for each sample using a primer complementary to the universal tag and miScprit primers specific to each miRNA. Expression levels were normalized to expression levels of small nuclear RNA RNU1A1. A CFX real-time detection system (Bio-Rad, Canada) was employed to detect SYBR green incorporation in amplified product.

Fold-changes were calculated according to the $2^{-\Delta\Delta CT}$ method using R software and significance using student t-test (R Development Core Team 2010).

4.3.6 Target Prediction for MiRNAs

Predicted targets for miRNAs were determined in TargetScan release 6.0 (http://www.targetscan.org) using TargetScan mouse as well as mouse orthologs of human annotations (as the 3'UTR of many genes are less well-annotated in mice than humans). The combined list of targets was employed for further analysis. The TargetScan seed-based algorithm (Lewis et al. 2005) predicts biological targets of miRNAs by searching for the occurrence of 8-mer and 7-mer sites matching the seed region of miRNAs.

4.3.7 Pathway Analysis for MiRNAs

Pathway analysis for each miRNA was done using DIANA LAB mirPath (Papadopoulos et al. 2009b). The DIANA-microT-3.0 (loose) software was employed for target prediction specific to mice. Cut-off for pathway analysis was set at $-\ln(P\text{-value}) \geq 3.00$, thus corresponding to $P\text{-value} \leq 0.05$. Pathway analysis for the gene expression data were conducted using a rank based test [Alvo et al. 2010] in R. The gene expression data were obtained from the National Center for Biotechnology Information Gene Expression Omnibus site (accession no. GSE35193; http://www.ncbi.nlm.nih.gov/projects/geo). The relative expression for the genes in a pathway was first aligned by subtracting the median

expression value for the combined treatment and control groups. These values were then ranked within each subject and the vector of average ranks was calculated for each treatment group. The distance between the two treatments was calculated and a permutation analysis was used to obtain a *P*-value for each pathway.

4.4 Results

4.4.1 Particle Characterization

Printex 90 CBNPs from the present study were characterized in extensive detail as described in (Bourdon et al. 2012b; Jacobsen et al. 2007; Saber et al. 2011). Briefly, the manufacturer-declared size is 14 nm with a measured geometric mean size of 65 nm (carbon spheres). The BET surface area is 295-338 m^2/g and the pycnometric particle density is 2.1 g/cm^3. Very low levels of total polycyclic aromatic hydrocarbons (PAH) (75 ng/g) (Jacobsen et al. 2008) and endotoxin (0.142 EU/mg) (Bourdon et al. 2012b) can be detected on the surface of Printex 90. Distribution was characterized in detail within instillation vehicle (0.9% NaCl MilliQ water containing 10% v/v acellular BAL for non-pregnant females and nanopure water for dams) (Bourdon et al. 2012b; Jackson et al. 2011a). The hydrodynamic number and size-distribution showed a major peak of approximately 2.6 µm and 3.1 µm in non-pregnant females, whereas values were in the range of 50-60 nm in dams.

4.4.2 *Global miRNA Expression*

A total of three differentially expressed miRNAs were found in non-pregnant females (none on day 1 or 3, but 3 on day 28) and 3 in dams (at weaning, 26-27 days). Comparison of treated non-pregnant females from day 28 and dams on day 26-27 revealed nearly identical profiles, with 2 miRNAs in common (miR-146b and miR-21) (Table 4.1). The complete microarray and gene expression array datasets are available through the Gene Expression Omnibus at NCBI (http://www.ncbi.nlm.nih.gov/geo/), SuperSeries GSE36199, SubSeries GSE36170 (dams) and GSE36171 (non-pregnant females). MiR-135b was confirmed by RT-PCR in both the dams and non-pregnant females, whereas, miR-146b and miR-21 were confirmed in non-pregnant females only (Figure 4.1). Due to the compressed dynamic range of miRNA arrays (Pradervand et al. 2012), the fold-changes detected by arrays were substantively higher using RT-PCR, as expected. RT-PCR analyses of miR-146a did not corroborate microarray findings in non-pregnant females (data not shown).

4.4.3 *Analysis of miRNA Targets*

Experimentally supported mRNA targets in humans were identified using TarBase version 5c (Papadopoulos et al. 2009a) for miR-21, but no experimentally validated targets were known for miR-146b and miR-135b. Mir-21 targets include Phosphatase and tensin homolog (*Pten*), Programmed cell death protein 4 (*Pdcd4*) and Tropomyosin 1 (*Tpm1*). No gene expression changes for these targets were

detected by microarrays in our previous studies (Bourdon et al. 2012a; Jackson et al. 2011b). RT-PCR analysis of *Pten* and *Pdcd4* in exposed females revealed down-regulation of *Pdcd4* on day 3 only (Table 4.2). Expression of two reported targets of miR-146a/b, Interleukin-1 receptor-associated kinase 1 (*Irak1*) and TNF receptor associated factor 6 (*Traf6*) (Taganov et al. 2006) was also unchanged (Table 4.2).

TargetScan 6.0 revealed 584, 180 and 240 predicted targets of miR-135b, miR-146 and miR-21, respectively. Because the expression of these miRNAs increased over time (reaching a maximum fold change on day 28) in non-pregnant females, we mined the gene expression profiles (Bourdon et al. 2012a) to identify genes showing decreased expression over time in order to narrow down potential targets. 298 genes were identified as having a fold-change of at least 1.4 on day 1 (statistical significance not considered) and decreased fold-change on days 3 and/or 28. Comparison of these genes with the predicted miRNA targets revealed 5 potential targets for miR-135b (*Adamts9*, *Bmper*, *Klf4*, *Cxcl12* and *Rrbp1*), 2 potential targets for miR-146b (*Klf4* and *Uhr1*) and 1 potential target for miR-21 (*Cxcl10*).

Kruppel-like factor 4 (*Klf4*) exhibited the most dramatic decrease from day 1 to day 28 out of the potential targets identified (fold-changes of 1.6, 2.2 and -1.6 on days 1, 3 and 28, respectively), and was a predicted target of both miR-135b

and miR-146b. However, RT-PCR analysis failed to support changes in *Klf4* gene expression for any of the post-exposure time-points (data not shown). Previous RT-PCR analysis revealed a modest up-regulation of the predicted miR-21 target C-X-C motif chemokine 10 (*Cxcl10*) on day 3, and no change in the miR-135b predicted target C-X-C motif chemokine 12 (*Cxcl12*) (Bourdon et al. 2012a). Thus, no convincing support was found for mRNA targets of the miRNAs.

4.4.4 Pathway Analysis for miRNAs

In order to elucidate the targeted pathways and potential down-stream effects of miRNA deregulation, pathway analysis was conducted on targets of miR-135b, miR-21 and miR-146b. The analysis revealed the most affected pathways (-ln(*P*-value) ≥ 3.0) for each miRNA, which included 10 KEGG pathways for miR-135b, 6 for miR-21 and 3 for miR-146b (Table 4.3). Concomitant transcriptomic analysis revealed that many of the mRNAs from the same pathways were also significantly perturbed by Printex 90 treatment. However, the statistical significance of these pathways and percentage of differentially expressed genes were consistent across the time-points, and thus did not appear to correlate with the miRNA profiles (e.g., increasing significance over time was only observed for thiamine metabolism whereas modest increase in percentage of differentially expressed genes was only observed for calcium signalling).

4.5 Discussion

Pulmonary instillation of Printex 90 revealed sustained and substantive induction of miR-135b, miR-146b and miR-21 in female mice up to 28 days post-exposure (up to 84-fold for miR-135b). The expression of these miRNAs increased over time after the initial exposure in non-pregnant females. miR-135b was the only miRNA confirmed by RT- PCR in the dams (24-fold induction). Analysis of known targets for miR-146b and miR-21 revealed neither changes in gene expression nor tendencies to decrease over the post-exposure time-points. *In silico* predicted targets of miR-135b, miR-146b and miR-21 did not exhibit concomitant changes in target expression, and mining of gene expression profiles revealed no tendencies for increased statistical significance in the miRNA-targeted pathways over time. Thus, the relevance of these miRNAs for toxicological response to nanoparticles is unclear and warrants further investigation.

Printex 90 exposed mice from the present study exhibited strong and persistent pulmonary inflammation (Bourdon et al. 2012b; Jackson et al. 2011a). Correspondingly, miR-135b, miR-146b and miR-21 have been implicated in inflammation and immune responses. For example, miR-146a/b are up-regulated in human monocytes during endotoxin-challenge (Taganov et al. 2006). These miRNAs down-regulate *Irak1* and *Traf6* and are thought to negatively regulate signal transduction pathways leading to NF-κB activation, thus averting over-

stimulation of inflammatory responses in human monocytes (Taganov et al. 2006). MiR-21 is induced in mouse lung and macrophages following endotoxin exposure (Lu et al. 2009). Both miR-146b and miR-21 are associated with resolution of acute inflammation (Recchiuti et al. 2011). Although miR-135b has yet to be fully characterized, it has been suggested to play a role in resolution of inflammation following exposure to nano-titanium dioxide (Halappanavar et al. 2011) and is expressed in human bronchial epithelial cells following diesel exhaust particle-induced inflammation (Jarim et al. 2009). Mice instilled with nano-titanium dioxide (Halappanavar et al. 2011) exhibit sizable changes (> 60-fold) in miR-135b, similar to Printex-90 instilled mice in the present study. Induction of miR-135b in primary human bronchial epithelial cells exposed to diesel exhaust particles (Jarim et al. 2009) provides human context to our findings. These data collectively suggest that miR-135b mediates important functions in pulmonary responses to particles and can potentially serve as an important biomarker of exposure. Thus, these miRNAs may play a role in inflammatory response and/or resolution of acute inflammation following pulmonary nanoparticle exposure, but target validation is essential to determine their mechanisms of action.

In addition to their potential roles in inflammation, miR-135b, miR-146b, and particularly miR-21, are also involved in DNA damage response and carcinogenesis. MiR-21 is an established oncomir and anti-apoptotic factor that is

aberrantly over-expressed in most human cancers (Farazi et al. 2011). Moreover, miR-21 suppresses p53 response (Papagiannakopoulos et al. 2008) and is up-regulated during ionizing radiation-induced DNA damage (Zhu et al. 2010). Induction of miR-21 in the non-pregnant females, but not the dams, is consistent with the elevated DNA strand breaks observed only in BAL of the non-pregnant females, relative to the dams (Bourdon et al. 2012b; Jackson et al. 2011a). MiR-135b is expressed in tumors isolated from the distal colon of chronically inflamed mice and is associated with inflammation induced-tumorigenic transformation (Necela et al. 2011). Mir-146b is implicated in DNA repair through its targeting of the Breast Cancer Type 1 Cancer Susceptibility gene (*Brca1*) (Garcia et al. 2011) and has reported tumor-suppressive and anti-metastatic effects (Xia et al. 2009). These data suggest that these miRNA may be responding to the genotoxicity observed in the non-pregnant female mice, but more importantly support the potential for mutagenic and carcinogenic outcome from exposure to CBNPs. Since carbon black is considered 'possibly carcinogenic to humans' (IARC Group 2B (IARC 1996)), the role of these miRNAs in particle-induced carcinogenesis should be investigated in more detail.

In conclusion, this study identified miR-135b as an important miRNA involved in pulmonary response to CBNP instillation in two mouse exposure models, but induction of miR-146b and miR-21 was exclusively observed in non-pregnant females. The reasons for these differences in miRNA responses in the

two models remain to be elucidated. Although molecular changes due to pregnancy may have concealed miRNA responses of miR-21 and miR-146b in dams, differences between the mice is most likely related to administration of a single large dose (vs. four doses in dams), differences in sampling time, and/or the absence of genotoxicity in the dams. We were unable to identify concomitant changes in known and predicted targets of miR-135b, miR-146b and miR-21 in the present study. Powerful tools have emerged to predict miRNA targets, however, miRNA-mRNA interactions are extremely complex. Although effects were expected at the transcriptional level, it is also possible that miR-135b, miR-21 and miR-146b may be acting at the translational level. To further complicate the issue, new evidence demonstrates that miRNAs can enhance translation (Vasudevan et al. 2007), and can affect miRNA regulation and function (Pasquinelli 2012). In addition, competing endogenous RNA can bind miRNAs and dilute their effects (Pasquinelli 2012). As such, the fate and function of miRNAs can be difficult to predict (Pasquinelli 2012). Further work must be undertaken to characterize the targets of these miRNAs in the context of these complex interactions in order to fully elucidate the role of miR-135b, miR-21 and miR-146b in biological responses to particulates. As miR-135b was dramatically induced by exposure to CBNPs in both of our mouse models, future work in our laboratory will focus on its role in inflammation and particle-induced responses.

4.6 Tables and Figures

Table 4.1. MiRNAs differentially expressed by exposure to Printex 90 CBNPs as identified by miRNA expression microarrays.

	Dose[a] = 0.162 mg Non-Pregnant Females						Dose[b] = 0.268 mg Dams	
	day 1		day 3		day 28		day 26-27	
miRNA	p-value	fold-change	p-value	fold-change	p-value	fold-change	p-value	fold-change
mmu-miR-135b	0.961	1.0	0.641	1.0	**0.000**	**1.2**	**0.000**	**1.8**
mmu-miR-146b	0.450	1.1	0.644	1.1	**0.014**	**1.5**	**0.011**	**1.5**
mmu-miR-21	0.226	1.4	0.620	1.4	**0.056**	**2.1**	**0.022**	**1.4**
mmu-miR-146a	0.519	1.1	0.644	1.1	**0.022**	**1.4**	0.526	1.2

[a]–single dose

[b]–4 x 0.067 mg

Table 4.2. RT-PCR gene expression of established targets for miR-21 (*Pten* and *Pdcd4*) and miR-146 (*Traf6* and *Irak1*) in Printex 90 CBNP exposed non-pregnant female mice relative to controls.

	Dose[a] = 0.162 mg Non-Pregnant Females					
	day 1		day 3		day 28	
Gene	p-value	fold-change	p-value	fold-change	p-value	fold-change
Phosphatase and tensin homolog (*Pten*)	0.106	0.8	0.958	1.0	0.512	0.8
Programmed cell death protein 4 (*Pdcd4*)	0.159	0.7	0.005	0.7	0.416	1.1
TNF receptor associated factor 6 (*Traf6*)	0.888	0.9	0.151	1.2	0.371	1.1
Interleukin-1 receptor-associated kinase 1 (*Irak1*)	0.141	1.2	0.073	1.3	0.106	1.3

[a]–1 x 0.162 mg

Table 4.3. Pathways expected to be perturbed by up-regulation of miR-135b, miR-21 and miR-146b expression.

KEGG pathway	Total Probes	% miRNA Targeted Genes[a]	% Genes Day 1[b]	% Genes Day 3[b]	% Genes Day 28[b]
mmu-miR-135b					
Wnt signaling pathway	298	13.7***	3.4*	3.0*	0.3
Axon guidance	278	5.5***	2.2*	1.8*	1.8*
Colorectal cancer	139	4.3***	3.6*	2.2**	1.4*
Basal cell carcinoma	59	9.1**	2.1*	2.1**	1.1
ErbB signaling pathway	196	1.7**	2.6*	1.0**	1.0
TGF-beta signaling pathway	155	4.0**	2.6**	2.6*	0.0*
Type II diabetes mellitus	101	10.3*	4.0**	4.0*	3.0**
Calcium signaling pathway	337	2.5*	1.2*	0.3*	0.9
Melanogenesis	188	5.9*	2.1*	0.5*	1.6
Leukocyte transendothelial migration	207	23.1*	3.4*	1.9**	3.4**
mmu-miR-21					
T cell receptor signaling pathway	224	2.1**	2.2**	2.7**	3.1**
Natural killer cell mediated cytotoxicity	215	1.8**	2.8**	1.9**	2.3**
Cytokine-cytokine receptor interaction	354	1.2*	10.5**	6.2**	8.2**
B cell receptor signaling pathway	157	1.1*	5.1*	3.2*	5.1**
Thiamine metabolism	7	7.7*	0.0	0.0*	0.0*
VEGF signaling pathway	149	1.2*	1.3*	0.0*	2.7*
mmu-miR-146b					
Toll-like receptor signaling pathway	161	1.7**	8.1**	7.5**	7.5**
Biosynthesis of steroids	35	2.9*	8.6**	17.1**	0.0
Bile acid biosynthesis	18	5.6*	11.1**	11.1**	11.1

[a]–Targets were identified using DIANA LAB mirPath and the % of miRNA predicted targets that are within that pathway is shown.

[b]–% of genes affected by CBNP exposure (0.162 mg Printex 90 exposed non-pregnant females vs. control) in the microarray data (unadjusted $P \leq 0.05$ and fold-change ≥ 1.4), with statistical significance of * ($P \leq 0.05$), ** ($P \leq 0.01$) and *** ($P \leq 0.001$).

Figure 4.1. RT-PCR validation of miR-135b, miR-146b and miR-21 in Printex 90 CBNP exposed mice relative to controls. *, ** refer to statistical significance of ≤ 0.1 and ≤ 0.05, respectively.

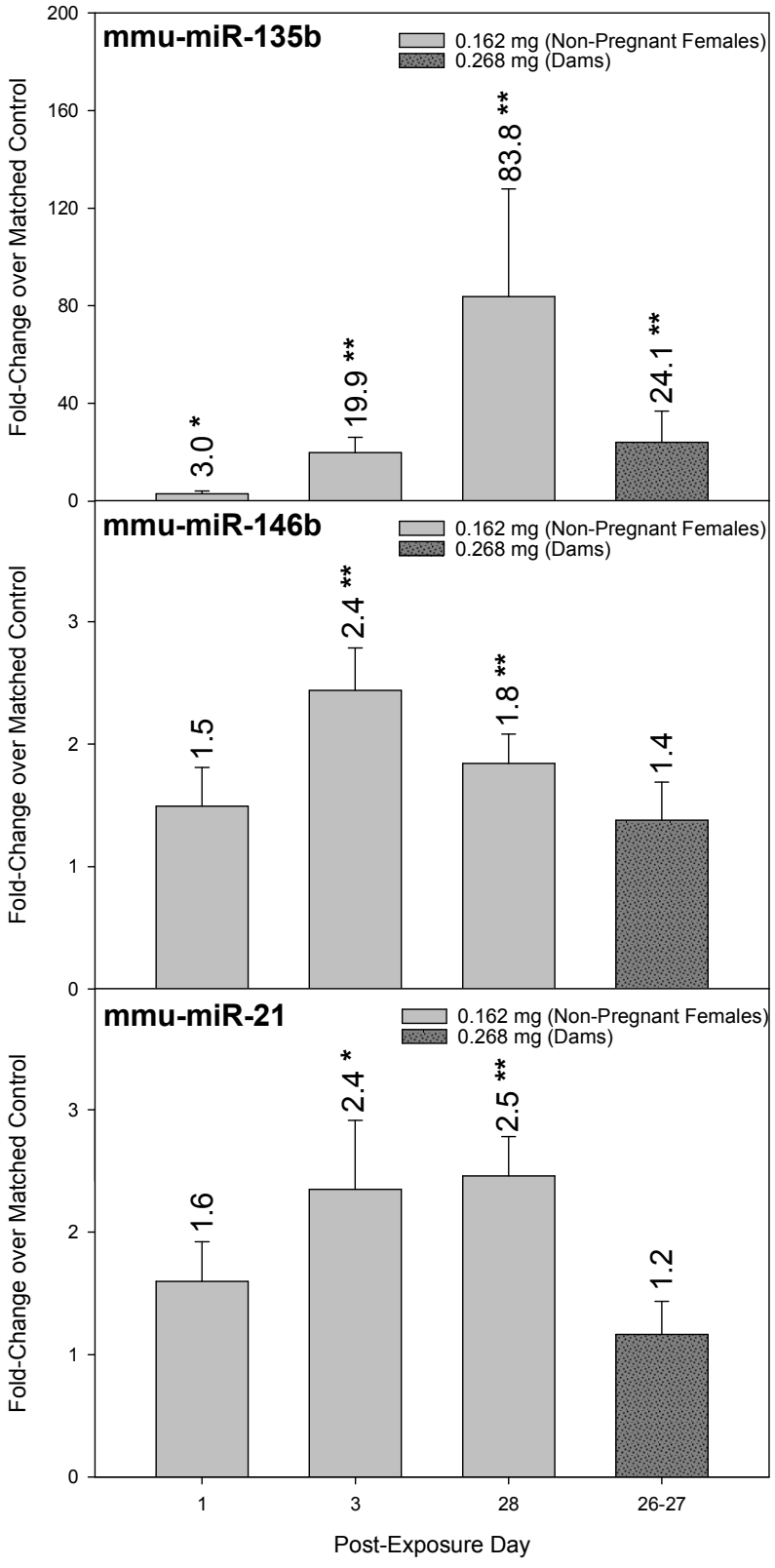

CHAPTER 5: CARBON BLACK NANOPARTICLE INTRATRACHEAL INSTILLATION ALTERS PLASMA LEVELS OF CELL ADHESION MOLECULES AND APOLIPOPROTEINS IN MICE IN THE ABSENCE OF CARDIAC TRANSCRIPTOMIC CHANGES

In preparation for peer-review: Bourdon, JA, Saber, AT, Jacobsen, NR, Halappanavar, S, Williams, A, Vogel, U, Wallin, H and Yauk, CL

5.1 Abstract

Exposure to fine and ultrafine particulate matter is associated with increased risk of cardiovascular disease, leading to concern over the widespread and increasing use of nanoparticles in consumer products. Mechanisms leading to adverse cardiovascular effects are suggested to involve perturbations of the autonomic nervous system with direct impacts on the heart, and inflammatory molecular signalling cascades involved in the progression of atherosclerosis. Previous toxicogenomics investigation in lung and liver support inflammatory molecular signalling cascades in initiating adverse cardiovascular effects, however, little is known on the possible impact on cardiac tissue directly. Here, we further characterize systemic responses within plasma with concomitant analysis of cardiac global gene and microRNA expression profiles in mice intratracheally instilled with vehicle or 0.162 mg Printex 90 carbon black nanoparticles (CBNPs) and sacrificed 1, 3 and 28 days after exposure. Plasma soluble cell adhesion molecules including sE-selectin, sICAM-1, sVCAM-1 in

addition to total PAI-1 were immediately induced and persisted to day 28. Decreases in plasma Apo-A1 and Apo-E were observed on post-exposure day 1, whereas total heart cholesterol was not affected. In contrast, gene expression in cardiac tissue was unperturbed by CBNP exposure in two separate experimental mouse groups, despite substantive changes in pulmonary and hepatic global gene expression profiles. RT-PCR analysis of the most differentially expressed genes revealed modest changes in *Adcy7* and *Fbn1* ($p \leq 0.1$ and fold changes $\geq$ 1.5). Cardiac microRNAs were also unperturbed by the exposure in heart tissue. These data further support the role of inflammation and the acute phase response in adverse cardiovascular effects with little effect on whole heart gene expression. Future work should determine whether expression changes can be detected in specific cell types (e.g., cardiomyocytes and cardiac endothelium) in order to draw firm conclusions with regards to direct cardiac impacts.

5.2 Introduction

It is well established that exposure to fine and ultrafine particulate matter (PM) is associated with adverse cardiovascular effects (Dockery et al. 1993; Miller et al. 2007; PopeIII et al. 2004). However, the mechanisms underlying this association remain to be fully elucidated. PM-induced cardiovascular effects are primarily hypothesized to occur through changes in the autonomic nervous system, leading to cardiac arrhythmia (Carr and Undem 2001; Chuang et al. 2007; Mills et al. 2009), or through systemic inflammatory signalling cascades, involved in increased blood coagulation and

progression of atherosclerotic plaque (Bonzini et al. 2010; Suwa et al. 2002). Several studies have demonstrated PM-associated atherosclerosis progression in animal models susceptible to plaque formation (e.g., hyperlipidemic rabbits, apoE$^{-/-}$ mice, LDLr$^{-/-}$ mice and mice with double knockout for apoE$^{-/-}$ and LDLr$^{-/-}$) following pulmonary exposure with ambient air particles/concentrated air pollution (Araujo et al. 2008; Chen and Nadziejko 2005; Sun et al. 2005; Suwa et al. 2002; Yatera et al. 2010), nano-carbon black (Niwa et al. 2007), single-wall carbon nanotubes (Li et al. 2007), nano-titanium dioxide (Mikkelsen et al. 2011) and nano-nickel (Kang et al. 2011). However, the potential for PM to induce arrhythmia suggests impacts on the cardiac tissue itself. Thus, direct impacts on heart tissue need to be addressed in further detail.

We previously established systemic inflammation as a potential driver of cardiovascular toxicities in C57BL/6 mice exposed to Printex 90 carbon black nanoparticles (CBNPs), an important reference material in the study of ultrafine air pollution. Briefly, mice were exposed by instillation to 0.018, 0.054 and 0.162 mg Printex 90/animal, corresponding to the mice being exposed at the current occupational exposure limit (i.e., 3.5 mg/m^3 as established by the Occupational Safety and Health Administration (OSHA) and the National Institute for Occupational Safety and Health (NIOSH)) for 1, 3 or 9 working days (8 hour/day) (Bourdon et al. 2012a). Global gene expression previously established in the lungs and livers of these Printex 90-exposed mice revealed molecular perturbations in pathways that could potentially play a role in adverse cardiovascular effects (Bourdon et al. 2012a). This included induction of pulmonary acute phase response, substantive pulmonary inflammatory responses and 3-

hydroxy-3-methyl-glutaryl-CoA reductase (HMG-CoA reductase) signalling in both lung and liver, all of which are strongly associated with onset and progression of cardiovascular disease (CVD) (Araujo 2011). Pulmonary inflammatory responses were supported by concomitant influx in polymorphonuclear cells that persisted 28 days post-exposure. The plasma of these mice had elevated serum amyloid A (SAA) and decreased levels of high density lipoprotein even 28 days after the exposure (Bourdon et al. 2012a). These findings suggest that systemic inflammation could play an important role in cardiovascular toxicities. However, the potential impact from the autonomic nervous system or other signalling mechanisms on cardiac tissue itself, and their potential implication in adverse cardiovascular toxicity, is currently unknown.

In this study, we further characterize systemic inflammation related changes associated with cardiovascular effects in plasma, including circulating cell adhesion molecules (e.g., soluble endothelial selectin (sE-Selectin), soluble intercellular adhesion molecule 1 (sICAM-1) and soluble vascular cell adhesionmolecule 1 (sVCAM-1)), total plasminogen activator inhibitor 1 (total PAI-1) and apolipoproteins (e.g., apolipoprotein A1 (Apo-A1) and apolipoprotein E (Apo-E)). In addition, we investigate transcriptomic changes (e.g., mRNA and microRNA perterbations) in whole heart tissue, in order to determine potential direct impacts on cardiac functions. This study is the first to investigate the effects of manufactured NPs on cardiac global gene expression via pulmonary exposure and provides insight into the systemic effects induced by CBNP-exposure relating to cardiovascular toxicities.

5.3 Materials and Methods

5.3.1 Particle Characterization

Printex 90 CBNPs were a gift from Evonik/Degussa (Frankfurt, Germany). They have been extensively characterized in (Bourdon et al. 2012b; Jacobsen et al. 2008; Saber et al. 2011). Hydrodynamic particle size distribution and agglomeration in exposure vehicle was determined by dynamic light scattering and transmission electron microscopy, as described previously (Bourdon et al. 2012b).

5.3.2 Animal Handling and Exposure

Protocols for animal handling and exposure have been described thoroughly in (Bourdon et al. 2012a; Bourdon et al. 2012b) and complied with EC Directive 86/609/EEC and Danish laws regulating experiments on animals (permit 2010/561-1179). The mouse exposure protocol described herein was done twice, as two separate experiments over different time periods. Thus, the entire experiment was performed twice to produce independent experimental subsets of mice referred to as subset 1 and subset 2 throughout. Briefly, C57BL/6 mice were supplied with food and water *ad libitum* and allowed to acclimatize prior to intratracheal instillation with vehicle (0.9% NaCl MilliQ water containing 10% v/v acellular BAL) and 0.162 mg Printex 90 CBNPs. This dose is expected to result in pulmonary deposition of Printex 90 that is equivalent to 9 working days at the occupational exposure limit of 3.5 mg/m^3 (Jacobsen et al. 2009) (as established by the Occupational Safety and Health Administration (OSHA) and the National Institute for Occupational Safety and Health (NIOSH). Prior to instillation, mice were anesthetised with equal volumes of Hypnorm and Dormicum. A 40 µl suspension of

sonicated CBNPs was administered via a 24 gauge BD incite catheter with a shortened needle (Becton Dickinson, Denmark) inserted in the trachea, followed by 150 µl of air. Following recovery from anaesthesia, the mice did not display signs of respiratory distress, decreased locomotor activity, lethargy or any other physical symptoms of exposure. Mice were sacrificed 24 hours, 3 days and 28 days after exposure. Heart blood was collected (800-1000 µl) and stabilized with M K_2EDTA. Plasma was isolated by centrifugation. Heart tissue, alongside lung and liver tissues were frozen in liquid nitrogen then stored at -80 °C.

5.3.3 Total RNA and miRNA Extraction

Total RNA was isolated from the hearts (random sections including both right and left ventricles) of 36 mice (subset 1, n=6 per group), using TRIzol reagent and purified using RNeasy MiniKits with on-column DNase treatment (Qiagen, Canada). Total RNA that included small RNAs was isolated from the hearts of an additional 36 mice (subset 2, n=6 per group, random section including both right and left ventricles) using the miRVana isolation kit (Ambion, Canada). RNA quality was confirmed by UV spectrophotometry (Nanodrop 2000, Thermo Scientific, Canada) and using an Agilent Bioanalyzer (Agilent Technologies, Canada) in all samples.

5.3.4 Gene Expression Microarray Hybridization

Complementary DNA was synthesized from 200 ng of total RNA from each sample (n=6 per group) and Stratagene universal mouse reference RNA (Agilent, Canada), using the Agilent Linear Amplification kit (Agilent Technologies, Canada). Experimental samples were labeled with cyanine 5-CTP whereas reference RNA was labeled with cyanine 3-CTP (Perkin-Elmer Life Sciences, Canada). The cyanine-labeled cRNA was *in vitro* transcribed using T7 polymerase and purified using RNeasy mini kits (Qiagen, Canada). Labeled sample and reference RNA samples for subset 1 (exposed to vehicle or 0.162 mg Printex 90, n=6 per treatment and time point) were combined and hybridized to Agilent 4 x 44K oligonucleotide microarrays (Agilent Technologies, Canada). The additional subset of mice treated in a separate identical experiment (subset 2, exposed to vehicle and 0.162 mg Printex 90, n=6 per treatment and time point) was hybridized to Agilent 8 x 60K oligonucleotide arrays (Agilent Technologies, Canada). For both experiments, hybridization took place for 17 hours at 60°C. The arrays were washed according to supplier instructions and then scanned on an Agilent G2505B scanner at 5 µm resolution. Data were acquired using Agilent Feature Extraction software version 9.5.3.1.

5.3.5 MiRNA Expression Microarray Hybridization

Total RNA from subset 2 was labelled with cyanine-3-cytidine biophosphate (pCp-Cy3) using the Agilent miRNA Complete Labelling and Hybridization kit (Agilent Technologies, Canada). Labelled RNA samples were

hybridized on 8 X 15K Agilent mouse miRNA array slides (Agilent Technologies, Canada) for 20 hours at 55°C then washed and scanned using an Agilent G2505B scanner (5 µm resolution). Data were acquired using Agilent Feature Extraction software version 9.5.3.1.

5.3.6 Statistical Analysis of Gene and MiRNA Expression Microarray Data

The analysis of the Agilent 4 x 44K oligonucleotide microarrays was conducted using a reference design (Kerr and Churchill 2001; Kerr 2003). For the Agilent 8 x 60K oligonucleotide microarrays, the relative expression (Sample/Reference) was analyzed using a linear model, treating the slide as a block effect. A similar linear model was applied to the absolute intensities for the miRNA data analysis.

All pre-processing of the data was conducted using R (R Development Core Team 2005). The median signal intensities for the expression arrays were normalized using the global lowess method (Yang et al. 2002) using the transform.madata function in the MAANOVA library (Wu et al. 2003). For the miRNA data, the non-background subtracted median signal intensities were cyclic-lowess normalized (Bolstad et al. 2003) followed by averaging the technical replicates using the median.

Ratio intensity plots were constructed for the raw and normalized data for each array and hierarchical clustering using complete and single linkages were generated to identify mircoarrays with poor data quality. This resulted in 6, 2 and 6 samples being removed from the final analysis for the 4 x 44k, 8 x 60k and the miRNA analyses.

Differentially expressed genes and miRNAs were identified using the MAANOVA library. The Fs statistic (Cui et al. 2005), a shrinkage estimator, was used for the gene-specific variance components and the associated *p*-values for all the statistical tests were estimated using the permutation method (30,000 permutations with residual shuffling). The *p*-values were then adjusted for multiple comparisons using the false discovery rate approach (FDR) (Benjamini and Hochberg 1995). The least-squares means (Goodnight and Harvey 1978; Searle et al. 1980) were used to estimate the fold changes for each pairwise comparison.

5.3.7 Real-Time Polymerase Chain Reaction

Primers were designed using Beacon designer 2.0 (Premier BioSoft International, USA). Primer specificity was assured by melting curve analysis and optimal annealing temperature was determined for each primer pair by gradient PCR. Heart total RNA (1 µg) was reverse transcribed to cDNA for each sample (n=6 per group), using the SuperScript III First-Strand Synthesis system

(Invitrogen, Canada). Experiments were performed on 10-fold cDNA dilutions in duplicate using a CFX96 real-time PCR detection system (Bio-Rad, Canada). Threshold cycle values were averaged. PCR efficiency for each gene was extrapolated from a 5-fold serial dilution standard curve of pooled RNA and normalized to *Hprt*. Using the delta CT value, differentially expressed genes were identified using a two-sample bootstrap test (t-Pivot method) assuming unequal variances using the R software (Efron and Tibshirani 1993; Higgins 2003). Standard errors for the fold-change for each comparison were estimated using the bootstrap method (Efron and Tibshirani 1993).

5.3.8 Lipid Extraction and Total Heart Cholesterol Analysis

Total lipids were extracted using the Folch method. Briefly, heart tissue was homogenized in 500 µl equal volumes of methanol and water. 5:1 chloroform:methanol was added and the lower phase was removed following centrifugation. Excess chloroform was removed under nitrogen gas flow. Collected lipids were re-suspended in 100 µl EnzyChrom™ assay buffer and stored at -20°C.

The EnzyChrom™ AF Cholesterol Assay Kit (BioAssay Systems, USA) was employed for quantification of total cardiac cholesterol in vehicle and 0.162 mg Printex 90 treatd mice (subset 2; n=6). Lipid extracts were diluted 10-fold and 50 µl aliquots were transferred to a clear 96-well plate with 6 standard dilutions

of cholesterol reference, in duplicate. Fifty µl of a dye reagent-enzyme mix (for cholesterol ester hydrolysis, oxidation and colour reaction) was added and the plate was incubated at room temperature for 30 min. The color intensity of the reaction product was measured by spectrophotometry at 570 nm and total cholesterol concentrations were determined by comparison to the standard curve. Data were normalized to tissue weight. Statistical significance was determined using an unpaired one-tailed *t*-test assuming unequal variances.

5.3.9 Plasma Cardiovascular Disease Biomarkers

Milliplex mouse cardiovascular disease (CVD) panels I and II were employed for plasma quantification of sE-Selectin, sICAM-1, sVCAM-1, total PAI-1, Apo-A1 and Apo-E. Multiplex assays were conducted according to the manufacturers guidelines provided with the kits. Plasma samples were diluted 1:100 for Panel 1, and 1:40,000 for Panel 2 using assay buffer. All measurements were performed in duplicate. Briefly, the biomarker standards were serially diluted using assay buffer before use. Standard, quality controls, or diluted sample (25 ul) were added to each well of a 96-well filter plate followed by 25 µl of assay buffer, and 25 ul of the antibody-immobilized bead suspension. The plate was sealed and incubated with agitation on a plate shaker overnight (16–18 h) at 4°C. After incubation, the plate was washed two times with wash buffer (200 ul/well), removing buffer by vacuum filtration between washes. Detection antibodies (25 ul) were added to each well, and the plate was incubated on a

shaker for 2 hours at room temperature. A streptavidin-phycoerythrin solution (25 µl) was then added to each well and the plate was left to shake at room temperature for 30 min. The plate was washed twice with wash buffer as before, and 100 ul of sheath fluid was added to the wells to resuspend the beads. A Luminex200 analyzer with xPONENT 3.1 analysis software (Luminex, Austin, TX) was used to evaluate the median fluorescent intensity (MFI) using the weighted 5-parameter logistic method to calculate analyte concentrations. Plasma of three mice displayed major inconsistencies throughout and were eliminated from the analysis.

5.4 Results

5.4.1 Particle Characterization

Particles have been described extensively in (Bourdon et al. 2012b; Jacobsen et al. 2008; Saber et al. 2011). Briefly, particles had a manufacturer declared particle size of 14 nm, BET surface area of 295-338 m^2/g and pycnometric particle density of 2.1 g/cm^3 with negligible quantities of surface contaminants (75 ng/g PAHs and 0.142 EU/mg endotoxin). The hydrodynamic diameter of the raw dispersion showed a major peak at approximately 2.6 µm and 3.1 µm, according to number and volume, respectively.

5.4.2 Global Cardiac Gene Expression

Global gene expression analysis was conducted on heart tissues from mice exposed to vehicle (control) or 0.162 mg of Printex 90 CBNPs by a single intratracheal instillation and necropsied 1, 3 and 28 days post-exposure. The entire experiment was

conducted twice, with two completely separate sets of animals and DNA microarrays (subset 1 and subset 2), with a sample of 6 mice per condition per experiment. This analysis revealed that very few genes in the heart were affected by the treatment (Table 1). Overall, statistically significant changes in mRNA levels (FDR p-value ≤ 0.05 and fold changes ≥ 1.5) were found for only four genes in subset 1 and one gene in subset 2, with no overlap in genes between subsets, for the DNA microarray datasets. However, the mRNA changes could not be confirmed by RT-PCR using a cut-off of $p \leq 0.05$ and fold changes ≥ 1.5. Marginal statistical significance ($p \leq 0.1$ and fold changes ≥ 1.5) was observed for Adenylate cyclase 7 (*Adcy7*) and Fibrillin 1 (*Fbn1*) in subset 1 (post-exposure day 1). The complete microarray datasets for Subsets 1 and 2 are available through the Gene Expression Omnibus at NCBI (http://www.ncbi.nlm.nih.gov/geo/, GSE37891, Sub-Series GSE37885 and GSE37887). All of the microarrays in the first experiment (subset 1) were run in parallel with microarrays on lung and liver reported in (Bourdon et al. 2012a). Thus, the lung and liver data serve as positive controls for the microarray work, and indicate that the technology is able to detect significant changes in gene expression when they exist (http://www.ncbi.nlm.nih.gov/geo/, GSE35284).

5.4.3 Global Cardiac miRNA Expression

MiRNA profiles were investigated in mice from Subset 2, using 8 X 14K Agilent miRNA arrays. The analysis revealed no significant changes in miRNAs from exposed relative to control mice (FDR p-value ≥ 0.8, data not shown). The complete microarray dataset has been submitted through the Gene Expression

Omnibus at NCBI (http://www.ncbi.nlm.nih.gov/geo/, GSE37891, Sub-Series GSE37890).

5.4.4 Total Heart Cholesterol

Since substantive perturbations of cholesterol homeostasis were observed in lung and liver of the mice (Bourdon et al. 2012a), total cholesterol was examined in heart. Heart total cholesterol was decreased by 13.6, 38.1 and 18.9% on days 1, 3 and 28 respectively, but these decreases did not attain statistical significance (day 1 p=0.24, day 3 p=0.15, day 28 p=0.16) (Figure 1).

5.4.5 Plasma Markers of Cardiovascular Disease

Six markers of cardiovascular disease were measured in the plasma of mice (i.e., sE-Selectin, sICAM-1, sVCAM-1, total PAI-1, Apo-A1 and Apo-E) (Figure 2). PAI-1, sE-Selectin, sICAM-1 levels were significantly elevated at all post-exposure time-points relative to controls, whereas sVCAM was elevated on post-exposure days 1 and 3. Apo-A1 and Apo-E were significantly decreased on day 1 but no changes were measured at later time-points.

5.5 Discussion

This study examines changes in mRNA and miRNA in whole heart tissue in parallel with markers of endothelial inflammation, fibrinolysis inhibition and lipid transport alterations in plasma of mice intratracheally instilled with vehicle and 0.162 mg

Printex 90 CBNPs and sacrificed 1, 3 and 28 days after exposure. We report that mRNA expression in whole cardiac tissue was unperturbed by CBNP exposure in two separate experimental mouse groups, despite previously reported substantive changes in pulmonary and hepatic gene expression (Bourdon et al. 2012a). RT-PCR failed to support changes in even the most differentially expressed genes; marginally significant changes concordant with microarray results were observed only for *Adcy7* and *Fbn1* ($p \leq 0.1$ and fold-change ≥ 1.5). Moreover, no significant changes in miRNAs were observed in the heart tissue of exposed mice at any time point. Despite lack of effects on the transcriptome, important changes in markers of endothelial inflammation, fibrinolysis inhibition and lipid transport were found in plasma. This included increases in sE-selectin, sICAM-1 and total PAI-1, which were immediately induced and persisted to day 28. In addition, decreases in Apo-A1 and Apo-E were observed on post-exposure day 1. Total heart cholesterol was not affected. These data reveal perturbations of plasma markers relevant to cardiovascular toxicities in the absence of cardiac transcriptomic profile alterations.

Only two genes, *Adcy7* and *Fbn1* were marginally affected in the hearts. *Adcy7* is involved in cyclic adenosine monophosphate (cAMP) production from ATP, a critical regulator of electric, mechanical and metabolic activity in cardiac myocytes (Iancu et al. 2007), whereas *Fbn1* is involved in maintenance of connective tissue elasticity and sequestering of transforming growth factor beta (Sherratt 2009). Although it is unclear whether the marginal changes in *Adcy7* and *Fbn1* are biologically significant, it is important to note that cAMP signalling and subsequent activation of protein kinase A

(PKA) is important in cardiac myocyte contractility (Dorn II and Molkentin 2004) and that maintenance of elasticity is a vital physiological property of arteries that can regulate blood pressure (Belz 1995). Thus, these genes may be involved in adverse cardiovascular toxicities.

It is possible that the lack of gene expression in this study may be related to sampling of whole heart tissue. Although subtle responses may have been detected by sampling of specific tissues (e.g., cardiomyocytes and arterial/cardiac endothelium, using laser capture microdissection), three previous studies of pulmonary exposure to concentrated air particulates demonstrate modest to substantive responses in whole cardiac tissue. Simkhovich et al. (2011) demonstrated that a three month inhalation exposure of male Fisher 344 rats to coarse and ultrafine concentrated ambient air particles led to up-regulation of thioredoxin interacting protein (*Txnip*) and cytochrome P450 (*Cyp2e1*), and a small number of additional genes in whole heart. Gene expression profiles in transgenic mice exhibiting severe dilated cardiomyopathy exposed to a single aspiration of concentrated ambient PM exhibited perturbations of cardiac sodium channel genes 36 hours post-exposure (Wang et al. 2011). Lastly, heart gene expression was substantially perturbed (367 differentially expressed genes) in male F344 rats exposed to concentrated air particulates by inhalation; these rats also exhibited considerable concomitant changes in pulmonary gene expression (Hasegawa et al. 2011). One additional study did not detect any cardiac or pulmonary gene expression changes in ApoE/LDLr double knockout mice (at lower exposure concentrations than in (Hasegawa et al. 2011), and with limited biological replicates) (Gunnison and Chen 2005). This

suggests the importance of pulmonary responses in initiating cardiac gene expression changes. Despite large changes in pulmonary gene expression, our data suggests that whole heart is relatively unperturbed by CBNP exposure. Thus, it is possible that sampling of whole heart diluted our ability to detect gene expression changes or that cardiovascular effects are more likely mediated by other signalling molecules.

Cell adhesion molecules (CAMs) are expressed on the surface of endothelial cells during pulmonary inflammatory responses, allowing tissue influx of leukocytes. Expression of CAMs in the arterial wall also plays a critical role in the initiation and progression of atherosclerotic plaque (Demerath et al. 2001). The selectin superfamily of CAMs (e.g., E-Selectin and P-Selectin) are early mediators of leukocyte-endothelial cell adhesion that function by attracting fucosylated carbohydrates on the surface of circulating leukocytes, forcing the leucocytes to decelerate and to "roll" across the cell surface of the endothelium (Tedder et al. 1995). Binding of leukocytes to the endothelium is thereafter facilitated by members of the immunoglobulin superfamily (e.g., ICAM-1 and VCAM-1), via interactions with integrins on the surface of the rolling leukocyte (Tedder et al. 1995), leading to leukocyte extravasation into the vessel wall, where the latter can accumulate lipids causing plaque formation and atherosclerosis (Blankenberg et al. 2003). For this reason, soluble forms of E-Selectin, ICAM-1 and VCAM-1 are detected at higher levels in the serum of individuals with CVD in comparison to healthy individuals (Demerath et al. 2001; Luc et al. 2003; Thorand et al. 2006). Here, we demonstrate that sVCAM-1, sE-Selectin and sICAM-1 are increased in plasma of CBNP exposed mice at relatively constant levels, with the latter two remaining elevated up to 28

days post-exposure. It is unclear whether increases in plasma E-Selectin, ICAM-1 and VCAM-1 observed herein were expressed at sites that promote plaque development (e.g., arterial wall) or were derived from pulmonary endothelium. Despite probable expression in the lungs in the process of transendothelial leukocyte migration, CAM induction was relatively constant across time-points, whereas pulmonary inflammation decreased substantially over time. Moreover, CAM expression was not altered in our microarray analysis of pulmonary tissue (Bourdon et al. 2012a), suggesting that the CAM induction originated at an extra-pulmonary site. Various other studies support the notion that CAM induction originates at plaque-forming sites following particle exposures. For example, pulmonary instillation with collected ambient air particulates results in ICAM-1 and VCAM-1 expression at sites of rabbit aortic plaques (Yatera et al. 2010). In addition, VCAM-1 is induced in brachiocephalic arteries of $ApoE^{-/-}$ transgenic mice exposed to carbon black nanotubes (Li et al. 2007), and titanium dioxide exposure stimulates leukocyte rolling and adhesion in the systemic microvascular wall of rats (Nurkiewicz et al. 2006). However, in a previous study of Printex 90, no changes in ICAM-1 or VCAM-1 were found in lung and aortic tissues of $ApoE^{-/-}$ mice (Vesterdal et al. 2010). Together, our findings and the results of others suggest the possible involvement of CAMs in particle-induced progression of atherosclerosis, but future work will be necessary to decipher the precise location of CAM expression.

Progression of atherosclerotic plaques is largely dependent on blood lipid availability and clearance from leukocytes that have crossed the vascular wall. Foam cells (i.e., derived from lipid laden macrophage) readily engulf circulating lipids (e.g., LDL)

which are subsequently oxidized and thus not readily metabolized, leading to bursting of the cell, deposition of fatty streaks, and onset of inflammation instigating additional leukocyte recruitment (Libby et al. 2011). Clearance of lipids from macrophages and prevention of LDL uptake in healthy individuals is mediated by HDL by promoting cholesterol efflux and the transport of excess lipids to the liver for excretion (Eckardstein et al. 2001). However, this process is significantly impaired during systemic inflammation in part by the displacement of Apo-A1 from HDL by acute phase serum amyloid A (Annema et al. 2010; Feingold and Grunfeld 2010; McGillicuddy et al. 2009). The present work demonstrates that both Apo-A1 and Apo-E, which are directly involved in reverse cholesterol transport via their association to HDL, are significantly decreased 24 hours after exposure to CBNPs. Our findings support previous reports of reduced HDL upon PM exposure in the mice studied herein (Bourdon et al. 2012a), and in humans (Rice et al. 2011), thus supporting the role of PM exposure in accelerating atherosclerosis progression.

Acute onset of adverse cardiovascular outcomes (e.g., myocardial infarction) is associated with rupturing of an atherosclerotic plaque and subsequent contact of blood coagulation components within the plaque's interior, resulting in a thrombus that can extend considerably into the vessel lumen or dislodge and relocate to smaller vessels, thus restricting blood flow (Libby et al. 2011). Therefore, the balance between circulating proteins involved in clotting and fibrinolysis is an important determinant of CVD risk (Rumley 1999). PAI-1 is increased during inflammatory responses and is involved in inhibiting the conversion of plasminogen into the active protease plasmin by binding and

neutralizing tissue plasminogen activator (t-PA) (Huber et al. 2001). Here, we demonstrate that PAI-1 is consistently increased on all post-exposure days. PAI-1 is also increased in the plasma of mice intratracheally instilled with collected ambient air PM (Cozzi et al. 2007) and in endothelial cells exposed to nano-copper oxide (Yu et al. 2010). This suggests an additional mechanism by which systemic changes in circulating proteins may promote CVD progression and risk.

In conclusion, CBNPs perturb plasma levels of molecules involved in endothelial inflammation, fibrinolysis inhibition and lipid transport in the absence of responses in cardiac tissue, at the time points examined. It is highly unlikely that the mice studied herein displayed any phenotypes of CVD. However, these data provide information on the propensity for CBNPs to promote CVD development. NP exposure may be particularly concerning for individuals who are already at risk of CVD due to poor lifestyle choices and genetic susceptibility. Our findings suggest that NPs most likely mediate adverse cardiovascular effects through inflammatory molecular signalling cascades and increased pulmonary expression of acute phase proteins, and not through autonomic perturbations leading to arrhythmia. However, it is also possible that gene expression changes were not detected due to random sampling of heart tissue that incorporated various cell types. Future work should apply laser capture microdissection to quantify *Adcy7* and *Fbn1* expression levels, among other genes, in different cardiac compartments. Moreover, the arterial wall of exposed mice should be examined for endothelial dysfunction and other markers of adverse cardiovascular toxicities. Future work should also establish the role of dose using chronic inhalation exposures to more

accurately mimic human exposure scenarios. This work is the first to investigate *in vivo* cardiac global gene expression following pulmonary exposure to manufactured NPs and provides important insight into the mechanisms of systemic cardiovascular toxicities caused by inhalation of NPs.

5.6 Tables and Figures

Table 5.1. Microarray analysis results of most differentially expressed genes (FDR *p*-value ≤ 0.05) (bold) in two separate experimental mouse groups (subset 1 and 2), with corresponding RT-PCR fold-changes and significance.

	Day 1				Day 3				Day 28			
Gene	**Microarray Fold-Change**	**FDR p-value**	**RT-PCR Fold-Change**	**p-value**	**Microarray Fold-Change**	**FDR p-value**	**RT-PCR Fold-Change**	**p-value**	**Microarray Fold-Change**	**FDR p-value**	**RT-PCR Fold-Change**	**p-value**
Mouse Heart 0.162 mg vs Control Subset 1												
Fibrillin 1 (*Fbn1*)	-2.0	0.000	-2.0	0.079	1.0	0.091	1.2	0.42	1.0	0.997	-1.4	0.144
Calreticulin 3 (*Calr3*)	1.9	0.000	1.2	0.215	1.5	0.241	1.1	0.431	1.3	0.943	-1.1	0.514
Adenylate cyclase 7 (*Adcy7*)	-2.0	0.000	-2.0	0.070	-1.1	0.794	1.1	0.588	-1.1	0.958	-1.3	0.338
Gamma-glutamyltransferase-like activity 1 (*Ggtla1*)	1.6	0.000	1.0	0.801	1.5	0.195	1.1	0.556	1.2	0.943	1.0	0.989
Bone morphogenetic protein 4 (*Bmp4*)	-1.4	0.258	-1.7	0.090	-1.7	0.000	-1.3	0.426	-1.3	0.943	-1.3	0.198
Tight junction protein 3 (*Tjp3*)	-1.1	0.863	-1.4	0.295	-1.4	0.000	-1.4	0.367	-1.3	0.943	-1.3	0.360
Mouse Heart 0.162 mg vs Control Subset 2												
D-aspartate oxidase (*Ddo*)	-1.1	1.000	1.0	0.971	-1.7	0.000	-1.1	0.237	-1.1	1.000	1.1	0.556
Glutamate-ammonia ligase (*Glul*)	1.0	1.000	1.2	0.079	-1.4	0.000	-1.3	0.062	1.0	1.000	1.0	0.833
Arginyltransferase 1 (*Ate1*)	1.1	1.000	1.2	0.110	1.0	0.992	1	0.907	-1.3	0.000	1.1	0.728

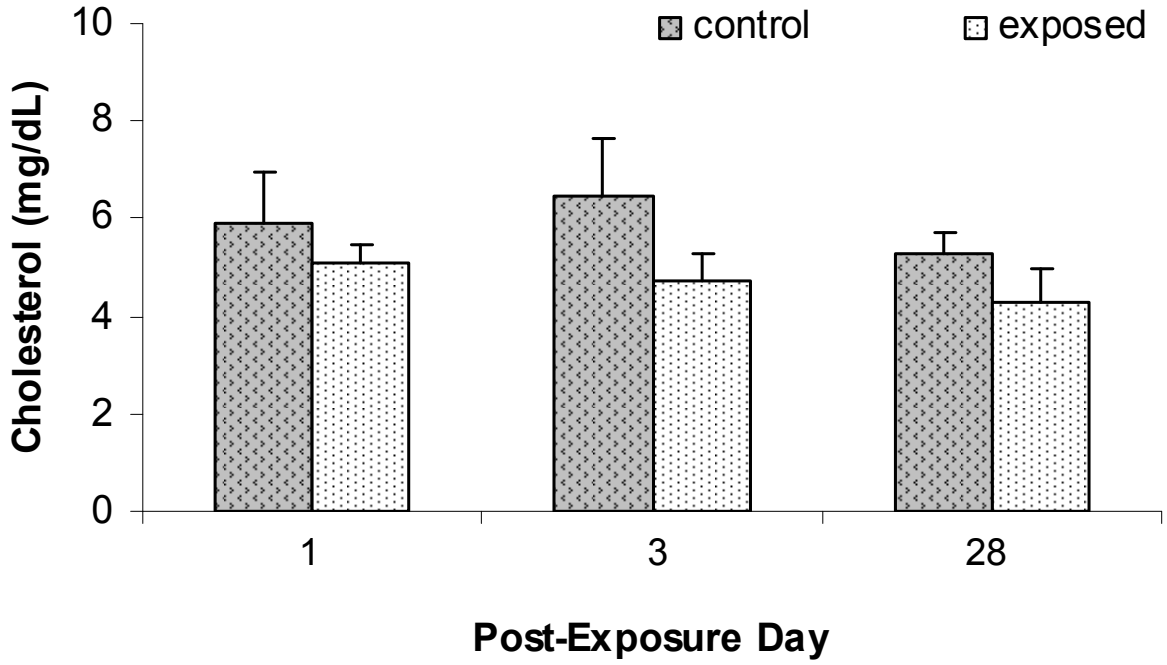

Figure 5.1. Total cardiac cholesterol in mice exposed to 0.162 mg CBNPs in comparison to vehicle controls (subset 2) 1, 3 and 28 days post-exposure.

	Day 1		Day 3		Day 28	
	Control	Exposed	Control	Exposed	Control	Exposed
sE-Selectin (ng/ml)	34.2 ± 3.2	68.8 ± 8.9 *	28.2 ± 2.5	47.5 ± 3.8 ***	22.4 ± 12.5	50.7 ± 6.0 **
sICAM-1 (ng/ml)	18.8 ± 1.4	20.2 ± 0.9 *	16.3 ± 0.9	20.2 ± 0.9 **	17.2 ± 2.0	23.0 ± 1.8 **
sVCAM-1 (ng/ml)	950.9 ± 57.2	1158.8 ± 27.0 **	910.0 ± 61.5	1108.3 ± 29.6 **	1005.5 ± 59.2	1224.9 ± 89.9
total PAI-1 (ng/ml)	0.4 ± 0.1	1.1 ± 0.3 *	0.4 ± 0.1	0.6 ± 0.0 *	0.3 ± 0.0	0.6 ± 0.1 *
Apo-A1 (µg/ml)	8870.0 ± 898.3	5070.7 ± 324.8 ***	6183.8 ± 498.6	6647.0 ± 586.2	7441.1 ± 1471.2	7087.1 ± 1095.9
Apo-E (µg/ml)	19.6 ± 4.1	7.0 ± 1.2 **	7.9 ± 0.9	14.3 ± 4.0	16.8 ± 5.1	15.0 ± 4.7

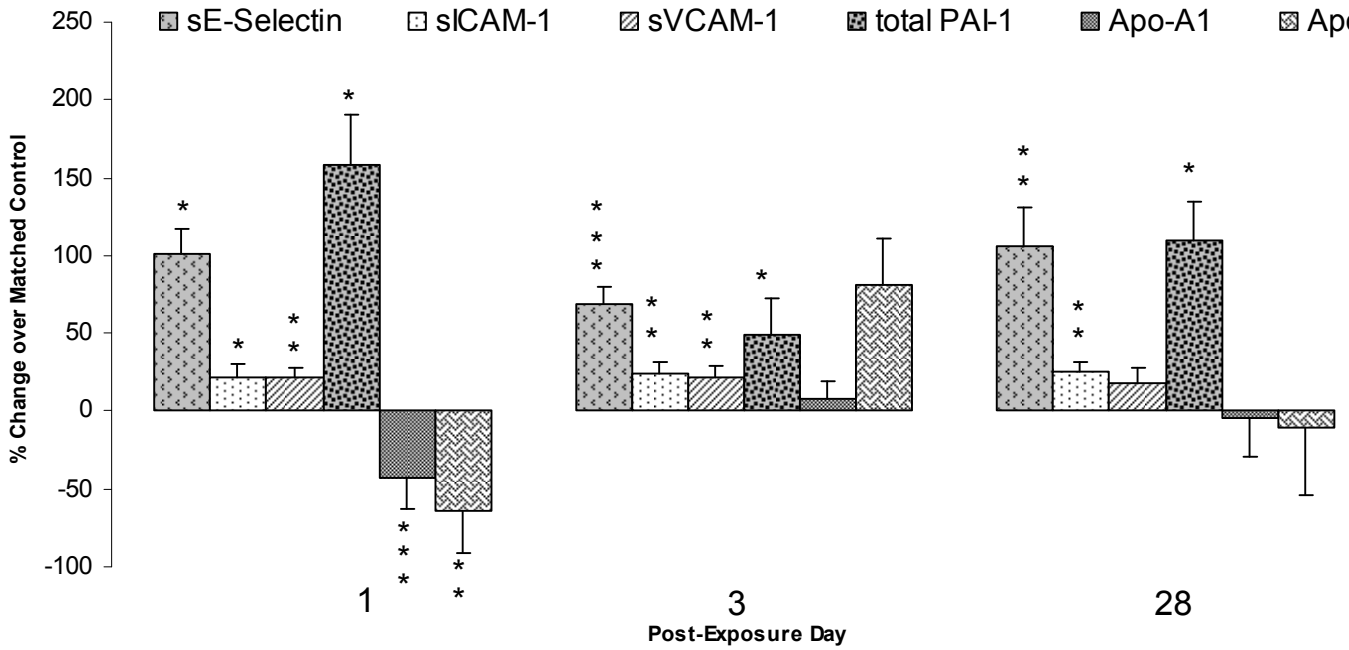

Figure 5.2. Plasma concentrations of sE-Selectin, sICAM-1, sVCAM-1, total PAI-1, Apo-A1 and Apo-E in mice exposed to 0.162 mg Printex 90 CBNP (subset 2), relative to vehicle exposed controls (top) on post-exposure days 1, 3 and 28, with percent change over matched control (bottom).

CHAPTER 6: GENE EXPRESSION PROFILING TO IDENTIFY POTENTIALLY RELEVANT DISEASE OUTCOMES AND SUPPORT HUMAN HEALTH RISK ASSESSMENT FOR CARBON BLACK NANOPARTICLE EXPOSURE

In preparation for peer-review: Bourdon, JA, Williams, A, Kuo, B, Moffat, I, White, PA, Halappanavar, S, Vogel, U, Wallin, H and Yauk, CL.

6.1 Abstract

New approaches are urgently needed to evaluate the potential hazards posed by exposure to nanomaterials. Gene expression profiling provides information on potential modes of action and human relevance, and tools have recently become available for pathway-based quantitative risk assessment. In this study, we explore the utility of toxicogenomics in human health risk assessment, using published gene expression data from C57BL/6 mice acutely exposed to 18, 54 and 162 μg Printex 90 carbon black nanoparticles (CBNP). Analysis of CBNP-perturbed pathways, networks and transcription factors revealed concomitant changes in predicted phenotypes (e.g., pulmonary inflammation and genotoxicity), that correlated with dose and time. Benchmark doses (BMDs) for apical endpoints were comparable to minimum BMDs for relevant pathway-specific expression changes. Comparison to inflammatory lung disease models (i.e., allergic airway inflammation, bacterial infection and tissue injury and fibrosis) and human disease profiles revealed that induced gene expression

changes in Printex 90 exposed mice were similar to those typicical for pulmonary injury and fibrosis. Very similar fibrotic pathways were perturbed in CBNP-exposed mice and human fibrosis disease models. Our synthesis demonstrate how toxicogenomics profiles may be used in human health risk assessment of nanoparticles and constitute an important step forward in the ultimate recognition of toxicogenomic endpoints in human health risk. As our knowledge of molecular pathways and their biological significance, dose-response characteristics and relevance to human disease continues to grow, we anticipate that toxicogenomics will become increasingly useful in assessing chemical toxicities and in human health risk assessment.

6.2 Introduction

Chronic inhalation of fine and ultrafine particulate matter has been associated with adverse pulmonary effects including fibrosis and cancer, as well as exacerbation of existing conditions such as asthma, bronchitis and chronic obstructive pulmonary disorder (Bonner 2007; Knaapen et al. 2004), in addition to cardiovascular disease (Dockery et al. 1993; PopeIII et al. 2004). Human exposure to manufactured nanomaterials (NMs), which have at least one size dimension that is less than 100 nm, may constitute an increased risk of adverse effects especially following inhalation exposure, and their potential to induce toxic effects is poorly understood (Handy and Shaw 2007). Moreover, the human health risks associated with inhalation exposure have not been adequately

investigated. Methods that can be effective in screening for NM toxicities are paramount, due to the countless variations in physical and chemical properties NPS in terms of size, shape, agglomeration and surface coatings.

Traditional assays used in human health risk assessment (HHRA) generally involve chronic and subchronic rodent exposures with concomitant analyses of tumor induction (e.g., two-year rodent cancer bioassay), in addition to various non-cancer endpoints, the most sensitive of which is used for regulatory decision-making (Meek et al. 1994). These approaches form the foundation of the chemical regulatory system and have been invaluable for HHRA. However, some of these assays, such as those based on chronic animal exposures at the maximum tolerated dose, are time and resource intensive, thus limiting broad application (Suter et al. 2004). Recent discussions have identified gene expression profiling as a potentially rapid and cost-effective approach for identifying and assessing prospective hazard, characterizing chemical (or particle) mode of action, and assessing human relevance in support of HHRA (National Academy of Sciences 2007). In order for gene expression data to become accepted for routine use in HHRA, it is necessary to demonstrate that mRNA/protein expression profiles can effectively predict the modes of action and biological outcomes of exposure at relevant doses, and to confirm that these data can be used to strengthen the foundation for HHRA and regulatory decisions. In this regard, it has been hypothesized that gene expression profiling

will be extremely useful in identifying effects at low doses, and moreover, useful for distinguishing between doses that elicit an adaptive response versus those that yield adverse effects (Boverhof and Zacharewski 2006). To date, the application of gene expression profiling in regulatory toxicology has largely focused on qualitative identification of chemical modes of action and transcription biomarkers that can predict specific toxicities. However, the utility of gene expression profiling in quantitative determination of threshold values (e.g., benchmark doses) has not yet been rigorously explored (Thomas et al. 2012).

In the present study we investigate the utility of gene expression profiles derived from mice exposed to Printex 90 carbon black nanoparticles (CBNPs) by intratracheal installation to identify potential hazards, modes of action, and doses above which adverse effects may be expected for specific toxicological outcomes. In addition, we quantitatively compare benchmark doses for pathways to those of apical endpoints derived from the same experimental animals. We employ Printex 90 as a model NM due to the rich database of traditional toxicity information on which our findings can be anchored. Briefly, Printex 90 consists almost entirely of carbon, with very low levels of impuritites in terms of polycyclic aromatic hydrocarbons and endotoxins (Bourdon et al. 2012b; Jacobsen et al. 2008; Saber et al. 2011). Printex90 generate reactive oxygen species (Jacobsen et al. 2008), induce DNA strand breaks *in vitro* and *in vivo*

(Jacobsen et al. 2009; Saber et al. 2005) and mutations *in vitro* (Jacobsen et al. 2007) that are associated with oxidative stress (Jacobsen et al. 2011). The data in this study are from previously published experiments investigating Printex 90 CBNP exposure in C57BL/6 mice at various doses (i.e., vehicle, 18, 54 and 162 μg) collected at several time-points (1, 3 and 28 days) following a single acute instillation (Bourdon et al. 2012a). We previously characterized widespread changes in gene expression involving acute phase response and inflammation, supported by concomitant influxes of pulmonary bronchoalveolar lavage cells (BAL) and increases in tissue-specific DNA strand breaks (Bourdon et al. 2012a; Bourdon et al. 2012b). In addition to the examination of BMDs and BMDLs, we compare CBNP-modified gene expression profiles to various models of lung disease in mice and humans reported in the litterature, in order to explore the utility of our data in predicting the potential risk of adverse health outcomes and the human relevance of expression changes. The work demonstrates one approach by which gene expression profiling may be integrated into HHRA to support or predict apical toxicological endpoints, dose-response, and relevance to human diseases.

6.3 Materials and Methods

6.3.1 Summary of Experimental Model and Published Results

Details of the mouse exposures, particle characterization and pulmonary phenotype were previously published in (Bourdon et al. 2012a; Bourdon et al.

2012b). Briefly, female C57BL/6 mice were exposed to a single installation of vehicle or Printex 90 (18, 54 or 162 μg) and sacrificed 1, 3 and 28 days post-exposure (n=6/group). The doses were selected to represent 1, 3 and 9 working days of exposure at the occupational exposure limit of 3.5 mg/m^3 of CB (as established by the Occupational Safety and Health Administration (OSHA) and the National Institute for Occupational Safety and Health (NIOSH))) for a mouse (assuming 1.8 L/h inhalation rate and 33.8% particle deposition in mouse, for an 8 h working day) (Dybing et al. 1997; Jacobsen et al. 2009). Printex 90 CBNPs were characterized and displayed the following properties: 14 nm primary particle size, 295-338 m^2/g BET surface area, 74.2 μg/g PAHs, 142 EU/g endotoxin, polydispersity index of 1, -10.7 mV zeta potential and hydrodynamic diameter peak of 2.6 μm and 3.1 μm according to particle number and volume-size-distribution (Bourdon et al. 2012b).

Analysis of BAL revealed neutrophilic inflammation that was sustained to day 28 at all doses. Tissue-specific genotoxicity as observed by DNA strand breaks that persisted up to day 28 at the two highest doses and FPG-sensitive sites at all doses on day 1 and the highest dose on day 3 (Bourdon et al. 2012b). Whole mouse genome DNA microarray revealed 487 and 81 differentially expressed genes (FDR adjusted *p*-value ≤ 0.1 and fold changes ≥ 1.5) overall in lung and liver, respectively (Bourdon et al. 2012a). The complete microarray dataset is available through the Gene Expression Omnibus at NCBI

(http://www.ncbi.nlm.nih.gov/geo/, Superseries GSE35284, SubSeries GSE35193). This dataset was previously used to examine molecular interactions between lung and liver upon CBNP exposure.

6.3.2 Rank-Based Pathway Analysis

To determine the most affected processes of CBNP exposure, pathway analysis of gene expression data was conducted using a rank based test in R (R Development Core Team 2011) as described in (Alvo et al. 2010). The relative expression for the genes in a pathway was first aligned by subtracting the median expression value for the combined treatment and control groups. These values were then ranked within each subject and the vector of average ranks was calculated for each treatment group. The distance between the two treatments was calculated and a permutation analysis was used to obtain a *p*-value for each pathway. Pathways with $p < 0.05$ were considered significant.

6.3.3 Ingenuity Pathway Analysis

Ingenuity Pathway Analysis (IPA) was employed to examine perturbed networks and pathways, and to identify potential transcription regulators in our dataset, using a data upload cut-off of FDR-adjusted $p < 0.1$ and a fold-change > 1.5. Based on the proportion of differentially expressed genes within a canonical pathway, statistical significance was determined (right-tailed Fisher's exact test). Network generation in IPA was done by overlaying differentially expressed

genes onto global molecular networks and by inter-connecting genes based on experimentally supported molecular relationships. Networks were then ranked according to size and connectivity. In order to substantiate assertions related to transcription factors that may be driving our gene expression patterns, a transcription regulator analysis was conducted. Transcriptional activators and repressors were identified for each condition and given a Z score according to the number and expression levels of down-stream genes. Transcription activators with $Z > 2.0$ or inhibitors with $Z < -2.0$ were identified as significantly affected transcription regulators.

6.3.4 Benchmark Dose (BMD)/Lower Confidence Limit Benchmark Dose(BMDL) Calculation for Apical Endpoints and RT-PCR Data

BMD10 (BMD representing an excess risk of 10% in exposed animals vs. controls) and BMDLs (95% confidence limit) were calculated for apical endpoint data (inflammation and genotoxicity) and for RT-PCR using EPA BMDS 2.2 (Davis et al. 2011). Only data that were statistically above control levels ($p < 0.05$) for at least two of the doses were included. Prior to running the analysis, the data were screened for homogeneity of variance, and then fit against five continuous dose-response models (i.e., hill, polynomial, linear, power and exponential). Goodness of fit > 0.05 and scaled residuals within ± 2.0 was applied as a cut off for selection of the appropriate model, and curves were also inspected visually.

When more than one model was suitable, the one with the lowest Akaike's Information Criterion (AIC) was selected.

6.3.5 BMD/BMDL Calculation for Genomic Data

In order to determine BMDs and BMDLs in gene expression data, BMDExpress was employed (Yang et al. 2007). Briefly, microarray probes with more than one representation on each array were averaged. Analyses were performed on genes that were identified as statistically significant by one-way ANOVA ($p < 0.05$) using the five following models: Hill, Power, Linear and Polynomial 2^o. The models exhibiting a nested chi-square test cut-off of 0.05 with the lowest AIC scores were selected as the best fit. Other settings included maximum iterations of 250, confidence level of 0.95, benchmark factor (BMR) of 1.349, and no restriction on the power. For functional classifications and analyses, the resulting BMD datasets were mapped to KEGG pathways with promiscuous probes removed (probes that mapped to multiple annotated genes). BMDs that exceeded the highest exposure dose (162 μg) were removed from the analysis.

6.3.6 Prediction Analysis for Microarrays

To determine the correlation between gene expression profiles of mice exposed to CBNPs with those of mouse pulmonary disease models, a prediction analysis for microarrays (PAM) (Tibshirani et al. 2002) was conducted in R (R Development Core Team 2011) using the pamr library (Hastie et al. 2011). Data

for this analysis encompassed 13 mouse lung disease models, and were obtained from the National Center for Biotechnology Information Gene Expression Omnibus (accession #GSE4231 and #GSE11037). The samples were labelled as belonging to one of three models of lung inflammation: Bacterial Infection, Lung Injury and Fibrosis, or Th2 Response (allergic airway inflammation). Probes with common GENBANK accessions were collapsed to a single measurement for each sample using the mean. Using the common accession numbers, a prediction model using shrunken centroids was estimated. Cross-validation of the nearest shrunken centroid classifier was conducted to identify an appropriate threshold. A threshold of 2 was selected, yielding a classifier with 753 GENBANK accessions. The means of the nine CBNP treatment conditions were then classified using the estimated prediction model.

6.3.7 Functional Analysis using Inflammatory Lung Disease Models

Functional analysis was conducted to establish molecular perturbations that were in common or discrepant between CBNP exposed mice and inflammatory lung disease models. The analysis was conducted on genes that were common between CBNP and each lung disease model, then again for genes that were unique to CBNP, using a cut-off of FDR-adjusted $p < 0.1$ and a fold-change > 1.5 for all datasets. The less stringent cut-off was employed for disease models because of the low power in several of the datasets. DAVID Bioinformatics Resources 6.7 was used to identify enriched biological functions

from terms with similar genes and biological meaning (Huang et al. 2009a; Huang et al. 2009b). DAVID Biological functions with enrichment scores > 1.3 were considered significant, in accordance with DAVID recommendations (Huang et al. 2009a).

6.3.8 Mining of Public Data Repositories for Disease Prediction

In order to predict potential disease outcomes of relevance to humans, gene expression profiles were mined against genomic data repositories. Disease prediction analysis was done in NextBio (http://nextbio.com) using the high dose exposure profiles as differentially expressed genes were identified at all time-points for this dose. Data from CBNP exposed mice were compared to curated datasets to identify disease studies with similar gene profiles, gene ranking and consistency. Pairwise gene signature correlations and rank-based enrichment statistics were employed in the calculation of NextBio scores for each disease. The disease that ranked highest in comparison with CBNP exposure was given a score of 100, and the rest of the results were normalized accordingly (Kupershmidt et al. 2010). Meta-analysis was performed using select disease models for mice, as well as for human studies representative of disease state. The analysis identified, ranked and scored all genes and biogroups that were common between the studies according to the scoring method described above for disease prediction (Kupershmidt et al. 2010). Biogroups were filtered for canonical pathways.

6.4 Results

6.4.1 Pathway Analysis

The rank-based pathway analysis revealed a total of 149, 150 and 106 differentially expressed KEGG pathways on days 1, 3 and 28, respectively. The most affected pathways were primarily related to inflammation on day 1, to steroid biosynthesis and DNA repair on day 3 and to apoptosis and inflammation on day 28. Significant pathways ($p < 0.05$) pertaining to genotoxicity (DNA damage and repair) and inflammatory and immune responses are summarized in Table 6.1, along with previously established phenotypes. All significant pathways are presented in Supplementary Table SP7. Analysis of the number of common pathways between doses for each time-point revealed that the molecular responses associated with the low doses (e.g., 18 and 54 μg) were also perturbed at the high dose (Figure 6.1).

6.4.2 Network Analysis

IPA analysis of differentially expressed genes (FDR $p < 0.1$ fold-change 1.5) revealed distinct molecular networks for the two highest doses on days 1 and 3 and for the highest dose on day 28 (Supplementary Figure SP4). Day 1 networks were mostly related to inflammatory responses, as well as DNA repair and lipid metabolism. Top canonical pathways included LXR/RXR activation and acute phase response signalling and the central nodes consisted of nuclear

factor kappa B (NFκB) (Supplementary Figure SP4). The most affected networks for day 3 involved lipid metabolism (54 μg) and DNA repair (162 μg), whereas central nodes consisted of tumour necrosis alpha (TNF) and transforming growth factor beta (TGF-β) at the medium and high dose, respectively. Most of the perturbed pathways at this time-point were involved in signalling in transitioning from an acute immune response to adaptive immunity. Day 28 networks and canonical pathways revealed inflammation and signalling to adaptive immunity, in which NFκB was the central node.

6.4.3 Regulators of Transcription

IPA revealed potential activation and inhibition of specific transcription factors in mice exposed to the highest dose of Printex 90 only, on post-exposure days 1 and 3. On day 1, gene expression profiles were indicative of activation of nuclear NFκB, NFκB p105 subunit (NFκB1), enhancer of zeste homolog 2 (EZH2), early growth response protein 1(EGR1), signal transducer and activator of transcription 3 (STAT3) and Notch homolog 1 (NOTCH1). On day 3, transcriptional activation was related to EZH2 and T-box transcription factor 2. Transcriptional inhibition on day 1 was mediated by krueppel-like factor 2 (KLF2), nuclear receptor subfamily 1 group H member 2 (NR1H2), NR1H3, peroxisome proliferator-activated receptor alpha (PPARA), PPAR delta (PPARD), PPAR gamma (PPARG), thyroid hormone receptor alpha (THRA), tumor protein 73 (TP73), forkhead box A2 (FOXA2) and hepatocyte nuclear

factor 4 alpha (HNF4A). Inhibition on day 3 was related to NR1H2, NR1H3, PPARD, FOXA2, nuclear receptor subfamily 3 group C member 1 (NR3C1), cyclin-dependent kinase inhibitor 2A (CDKN2A), transcription factor 3 (TCF3) and SWI/SNF-related matrix-associated actin-dependent regulator of chromatin subfamily B member 1 (SMARCB1). The interaction of these transcriptional regulators with genes that were differentially expressed in CBNP exposed mice is presented in Supplementary Figure SP5.

Because substantial inflammation and DNA strand breaks were observed in the mice, we focused on transcription factors involved in inflammation and DNA damage. NFκB was selected as it was identified as the most significant transcription activator on Day 1, and was often central in the most significant IPA generated networks (Supplementary Figure SP4). Although TP53 was not identified as a significant transcription regulator, it was selected on the basis of being the primary transcription factor involved in the DNA damage responses. IPA revealed that many differentially expressed genes were associated with these two transcription factors. The fifty most significant gene interactions for each of these two transcription factors are shown in Figure 6.2.

6.4.4 BMD and BMDL

EPA BMDS 2.2 BMDs and BMDLs were generated for apical endpoints and RT-PCR data (Table 6.2) (curves are presented in Supplementary Figure

SP6). Although many of the apical endpoints and RT-PCR data were not suitable for modelling, BMD and BMDL values generally increased over post-exposure time as expected. The mean BMDs for inflammatory apical endpoints were 0.9, 1.2 and 9.6 μg, and BMDLs were 0.6, 0.9 and 6.5 μg on days 1, 3 and 28 respectively. BMD values for RT-PCR data of genes involved in inflammation tended to be higher than for apical endpoints. Mean BMDs of inflammatory genes were 22.5, 16.7 and 29.0 μg, and mean BMDLs were 19.5, 9.1 and 20.1 μg, on days 1, 3 and 28, respectively.

BMDs and BMDLs were also generated for microarray gene expression profiles using BMDExpress. Median BMD and BMDL, and 5th percentile BMD, are presented in Table 6.3, for pathways of relevance to the apical endpoints measured. Even the 5th percentile BMDs tended to be higher than BMDs generated for apical endpoints, with mean values of 33.1, 31.1 and 85.1 μg for inflammatory responses and 37.3, 20.3 and 71.1 μg for genotoxicity, on post-exposure days 1, 3 and 28, respectively. The means for the median pathway BMDs/BMDLs were 89.5/59.1 μg, 73.1/43.8 μg and 108.7/64.9 μg for inflammatory pathways, whereas these values for genotoxicity were 94.1/61.5 μg, 74.2/41.7 μg and 59.9/33.6 μg on days 1, 3 and 28, respectively. The lowest median pathway BMDs and BMDLs (values presented in parentheses) were non-small cell lung cancer (4.4 and < 0.0001 μg) on day 1, aminophosphonate

metabolism (0.2 and < 0.0001 μg) on day 3 and glycine, serine and threonine metabolism (< 0.0001 and < 0.0001 μg) on day 28.

Distribution of the most sensitive BMDs and BMDLs (minimum BMDs and BMDLs, representing the most sensitive gene within the pathway) for pathways involved in inflammation and genotoxicity are compared with BMD and BMDL values generated for apical endpoints (apical endpoint data presented in table 6.2) (Figure 6.3). BMD and BMDL values for apical endpoints of inflammation generally fell within the upper quartile except on day 1 which exceeded the 75th percentile. Genotoxicity BMDs all fell within the lower quartile, whereas the comparison of genotoxicity apical endpoint data (DNA strand breaks) to pathway minimum BMDL distribution was much more varied. The data indicate that apical endpoint BMDs and BMDLs are relatively comparable to minimum BMDs and BMDLs generated for relevant pathways.

6.4.5 Prediction Analysis for Microarray

PAM was used to compare the Printex 90 gene expression dataset to 13 pulmonary gene expression profiles that represent a range of murine pulmonary disease models (e.g., transgene over-expression, treatments with infectious agents, toxic chemicals and allergens) as described in (Lewis et al. 2008; Thomson et al. 2012). The models were classified according to the three following sub-

groups: 1) bacterial infection, 2) lung injury and fibrosis, and 3) Th2 response (allergic airway inflammation).

Clustering of the models using PAM is shown in Figure 6.4A. Two CBNP exposure conditions (day 28 low and medium doses) did not cluster with other CBNP exposure condition or other disease models, likely due to lack of response. Models of bacterial infection did not cluster with other disease models or CBNP exposure. PAM analysis revealed an association between CBNP exposure, Th2 responses and lung injury/fibrotic responses. Although Th2 response and lung injury/fibrotic responses were more closely associated with one another than with CBNP exposure, PAM analysis revealed that CBNP exposure was more closely related to lung injury/fibrotic responses than to Th2 responses, which is also supported by probability statistics comparing CBNP exposure with each disease sub-group (Figure 6.4B).

6.4.6. Functional Analysis

In order to examine commonalities and discrepancies between disease models and CBNP exposure in more detail, functional analysis was conducted on 1) genes that were in common between CBNP and each disease model and 2) genes that were unique to CBNP. The number of significant genes used for each analysis is presented in Supplementary Table SP8. The DAVID biological functions are summarized in Table SP9. This analysis demonstrates that

inflammation was common between most models at all time-points (excluding Aspergillus extract). On day 1, commonalities for CBNP exposure were observed with bacterial infection models (i.e., due to the acute phase response) and with injury and fibrosis models (i.e., due to changes in tissue morphogenesis related genes). Day 3 revealed inflammation and cell cycle disturbances in most of the models. However, CBNP responses were more similar to bleomycin-induced lung injury as shown by the high degree of overlapping biological functions on day 3 (Table 6.3). CBNPs triggered an adaptive immune response on day 28 that was only also apparent in lung injury and fibrosis models. Complete information on significant biological functions identified in DAVID (score > 1.3) is presented in Supplementary Table SP9.

6.4.7 Disease Prediction

Gene expression profiles from the high dose CBNP-exposed mice versus control were analyzed in NextBio to identify closely-related respiratory disease profiles. On all post-exposure days, severe acute respiratory syndrome (SARS), congenital cystic adenomatoid malformation, and injury of lung, were identified as the top three respiratory diseases associated with CBNP exposure. Scores for all significant diseases identified are presented in Supplementary Table SP10. Interestingly, fibrosis was identified as a predicted disease outcome of CBNP exposure that increased considerably with time (e.g., score of 14 on day 1, 35 on day 3 and 45 on day 28). In order to examine the molecular mechanisms that may

be involved in fibrosis in more detail, a meta-analysis was completed using curated studies within NextBio that identified fibrosis as a phenotype. Meta-analysis in mouse employed 36 models that included fibrosis-induced by injury with naphthalene, bleomycin and ganciclovir, doxycycline-induced over-expression, and TGF-β over-expression in a variety of mouse models (wild type, inflammation resistant/susceptible). Meta-analysis using CBNP gene expression profiles in mouse ranked 473 canonical pathways and 21,277 genes present in at least one of the studies on select models of pulmonary fibrosis and lung injury (identified in NextBio disease correlation profiles). In order to establish human-relevance, the analysis was repeated using human studies curated in NextBio. Meta-analysis encompassed 4 studies from lung biopsies of patients affected with fibrosis, with intermediate to severe pulmonary hypertension, pneumonia and exacerbation of idiopathic pulmonary fibrosis. Overall, 472 canonical pathways and 15,795 genes were ranked as present in at least one of the studies.

The top ranked pathways and genes for the mouse and human meta-analyses are presented in Table 6.5. Interestingly, comparison of fold-ranks between the mouse and human analysis revealed that the most affected pathways were the same in both species. However, the genes that were most perturbed during fibrotic responses were considerably different in CBNP-exposed mice compared to human diseases, with the exception of glycerol-3-

phosphate dehydrogenase (*GDP1*), kruppel-like factor 4 (*KLF4*), secreted phosphoprotein 1 (*SPP1*) and ceruloplasmin (*CP*).

6.5 Discussion

It is now widely accepted that toxicity is preceded by, and accompanied by, transcriptional changes, thus providing molecular signatures of direct and indirect toxic effects (Auerbach et al. 2010; Fielden et al. 2011; Gatzidou et al. 2007). It is hypothesized that toxicogenomic profiling can be used as a screening tool to prioritize the specific assays that should be conducted from the standard battery of tests, thus minimizing animal use, cost and time (Dix et al. 2007). Moreover, global analyses of transcriptional changes provide a wealth of information that can be used to identify putative modes of action and to query relevance to human adverse health outcomes (Currie 2012). This type of approach is the general premise of the widely supported paradigm outlined in 'Toxicity Testing in the 21st Century' (National Academy of Sciences 2007). However, substantive work demonstrating the ability of gene expression profiles to identify hazards, to assess risk of exposure via quantitative dose-response analysis, and to identify adverse outcomes associated with specific modes of action is required before these endpoints can be used in HHRA. The present study applies pathway- and network-based approaches, BMD modelling, and disease prediction tools to gene expression data to explore the relationship between apical endpoints and transcriptional profiles. The work investigates the

potential utility of gene expression profiling in determining hazard and mode of action of NPs, in characterizing dose-response relationships and in predicting the relevance of these findings to potential disease-outcomes and human health effects for HHRA.

6.5.1 Hazard Identification, Mode of Action and Prediction of Apical Endpoints

The utility of gene expression profiling in hazard identification has been examined for a limited number of chemicals, including dibutyl phthalate and acetaminophen (Euling et al. 2011; Kienhuis et al. 2011; Makris et al. 2010). Toxicogenomic profiles of alachlor exposure in rat olfactory mucosa (Genter et al. 2002) and dimethylarsenic acid (DMA) exposure in human cultured bladder cells and rat bladder epithelium (Sen et al. 2005; US EPA 2005) have also provided useful information for two final assessments of acetochlor and arsenicals (US EPA 2004; US EPA 2006). Our data demonstrate that gene expression profiles can also be viewed as effective predictors of the biological effects of CBNP exposure. For example, inflammatory responses manifested at the gene expression level and detected using DNA microarrays, which were classified using KEGG pathway analyses (e.g., perturbations in cytokine-cytokine receptor interaction, toll-like receptor signalling), examination of top-ranked molecular networks (e.g., cellular movement, inflammation, immune cell trafficking), and activation of transcription factors involved or affected by inflammation (e.g., *NFκB* and *Stat3*), are for the most part consistent with the observed pulmonary influx of

inflammatory markers (e.g., neutrophils, eosinophils and lymphocytes). The number of genes perturbed and the magnitude of expression changes in these pathways correlates with dose and time. In addition, observed transcriptomic changes associated with perturbations of cell cycle networks, alterations of non-homologous end-joining, and p53 signalling support the sustained genotoxicity observed in the mice, although dose and time correlations were not as apparent (e.g., levels of DNA strand breaks remained relatively constant at the two highest exposure doses (Bourdon et al. 2012b) whereas induction of DNA repair genes increased with dose and time). The transcriptomic changes associated with alterations in glutathione metabolism and free radical scavenging correlate with induction of DNA formamidopyrimidine DNA glycoslase (FPG) sensitive sites (an indicator of oxidative DNA damage) early after the exposure. The persistence of this response is an indication of an adaptive response to oxidative stress in the lungs of the mice. Interestingly, CBNP-induced alterations in gene expression profiles also revealed a pulmonary acute phase response and unexpected changes in lipid homeostasis, which were subsequently supported by measured decreases in plasma high density lipoprotein (HDL) (Bourdon et al. 2012a). The strong association between CBNP-induced gene expression profiles and apical endpoints collectively support the use of toxicogenomics for hazard identification of NMs, and perhaps more importantly, for highlighting unexpected adverse outcomes. Overall, our data suggest that gene expression

profiles can be effectively used to identify putative mode(s) of action and hazards of NP exposure, in the absence of phenotypic data.

6.5.2 Dose-Response Characterization

In addition to identification of hazard, it has been suggested that gene expression profiles may be useful for quantitative assessment (e.g., establishment of reference doses) of responses related to both cancer and non-cancer endpoints (Thomas et al. 2007). Calculation of benchmark doses (BMDs) provide an important measure to quantitatively assess risk of exposure using all characterized doses, when the no observable adverse effect level (NOAEL) is not available (Crump et al. 1995). Because alterations in gene expression can be initiated in the absence of biological effects (e.g., adaptive or stress response pathways effective in mitigating toxic effects), it is expected that BMDLs for genomics endpoints may be too sensitive for use in HHRA. However, analysis of 5 chemicals (i.e., 1,4-dichlorobenzene, propylene glycol mono-t-butyl ether, 1,2,3-trichloropropane, methylene chloride and naphthalene) showed that median BMD and BMDLs for the most sensitive pathways and GO categories were highly correlated with BMD and BMDLs of cancer and non-cancer endpoints (Thomas et al. 2011; Thomas et al. 2012).

In the current study, rather than choosing the most sensitive (i.e., lowest) BMDs, we focussed on the analysis of pathways that were specific to biological

outcomes observed in the mice (i.e., phenotypically anchored), and calculated BMDs for these relevant genes and pathways. Although the pathway-based BMDs and BMDLs calculated here were actually less sensitive than the observed apical endpoints, the minimum BMD and BMDL values were within the appropriate dose range. However, median BMDs and BMDLs for the most sensitive pathways (e.g., non-small cell lung cancer, aminophosphonate metabolism and glycine, serine and threonine metabolism) did correlate more closely with apical endpoints even though the pathways were not necessarily relevant to these endpoints. This finding supports previous examples demonstrating a 1:1 correlation between BMDs for gene expression and apical endpoints (Thomas et al. 2011; Thomas et al. 2012). These data suggest the potential utility of using gene expression profiles in determining acceptable exposure limits for NPs. In order to determine the specific utility of pathway derived BMDs in HHRA, it will be necessary to establish a comprehensive catalogue of pathways that are actually perturbed in the event of specific adverse effects.

6.5.3 Disease Prediction and Relevance to Humans

Perhaps the principal motivation for including gene expression profiling in HHRA is the wealth of information that can be used to identify key events that are correlated with adverse outcomes that are relevant to human disease, and moreover can be used to predict the likelihood of a human disease. Identification

of key events at the transcriptional level can facilitate the identification of processes that are critical for disease initiation and progression, thus allowing information from animal experiments to be queried and used for extrapolation to human scenarios (Edwards and Preston 2008). Comparison of our data with specific models of lung disease, including bacterial infection, airway hypersensitivity and lung injury revealed that CBNPs induced responses that were more closely related to lung injury and fibrosis than to other models. This finding was further supported by comparison of the expression profiles of CBNP exposed mice to those of curated studies of animals and humans exhibiting a myriad of pulmonary disease phenotypes. This analysis demonstrates that CBNP exposure perturbs genes that are known to be involved in tissue injury and fibrosis and that fibrotic pathways are very similar in both mice and humans (52% of the top 50 pathways found were common between mouse and human). Although top-ranked CBNP-related genes involved in fibrosis differed considerably between the species, many of the genes in mice and humans had similar functions, including inflammatory and acute phase responses (e.g., *Saa3*, *Scocs3* and *Mt2* in mice and *CP*, *VNN2* and *CXCL10* in humans), cell cycle progression (*Cdkn1a* in mice and *KLF4* in humans) and bone and tissue modelling (*Mmp14*, *Timp1*, *Eln* and *Ogn* in mice and *SPP1* in humans). Likewise, fibrosis has been identified as an outcome of exposure to various particles and NPs in animals (Bermudez et al. 2004; Shvedova et al. 2008), including Printex 90 (e.g., 28-day nose only inhalation in Wistar WU rats) (Bellmann et al. 2009), as

well as in humans (Lkhasuren et al. 2007; Wang and Christiani 2003). The process of pulmonary fibrosis is closely related to progression of carcinogenic outcome (Hubbard et al. 2000). These data demonstrating very similar fibrotic pathways in mice and humans and a significant overlap with CBNP-induced gene expression changes thus support the use of pathway-based approaches in identifying molecular mechanisms of disease onset and progression, and using gene expression profiles to support HHRA.

6.5.4 Conclusions and Recommendations

This study confirms several key elements that are necessary for the application of gene expression profiling for HHRA of toxicant exposures in general. First, transcriptional profiles can effectively predict the biological effects of chemical exposures. Specifically, in the absence of data for any apical endpoints, our data would have suggested that mice exposed to CBNPs exhibit an inflammatory response, oxidative stress, DNA damage and perturbations in cholesterol metabolism. Second, a comparison of BMDs and BMDLs of relevant pathways and apical endpoints confirms that minimum pathway BMDs and BMDLs are in the same range as those of apical endpoints. Third, that expression profiles can be fairly easily mined to identify potential adverse outcomes (i.e., diseases) that are relevant to humans, and might reasonably be expected to occur in humans exposed to substances that elicit specific gene expression patterns in experimental animals. We believe that our work constitutes a significant step

towards the ultimate recognition of toxicogenomic endpoints for routine assessment of human health risk.

Gene expression profiling offers a promising approach to decipher the largely unknown hazards of NP exposure. Due to the unique properties of NPs, powerful technologies that can assess a multitude of adverse outcome possibilities will be required to decipher their modes of action and potential impacts on human health within a time-frame that is suitable for prompt regulatory decision making. This same premise should hold true for any new chemical products, for which toxicity is largely or completely unknown. In order to establish a strong foundation for the integration of gene expression profiling into HHRA, it will be necessary for the approach employed here to be applied to a variety of additional chemicals/particles that span a wide range of toxicological potencies and modes of action, and using a variety of experimental designs (e.g., multiple doses and time-point). As our knowledge of molecular pathways, and of the diverse tools used to decipher their biological significance, dose-response characteristics and relevance to human disease continues to grow, we anticipate that toxicogenomics will become increasingly useful in assessing the toxicological hazards of a wide range of test articles, and by extension, for HHRA.

6.6 Tables and Figures

Table 6.1. Summary of significant KEGG pathways ($p \leq 0.05$) relating to DNA damage and repair pathways and inflammatory and immune responses, established using the rank-based approach in CBNP exposed C57BL/6 mice. Phenotypes established in Bourdon et al., 2012 are presented.

	Day 1			Day 3			Day 28		
	DNA Damage and Repair Pathways	Inflammatory and Immune Response Pathways	Phenotype	DNA Damage and Repair Pathways	Inflammatory and Immune Response Pathways	Phenotype	DNA Damage and Repair Pathways	Inflammatory and Immune Response Pathways	Phenotype
18 ug	Apoptosis	NOD-like receptor signaling	DNA strand breaks; FPG sensitive sites; Neutrophil influx			Neutrophil influx; Eosinophil influx; Lymphocyte influx; Macrophage influx	Apoptosis		Neutrophil influx
54 ug	Nucleotide Excision Repair; Glutathione metabolism	NOD-like receptor signaling; Toll-like receptor signaling; Cytokine-cytokine receptor signaling; Antigen processing and presentation	DNA strand breaks; FPG sensitive sites; Neutrophil influx	Homologous recombination; Base excision repair; Cell cycle; p53 signaling; Nucleotide excision repair; Non-homologous end-joining	T Cell receptor signaling; Hematopoietic cell lineage; MAPK signaling; Antigen processing and presentation; Toll-like receptor signaling; NOD-like receptor signaling; Jak-STAT signaling; B cell receptor signaling	DNA strand breaks; Eosinophil influx; Lymphocyte influx	Apoptosis		DNA strand breaks; Eosinophil influx; Lymphocyte influx
162 ug	Glutathione metabolism; Mismatch repair; Cell cycle; Nucleotide excision repair; Homologous recombination; Non-homologous end-joining; Base excision repair; p53 signaling	NOD-like receptor signaling; Antigen processing and presentation; Cytokine-cytokine receptor interaction; Toll-like receptor signaling; T cell receptor signaling; Hematopoietic cell lineage; Jak-STAT signaling; MAPK signaling; Chemokine signaling; B cell receptor signaling	DNA strand breaks; FPG sensitive sites; Neutrophil influx	Homologous recombination; Glutathione metabolism; Cell cycle; Mismatch repair; Nucleotide excision repair; Base excision repair; Non-homologous end-joining; p53 signaling	Antigen processing and presentation; NOD-like receptor signaling; Hematopoietic cell lineage; Cytokine-cytokine receptor interaction; Jak-STAT signaling; Toll-like receptor signaling; Chemokine signaling pathway; Complement and coagulation cascades	DNA strand breaks; FPG sensitive sites; Neutrophil influx; Eosinophil influx	Glutathione metabolism; Non-homologous end-joining	NOD-like receptor signaling; Cytokine-cytokine receptor interaction; Jak-STAT signaling; Antigen processing and presentation; B cell receptor signaling; Toll-like receptor signaling; Hematopoietic cell lineage	DNA strand breaks; Neutrophil influx; Lymphocyte influx

Table 6.2. BMD and BMDL for apical endpoints and RT-PCR confirmed gene expression involved in inflammation and DNA damage responses. Apical endpoints were modelled according to hill (HL), polynomial (PL), power (PW), linear (LN) and exponential models and the best model was selected for determination of BMD/BMDL. Only data that were significant for at least two doses and with appropriate fit for modelling ($p \geq 0.05$) are reported.

	Day 1				Day 3				Day 28			
	model	Goodness of Fit	BMD (µg)	BMDL (µg)	model	Goodness of Fit	BMD (µg)	BMDL (µg)	model	Goodness of Fit	BMD (µg)	BMDL (µg)
Pulmonary Inflammation												
Neutrophil Influx	PL	>0.1	0.5	0.3	PL	>0.1	1.8	1.2	PW	>0.1	3.7	2.2
Eosinophil influx					HL	>0.1	0.6	0.6				
Lymphocyte influx									PL	>0.1	15.5	10.7
Total BAL Cell influx	PL	>0.1	1.3	0.8								
Saa3	PW	>0.05	0.3	0.2	LN	>0.1	3.8	2.7	PW	>0.1	33.2	21.7
Il6	LN	>0.1	32.5	23.6	PL	>0.1	22.5	11.8				
Cxcl5	HL	>0.1	46.6	46.6	PL	>0.1	15.6	7.0				
Tnf									LN	>0.05	24.7	18.4
Il1r2	PL	>0.1	10.7	7.4								
Cxcl1					PL	>0.1	13.5	8.9				
Ccl2					PL	>0.05	12.4	8.3				
Ccl7					LN	>0.05	25.9	8.3				
Ccl17					PL	>0.1	15.1	9.7				
Cxcl10					LN	>0.1	25.1	15.7				
Genotoxicity												
DNA strand breaks	HL	>0.1	< 0.0001	< 0.0001	PL	>0.1	4.5	3	PL	>0.1	2.4	1.6

Table 6.3. Median BMD, 5th percentile BMD and median BMDL for KEGG pathways involved in inflammation and DNA damage response. Analyses were performed on genes that were significant by one-way ANOVA ($p \leq 0.05$) using the five following models: Hill, Power, Linear and Polynomial 2^{o}. BMDs with goodness of fit < 0.05 or that exceeded the highest exposure dose (162 µg) were removed from the analysis.

	Day 1				Day 3				Day 28			
	% Genes BMD p >0.05	BMD Median (µg)	BMD 5th Percentile (µg)	BMDL median(µg)	% Genes BMD p >0.05	BMD Median (µg)	BMD 5th Percentile (µg)	BMDL median(µg)	% Genes BMD p >0.05	BMD Median (µg)	BMD 5th Percentile (µg)	BMDL median(µg)
Pulmonary Inflammation												
Antigen processing and presentation	22.0	33.6	26.1	19.0	18.3	120.8	66.3	78.5	13.4	108.5	95.4	70.7
B cell receptor signaling pathway	18.2	112.8	27.7	73.6	24.2	46.0	12.9	22.2	21.2	116.4	80.5	65.1
Complement and coagulation cascades	20.0	45.1	23.9	30.6	11.4	74.0	28.0	46.6	20.0	109.5	88.1	71.3
Cytokine-cytokine receptor interaction	25.8	96.2	28.1	65.4	18.5	33.2	25.6	19.3	18.0	113.0	73.7	65.1
Hematopoietic cell lineage	26.2	118.0	55.7	76.1	28.6	107.6	20.2	72.1	15.5	89.5	74.6	61.1
Jak-STAT signaling pathway	20.8	94.6	27.3	64.5	13.9	44.5	30.2	21.6	10.4	97.9	94.8	62.3
Leukocyte transendothelial migration	17.7	111.9	48.6	73.3	12.4	40.0	34.6	14.1	11.5	77.7	73.0	54.6
MAPK signaling pathway	16.5	101.7	31.3	68.3	15.3	103.1	39.3	66.5	10.2	143.7	131.2	72.2
T cell receptor signaling pathway	17.0	105.1	44.4	69.9	22.3	116.6	29.1	76.5	17.0	116.4	59.0	58.6
Toll-like receptor signaling pathway	29.2	75.8	17.5	50.6	21.9	45.0	24.3	20.4	15.6	114.6	81.0	67.8
Genotoxicity												
Apoptosis	18.5	31.9	22.2	18.5	25.9	43.2	19.6	21.5	12.4	80.7	57.5	37.2
Base excision repair	27.3	118.1	27.5	76.2	24.2	30.7	7.6	3.5E-04	n/a	n/a	n/a	n/a
Cell cycle	25.9	99.1	12.5	66.3	13.9	115.4	37.6	75.9	2.8	3.4E-04	n/a	3.4E-04
Homologous recombination	15.4	124.9	86.3	78.7	3.9	125.4		80.7	n/a	n/a	n/a	n/a
Mismatch repair	28.6	128.6	32.0	80.8	19.1	66.2	28.9	43.1	n/a	n/a	n/a	n/a
Non-homologous end-joining	25.0	72.0	61.8	51.8	41.7	34.2	6.7E-13	7.8E-06	8.3	125.6	125.6	78.6
p53 signaling pathway	21.9	83.7	18.4	58.5	20.3	104.3	28.1	70.4	10.9	33.4	30.2	18.7

na=not available

Table 6.4. Functional analysis of genes that are common between CBNPs and lung disease models ($p \leq 0.1$ and a fold-change ≥ 1.5) (grey) and genes unique to CBNPs for each model (black) for 162 µg exposed mice using DAVID functional annotation clustering.

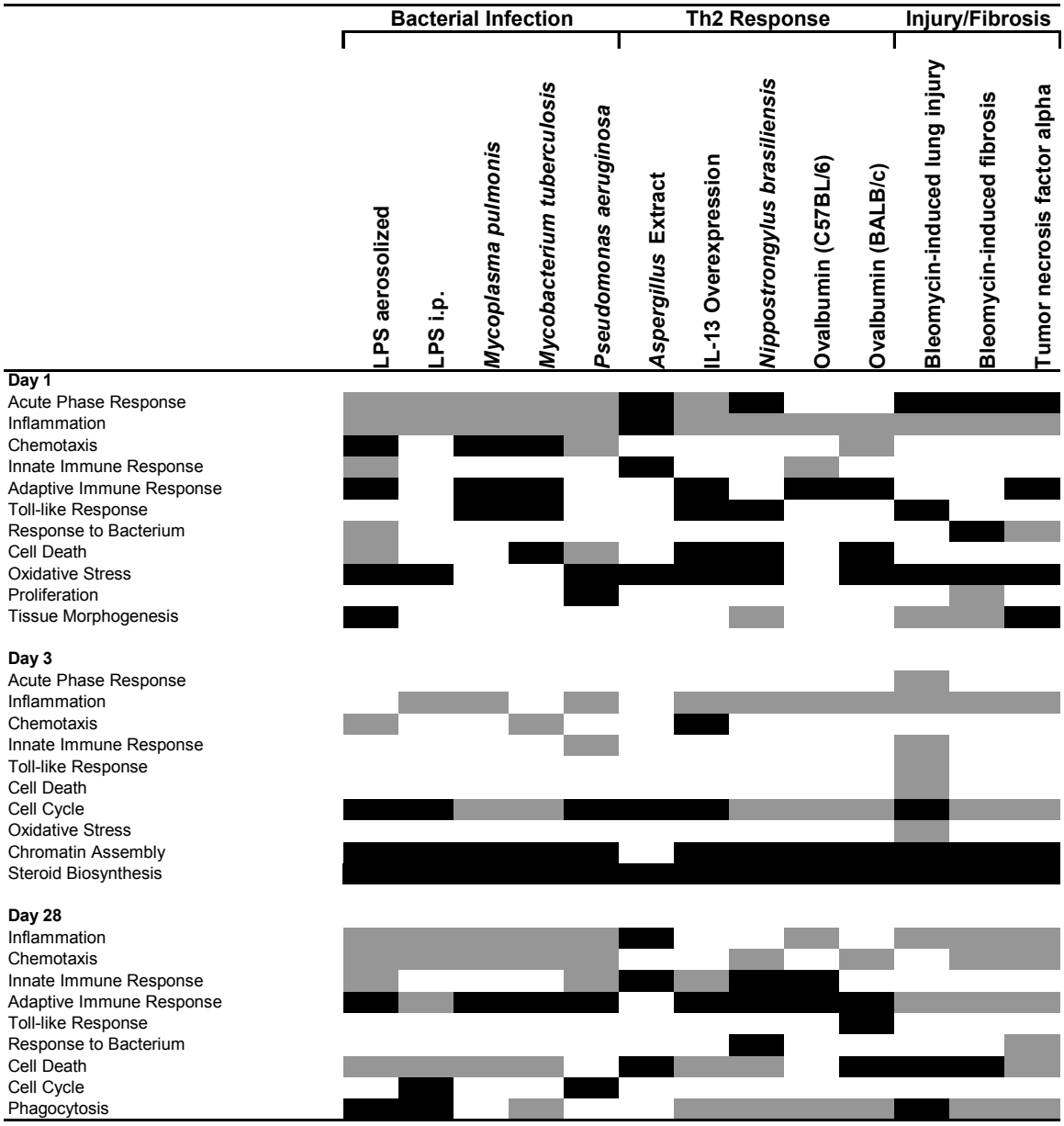

Table 6.5. Meta-analyses of curated studies in NextBio, using mouse or human genomic profiles in which fibrosis was identified as a phenotype. Top 10 ranked canononical pathways (n=473 mouse and n=472 humans) and genes (n=21,277 mouse, n=15,795 human) are presented. Values in parentheses represent ranking for the other meta-analysis (mouse or human).

Rank 1 (Rank 2)	Pathway	Rank 1 (Rank 2)	Gene (Symbol)
Mouse			
1 (1)	Cytokine cytokine receptor interaction	1 (698)	cyclin-dependent kinase inhibitor 1a (*Cdkn1a*)
2 (13)	p53 signaling pathway	2 (158)	matrix metalloproteinase 14 (*Mmp14*)
3 (28)	focal adhesion	3 (2353)	tissue inhibitor of metalloporteinase 1 (*Timp1*)
4 (22)	Cell cycle	4 (535)	metallothionein 2 (*Mt2*)
5 (2)	Toll-like receptor signaling pathway	5 (786)	thymidine kinase 1 (*Tk1*)
6 (15)	Cell communication	6 (2936)	osteoglycin (*Ogn*)
7 (29)	ECM Receptor interaction	7 (-)	elastin (*Eln*)
8 (16)	Cell cycle G1 to S reactome	8 (594)	suppressor of cytokine signaling 3 (*Socs3*)
9 (19)	Cell cycle G1/S checkpoint	9 (273)	lysloxidase (*Lox*)
10 (3)	Hematopoitic cell lineage	10 (491)	serum amyloid a3 (*Saa3*)
Human			
1 (1)	Cytokine cytokine receptor interaction	1 (1001)	mucin 4 (*MUC4*)
2 (5)	Toll-like receptor signaling pathway	2 (652)	glutathione S-transferase alpha 1 (*GSTA1*)
3 (10)	Hematopoitic cell lineage	3 (56)	Kruppel-like factor 4 (*KLF4*)
4 (17)	Erythrocyte differentiation pathway	4 (4161)	golgi membrane protein 1 (*GOLM1*)
5 (14)	IL-1R Pathway	5 (48)	glycerol-3-phosphate dehydrogenase 1 (*GPD1*)
6 (12)	Calcineurin Nf At Signaling	6 (1366)	spermatogenesis associated, serine-rich 1 (*SPATS2L*)
7 (26)	Local acute inflammatory response pathway	7 (76)	secreted phosphoprotein 1 (*SPP1*)
8 (27)	Cytokines and Inflammatory pathway	8 (620)	chemokine (C-X-C motif) ligand 10 (*CXCL10*)
9 (21)	MMP cytokine connection	9 (89)	ceruloplasmin (*CP*)
10 (30)	Msp/RON Receptor Signaling Pathway	10 (-)	vanin 2 (*VNN2*)

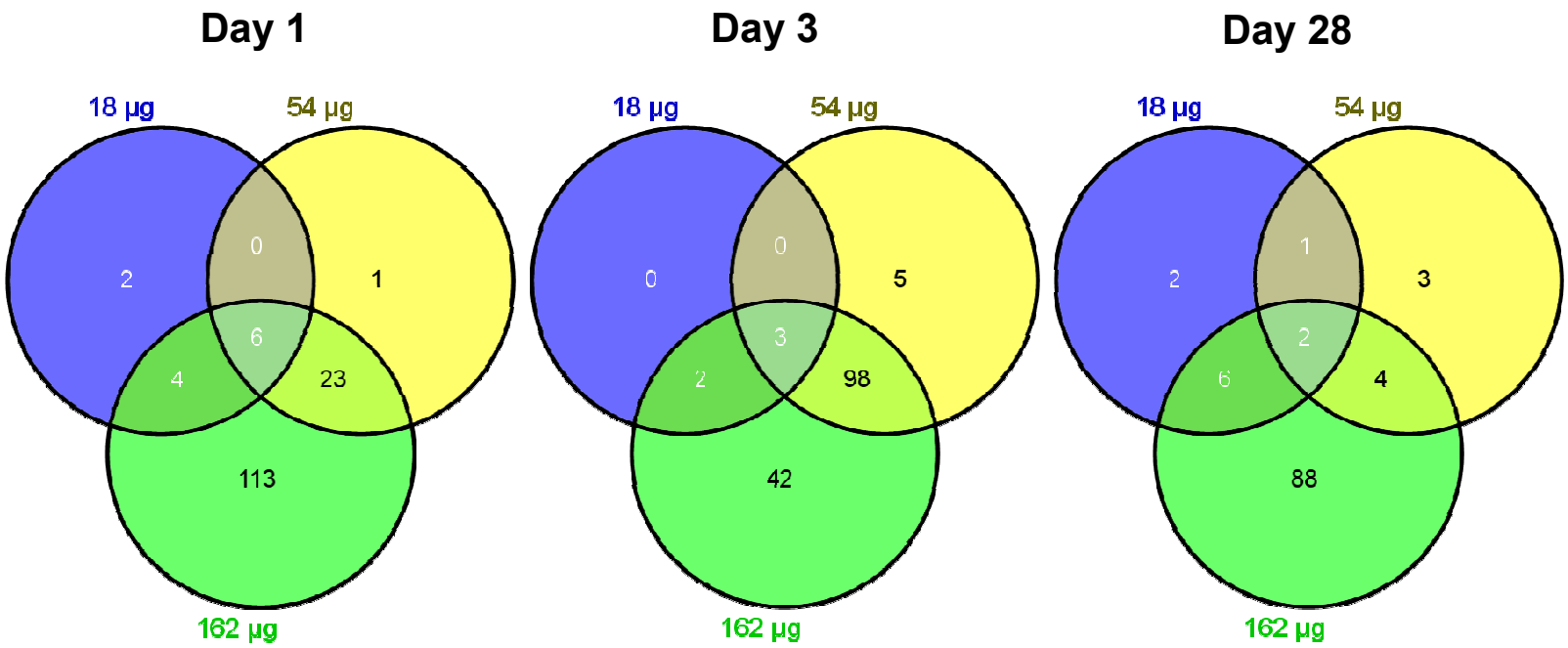

Figure 6.1. Venn diagrams illustrating overlap of significant pathways ($p \leq 0.05$) according to dose, for each post-exposure day (1, 3 and 28 days) in C57BL/6 mice exposed to CBNPs.

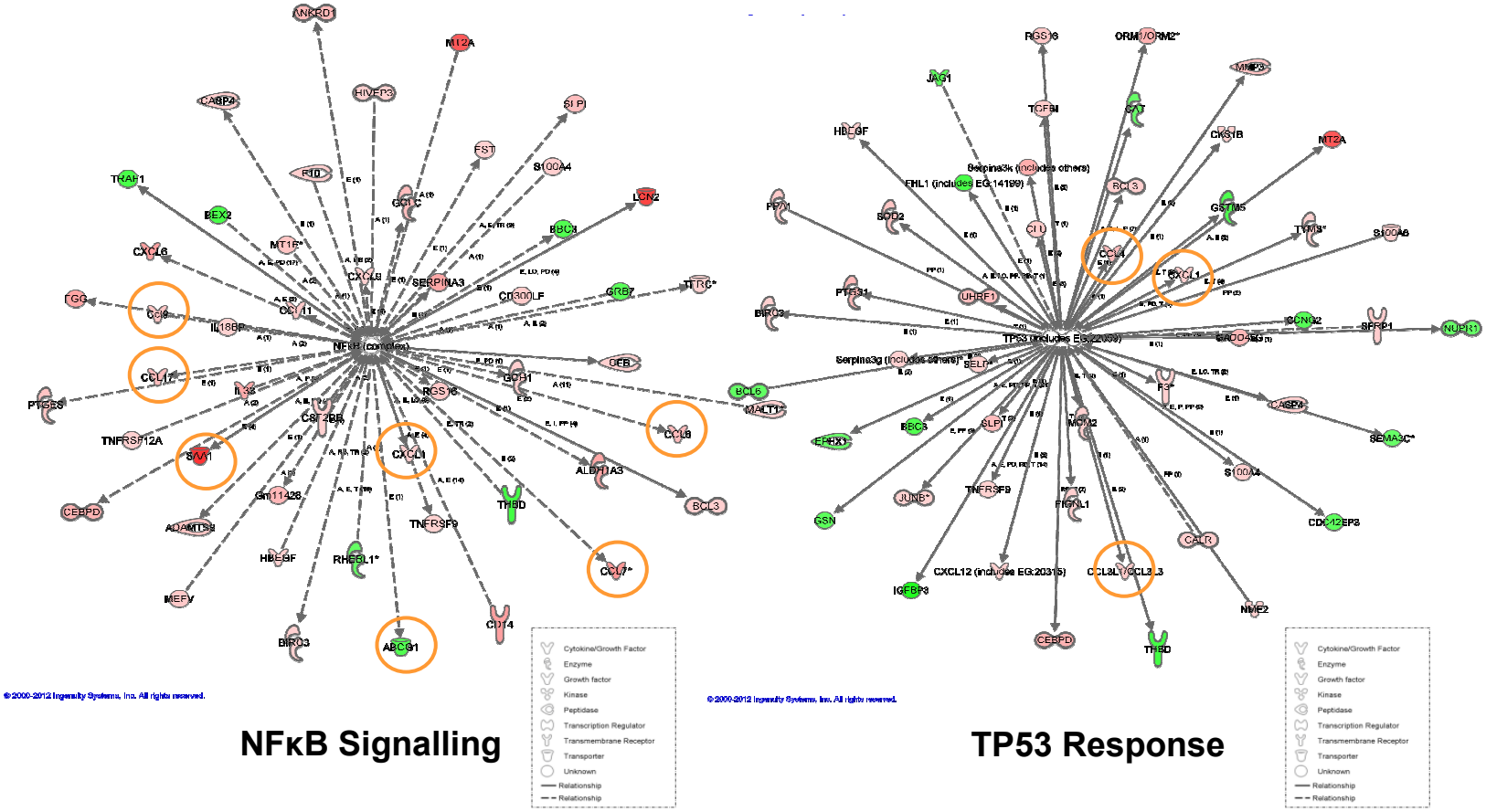

Figure 6.2. Top 50 most significant gene interactions (FDR $p < 0.1$ and fold-change > 1.5) up-stream and down-stream of NFκB and TP53. Genes coloured in red are up-regulated whereas genes in green are down-regulated. Intensity of the colour refers to more substantive fold-changes. Direct relationships are presented by solid lines and indirect relationships by dashed lines. Genes circled in yellow were validated by RT-PCR.

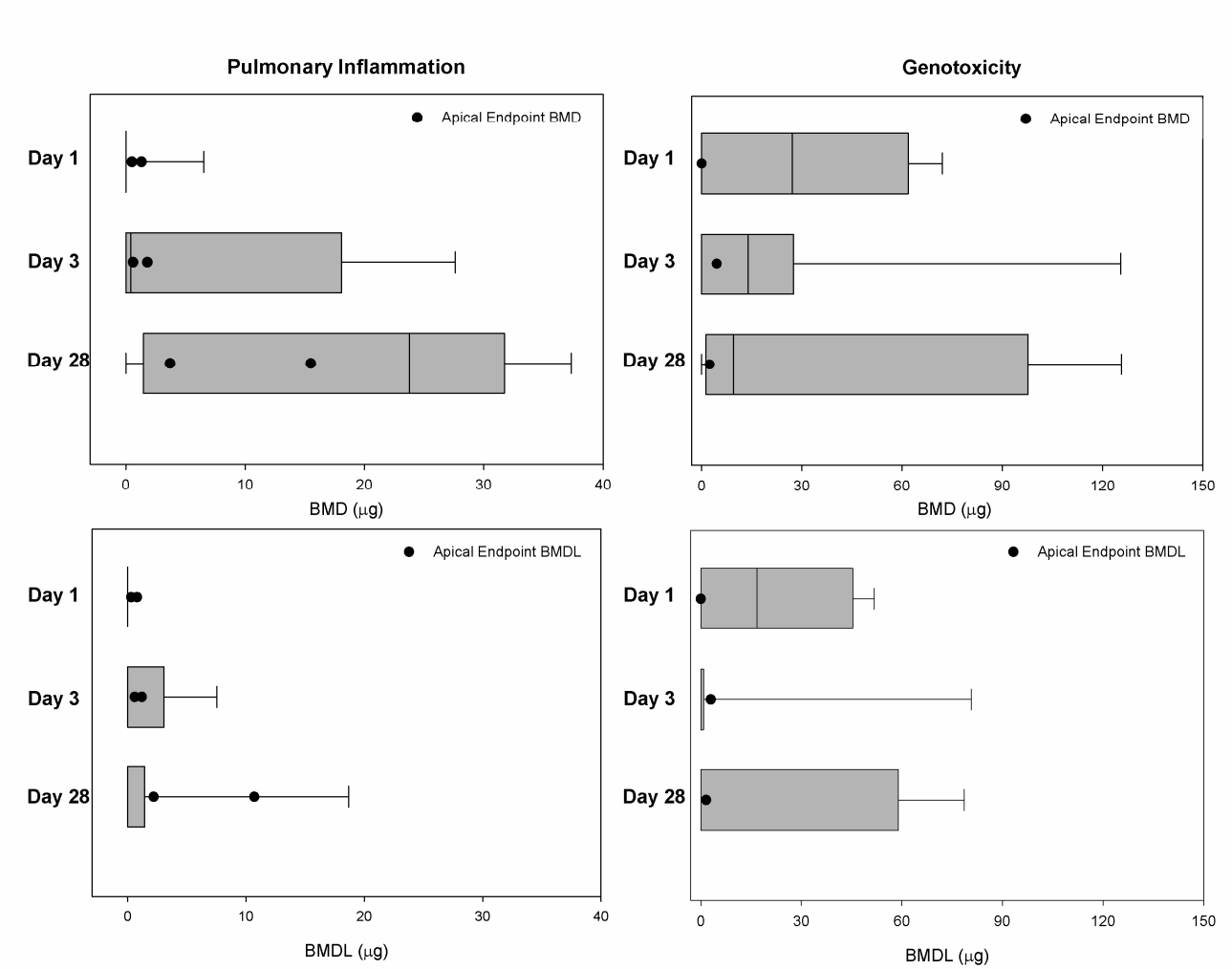

Figure 6.3. Box plots representing distribution of minimum BMD and minimum BMDL values for pathways relevant to pulmonary inflammation and genotoxicity. Relevant apical endpoint BMD and BMDL values are superimposed (inflammatory cell influx for pulmonary inflammation and DNA strand breaks for genotoxicity).

A)

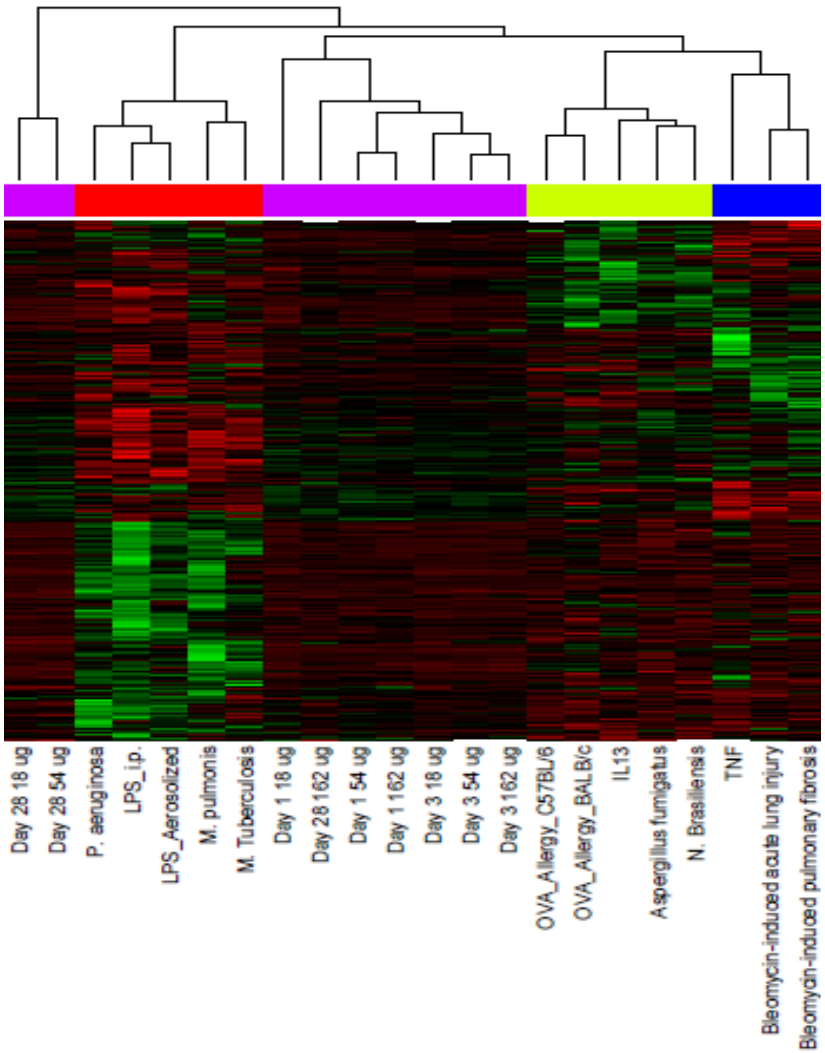

B)

Groups	Predicted Class	Bacterial Infection	Bleomycin Injury	Th2 Response
Day 1 18 µg	Bleomycin Injury	0.000	1.000	0.000
Day 1 54 µg	Bleomycin Injury	0.000	1.000	0.000
Day 1 162 µg	Bleomycin Injury	0.000	1.000	0.000
Day 3 18 µg	Bleomycin Injury	0.000	0.999	0.001
Day 3 54 µg	Bleomycin Injury	0.000	0.997	0.003
Day 3 162 µg	Bleomycin Injury	0.000	1.000	0.000
Day 28 18 µg	Th2 Response	0.000	0.123	0.877
Day 28 54 µg	Bleomycin Injury	0.000	0.964	0.036
Day 28 162 µg	Bleomycin Injury	0.000	1.000	0.000

Figure 6.4. PAM using mouse gene expression profiles from 13 lung disease models and CBNP exposed mice. A) Represents clustering of 753 genes as selected by a PAM threshold cut-off of 2. Sample are classified according to CBNP exposure (purple), Th2 response (yellow), injury and fibrosis (blue) and bacterial infection (red). B) Represents the probability statistics comparing CBNP exposure for each disease sub-group.

CHAPTER 7: RESEARCH SUMMARY AND CONCLUSIONS

7.1 Hypothesis Testing and Summary of Study Outcomes

The overall objectives of this thesis were to employ systems biology to 1) examine NP mode of action and to determine the relationship between molecular pathways and more conventional toxicity assessment endpoints; 2) elucidate molecular signalling cascades and impacts on non-targeted tissues; and 3) query the biological relevance of the observed responses to human diseases, and to determine the utility of systems biology endpoints in qualitative and quantitative human health risk assessment. The outcomes of the specific hypotheses tested are briefly described for each experimental chapter below.

Chapter 2

Hypotheses: Intratracheal instillation of CBNPs causes *in vivo* pulmonary inflammation and genotoxicity that is associated with oxidative stress. Genotoxicity extends to hepatic tissue.

Outcome: These hypotheses were supported. Pulmonary exposure to CBNPs caused *in vivo* lung inflammation, as shown by a persistent influx of polymorphonuclear cells that was dominated by neutrophils at all doses and time-points. Genotoxicity was sustained in lung following exposure, as shown by DNA strand break induction in lung tissue (all doses on day 1, and two highest doses on days 3 and 28) and isolated bronchoalveolar lavage cells (at least at the

highest dose on all post-exposure days). The results of the formamidopyrimidine DNA glycosylase comet assay supported the role of oxidative stress as a mediator of DNA damage (all doses on day 1 and highest dose on day 3). Genotoxicity extended to the liver, as shown by DNA stand break induction (all doses on day 1 and day 28).

Conclusions: CBNP exposure causes persistent inflammation and sustained genotoxicity in the lungs of exposed mice. Oxidative stress participates in pulmonary genotoxic effects. DNA strand breaks extend to secondary tissue (i.e., the liver).

Chapter 3

Hypothesis: CBNP-induced transcriptional changes occurring in the lung initiate signalling cascades that regulate molecular pathways in the liver.

Outcome: This hypothesis was supported. Inflammatory and acute phase responses (APR) were initiated in the lungs as shown by induction of various genes including *Saa1* and *Saa3*. These molecular changes were associated with changes in plasma protein profiles measured at the high dose including increased serum amyloid A (days 1 and 28) and decreased high density lipoprotein (days 3 and 28). Plasma changes were associated with up-regulation of the 3-hydroxy-3-methylglutaryl-coenzyme A (HMG-CoA) reductase pathway in liver by induction of genes including *Hmgcr*, *Sqle*, *Fdps* and *Dhcr7* at the

highest dose on day 1 and at all doses on day 28. A modest increase in plasma low density lipoprotein was observed on day 28.

Conclusions: Pulmonary exposure to CBNPs results in APR-mediated systemic effects in plasma and liver of exposed mice that perturb cholesterol homeostasis and that suggest probable adverse cardiovascular effects.

Chapter 4

Hypotheses: Changes in miRNA expression occur upon CBNP exposure. These miRNAs mediate transcriptional responses in the lungs of exposed mice.

Outcome: The first hypothesis was supported. CBNP-induced differential miRNA expression in the lungs using two separate mouse models (dams and non-pregnant female mice). Non-pregnant females exhibited large up-regulation of miR-135b that increased over post-exposure time-point (up to 84 fold over control on day 28), whereas more conservative changes in miR-146b and miR-21 were observed on days 3 and 28. Dams exhibited increased miR-135b at weaning (26-27 days post-exposure). However, the second hypothesis concerning miRNA involvement in transcriptional responses was not supported. Examination of transcriptional profiles over-time did not reveal any temporal patterns that would suggest miRNA regulation of known targets (e.g., *Pten*, *Pdcd4*, *Traf6* and *Irak1*), predicted targets, and pathways targeted by miR-135b, miR-146b or miR-21.

Conclusions: MiR-135b is involved in mediating pulmonary responses to CBNP exposure. However, the precise mechanisms by which it participates in these responses could not be elucidated from transcriptional profiles. Although miRNAs have been shown to act primarily in degradation of mRNA targets within mammalian systems, it is possible that the complex nature of miRNA function and fate impedes the ability to identify direct targets from gene expression profiles or that targets may differ from those already established or predicted *in silico*.

Chapter 5

Hypotheses: Intratracheal installation of CBNPs causes transcriptional changes in cardiac tissue and systemic inflammation related changes associated with adverse cardiovascular effects in plasma.

Outcome: The first hypothesis concerning cardiac gene and miRNA expression was not supported as neither mRNAs nor miRNAs were differentially expressed in the heart as a result of CBNP exposure (at any of the post-exposure time-points, using the high dose only). Expression changes did not occur despite concomitant changes in lung and liver of the mice and as verified in the hearts of an additional set of mice. However, the second hypothesis concerning alterations in plasma proteins was supported. This included increases in cellular adhesion molecule VCAM-1 (days 1 and 3), ICAM-1 (all days) and E-Selectin (all days),

increases in plasminogen activator inhibitor PAI-1 (all days) and decreases in apolipoproteins Apo-E and Apo-A1 (day 1).

Conclusions: Whole heart gene and miRNA gene expression is releatvely unperterbed by CBNP exposure. Findings in plasma further support the role of indirect mechanisms such as pulmonary inflammation and pulmonary acute phase response in mediating adverse cardiovascular effects.

Chapter 6

Hypotheses: Global gene expression profiles can be used in human health risk assessment of nanoparticles to identify modes of action and to predict biological outcomes of exposure. Expression profiling can also be used to quantitatively assess dose-responses (i.e., by deriving benchmark doses) and to identify potential disease outcomes of relevance to humans.

Outcome: These hypotheses were supported. Analysis of pathways, networks and transcription factors perturbed by CBNP exposure revealed concomitant changes in predicted phenotypes (e.g., pulmonary inflammation and genotoxicity) that correlated with dose and time. Calculation of BMDs for apical endpoints, and for pathways specifically related to these endpoints, revealed that pathway specific minimum BMDs were comparable to their corresponding endpoints. Comparison of our profiles with those of inflammatory lung disease models (i.e., allergic airway inflammation, bacterial infection and tissue injury and fibrosis, using prediction analysis for microarray) and with expression

profiles available in transcriptomic data repositories (i.e., NextBio), suggests an association between CBNP exposure and pulmonary injury and fibrosis. Further characterization of the responses in NextBio, using mouse and human respiratory disease models, revealed very similar fibrotic pathways in both species hypothetically perturbed by Printex 90 exposure.

Conclusions: Gene expression profiling can be useful for human health risk assessment. This study constitutes a step forward in the acceptance of gene expression profiling for regulatory toxicology, but additional studies demonstrating the utility of systems biology will be necessary to fully implement such approaches in routine risk assessments.

7.2 General Conclusions and Contributions to Scientific Knowledge

The results presented in this Ph.D. thesis provide important insight into the utility of systems biology approaches in deciphering toxicant modes of action and in predicting potentially adverse health effects of nanoparticle exposure. Specific contributions are noted as follows:

7.2.1 Systemic Responses to NP Exposure

Studies of NP toxicity have mostly focused on cultured cells or the lungs of exposed rodents (Borm et al. 2006; Seaton et al. 2010). In this thesis, systemic effects of exposure in extra-pulmonary tissues (i.e., liver and heart), as well as plasma, were investigated in detail. We established that pulmonary exposure to

CBNPs causes substantive transcriptomic alterations within lung that are associated with systemic toxicities, as shown by alterations in hepatic gene expression (e.g., HMG-CoA reductase pathway), hepatic genotoxicity and perturbations of plasma lipids (i.e., HDL and LDL) and proteins potentially involved in progression of cardiovascular disease (i.e., ICAM-1, VCAM-1, E-Selectin, PAI-1, Apo-E, Apo-A1). All of these observations are closely associated with the onset of systemic inflammation (Libby et al. 2002). Thus, this work strongly supports chronic inflammation as a driving factor in CBNP-induced systemic toxicities that is mostly relevant to cardiovascular disease. It is important to note that the current poor state of cardiovascular health in industrialized countries, largely due to nutritional choices and lack of exercise, indicates that a large segment of the population is susceptible to development of adverse cardiovascular outcomes. Data reported within this thesis suggest mechanisms by which CBNP inhalation may accelerate the progress of atherosclerosis and adverse cardiovascular outcomes and thus, these susceptibilities must be taken into consideration when evaluating risk of NP exposure.

7.2.2 Dose and Time Response to NP Exposure

Although genotoxicity and inflammation are established modes of action of NP exposure, the relevance of dose and post-exposure time remained to be elucidated. Data within this thesis demonstrate that genotoxicity in lung tissue

occurs at lower doses and is sustained at later time-points than previously documented (Totsuka et al. 2009). Moreover, CBNP intratracheal instillation-induced hepatic genotoxicity was established for the first time. It is interesting that a single exposure resulted in effects that persisted even 28 days post-exposure. These effects included genotoxicity (i.e., in lung, BAL cells and liver), pulmonary influx of inflammatory leukocytes, decrease in plasma HDL, and increases in plasma SAA, PAI-1 and soluble CAMs (i.e., ICAM and E-Selectin). Expression of miRNAs (i.e., miR-135b, miR-21 and miR-146b) actually increased over time after the exposure. These data suggest that the effects of CBNP, even at relatively low doses, are not readily resolved after exposure. Thus, daily exposure in occupational settings, in addition to the likelihood of NP accumulation over-time, suggests that CBNP inhalation may be causing chronic inflammatory responses and ongoing DNA damage, which may be driving adverse health effects of exposure including pulmonary fibrosis and carcinogenesis, and cardiovascular disease. This work demonstrates that exposure corresponding to one day at the occupational exposure limit, and scaled down to a mouse, is sufficient to induce persistent toxicities in lung and liver. Thus, these findings suggest that the current occupational exposure limit (3.5 mg/m^3 TWA) currently in practice for most countries (see Table 1.1) should be revised in order to adequately address human health risks of exposure.

7.2.3 Applications of Toxicogenomics and Systems Biology Data to Human Health Risk Assessment

Although many reports have alluded to the utility of toxicogenomics and systems biology approaches in human health risk assessment (Boverhof and Zacharewski 2006; Currie 2012; National Academy of Sciences 2007; Pennie et al. 2004; Waters and Fostel 2004), only two assessments have concretely integrated gene expression profiles to determine mechanism of action in the weight of evidence analysis: acetochlor (US EPA 2004) and dimethylarsenic acid (US EPA 2006). In order for gene expression profiling to be used in routine regulatory decision-making, it will be necessary to demonstrate how expression endpoints correlate with apical endpoints (concrete measures of toxicity) and to establish precise guidelines for how to use the data. Data within this thesis provide clear evidence of how gene expression can be used to determine mode of action of CBNPs and more importantly, provide evidence of the utility of gene expression profiles in human health risk assessment. We demonstrate that perturbed pathways, networks and transcription factors can effectively predict phenotypes (e.g., pulmonary inflammation and genotoxicity), in a way that is correlated with doses and time. We further demonstrate that BMDs for apical endpoints are comparable to minimum BMDs for relevant pathway-specific expression changes. Furthermore, comparison of pulmonary gene expression profiles to various models of lung disease strongly identified fibrotic pathways as mechanisms of CBNP toxicity of relevance to humans. Ongoing work within the

Organisation for Economic Co-Operation and Development (OECD) is actively developing adverse outcome pathways (AOP) approaches that are expected to provide tangible methods by which systems biology endpoints can be used in human health risk assessment. Toxicogenomics data that examine responses over dose and time in a variety of tissues can be very useful for such applications, as illustrated for CBNP exposure in Figure 7.1. Thus, this work provides clear examples of how toxicogenomic profiles may be used in human health risk assessment of nanoparticles and for chemicals in general. Moreover, the findings lend support to the notion that gene expression profiling can be used to support hazard identification and risk assessment of the large number of chemicals with little to no toxicological data that are part of Health Canada's Chemical Management Plan. These efforts presented in this thesis constitute important steps forward in the ultimate recognition of toxicogenomic endpoints in human health risk assessment.

7.3 Future Directions

This thesis revealed many avenues of research in the fields of nanotoxicology and human health risk assessment that should be explored in further detail. Specific recommendations for future work in these areas are proposed bellow:

- As many effects were observed at low doses of exposure (e.g., DNA strand breaks in lung and liver, FPG-sensitive sites, pulmonary influx of PMN), it

will be important to establish the no observable adverse effect levels (NOAEL) and lowest observable adverse effect levels (LOAEL) for each endpoint. Likewise, many endpoints persisted or were increased on day 28 (e.g., DNA strand breaks in lung and liver, pulmonary influx of PMN, mRNA and miRNA expression). Thus, it will be important to evaluate the duration of these responses. This will require additional exposures using lower doses and extended time-points.

- To more closely mimic human responses and to further support human health risk assessment, it will be necessary to conduct chronic inhalation studies in multiple species and in animals of both sexes.
- Although particle translocation is expected to be minimal, the potential for relocation of CBNPs to extra-pulmonary organs is not addressed in this thesis. Carbon-based particles are especially difficult to quantify within tissues using standard electron microscopy, but certain methods including light extinction techniques (Henderson et al. 1987; Rudd and Strom 1981) can be used in quantifying CBNPs in extra-pulmonary organs. Alternatively, additional exposures using radio-labelled carbon could be used to examine particle translocation (Oberdorster et al. 2002). Moreover, these techniques should be used to investigate lung burdens of CBNPs (e.g., clearance of deposited CBNPs) over post-exposure time-point.
- To identify effects that are specific to the nano-features of the studied particles, it will be important to address toxic effects of dispered particles

in comparison to agglomerated particles. These experiments may be achieved using centrifugation or administration of NPs in various vehicles.

- Data in this thesis suggest that molecular responses initiated in lung can trigger biological responses in extra-pulmonary tissues. Thus, it will be important to extend the analyses to determine what additional tissues that may be impacted by systemic molecular signalling cascades. Although translocation is expected to be minimal, potential NP relocation to systemic circulation, to the gastro-intestinal tract and to brain (i.e., via the olfactory bulb) (Geiser and Kreyling 2010) warrant further toxicological investigations.
- This study investigated whole tissue responses to CBNPs. Follow-up studies should investigate gene expression and toxicities in cells that are focal to specific adverse health outcomes such as cancer (e.g., pulmonary epithelium and hepatocytes) and cardiovascular disease (e.g., vascular endothelium). Thus, it will be important to carry out further investigations on specific cell types isolated by laser capture microdissection.
- This study identified substantive up-regulation of miR-135b. Future work should determine whether miR-135b is a CB-specific response, or whether sustained induction of miR-135b results following any type of particle exposure or inflammatory response. The biological implications of miR-

135b up-regulation should be investigated in detail, using miRNA over-expression and knockout/knockdown experiments.

- Investigations of metabolomic and proteomic profiles and their utility in the human health risk assessment of NPs will be essential to further support integration of systems biology approaches to regulatory toxicology.
- Much more research is needed in the area of integrating toxicogenomics to human health risk assessment. This includes additional studies establishing the correlation between apical endpoints and toxicity pathways identified by gene expression profiles, and thorough evaluations of the accuracy and sensitivity of gene expression profiles in predicting adverse health outcomes. Furthermore, it will be necessary to establish additional collaborations linking the scientific and regulatory communities, in order to work towards routine integration of toxicogenomics and systems biology approaches into human health risk assessment.

7.4 Concluding Remarks

This thesis demonstrates the power of systems biology approaches in deciphering NP modes of action and systemic toxicities, and for human health risk assessment. The work presented herein constitutes an important step

forward in understanding NP toxicities and the eventual acceptance of systems biology approaches in regulatory toxicology.

7.5 Tables and Figures

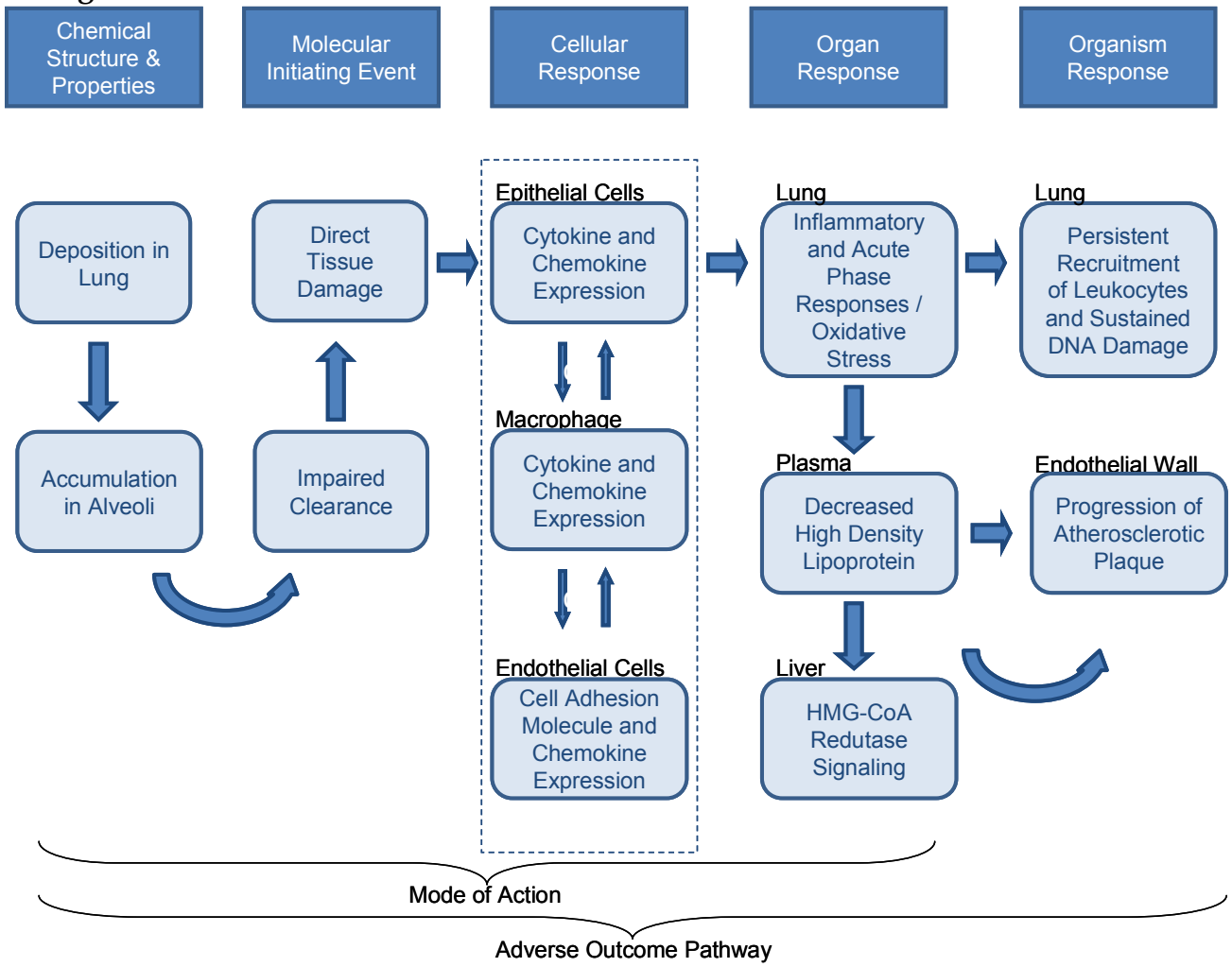

Figure 7.1. Adverse outcome pathway established for CBNP exposure according to OECD guidelines.

REFERENCES

Alvo M, Liu Z, Williams A, Yauk C. 2010. Testing for mean and correlation changes in microarray experiments: an application for pathway analysis. BMC Bioinformatics 11(60).

Annema W, Nijstad N, Tolle M, deBoer JF, Buijs RVC, Heeringa P, vanderGiet M, Tietge JF. 2010. Myeloperoxidase and serum amyloid A contribute to impaired in vivo reverse cholesterol transport during the acute phase response but not group IIA secretory phospholipase A2. Journal of Lipid Research 51:743-754.

Araujo J. 2011. Particulate air pollution, systemic oxidative stress, inflammation, and atherosclerosis. Air Quality, Atmosphere and Health 4:79-93.

Araujo J, Barajas B, Kleinman M, Wang X, Bennett B, Gong K, Navab M, Harkema J, Sioutas C, Lusis A and others. 2008. Ambient particulate pollutants in the ultrafine range promote early atherosclerosis and systemic oxidative stress. Circulation Research 102:589-596.

ASTM International. 2005. Standard test methods for carbon black used in rubber products (standard no. D305-84). Philadelphia, PA: American Society for Testing on Materials.

Auchter JF. 2005. Chemical economics handbook: carbon black. Menlo Park, CA: SRI Consulting.

Auerbach S, Shah R, Mav D, Smith C, Walker N, Vallant M, Boorman G, Irwin R. 2010. Predicting the hepatocarcinogenic potential of alkenylbenzene flavoring agents using toxicogenomics and machine learning. Toxicology and Applied Pharmacology 243:300-314.

Babior B. 2000. Phagocytes and oxidative stress. American Journal of Medicine 109(1):33-44.

Ballantyne CM, Hoogeveen RC, Bang H, Coresh J, Folsom AR, Heiss G, Sharrett R. 2004. Lipoprotein-associated phospholipase A2, high-sensitivity c-reactive protein, and risk for incident coronary heart disease in middle-ages men and women in the atherosclerosis risk in communities (ARIC) study. Circulation 109:837-842.

Bellmann B, Creutzenberg H, Ernst H, Muhle H. 2009. Rat inhalation test with particles from biomass combustion and biomass co-firing exhaust. Journal of Physics: Conference Series 151:doi:10.1088/1742-6596/151/1/012067.

Belz G. 1995. Elastic properties and Windkessel function of the human aorta. Cardiovacular Drugs and Therapy 9(1):73-83.

Benjamini Y, Hochberg Y. 1995. Controlling the false discovery rate: a practical and powerful approach to multiple testing. Journal of the Royal Statistical Society, Series B, Statistical Methodology 57:289-300.

Bermudez E, Mangum J, Wong B, Bahman A, Hext P, Warheit D, Everitt J. 2004. Pulmonary responses of mice, rats, and hamsters to subchronic inhalation of ultrafine titanium dioxide particles. Toxicological Sciences 77:347-357.

Bhabra G, Sood A, Fisher B, Cartwright L, Saunders M, Evans WH, Surprenant A, Lopez-Castejon G, Mann S, Davis SA and others. 2009. Nanoparticles can cause DNA damage across a cellular barrier. Nature Nanotechnology 4:876-883.

Blankenberg S, Barbaux S, Tiret L. 2003. Adhesion molecules and atherosclerosis. Atherosclerosis 170(2):191-203.

Bolstad B, Irizarry R, Astrand M, Speed T. 2003. A comparison of normalization methods for high density oligonucleotide array data based on variance and bias. Bioinformatics 19:185-193.

Bonner JC. 2007. Lung fibrotic responses to particle exposure. Toxicological Pathology 35(1):148-153.

Bonzini M, Tripodi A, Artoni A, Tarantini L, Marinelli B, Bertazzi P, Apostoli P, Baccarelli A. 2010. Effects of inhalable particulate matter on blood coagulation. Journal of Thrombosis and Haemostasis 8(4):662-668.

Borm P, Cakmak G, Jermann E, Weishaupt C, Kempers P, Van Schooten F, Oberdorster G, Schins R. 2005. Formation of PAH-DNA adducts after in vivo and in vitro exposure of rats and lung cells to different commercial carbon blacks Toxicology and Applied Pharmacology 205:157-167.

Borm P, Robbins D, Haubold S, Kuhlbusch T, Fissan H, Donaldson K, Schins R, Stone V, Kreyling W, Lademann J and others. 2006. The potential risks of nanomaterials: a review carried out for the ECETOC. Particle and Fibre Toxicology 3(11).

Bornholdt J, Dybdahl M, Vogel U, Hansen ML, Loft S, Wallin H. 2002. Inhalation of ozone induces DNA strand breaks and inflammation in mice. Mutation Research 520:63-72.

Bornholdt J, Saber A, Sharma A, Savolainen K, Vogel U, Wallin H. 2007. Inflammatory response and genotoxicity of seven wood dusts in the human epithelial cell line A549. Mutation Research- Genetic Toxicology and Environmental Mutagenesis 632:78-88.

Bourdon J, Halappanavar S, Saber A, Jacobsen N, Williams A, Wallin H, Vogel U, Yauk C. 2012a. Hepatic and pulmonary toxicogenomic profiles in mice intratracheally instilled with carbon black nanoparticles reveal pulmonary inflammation, acute phase response and alterations in lipid homeostasis. Toxicological Sciences:doi:10.1093/toxsci/kfs119.

Bourdon J, Saber A, Jacobsen N, Jensen K, Madsen A, Lamson J, Wallin H, Moller P, Loft S, Yauk C and others. 2012b. Carbon black nanoparticle instillation induces sustained inflammation and genotoxicity in mouse lung and liver. Particle and Fibre Toxicology 9(5).

Boverhof D, Zacharewski T. 2006. Toxicogenomics in risk assessment: applications and needs. Toxicological Sciences 89(2):352-360.

Bradley J, Nordan M, Tassinari O. 2009. The recession's ripple effect on nanotech. Boston, MA: Lux Research Inc.

Brook R. 2008. Cardiovascular effects of air pollution. Clinical Science 115:175-187

Brown DM, Stone V, Findlay P, MacNee W, Donaldson K. 2000. Increased inflammation and intracellular calcium caused by ultrafine carbon black is independent of transition metals or other soluble components. Occupational and Environmental Medicine 57:685-691.

Buchte SF, Morfeld P, Wellmann J, Bolm-Audorff, McCunney RJ, Piekarski C, ICBA. 2006. Lung cancer mortality and carbon black exposure: a nested-control study at

a German carbon black production plant. Journal of Occupational and Environmental Medicine 48:1242-1252.
Buzea C, Blandino I, Robbie K. 2007. Nanomaterials and nanoparticles: sources and toxicity. Biointerphase 2(4):MR17-MR172.
Carr M, Undem B. 2001. Inflammation-induced plasticity of the afferent innervation of the airways. Environmental Health Perspectives 109:567-571.
Chen HW, Su SF, Chien CT, Lin WH, Yu SL, Chou CC, Chen JJ, Yang PC. 2006. Titanium dioxide nanoparticles induce emphysema-like lung injury in mice. Journal of the Federation of American Societies for Experimental Biology 20:2393-2395.
Chen L, Nadziejko C. 2005. Effects of subchronic exposures to concentrated ambient particles (CAPs) in mice. V.CAPs exacerbate aortic plaque development in hyperlipidemic mice. Inhalation Toxicology 17:217-224.
Cheng K, Cahill D, Kasai H, Nishimura S, Loeb L. 1992. 8-hydroxyguanine, an abundant form of oxidative DNA damage, causes G----T and A----C substitutions. J Biol Chem 267:166-172.
Cheng TJ, Hwang JS, Wang PY, Tsai CF, Chen CY, Lin SH, Chan CC. 2003. Effects of concentrated ambient particles on heart rate and blood pressure in pulmonary hypertensive rats. Environmental Health Perspectives 111(2):147-150.
Cho W-S, Kim S, Han BS, Son WC, Jeong J. 2009. Comparison of gene expression profiles in mice liver following intravenous injection of 4 and 100 nm-sized PEG-coated gold nanoparticles. Toxicology Letters 191(1):96-102.
Choi HS, Ashitate Y, Lee JH, Kim SH, Matsui A, Insin N, Bawendi MG, Semmler-Behnke M, Frangioni JV, Tsuda A. 2010. Rapid translocation of nanoparticles from the lung airspaces to the body. Nature Biotechnology 28(12):1300-1303.
Chuang K-J, Chan C-C, Su T-C, Lee C-T, Tang C-S. 2007. The effect of urban air pollution on inflammation, oxidative stress, coagulation, and autonomic dysfunction in young adults. American Journal of Respiratory and Critical Care Medicine 176(4):370-376.
Cooke M, Evans M, Dizdrogla M, Lunec J. 2003. Oxidative DNA damage: mechanisms, mutation, and disease. FASEB J 17(10):1195-1214.
Coussen L, Werb Z. 2002. Inflammation and cancer. Nature 420:860-867.
Cozzi E, Wingard C, Cascio W, Devlin R, Miles J, Bofferding A, Lust R, Van Scott M, Henriksen R. 2007. Effect of ambient particulate matter exposure on homeostasis. Translational Research 149(6):324-332.
Crosbie W. 1986. Respiratory survey on carbon black workers in the U.K. and the U.S. Archives of Environmental Health 41:346-353.
Crump K, Allen BC, Faustman E. 1995. The use of the benchmark dose approach in health risk assessment. Washington, DC: US Environmental Protection Agency.
Cui X, Hwang JT, Qiu J, Blades NJ, Churchill GA. 2005. Improved statistical tests for differential gene expression by shrinking variance components estimates. Biostatistics 6:59-75.
Currie R. 2012. Toxicogenomics: the challenges and opportunities to identify biomarkers, signatures and thresholds to support mode-of-action. Mutation Research/Genetic Toxicology and Environmental Mutagenesis:doi: 10.1016/j.mrgentox.2012.03.002.

Danielsen P, Loft S, Jacobsen N, Jensen K, Autrup H, Ravanat J-L, Wallin H, Moller P. 2010. Oxidative stress, inflammation, and DNA damage in rats after intratracheal instillation or oral exposure to ambient air and wood smoke particulate matter. Toxicological Sciences 118(2):574-585.

Davis J, Gift J, Zhao Q. 2011. Introduction to benchmark dose methods and U.S. EPA's benchmark dose software (BMDS) version 2.1.1. Toxicology and Applied Pharmacology 254(2):181-191.

de Haar C, Hassing I, Bol M, Bleumink R, Pieters R. 2005. Ultrafine carbon black particles cause early inflammation and have adjuvant activity in a mouse allergic airway disease model. Toxicological Sciences 87(2):409-418.

Dell LD, Mundt KA, Luippold RS, Nunes AP, Cohen L, Burch MT, Heidenreich MJ, Bachand AM, ICBA. 2006. A cohort mortality study of employees in teh U.S. carbon black industry. Journal of Occupational and Environmental Medicine 48:1219-1229.

Demerath E, Towne B, Blangero J, Siervogel R. 2001. The relationship of soluble ICAM-1, VCAM-1, P-selectin and E-selectin to cardiovascular disease risk factors in healthy men and women. Annals of Human Biology 28(6):664-678.

Dix D, Martin H, Richard A, Setzer R, Kavlock R. 2007. The ToxCast program for prioritizing toxicity testing of environmental chemicals. Toxicological Sciences 95(1):5-12.

Dockery D, Pope C, Xu X, Spengler J, Ware J, Fay M, Ferris B, Speizer F. 1993. An association between air pollution and mortality in six U.S. cities. New England Journal of Medecine 329(24):1753-1759.

Don Porto Carero A, Hoet PHM, Verschaeve L, Schoeters G, Nemery B. 2001. Genotoxic effects of carbon black particles, diesel exhaust particles, and urban air particulates and their extracts on a human alveolar epithelial cell line (A549) and a human monocytic cell line (THP-1). Environmental and Molecular Mutagenesis 37:155-163.

Donaldson K, Borm P, Oberdorster G, Pinkerton K, Stone V, Tran C. 2008. Concordance between in vitro and in vivo dosimetry in the proinflammatory effects of low-toxicity, low-solubility particles: the key role of the proximal alveolar region. Inhal Toxicol 20(1):53-62.

Dong L, Li H, Wang S, Li Y. 2009. Different doses of lipopolysacharides regulate the lung inflammation of asthmatic mice via TLR4 pathway in alveolar macrophage. J Asthma 46(3):229-233.

Dong Z, Wu T, Qin W, An C, Wang Z, Zhang M, Zhang Y, Zhang C, An F. 2011. Serum amyloid A directly accelerates the progression of atherosclerosis in apolipoprotein E-deficient mice. Molecular Medicine 17(11-12):1357-1364.

Dorn II G, Molkentin J. 2004. Manipulating cardiac contractility in heart failure. Circulation 109:150-158.

Driscoll KE, Carter JM, Howard BW, Hassenbein DG, Pepelko W, Baggs RB, Oberdorster G. 1996. Pulmonary inflammation, chemokine, and mutagenic responses in rats after subchronic inhalation of carbon black. Toxicology and Applied Pharmacology 136:372-380.

Dybing E, Sanner T, Roelfzema H, Kroese D, Tennant R. 1997. T25: a simplified carcinogenic potency index: description of the system and study of correlations

between carcinogenic potency and species/site specificity and mutagenicity. Pharmacological Toxicology 80(6):272-279.
Eckardstein v, Nofer J-R, Assmann G. 2001. High density lipoproteins and arteriosclerosis: role of cholesterol efflux and reverse cholesterol transport. Arteriosclerosis, Thrombosis, and Vascular Biology 21:13-27.
Edwards SW, Preston RJ. 2008. Systems biology and mode of action based risk assessment. Toxicological Sciences 106(2):312-318.
Efron B, Tibshirani R. 1993. An introduction to the bootstrap. Boca Raton, FL: Chapman & Hall/CRC.
Elder A, Gelein R, Finkelstein JN, Driscoll KE, Harkema J, Oberdorster G. 2005. Effects of subchronically inhaled carbon black in three species. I.retention kinetics, lung inflammation, and hisopathology. Toxicological Sciences 88:614-629.
Elder A, Gelein R, Silva V, Feikert T, Opanashuk L, Carter J, Potter R, Maynard A, Ito Y, Finkelstein J and others. 2006. Translocation of inhaled ultrafine manganese oxide particles to the central nervous system. Environmental Health Perspectives 114(8):1172-1178.
Erdely A, Liston A, Salem-Muniz R, Hulderman T, Young S-H, Zeidler-Erdely P, Castranova V, Simeonova P. 2011. Identification of systemic markers from a pulmonary carbon nanotube exposure. J Occup Environ Med 53:580-586.
Euling SY, White LD, Kim AS, Sen B, Wilson VS, Keshava C, Keshava N, Hester S, Ovacik AM, Ierapetritou MG and others. 2011. Use of genomic data in risk assessment case study: II. Evaluation of the dibutyl phthalate toxicogenomic data set. Toxicology and Applied Pharmacology:doi:10.1016/j.taap.2011.06.014.
Farazi T, Spitzer J, Morozov P, Tuschl T. 2011. miRNAs in human cancer. Journal of Pathology 223:102-115.
Federico A, Morgillo F, Tuccillo C, Ciardiello F, Loguerico C. 2007. Chronic Inflammation and oxidative stress in human carcinogenesis. Int J Cancer 121:2381-2386.
Feingold KR, Grunfeld C. 2010. The acute phase response inhibits reverse cholesterol transport. Journal of Lipid Research 51(4):682-684.
Feingold KR, Hardardottir I, Memon R, Kral EJ, Moser AH, Taylor JM, Grunfeld C. 1993. Effects of endotoxin on cholesterol biosynthesis and distribution in serum lipoproteins in syrian hamsters. Journal of Lipid Research 34:2147-2158.
Feingold KR, Pollock AS, Moser AH, Shigenaga JK, Grunfeld C. 1995. Discordant regulation of proteins of cholesterol metabolism during the acute phase response. Journal of Lipid Reseach 36:1474-1482.
Ferin J, Oberdorster G, Penney D. 1992. Pulmonary retention of ultrafine and fine particulates in rats. American Journal of Respiratory Cell and Molecular Biology 6(5):535-542.
Fernandez-Urrusuno R, Fattal E, Feger J, Couvreur P, Therond P. 1997. Evaluation of hepatic antioxidant systems after intravenous administration of polymeric nanoparticles. Biomaterials 18:511-517.
Fielden M, Adai A, Dunn II RT, Olaharski A, Searfoss G, Sina J, Aubrecht J, Boitier E, Nioi P, Auerbach S and others. 2011. Development and evaluation of a genomic signature for the prediction and mechanistic assessment of nongenotoxic hepatocarcinogens in the rat. Toxicological Sciences 124(1):54-74.

Firestone M, Kavlock R, Zenick H, Kramer M, U.S. EPA Eorking Group on the Future of Toxicity Testing. 2010. The U.S. Environmental Protection Agency strategic plan for evaluating the toxicity of chemicals. Journal of Toxicology and Environmental Health, Part B: Critical Reviews 13(2-4):139-162.

Folkmann J, Loft S, Moller P. 2007. Oxidatively damaged DNA in aging dyslipidemic ApoE$^{-/-}$ and wild-type mice. Mutagenesis 22(2):105-110.

Forchhammer L, Brauner E, Folkmann J, Danielsen P, Nielsen C, Jensen A, Loft S, Friis G, Moller P. 2008. Variation in assessment of oxidatively damaged DNA in mononuclear blood cells by the comet assay with visual scoring. Mutagenesis 23(3):223-231.

Forchhammer L, Johansson C, Loft S, Moller L, Godschalk R, Langie S, Jones G, Rachel W, Collins A, Azqueta A and others. 2009. Variation in the measurment of DNA damage by comet assay measured by the ECVAG inter-laboratory validation trial. Mutagenesis 25(2):113-123.

Foucaud L, Goulaouic S, Bennasroune A, Laval-Gilly P, Brown D, Stone V, Falla J. 2010. Oxidative stress induction by nanoparticles in THP-1 cells with 4-HNE production: stress biomarker or oxidative stress signalling molecule? Toxicology In Vitro 24(6):1512-1520.

Fujii T, Hayashi S, Hogg JC, Mukae H, Suwa T, Goto Y, Vincent R, Van Eeden SF. 2002. Interaction of alveolar macrophages and airway epithelial cells following exposure to particulate matter produces mediators that stimulate the bone marrow. American Journal of Respiratory Cell and Molecular Biology 27(34-41).

Fujii T, Hayashi S, Hogg JC, Vincent R, Van Eeden SF. 2001. Particulate matter induces cytokine expression in human bronchial epithelial cells. American Journal of Respiratory Cell and Molecular Biology 25(265-271).

Fujita K, Horie M, Kato H, Endoh S, Suzuki M, Nakamura A, Miyauchi A, Yamamoto K, Kinugasa S, Nishio K and others. 2009. Effects of TiO2 particles on gene expression profile in human keratinocytes without illumination: involvement of extracellular matrix and cell adhesion. Toxicology Letters 191(2-3):109-117.

Gallagher J, Sams R, Inmon J, Gelein R, Elder A, Oberdorster G, Prahalad AK. 2003. Formation of 8-oxo-7, 8-dihydro-2'-deoxyguanosine in rat lung DNA following subchronic inhalation of carbon black. Toxicology and Applied Pharmacology 190(3):224-231.

Garcia A, Buisson M, Bertrand P, Rimokh R, Rouleau E, Lopez B, Lidereau R, Mikaelian I, Mazoyer S. 2011. Down-regulation of BRCA1 expression by miR-146a and miR-146b-5p in triple negative sporadic breast cancers. EMBO Molecular Medicine 3(5):279-290.

Gardiner K, Trethowan N, Harrington J, Rossiter C, Calvert I. 1993. Respiratory health effects of carbon black: a survey of European carbon black workers. British Journal of Industrial Medicine 50:1082-1096.

Gardiner K, Van Tongeren M, Harrington JM. 2001. Respiratory health effects from exposure to carbon black: results of the phase II and II cross-sectional studies in the European carbon black manufacturing industy. Occupational and Environmental Medicine 58:496-503.

Gatzidou E, Zira A, Theocharis E. 2007. Toxicogenomics: a pivotal piece in the puzzle of toxicological research. Journal of Applied Toxicology 27:302-309.

Geiser M, Kreyling W. 2010. Deposition and biokinetics of inhaled nanoparticles. Particle and Fibre Toxicology 7(2).

Geiser M, Rothen-Rutishauser B, Kapp N, Schurch S, Kreyling W, Schulz H, Semmler M, Hof VI, Heyder J, Gehr P. 2005. Ultrafine particles cross cellular membranes by nonphagocytic mechanisms in lungs and in cultured cells. Environmental Health Perspectives 113(11):1555-1560.

Genter MB, Burman DM, Vijayakumar S, Ebert CL, Aronow BJ. 2002. Genomic analysis of alachlor-induced oncogenesis in rat olfactory mucosa. Physiological Genomics 12:35-45.

Gerloff K, Albrecht C, Boots A, Forster I, Schins R. 2009. Cytotoxicity and oxidative damage by nanoparticles in human intestinal Caco-2 cells. Nanotoxicology 3(4):355-364.

Goncalves DM, de Liz R, Girard D. 2011. Activation of neutrophils by nanoparticles. The Scientific World Journal 11:1877-1885.

Goodnight J, Harvey W. 1978. Least-square means in the fixed-effects general linear models. Technical Report R-103, SAS Institute Inc, NC.

Green T, Fisher J, Stone M, Wroblewski B, Ingham E. 1998. Polyethylene particles of critical size are necessary for the induction of cytokines by macrophages *in vitro*. Biomaterials 19:2297-2302.

Gunnison A, Chen L. 2005. Effects of subchronic exposures to concentrated ambient particles in mice: VI. gene expression in heart and lung tissue. Inhalation Toxicology 17:225-233.

Guo H, Ingolia NT, Weissman JS, Bartel DP. 2010. Mammalian microRNAs predominantly act to decrease target mRNA levels. Nature 466:835-841.

Halappanavar S, Jackson P, Williams A, Jensen KA, Hougaard KS, Vogel U, Yauk CL, Wallin H. 2011. Pulmonary responses to surface-coated nanotitanium dioxide particles includes induction of acute phase response genes, inflammatory cascades, and changes in microRNAs: a toxicogenomic study. Environmental and Molecular Mutagenesis 52(6):425-439.

Halligan E, Lunec J. 2008. Toxicogenomics: unlocking the potential of the human genome. Advances in Experimental Biology 2:1-20.

Handy RD, Shaw BJ. 2007. Toxic effects of nanoparticles and nanomaterials: implications for public health, risk assessment and the public perception of nanotechnology. Health, Risk and Society 9(2):125-144.

Harber P, Muranko H, Shvartsblat S, Solis S, Torossian A, Oren T. 2003a. A triangulation approach to historical exposure assessment for the carbon black industry. Journal of Occupational and Environmental Medicine 45:131-143.

Harber P, Muranko H, Solis S, Torossian A, Merz B. 2003b. Effects of carbon black exposure on respiratory function and symptoms. Journal of Occupational and Environmental Medicine 45(2):144-155.

Hasegawa G, Hirano M, Ishihara Y. 2011. Differential gene expression associated with inflammation and blood pressure regulation by concentrated ambient particle exposure. Inhalation Toxicology 23(14):897-905.

Hastie T, Tibshirani R, Narasimhan B, Chu G. 2011. Pamr: pam: prediction analysis for microarrays.

Heijne W, Kienhuis A, van Ommen B, Stierum R, Groten J. 2005. Systems toxicology: applications of toxicogenomics, transcriptomics, proteomics and metabolomics in toxicology. Expert Reviews in Proteomics 2(5):767-780.

Heinrich U, Fuhst R, Rittinghausen R, Creutzenberg O, Bellmann B, Koch W, Levsen K. 1995. Chronic inhalation exposure of wistar rats and two different strains of mice to diesel exhaust, carbon black and titanium dioxide. Inhalation Toxicology 7:533-556.

Hellstrand E, Lynch I, Andersson A, Drakenburg T, Dahlback B, Dawson KA, Linse S, Cedervall T. 2009. Complete high-density lipoproteins in nanoparticle corona. Federation of European Biochemical Societies (FEBS) Journal 276:3372-3381.

Henderson RF, Waide J, Mauderly J, McClellan R. 1987. A rapid method for determining soot content of lungs in diesel-exposed rodents. Journal of Applied Toxicology 7(6):357-360.

Higgins JJ. 2003. An introduction to modern nonparametric statistics. Pacific Grove, CA: Brooks/Cole.

Hodgson J, Jones R. 1985. A mortality study of carbon black workers employed at five United Kingdom factories between 1947-1980. Archives of Environmental Health 40:261-268.

Hollan I, Scott H, Saatvedt K, Prayson R, Mikkelsen K, Nossent HC, Kvelstad IL, Liang MH, Forre OT. 2007. Inflammatory rheumatic disease and smoking are predictors of aortic inflammation: a controlled study of biopsy specimens obtained at coronary artery surgery. Arthritis and Rheumatism 56(6):2072-2079.

Huang D, Sherman B, Lempicki R. 2009a. Bioinformatics enrichment tools: paths toward the comprehensive functional analysis of large gene lists. Nucleic Acids Research 37:1-13.

Huang D, Sherman B, Lempicki R. 2009b. Systematic and integrative analysis of large lists using DAVID bioinformatics resources. Nature Protocols 4:44-57.

Hubbard R, Venn A, Lewis S, Britton J. 2000. Lung cancer and cryptogenic fibrosing alveolitis: a population-based cohort study. American Journal of Respiratory and Critical Care Medicine 161:5-8.

Hubbs A, Mercer R, Benkovic S, Harkema J, Sriram K, Schwegler-Berry D, Goravanahally M, Nurkiewicz T, Castranova V, Sargent L. 2011. Nanotoxicology- a pathologist's perspective. Toxicologic Pathology 39:301-324.

Huber K, Christ G, Wojta J, Gulba D. 2001. Plasminogen activator inhibitor type-1 in cardiovascular disease. Thrombosis Research 103:S7-S19.

Hussain S, Boland S, Baeza-Squiban A, Hamel R, Thomassen LCJ, Martens JA, Billon-Galland MA, Fleury-Feith J, Moisan F, Pairon J-C and others. 2009. Oxidative stress and proinflammatory effects of carbon black and titanium dioxide nanoparticles: role of particle surface area and internalized amount. Toxicology 260:142-149.

Iancu R, Jones S, Harvey R. 2007. Compartmentation of cAMP signaling in cardiac myocytes: a computational study. Biophysical Journal 92:3317-3331.

IARC. 1996. IARC monographs. 93.

IARC. 2010. Carbon black IARC monographs. International Agency for Research on Cancer. monographs.iarc.fr/ENG/Monographs/vol93/mono93-6.pdf p.

ICBA. 2006. Carbon Black User's Guide: safety, Health, & Environmental Information.

ICRP. 1994. Human respiratory tract model for radiological protection: a report of the task group of the International Commission on Radiological Protection. Annals of the ICRP 24(1-3):1-482.

Ilker-Yilmaz M, Baykal Y, Kilic M, Sonmez A, Bulucu F, Aydin A, Sayal A, Hakki-Kocar I. 2003. Effects of statins on oxidative stress. Biological Trace Element Research 98:119-127.

Ingalls TH. 1950. Incidence of cancer in the carbon black industry. Archives of Industrial Hygiene and Occupational Medicine 1:662-676.

Ingalls TH, Risquez-Iribarren R. 1961. Periodic search for cancer in the carbon black industry. Archives of Environmental Health 2:429-433.

Inoue K-I, Tukano H, Yanagisawa R, Sakurai M, Ichinose T, Sasakane K, Yoshikawa T. 2005. Effects of nanoparticles on antigen-related airway inflammation in mice. Respiratory Research 6(106):-12.

Jackson P, Hougaard KS, Boisen AMZ, Jacobsen NR, Jensen KA, Moller P, Brunborg G, Gutzkow KB, Andersen O, Loft S and others. 2011a. Pulmonary exposure to carbon black by inhalation or instillation in pregnant mice: effects on liver DNA strand breaks in dams and offspring. Nanotoxicology:doi: 10.3109/17435390.2011.587902.

Jackson P, Hougaard KS, Vogel U, Wu D, Casavant L, Williams A, Wade M, Yauk CL, Wallin H, Halappanavar S. 2011b. Exposure of pregnant mice to carbon black by intratracheal instillation: toxicogenomic effects in dams and offspring. Mutation Research/Genetic Toxicology and Environmental Mutagenesis:doi:10.1016/j.mrgentox.2011.09.018.

Jacobsen N, Moller P, Jensen K, Vogel U, Ladefoged O, Loft S, Wallin H. 2009. Lung inflammation and genotoxicity following pulmonary exposure to nanoparticles in ApoE-/- mice. Particle and Fibre Toxicology 6(2).

Jacobsen N, Pojana G, White P, Gingerich J, Moller P, Saber A, Douglas G, Vogel U, Wallin H. 2011. Mutation spectrum in FE1-muta^{TM}mouse lung epithelial cells. Environmental and Molecular Mutagenesis 52:331-337.

Jacobsen N, Saber A, White P, Pojana G, Vogel U, Loft S, Gingerich J, Soper L, Douglas G, Wallin H. 2007. Increased mutant frequency by carbon black, but not quartz, in the LacZ and cII transgenes of Muta^{TM}Mouse lung epithelial cells. Environmental and Molecular Mutagenesis 48:451-461.

Jacobsen NR, Pojana G, White P, Moller P, Cohn CA, Korsholm KS, Vogel U, Wallin H. 2008. Genotoxicity, cytotoxicity, and reactive oxygen species induced by single-walled carbon nanotubes and C(60) fullrenes in the FE1-Muta^{TM}Mouse lung epithelial cells. Environmental and Molecular Mutagenesis 49:476-487.

Jarim M, Fry R, Jaspers I, Dailey L, Diaz-Sanchez D. 2009. Disruption of microRNA expression in human airway cells by diesel exhaust particles is linked to tumorigenesis-associated pathways. Environmental Health Perspectives 117(11):1745-1751.

Jensen A, Lohr M, Eriksen L, Gronbaek M, Dorry E, Loft S, Moller P. 2012. Influence of the Ser326Cys polymorphism on oxidatively damaged DNA and repair activity. Free Radical Biology and Medicine 52(1):118-125.

Johansson C, Moller P, Forchhammer L, Loft S, Godschalk R, Langie S, Lumeij S, Jones G, Kwok R, Azqueta A and others. 2010. An ECVAG dagger trial on assessment

of oxidative damage to DNA measured by the comet assay. Mutagenesis 25(2):125-132.
Kang GS, Gillespie PA, Gunnison A, Moreira AL, Tchou-Wong K-M, Chen L-C. 2011. Long-term inhalation exposure to nickel nanoparticles exacerbated atherosclerosis in a susceptible mouse model. Environmental Health Perspectives 119(2):176-181.
Kawabata Y, Iwai K, Udagawa T, Tukagoshi K, Higuchi K. 1986. Effects of diesel soot on unscheduled DNA synthesis of tracheal epithelium and lung tumor formation. Developments in Toxicology & Environmental Science 13:213-222.
Kawata K, Osawa M, Okabe S. 2009. In vitro toxicity of silver nanoparticles at nontoxic doses to HepG2 human hepatoma cells Environmental Science and Technology 43(15):6045-6051.
Kerr M, Churchill G. 2001. Statistical design and the analysis of gene expression microarray data. Genetics Research 77(2):123-128.
Kerr MK. 2003. Design considerations for efficient and effective micro-array studies. Biometrics 59:822-828.
Kienhuis AS, Bessems JGM, Pennings JLA, Driessen M, Luijten M, van Delft JHM, Peijnenburg AACM, van der Ven LTM. 2011. Application of toxicogenomics in hepatic systems toxicology for risk assessment: acetaminophen as a case study. Toxicology and Applied Pharmacology 250:96-107.
Knaapen AM, Borm PJA, Albrecht C, Schins RPF. 2004. Inhaled particles and lung cancer. Part A: mechanisms. International Journal of Cancer 109:799-809.
Knust J, Ochs M, Gundersen H, Nyengaard J. 2009. Stereological estimates of alveolar number and size capillary length and surface area in mice lungs. Anat Rec 292(1):113-122.
Kreyling WG, Semmler M, Erbe F, Mayer P, Takenaka S, Schulz H, Oberdorster G, Ziesenis A. 2002. Minute translocation of ultrafine insoluble iridium particles from lung epithelium to extrapulmonary organs is size dependant but very slow. Journal of Toxicology and Environmental Health Part A 65:1513-1530.
Kroll A, Dierker C, Rommel C, Hahn D, Wohlleben W, Schulze-Isfort C, Gobbert C, Voetz M, Hardinghaus F, Schnekenburger J. 2011. cytotoxicity screening of 23 engineered nanomaterials using a test matrix of ten cell lines and three different assays. Part and Fibre Toxicol 8(9):-27.
Kuhlbusch TA, Neumann S, Fissan H. 2004. Number size distribution, mass concentration, and particle composition of PM1, PM2.5, and PM10 in bag filling areas of carbon black production. Journal of Occupational and Environmental Hygiene 1:660-671.
Kupershmidt I, Su QJ, Grewal A, Sundaresh S, Halperin I, Flynn J, Shekar M, Wang H, Park J, Cui W and others. 2010. Ontology-based meta-analysis of global collections of high-throughput public data. Public Library of Science ONE 5(9).
Lema C, Cunningham M. 2010. MicroRNAs and their implications in toxicological research. Toxicology Letters 198(2):100-105.
Lewis B, Burge C, Bartel D. 2005. Conserved seed pairing, often flanked by adenosines, indicates that thousands of human genes are microRNA targets. Cell 120(1):15-20.

Lewis CC, Yang JYH, Huang X, Banerjee SK, Blackburn MR, Baluk P, McDonald DM, Blackwell TS, Nagabhushanam V, Peters W and others. 2008. Disease-specific gene expression profiling in multiple models of lung disease. American Journal of Respiratory Critical Care Medicine 177:376-387.

Li JJ, Muralikrishnan S, Ng C-T, Yung L-YL, Bay B-H. 2010. Nanoparticle-induced pulmonary toxicity. Experimental Biology and Medicine 235:1025-1033.

Li N, Sioutas C, Cho A, Schmitz D, Sempf J, Oberly T, Freines J, Nel A. 2003. Ultrafine particulate pollutants induce oxidative stress and mitochondrial damage. Environmental Health Perspectives 111:455-460.

Li S, Wang H, Qi Y, Tu J, Bai Y, Tian T, Huang N, Wang Y, Xiong F, Lu Z and others. 2011a. Assessment of nanomaterial cytotoxicity with SOLiD sequencing-based microRNA expression profiling. Biomaterials 32(34):9021-9030.

Li S, Wang Y, Wang H, Bai Y, Liang G, Wang Y, Huang N, Xiao Z. 2011b. MicroRNAs as participants in cytotoxicity of CdTe quantum dots in NIH/3T3 cells. Biomaterials 32(15):3807-3814.

Li XY, Brown D, Smith S, McNee W, Donaldson K. 1999. Short-term inflammatory responses following intratracheal instillation of fine and ultrafine carbon black in rats. Inhalation Toxicology 11:709-731.

Li Z, Hulderman T, Salmen R, Chapman R, Leonard S, Young S, Shvedova A, Luster M, Simeonova P. 2007. Cardiovascular effects of pulmonary exposure to single-wall carbon nanotubes. Environmental Health Perspectives 115:377-382.

Liao JK. 2002. Isoprenoids as mediators of the biological effects of statins. Journal of Clinical Investigation 110(3):285-288.

Libby P, Ridker P, Hansson G. 2011. Progress and challenges in translating the biology of atherosclerosis. Nature 473:317-325.

Libby P, Ridker P, Maseri A. 2002. Inflammation and atherosclerosis. Circulation 105:1135-1143.

Lkhasuren O, Takahashi K, Dash-Onolt L. 2007. Occupational lung diseases and the mining industry in Mongolia. International Journal of Occupational Health 13:195-201.

Loft S, Poulsen H. 1996. Cancer risk and oxidative DNA damage in man. J Mol Med 74:297-312.

Loft S, Svoboda P, Kasai H, Tjonneland A, Vogel U, Moller P, Overvad K, Raaschou-Nielson O. 2006. Prospective study of 8-oxo-7,8-dihydro-2'-deoxyguanosine excretion and risk of lung cancer. Carcinogenesis 27:1245-1250.

Loft S, Svoboda P, Kawai K, Kasai H, Sorensen M, Tjonneland A, Vogel U, Moller P, Overvad K, Raaschou-Nielson O. 2011. Association between 8-oxo-7,8-dyhydroguanine excretion and risk of lung cancer in a prospective study. Free Rad Biol Med (in press):DOI:10.1016/j.freeradbiomed.2011.10.439.

Lu T, Munitz A, Rothenberg M. 2009. MicroRNA-21 is up-regulated in allergic airway inflammation and regulates IL-12p35 expression. Journal of Immunology 182(8):4994-5002.

Luc G, Arveiler D, Evans A, Amouyel P, Ferrieres J, Bard J-M, Elkhalil L, Fruchart J-C, Ducimetiere P. 2003. Circulating soluble adhesion molecules ICAM-1 and VCAM-1 and incident coronary heart disease: The PRIME study. Atherosclerosis 170:169-176.

Madsen A, Saber A, Nordly P, Sharma A, Wallin H, Vogel U. 2008. Inflammation but no DNA (deoxyribonucleic acid) damage in mice exposed to airborne dust from a biofuel plant. Scandinavian Journal of Work and Environmental Health 34(4):278-287.

Maes O, Chertkow H, Wang E, Schipper H. 2009. MicroRNA: Implication for Alzheimer Disease and other human CNS disorders. Current Genomics 10(3):154-168.

Magari SR, Hausser R, Schwartz J, William PL, Smith TJ, Christiani DC. 2001. Association of heart rate variability with occupational and environmental exposure to particulate air pollution. Circulation 104(9):986-991.

Magrez A, Kasas S, Salicio V, Pasquier N, Seo JW, Celio M, Catsicas S, Schwaller B, Forro L. 2006. Cellular toxicity of carbon-based nanomaterials. Nano Letters 6(6):1121-1125.

Mahmood M, Li Z, Casciano D, Khodakovskaya M, Chen T, Karmakar A, Dervishi E, Xu Y, Mustafa T, Watanabe F and others. 2011. Nanostrctural materials increase mineralization in bone cells and affect gene expression through miRNA regulation. Journal of Cellular and Molecular Medicine 15(11):2297-2306.

Makris SL, Euling SY, Early Gray Jr L, Benson R, Foster PMD. 2010. Use of genomic data in risk assessment case study: I. Evaluation of the dibutyl phthalate male reproductive development toxicity data set. Toxicology and Applied Pharmacology:doi:10.1016/j.taap.2010.09.006.

McGillicuddy FC, delaLleraMoya M, Hinkle CC, Joshi MR, Chiquoine EH, Billheimer JT, Rothblat GH, Reilly MP. 2009. Inflamation impairs reverse cholesterol transport. Circulation 119:1135-1145.

Medalia AI, Rivin D, Sanders DR. 1983. A comparison of carbon black with soot. The Science of the Total Environment 31:1-22.

Meek M, Newhook R, Liteplo R, Armstrong V. 1994. Approach to assessment of risk to human health for priority substances under the Canadian Environmental Protection Act. Journal of Environmental Science and Health, Part C: Environmental Carcinogenesis and Ecotoxicology Reviews C12:105-134.

Memon RA, Grunfeld C, Moser AH, Feingold KR. 1993. Tumor necrosis factor mediates the effects of endotoxin on cholesterol and triglyceride metabolism in mice. Endocrinology 132(5):2246-2253.

Mikkelsen L, Sheykhzade M, Jensen K, Saber A, Jacobsen N, Vogel U, Wallin H, Loft S, Moller P. 2011. Modest effect on plaque progression and vasodilatory function in atherosclerosis-prone mice exposed to nanosized TiO_2. Particle and Fibre Toxicology 8(32).

Miller K, Siscovick D, Sheppard L, Shepherd K, Sullivan J, Anderson G, Kaufman J. 2007. Long-term exposure to air pollution and incidence of cardiovascular events in women. New England Journal of Medecine 356:447-458.

Mills N, Donaldson K, Hadoke P, Boon N, MacNee W, Cassee F, Sandstrom T, Blomberg A, Newby D. 2009. Adverse cardiovascular effects of air pollution. Nature Clinical Practice Cardiovascular Medicine 6(1):36-44.

Mitsubishi Chemical Corporation. 2006. Manufacturing process of carbon black.

Moller P. 2006. The alkaline comet assay: towards validation in biomonitoring of DNA damaging exposures. Basic Clin Pharmacol Toxicol 98(4):336-345.

Moller P, Friis G, Christensen P, Risom L, Plesner G, Kjaersqaard J, Vinzents P, Loft S, Jensen A, Tved M. 2004a. Intra-laboratory comet assay sample scoring exercise for determination of formamidopyrimidine DNA glycosylase sites in human mononuclear blood cell DNA. Free Rad Res 38(11):1207-1214.

Moller P, Jacobsen NR, Folkmann JK, Danielsen PH, Mikkelsen L, Hemmingsen JG, Vesterdal LK, Forchhammer L, Wallin H, Loft S. 2010a. Role of oxidative damage in toxicity of particulates. Free Radical Research 44(1):1-46.

Moller P, Loft S. 2010. Oxidative damage to DNA and lipids as biomarkers of exposure to air pollution. Environ Health Perspect 118(8):1126-1136.

Moller P, Moller L, Godschalk R, Jones G. 2010b. Assessment and reduction of comet assay variation in relation to DNA damage: studies from the European comet assay validation group. Mutagenesis 25(2):109-111.

Moller W, Haubinger K, Winkler-Heils, Stahlhofen W, Meyer T, Hofmann W, Heyder J. 2004b. Mucociliary and long-term particle clearance in the airways of healthy nonsmoker subjects. Journal of Applied Physiology 97:2200-2206.

Morfeld P, Buchte SF, McCunney RJ, Piekarski C, ICBA. 2006. Lung cancer mortality and carbon black exposure: uncertainties of SMR analyses in a cohort study at a German carbon black production plant. Journal of Occupational and Environmental Medicine 48:1253-1264.

Mroz R, Schins R, Drost E, MacNee W, Donaldson K. 2007. Nanoparticle carbon black driven DNA damage induces growth arrest AP-1 and NFkB DNA binding in lung epithelial cells. Journal of Physiology and Pharmacology 58(5):461-470.

Mroz R, Schins R, Li H, Jimenez L, Drost E, Holownia A, MacNee W, Donaldson K. 2008. Nanoparticle-driven DNA damage mimics irradiation-related carcinogenesis pathways. European Respiratory Journal 31(2):241-251.

Muranko HJ, Hethmon TA, Smith RG. 2001. 'Total' and respirable dust exposures in the US carbon black manufacturing industry. American Industrial Hygiene Association Journal 62:57-64.

National Academy of Sciences. 2007. Toxicity testing in the twenty-first century: a vision and strategy. Washington, DC: Committe on Toxicity Testing and Assessment of Environmental Agents.

Necela B, Carr J, Asmann Y, Thompson E. 2011. Diferential expression of microRNAs in tumors from chronically inflammed mice or genetic (APC Min/+) models of colon cancer. PLoS ONE 6(4).

Nel A, Xia T, Mudler L, Li N. 2006. Toxic potential of materials at the nanolevel. Science 311(5761):622-627.

Ng C-T, Dheen T, Yip W-C, Ong C-N, Bay B-H, Yung L-Y. 2011. The induction of epigenetic regulation of PROS1 gene in lung fibroblasts by gold nanoparticles and implications for potential lung injury. Biomaterials 32(30):7609-7615.

Ng C-T, Li JJ, Bay B-H, Yung L-YL. 2010. Current studies into the genotoxic effects of nanomaterials. Journal of Nucleic Acids:doi: 10.4061/2010/947859.

Nikula KJ, Snipes MB, Barr EB, Griffith WC, Henderson RF, Mauderly JL. 1995. Comparative pulmonary toxicities and carcinogenicities of chronically inhaled diesel exhaust and carbon black in F344 rats. Fundamental and Applied Toxicology 25(1):80-94.

Niwa Y, Hiura Y, Murayama T, Yokode M, Iwai N. 2007. Nano-sized carbon black exposure exacerbates atherosclerosis in LDL-receptor knockout mice. Circulation Journal 71:1157-1161.

Nurkiewicz TR, Porter DW, Barger M, Millecchia L, Rao KM, Marvar PJ, Hubbs AF, Castranova V, Boegehold MA. 2006. Systemic microvascular dysfunction and inflammation after pulmonary particulate matter exposure. Environmental Health Perspectives 114(3):412-419.

Oberdorster G. 2001. Pulmonary effects of inhaled ultrafine particles. International Archives of Occupational and Environmental Health 74:1-8.

Oberdorster G, Oberdorster E, Oberdorster J. 2005. Nanotoxicology: an emerging discipline evolving from studies of ultrafine particles. Environmental Health Perspectives 113(7):823-839.

Oberdorster G, Sharp Z, Atudorei V, Elder A, Gelein R, Lunts A, Kreyling W, Cox C. 2002. Extrapulmonary translocation of ultrafine carbon particles following whole-body inhalation exposure of rats. Journal of Toxicology and Environmental Health 65:1531-1543.

Ovrevik J, Lag M, Holme JA, Scharze PE, Refsnes M. 2009. Cytokine and chemokine expression in lung epithelial cells exposed to components characteristic of particulate air pollution Toxicology 259(1-2):46-53.

Papadopoulos G, Reczko M, Sethupathy P, Hatzigeorgiou A. 2009a. The database of experimentally supported targets: a functional update of TarBase. Nucleic Acids Research 37:D155-158.

Papadopoulos GL, Alexiou P, Maragkakis M, Reczko M, Hatzigeorgiou AG. 2009b. DIANA-mirPath: integrating human and mouse microRNAs in pathways. Bioinformatics 25(15):1991-1993.

Papagiannakopoulos T, Shapiro A, Kosik K. 2008. MicroRNA-21 targets a network of key tumor-suppressive pathways in glioblastoma cells. Cancer Research 68(19):8164-8172.

Papatheofanis F, Barmada R. 1991. Polymorphonuclear leukocyte degranulation with exposure to polymethylmethacrylate nanoparticles. Journal of Biomedical Materials Research 25(6):761-771.

Parent ME, Siemiatycki J, Fritschi L. 2000. Workplaces exposures and oesophageal cancer. Occupational and Environmental Medicine 57:325-334.

Parent ME, Siemiatycki J, Renaud G. 1996. Case-control study of exposure to carbon black in the occupational setting and risk of lung cancer. American Journal of Industrial Medicine 30:285-292.

Pasquinelli AE. 2012. MicroRNAs and their targets: recognition, regulation and an emerging reciprocal relationship. Nature Reviews:doi:10.1038/nrg3162.

Pennie W, Pettit S, Lord P. 2004. Toxicogenomics in risk assessment: an overview of an HESI collaborative research program. Environmental Health Perspectives 112(4):417-419.

Pfaffl MW, Horgan GW, Dempfle L. 2002. Relative expression software tool (REST©) for group-wise comparison and statistical analysis of relative expression results in real-time PCR. Nucleic Acid Research 30(9):e36.

Pope C, Dockery D, Schwartz J. 1995. Review of epidemiological evidence of health effects of particulate air pollution. Inhalation Toxicology 7(1):1-18.

Pope III C, Burnett R, Thuns M, Calle E, Krewski D, Ito K, Thurston G. 2002. Lung cancer, cardiopulmonary mortality, and long-term exposure to fine particulate pollution. Journal of the American Medical Association 287(9):1132-1141.

PopeIII CA, Burnett RT, Thurston GD, Thun MJ, Calle EE, Krewski D, Godleski JJ. 2004. Cardiovascular mortality and long-term exposure to particulate air pollution: epidemiological evidence of general pathophysiological pathways of disease. Circulation 109:71-77.

Pradervand S, Weber J, Thomas J, Bueno M, Wirapati P, Lefort K, Dotto GP, Harshman K. 2012. Impact of normalization on miRNA microarray expression profiling. RNA 15:493-501.

Puntoni M, Ceppi M, Reggiardo G, Merlo F. 2001. Occupational exposure to carbon black and risk of bladder cancer. Lancet 358:562.

Puntoni R, Ceppi M, Gennaro V, Ugolini D, Puntoni M, La Manna G, Casella C, Merlo DF. 2004. Occupational exposure to carbon black and risk of cancer. Cancer Causes and Control 15(5):511-516.

R Development Core Team. 2005. R: A language and environment for statistical computing. Vienna, Austria.

R Development Core Team. 2010. R: a language and environment for statistical computing.

R Development Core Team. 2011. R: a language and environment for statistical computing. Vienna, Austria: R Foundation for Statistical Computing.

Raaschou-Nielson O, Andersen Z, Hvidberg M, Jensen S, Ketzel M, Sorensen M, Hansen J, Loft S, Overvad K, Tjonneland A. 2011. Air pollution from traffic and cancer incidence: a Danish cohort study. Environ Health 10(67):1-11.

Recchiuti A, Krishnamoorthy S, Fredman G, Chiang N, Serhan C. 2011. MicroRNAs in resolution of acute inflammation: identification of novel resolvin D1-miRNA circuits. Journal of the Federation of American Societies for Experimental Biology 25(2):544-560.

Renwick L, Donaldson K, Clouter A. 2001. Impairment of alveolar macrophage phagocytosis by ultrafine particles. Toxicology and Applied Pharmacology 172:119-127.

Rice M, Cavallari J, Fang S, Christiani D. 2011. Acute decrease in HDL cholesterol associated with exposure to welding fumes. Journal of Occupational and Environmental Medicine 53(1):17-21.

Rikitake Y, Liao JK. 2005. Rho GTPases, statins, and nitric oxide. Circulation Research 97:1232-1235.

Risom L, Moller P, Vogel U, Kristjansen P, Loft S. 2003. X-ray-induced oxidative stress: DNA damage and gene expression of HO-1, ERCC1 and OGG1 in mouse lung. Free Rad Res 37(9):957-966.

Robertson JM, Ingalls TH. 1980. A mortality study of carbon black workers in the United States from 1935 to 1974. Archives of Environmental Health 35:181-186.

Robertson JM, Ingalls TH. 1989. A case-control study of circulatory, malignant, and respiratory morbidity in carbon black workers in the United States. American Industrial Hygiene Association Journal 50:510-515.

Robertson JM, Inman KJ. 1996. Mortality in carbon black workers in the United States. Journal of Occupational and Environmental Medicine 38:569-570.

Rocco M. 2005. Environmentally responsible development of nanotechnology. Environ Sci Technol 39(5):106A-112A.
Roduner E. 2006. Size matters: why nanomaterials are different. Chemical Society Reviews 35(7):583-592.
Rudd C, Strom K. 1981. A spectrophotometric method for the quantification of diesel exhaust particles in guinea pig lung. Journal of Applied Toxicology 1(2):83-87.
Rumley L. 1999. Coagulation, fibrinolysis and cardiovascular disease. Fibrinolysis and Proteolysis 13(2):91-98.
Saber A, Jensen K, Jacobsen N, Birkedal R, Mikkelsen L, Moller P, Loft S, Wallin H, Vogel U. 2011. Inflammatory and genotoxic effects of nanoparticles designed for inclusion in paints and laquers. Nanotoxicology:doi:10.3109/17435390.17587900.
Saber AT, Bornholdt J, Dybdahl M, Sharma AK, Loft S, Vogel U, Wallin H. 2005. Tumor necrosis factor is not required for particle induced genotoxicity and pulmonary inflammation. Archives of Toxicology 79:177-182.
Saber AT, Halappanavar S, Folkmann JK, Bornholdt J, Boisen AMZ, Moller P, Williams A, Yauk C, Vogel U, Loft S and others. 2009. Lack of acute phase response in the livers of mice exposed to diesel exhaust particles or carbon black by inhalation. Particle and Fibre Toxicology 6(12).
Sadauskas E, Jacobsen NR, Danscher G, Stoltenberg M, Vogel U, Larsen A, Kreyling W, Wallin H. 2009a. Biodistribution of gold nanoparticles in mouse lung following intratracheal instillation. Chemistry Central Journal 3(16).
Sadauskas E, Wallin H, Stoltenberg M, Vogel U, Doering P, larsen A, Danscher G. 2009b. Kupffer cells are central in the removal of nanoparticles from the organism. Part Fibre Toxicol 4(10).
Sager TM, Castranova V. 2009. Surface area of particle administered versus mass in determining the pulmonary toxicity of ultrafine and fine carbon black: comparison to ultrafine titanium dioxide. Particle and Fibre Toxicology 6:15-46.
Sandhu RS, Petroni DH, George WJ. 2005. Ambient particulate matter, c-reactive protein, and coronary artery disease. Inhalation Toxicology 17:409-413.
Schins RPF, Knaapen AM. 2007. Genotoxicity of poorly soluble particles. Inhalation Toxicology 19:189-198.
Schwe T-T, Yamamoto S, Ahmed S, Kakeyama M, Kobayashi T, Fujimaki H. 2006. Brain cytokine and chemokine mRNA expression in mice induced by intranasal instillation with ultrafine carbon black. Toxicology Letters 163:153-160.
Searle S, Speed F, Milliken G. 1980. Population marginal means in the linear model: an alternative to least squares means. The American Statistician 34(216-221).
Seaton A, Tran L, Aitken R, Donaldson K. 2010. Nanoparticles, human health hazard and regulation. Journal of the Royal Society Interface 7:119-129.
Sen B, Wang A, Hester S, Robertson J, Wolf D. 2005. Gene expression profiling of responses to dimethylarsinic acid in female F344 rat urothelium. Toxicology 215(214-226).
Sherratt M. 2009. Tissue elasticity and the ageing elastic fibre. Age 31:305-325.
Shvedova A, Kisin E, Murray A, Johnson V, Gorelik O, Arepalli S, Hubbs A, Mercer R, Keohavong P, Sussman N and others. 2008. Inhalation vs. aspiration of single-walled carbon nanotubes in C57BL/6 inflammation , fibrosis, oxidative stress, and

mutagenesis. American Journal of Physiology Lung Cellular and Molecular Physiology 295:L552-L565.
Singh N, Manshian B, Jenkins GJ, Griffiths SM, Williams PM, Maffeis TG, Wright CJ, Doak SH. 2009. NanoGenotoxicology: the DNA damaging potential of engineered nanomaterials. Biomaterials 30:3891-3914.
Smith RG, Musch DC. 1982. Occupational exposure to carbon black: a particulate sampling study. American Industrial Hygiene Association Journal 43:925-930.
Soll-Johanning H, Bach E, Olsen J, Tuchsen F. 1998. Cancer incidence in urban bus drivers and tramway employees: a retrospective cohort study. Occup Environ Med 55:594-598.
Sorohan T, Harrington JM. 2007. A "lugged" analysis of lung cancer risks in the UK carbon black production workers, 1951-2004. American Journal of Industrial Medicine 50:555-564.
Sorohan TL, Hamilton M, van Tongeren, Gardiner K, Harrington J. 2001. A cohort mortality study of the U.K. carbon black workers 1951-96. American Journal of Industrial Medicine 39:158-170.
Stern S, McNeil S. 2008. Nanotechnology safety concerns revisited. Toxicological Sciences 101(1):4-21.
Straif K, Keil U, Taeger D, Holthenrich D, Sun Y, Bungers M, Weiland SK. 2000. Exposure to nitrosamines, carbon black, asbestos, and talc and mortality from stomach, lung and laryngeal cancer in a cohort of rubber workers. American Journal of Epidemiology 152:297-306.
Sun Q, Wang A, Jin X, Natanzon A, Duquaine D, Brook R, Aguinaldo J, Fayad Z, Fuster V, Lippmann M and others. 2005. Long-term air pollution exposure and acceleration of atherosclerosis and vascular inflammation in an animal model. Journal of the American Medical Association 294:3003-3010.
Suter L, Babiss L, Wheeldon E. 2004. Toxicogenomics in predictive toxicology in drug development. Chemistry and Biology 11(2):161-171.
Suwa T, Hogg J, Quinlan K, Ohgami A, Vincent R, van Eeden S. 2002. Particulate air pollution induces progression of atherosclerosis. Journal of the American College of Cardiology 39:935-942.
Taganov K, Boldin M, Chang K-J, Baltimore D. 2006. NF-kB-dependant induction of microRNA miR-146, an inhibitor targeted to signaling proteins of innate immune responses. Proceedings of the National Academy of Sciences 103(33):12481-12486.
Tedder T, Steeber D, Chen A, Engel P. 1995. The selectins: vascular adhesion molecules FASEB Journal 9:866-873.
Thomas RS, Allen BC, Nong A, Yang L, Bermudez E, Clewell III HJ, Andersen ME. 2007. A method to integrate benchmark dose estimates with genomic data to assess the functional effects of chemical exposure. Toxicological Sciences 98(1):240-248.
Thomas RS, Clewell HJ, Allen BC, Wesselkamper SC, Wang NCY, Lambert JC, Hess-Wilson JK, Zhao QJ, Andersen ME. 2011. Application of transcriptional benchmark dose values in quantitative cancer and noncancer risk assessment. Toxicological Sciences 120(1):194-205.

Thomas RS, Clewell III HJ, Allen BC, Yang L, Healy E, Andersen ME. 2012. Integrating pathway-based transcriptomic data into quantitative chemical risk assessment: a five chemical case study. Mutation Research/Genetic Toxicology and Environmental Mutagenesis:doi:10.1016/j.mrgentox.2012.01.007.

Thomson EM, Williams A, Yauk CL, Vincent R. 2012. Overexpression of tumor necrosis factor-alpha in the lungs alters immune response, matrix remodeling, and repair and maintenance pathways. American Journal of Pathology 180(4).

Thorand B, Baumert J, Doring A, Schneider A, Chambless L, Lowel H, Kolb H, Koenig W. 2006. Association of cardiovascular risk factors with markers of endothelial dysfunction in middle-aged men and women. Results from the MONICA/KORA Augsburg study. Thrombosis and Haemostasis 95(1):134-141.

Tibshirani R, Hastie T, Narasimhan B, Chu G. 2002. Diagnosis of multiple cancer types by shrunken centroids of gene expression. Proceedings of the National Academy of Sciences of the United States of America 99(10):6567-6572.

Tong H, McGee JK, Saxena RK, Kodavanti UP, Devlin RB, Gilmour MI. 2009. Influence of acid functionalization on the cardiopulmonary toxicity of carbon nanotubes and carbon black particles in mice. Toxicology and Applied Pharmacology 239:224-232.

Totsuka Y, Higuchi T, Imai T, Nishikawa A, Nohmi T, Kato T, Masuda S, Kinae N, Hiyoshi K, Ogo S and others. 2009. Genotoxicity of nano/microparticles in in vitro micronuclei, in vivo comet, in vivo comet and mutation assay systems. Particle and Fibre Toxicology 6(23).

Trouiller B, Reliene R, Westbrook A, Solaimani P, Schiestl H. 2009. Titanium dioxide nanoparticles induce DNA damage and genetic instability in vivo in mice. Cancer Research 66(22):8784-8789.

Unfried K, Albrecht C, Koltz L-O, von Mikecz A, Grether-Beck S, Schins P. 2007. Cellular responses to nanoparticles: target structures and mechanisms. Nanotoxicology 1(1):52-71.

US EPA. 2004. Acetochlor report of the cancer assessment review committe (CARC). fourth evaluation. Washington, DC: Environmental Protection Agency.

US EPA. 2005. Science Issue Paper: mode of carcinogenic action for cadodylic acid and recommendations for dose response extrapolation. Washington, DC: Environmental Protection Agency.

US EPA. 2006. Revised reregistration eligibility decision document (RED) for MSMA; DSMA, and CAMA and cacodylic acid. Washington, DC: Environmental Protection Agency.

Valko M, Izakovic M, Mazur M, Rhodes C, Telser J. 2004. Role of oxygen radicals in DNA damage and cancer incidence. Mol Cell Biochem 266:37-56.

van Tongeren M, Kromhout H, Gardiner K. 2000. Trends in levels of inhalable dust exposure, exceedance and overexposure in the European carbon black manufacturing industry. Annals of Occupational Hygiene 44:271-280.

van Tongeren MJA, Gardiner K, Rossiter CE, Beach J, Harber P, Harrington MJ. 2002. Longitudinal analyses of chest radiographs from the European carbon black respiratory morbidity study. European Respiratory Journal 20(2):417-425.

Vasudevan S, Tong Y, Steitz JA. 2007. Switching from repression to activation: microRNAs can up-regulate translation. Science 318:1931-1934.

Vesterdal LK, Folkmann JK, Jacobsen NR, Sheykhzade M, Wallin H, Loft S, Moller P. 2010. Pulmonary exposure to carbon black nanoparticles and vascular effects. Particle and Fibre Toxicology 7(33).

Videira MA, Botelho MF, Santos AC, Gouveia LF, De Lima JJA, A J. 2002. Lymphatic uptake of pulmonary delivered radiolabeled solid lipid nanoparticles. Journal of Drug Targeting 10:607-613.

Vishwakarma V, Samal S, Manoharan N. 2010. Safety and risk associated with nanoparticles- a review. Journal of Minerals & Materials Characterization and Engineering 9:455-459.

Voll M, Kleinschmit P. 2002. Carbon. Ullmann's encyclopedia of industrial chemistry. New-York: Wiley-VCH Verlag GmbH & Co.

Wang T, Lang G, Moreno-Vinasco L, Huang Y, Goonewardena S, Peng Y-J, Svensson E, Natarajan V, Lang R, Linares J and others. 2011. Particulate matter induces cardiac arrhythmias via dysregulation of carotid body sensitivity and cardiac sodium channels. American Journal of Respiratory Cell and Molecular Biology 46(4):524-531.

Wang X, Christiani D. 2003. Occupational lung disease in China. International Journal of Occupational and Environmental Health 9:320-325.

Waters M, Fostel J. 2004. Toxicogenomics and systems toxicology: aims and pospects. Nature Reviews Genetics 5:936-948.

Watson AY, Valberg PA. 2001. Carbon black and soot: two different substances. American Industrial Hygiene Association Journal 62(2):218-228.

Wellmann J, Weiland SK, Neiteler G, Klein G, Straif K. 2006. Cancer mortality in German carbon black workers 1976-98. Occupational and Environmental Medicine 63:513-521.

Williams T, Harris R, Arp E, Symons M, Van Ert M. 1980. Worker exposure to chemical agents in the manufacture of rubber tires and tubes: particulates. American Industrial Hygiene Association Journal 41:204-211.

Wolff RK, Bond JA, Henderson RF, Karkema JR, Mauderly JL. 1990. Pulmonary inflammation and DNA adducts in rats inhaling diesel exhaust or carbon black. Inhalation Toxicology 2:241-254.

Wu H, Kerr M, Cui X, Churchill G. 2003. MAANOVA: A software package for the analysis of spotted cDNA microarray experiments. The Analysis of Gene Expression Data. p 313-341.

Xia H, Qi Y, Ng S, Chen X, Li D, Chen S, Ge R, Jiang S, Li G, Chen Y and others. 2009. MicroRNA-146b inhibits glioma cell migration and invasion by targeting MMPs. Brain Research 1269:158-165.

Yamawaki H, Iwai N. 2006. Mechanisms underlying nano-sized air-pollution-mediated progression of atherosclerosis: carbon black cause cytotoxic injury/inflammation and inhibits cell grwoth in vascular endothelial cells. Circulation Journal 70:129-140.

Yang H, Liu C, Yang D, Zhang H, Xi Z. 2008. Comparative study of cytotoxicity, oxidative stress and genotoxicity induced by four typical nanomaterials: the role of particle size, shape and composition. Applied Toxicology 29:69-78.

Yang H, Liu C, Yang D, Zhang H, Xi Z. 2009. Comparative study of cytotoxicity, oxidative stress and genotoxicity induced by four typical nanomaterials: the role

of particle size, shape and composition. Journal of Applied Toxicology 29(1):69-78.
Yang L, Allen B, Thomas R. 2007. BMDExpress: a software tool for the benchmark dose analyses of genomic data. BMC Genomics 8(387).
Yang Y, Dudoit S, Lin D, Peng V, Ngai J, Speed T. 2002. Normalization for cDNA microarray data: A robust composite method addressing single and multiple slide variations. Nucleic Acids Research 2002(30):1-e15.
Yatera K, Hsieh J, Hogg J, Tranfield E, Suzuki H, Shih C-H, Behzad A, Vincent R, van Eeden S. 2010. Particulate matter air pollution exposure promotes recruitment of monocytes into atherosclerotic plaques. American Journal of Physiology- Heart and Circulatory Physiology 121(21):2331-2378.
Yoshida M. 2003. Potential roles of statins in inflammation and atherosclerosis. Journal of Atherosclerosis and Thrombosis 10(3):140-144.
Yu LE, Yung L-YL, Ong C-N, Tan Y-L, Balasubramanium KS, Hartono D, Shui G, Wenk MR, Ong W-Y. 2007. Translocation and effect of gold nanoparticles after inhalation exposure in rats. Nanotoxicology 1(3):235-242.
Yu M, Mo Y, Wan R, Chien S, Zhang X, Zhang Q. 2010. Regulation of plasminogen activator inhibitor-1 expression in endothelial cells with exposure to metal nanoparticles. Toxicology Letters 195(1):82-89.
Zhou H, Kobzik L. 2007. Effect of concentrated ambient particles on macrophage phagocytosis and killing of Streptococcus pneumoniae. American Journal of Respiratory Cell and Molecular Biology 36:460-465.
Zhu Y, Yu X, Fu H, Wang H, Wang P, Zheng X, Wang Y. 2010. MicroRNA-21 is involved in ionizing radiation-promoted liver carcinogenesis. International Journal of Clinacal and Experimental Medicine 3(3):211-222.

SUPPLEMENTARY TABLES

SP1. Differentially expressed genes (fold-change > 1.5 and FDR p-value < 0.1) for at least one condition in C57/BL6 mouse lung following intratracheal instillation with Printex 90 CBNPs, relative to controls.

			Day 1						Day 3						Day 28					
			0.018 µg		0.054 µg		0.162 µg		0.018 µg		0.054 µg		0.162 µg		0.018 µg		0.054 µg		0.162 µg	
Gene Name	Genbank	Gene Description	FDR p-value	Fold change	FDR p-value	Fold change	FDR p-value	Fold change	FDR p-value	Fold change	FDR p-value	Fold change	FDR p-value	Fold change	FDR p-value	Fold change	FDR p-value	Fold change	FDR p-value	Fold change
0610011I04Rik	NM_025326	Mus musculus RIKEN cDNA 0610011I04 gene (0610011I04Rik), mRNA [NM_025326]	0.88	1.2	0.07	1.6	0.05	1.5	1.00	1.1	0.90	1.3	0.14	1.4	0.95	0.0	0.98	0.0	0.70	1.2
1100001G20Rik	NM_183249	Mus musculus RIKEN cDNA 1100001G20 gene (1100001G20Rik), mRNA [NM_183249]	0.89	1.3	0.17	2.2	0.38	1.5	1.00	1.8	0.00	2.8	0.01	2.7	0.80	1.7	0.98	1.8	0.00	3.6
1110018M03Rik	NM_026271	Mus musculus RIKEN cDNA 1110018M03 gene (1110018M03Rik), mRNA [NM_026271]	0.89	1.2	0.95	-1.0	0.67	-1.2	1.00	-1.3	0.93	-1.2	0.10	-1.6	0.82	-1.2	1.00	-1.0	0.62	-1.2
1110021J02Rik	AK003900	Mus musculus 18-day embryo whole body cDNA, RIKEN full-length enriched library, clone:1110021J02 product:hypothetical protein, full insert sequence. [AK003900]	0.87	1.2	0.15	1.5	0.02	1.6	1.00	1.2	0.90	1.2	0.35	1.2	0.94	1.0	0.98	1.1	0.87	1.1
1300002K09Rik	NM_028788	Mus musculus RIKEN cDNA 1300002K09 gene (1300002K09Rik), mRNA [NM_028788]	0.99	-1.0	0.99	1.0	0.43	1.2	1.00	1.2	0.90	1.3	0.18	1.3	0.95	1.0	0.98	1.1	0.03	1.6
1600029D21Rik	NM_029639	Mus musculus RIKEN cDNA 1600029D21 gene (1600029D21Rik), mRNA [NM_029639]	0.94	1.1	0.63	1.2	0.99	1.0	1.00	1.2	0.45	1.6	0.11	1.4	0.80	1.2	0.98	1.1	0.07	1.6
1810007E14Rik	ENSMUST00000061360	Mus musculus RIKEN cDNA 1810007E14 gene (1810007E14Rik), mRNA [NM_025308]	0.99	1.0	0.44	1.3	0.19	1.3	1.00	1.1	0.90	1.3	0.00	1.7	0.81	1.2	0.98	1.1	0.57	1.2
1810010H24Rik	XM_286373	PREDICTED: Mus musculus RIKEN cDNA 1810010H24 gene (1810010H24Rik), mRNA [XM_286373]	0.91	-1.2	0.61	-1.2	0.08	-1.5	1.00	-1.2	1.00	-1.0	0.78	-1.1	0.96	1.0	1.00	1.0	0.94	-1.0
1810026B05Rik	AK140938	Mus musculus 16 days embryo head cDNA, RIKEN full-length enriched library, clone:C130076G01 product:unclassifiable, full insert sequence [AK140938]	0.83	-1.5	0.28	-1.7	0.08	-1.7	1.00	-1.2	0.91	-1.2	0.10	-1.7	0.97	-1.0	0.98	1.1	0.97	1.0
2010004A03Rik	NM_029646	Mus musculus RIKEN cDNA 2010004A03 gene (2010004A03Rik), mRNA [NM_029646]	0.91	-1.1	1.00	1.0	0.25	1.2	1.00	1.1	0.92	1.1	0.42	1.2	0.80	1.2	0.98	1.3	0.00	1.6

2610307O08Rik	BC046640	Mus musculus RIKEN cDNA 2610307O08 gene, mRNA (cDNA clone MGC:49267 IMAGE:5067343), complete cds. [BC046640]	0.99	-1.0	0.55	1.2	0.01	1.6	1.00	1.2	0.90	1.3	0.21	1.3	0.91	1.1	0.98	1.1	0.45	1.3
2810003C17Rik	NM_145144	Mus musculus RIKEN cDNA 2810003C17 gene (2810003C17Rik), mRNA [NM_145144]	0.99	-1.0	0.95	1.0	0.01	1.5	1.00	1.0	0.95	-1.1	0.88	1.0	0.84	1.1	0.98	1.1	0.77	-1.1
2810409K11Rik	AK031040	Mus musculus adult male thymus cDNA, RIKEN full-length enriched library, clone:5832424I11 product:weakly similar to ZFP71P homolog [Mus musculus], full insert sequence. [AK031040]	0.61	-1.3	0.15	-1.3	0.00	-1.5	1.00	1.0	0.92	-1.1	0.32	-1.2	0.91	1.1	0.98	1.1	0.61	1.1
2810474O19Rik	NM_026054	Mus musculus RIKEN cDNA 2810474O19 gene (2810474O19Rik), mRNA [NM_026054]	0.87	1.2	0.53	1.2	0.28	1.3	1.00	1.0	0.90	1.3	0.04	1.5	0.99	-1.0	0.98	-1.2	0.83	-1.1
3110023G01Rik	AK014074	Mus musculus 13 days embryo head cDNA, RIKEN full-length enriched library, clone:3110023G01 product:hypothetical AAA ATPase superfamily containing protein, full insert sequence [AK014074]	0.97	-1.1	0.99	1.0	0.99	-1.0	1.00	1.3	0.76	1.6	0.08	1.6	0.83	1.2	0.98	1.1	0.97	1.0
3110049J23Rik	NM_026085	Mus musculus RIKEN cDNA 3110049J23 gene (3110049J23Rik), mRNA [NM_026085]	1.00	1.0	0.75	1.1	0.95	1.0	1.00	1.2	0.90	1.2	0.00	1.7	0.80	1.3	0.98	1.3	0.04	1.6
4632423N09Rik	NM_028149	Mus musculus RIKEN cDNA 4632423N09 gene (4632423N09Rik), mRNA [NM_134030]	0.87	-1.2	0.35	-1.3	0.01	-1.5	1.00	-1.1	0.94	-1.1	0.15	-1.3	0.99	1.0	0.98	1.1	0.96	1.0
4833422F24Rik	NM_029021	Mus musculus RIKEN cDNA 4833422F24 gene (4833422F24Rik), mRNA [NM_029021]	0.95	1.1	0.41	1.2	0.00	1.8	1.00	1.0	0.98	1.0	0.36	1.2	0.92	-1.1	1.00	-1.0	0.85	1.1
4932435O22Rik	AK053334	Mus musculus RIKEN cDNA 4932435O22 gene (4932435O22Rik), mRNA [NM_177008]	0.98	1.0	0.94	-1.0	0.86	1.1	1.00	1.3	0.90	1.2	0.05	1.5	0.86	1.1	0.99	-1.0	0.65	1.2
4933403G17Rik	AK016633	Mus musculus adult male testis cDNA, RIKEN full-length enriched library, clone:4933403G17 product:hypothetical protein, full insert sequence. [AK016633]	0.94	1.1	0.49	1.3	0.03	1.5	1.00	1.2	0.92	1.1	0.20	1.3	0.80	1.4	0.98	1.2	0.41	1.4
5730507H05Rik	AJ237585	Mus musculus mRNA for hypothetical protein expressed in thymocytes (clone MFT.M05.13 [AJ237585]	0.92	-1.1	0.70	1.2	0.43	1.3	1.00	1.2	0.90	1.3	0.07	1.6	0.89	-1.1	0.98	-1.3	0.94	1.0
5730557B15Rik	NM_026153	Mus musculus RIKEN cDNA 5730557B15 gene (5730557B15Rik), transcript variant 1, mRNA [NM_026153]	0.87	-1.2	0.46	-1.3	0.05	-1.5	1.00	-1.2	1.00	1.0	0.98	1.0	0.90	-1.1	0.99	-1.0	0.59	-1.2
6330403K07Rik	NM_134022	Mus musculus RIKEN cDNA 6330403K07 gene (6330403K07Rik), mRNA [NM_134022]	1.00	1.0	0.97	-1.0	0.04	-1.5	1.00	1.0	0.91	1.2	0.92	1.0	0.85	1.1	0.98	1.1	0.91	1.0
9030425E11Rik	NM_133733	Mus musculus RIKEN cDNA 9030425E11 gene (9030425E11Rik), mRNA [NM_133733]	0.74	1.4	0.00	1.8	0.00	1.8	1.00	1.0	0.92	1.1	0.11	1.4	0.89	1.1	0.98	-1.2	0.58	1.2
9230117N10Rik	NM_133775	Mus musculus RIKEN cDNA 9230117N10 gene (9230117N10Rik), mRNA [NM_133775]	0.95	-1.1	0.64	1.3	0.00	2.9	1.00	1.4	0.90	1.5	0.01	2.1	0.97	1.1	0.98	1.2	0.54	1.4

9530013L04Rik	AK020555	Mus musculus adult male urinary bladder cDNA, RIKEN full-length enriched library, clone:9530013L04 product:unclassifiable, full insert sequence. [AK020555]	0.72	-1.5	0.28	-1.5	0.06	-1.6	1.00	-1.2	0.90	-1.3	0.24	-1.4	0.82	-1.2	0.99	-1.1	0.80	-1.1
9530077C05Rik	NM_026739	Mus musculus RIKEN cDNA 9530077C05 gene (9530077C05Rik), mRNA [NM_026739]	0.98	-1.0	0.85	1.1	0.00	1.7	1.00	1.2	0.91	1.1	0.03	1.5	0.85	1.1	0.98	1.1	0.63	1.2
A_51_P144143	A_51_P144143	Unknown	0.95	1.1	0.26	1.4	0.03	1.6	1.00	1.2	0.46	1.5	0.05	1.5	0.86	1.1	0.99	1.0	0.03	1.7
A_51_P237890	A_51_P237890	Unknown	0.89	-1.2	0.31	-1.4	0.02	-1.5	1.00	-1.1	0.96	-1.1	0.36	-1.2	0.82	-1.2	0.99	-1.0	0.91	-1.0
A_52_P517668	A_52_P517668	Unknown	0.96	1.1	0.54	1.3	0.86	1.1	1.00	1.3	0.67	1.6	0.00	1.9	0.82	1.2	1.00	-1.0	0.02	1.8
A_52_P764117	A_52_P764117	Unknown	0.87	-1.2	0.51	-1.2	0.01	-1.5	1.00	-1.1	0.90	-1.2	0.30	-1.2	0.87	1.1	0.98	1.2	0.73	1.1
A030006P16Rik	CK791701	AGENCOURT_18667722 NIH_MGC_230 Mus musculus cDNA clone IMAGE:30848973 5', mRNA sequence [CK791701]	0.89	-1.3	0.43	-1.5	0.00	-3.0	1.00	-1.1	0.98	1.1	0.87	-1.1	0.80	1.5	0.98	1.3	0.83	1.1
A030009B12Rik	NM_026588	Mus musculus RIKEN cDNA A030009B12 gene (A030009B12Rik), mRNA [NM_026588]	0.98	1.0	0.82	1.1	0.91	1.1	1.00	1.2	0.90	1.3	0.07	1.5	0.80	1.3	0.98	1.2	0.18	1.5
A930038C07Rik	NM_172399	Mus musculus RIKEN cDNA A930038C07 gene (A930038C07Rik), mRNA [NM_172399]	0.85	1.4	0.28	1.5	0.63	1.2	1.00	1.3	0.65	1.6	0.05	1.6	0.81	1.2	0.98	1.2	0.69	1.2
AA733629	AA733629	AA733629 vu74b08.r1 Stratagene mouse skin (#937313) Mus musculus cDNA clone IMAGE:1197111 5' similar to gb:K02782 Mouse complement component C3 mRNA, alpha and beta subunits, (MOUSE);, mRNA sequence [AA733629]	0.90	1.1	0.10	1.5	0.05	1.4	1.00	1.1	0.95	1.1	0.81	1.1	0.92	1.1	0.98	1.2	0.49	1.3
AB069910	AB069910	Mus musculus V303-D-J-C mu mRNA, partial cds, sequence:R2-10. [AB069910]	0.99	1.0	0.67	1.1	0.95	1.0	1.00	-1.0	0.94	-1.1	0.65	-1.1	0.93	1.1	0.98	1.1	0.06	1.5
Abca8a	NM_153145	Mus musculus ATP-binding cassette, sub-family A (ABC1), member 8a (Abca8a), mRNA [NM_153145]	0.98	1.0	0.99	-1.0	0.07	-1.5	1.00	-1.1	0.98	1.1	0.31	-1.3	0.83	1.2	0.98	1.2	0.85	1.1
Abcg1	NM_009593	Mus musculus ATP-binding cassette, sub-family G (WHITE), member 1 (Abcg1), mRNA [NM_009593]	0.99	1.0	0.62	-1.2	0.03	-1.7	1.00	-1.2	0.95	-1.1	0.54	-1.2	0.83	-1.2	0.99	-1.0	0.59	1.3
Acsl4	NM_019477	Mus musculus acyl-CoA synthetase long-chain family member 4 (Acsl4), transcript variant 2, mRNA [NM_019477]	0.97	1.0	0.61	1.2	0.02	1.5	1.00	1.1	0.92	1.1	0.19	1.3	0.99	1.0	0.99	1.0	0.87	1.1
Acss1	NM_080575	Mus musculus acyl-CoA synthetase short-chain family member 1 (Acss1), mRNA [NM_080575]	0.89	-1.1	0.39	-1.3	0.00	-1.7	1.00	-1.0	0.90	-1.2	0.32	-1.2	0.94	1.0	0.98	1.1	0.95	-1.0
Acta2	NM_007392	Mus musculus actin, alpha 2, smooth muscle, aorta (Acta2), mRNA [NM_007392]	0.92	1.2	0.31	1.6	0.09	1.7	1.00	1.0	0.96	1.1	0.87	1.1	0.82	1.2	0.98	1.1	0.93	-1.1
Adam8	NM_007403	Mus musculus a disintegrin and metallopeptidase domain 8 (Adam8), mRNA [NM_007403]	1.00	-1.0	0.40	1.7	0.10	1.9	1.00	1.4	0.90	1.5	0.18	1.7	0.80	1.8	0.98	1.4	0.23	2.0

Adamts9	AK007436	Mus musculus 10 day old male pancreas cDNA, RIKEN full-length enriched library, clone:1810011L16 product:similar to ADAMTS-9 PRECURSOR (EC 3.4.24.-) (A DISINTEGRIN AND METALLOPROTEINASE WITH THROMBOSPONDIN MOTIFS 9) (ADAM-TS 9) (ADAM-TS9) [Homo sapie...	0.49	1.9	0.00	2.2	0.02	2.0	1.00	1.3	0.90	1.5	0.31	1.4	0.93	-1.1	0.98	-1.2	0.77	-1.2
Agtrl1	NM_011784	Mus musculus angiotensin receptor-like 1 (Agtrl1), mRNA [NM_011784]	0.94	-1.1	0.41	-1.3	0.01	-1.7	1.00	-1.0	0.98	1.0	0.30	-1.3	0.94	1.1	1.00	-1.0	0.57	-1.2
AI451617	AK136456	Mus musculus adult male colon cDNA, RIKEN full-length enriched library, clone:9030414N23 product:similar to Tripartite motif protein 30 (Down regulatory protein of interleukin 2 receptor) [Mus musculus], full insert sequence. [AK136456]	0.90	1.1	0.37	1.4	0.64	1.2	1.00	1.1	0.96	1.1	0.36	1.3	0.83	1.1	0.98	1.2	0.04	1.6
AI987662	NM_178899	Mus musculus expressed sequence AI987662 (AI987662), mRNA [NM_178899]	0.87	-1.2	0.26	-1.4	0.01	-1.6	1.00	-1.1	0.92	-1.1	0.11	-1.4	0.87	-1.1	0.99	1.0	0.62	-1.2
AK033738	AK033738	Mus musculus adult male cecum cDNA, RIKEN full-length enriched library, clone:9130604L22 product:weakly similar to HAI-2 RELATED SMALL PROTEIN (IMMORTALIZATION-UPREGULATED PROTEIN 1) (HEPATOCYTE GROWTH FACTOR ACTIVATOR INHIBITOR TYPE 2-RELATED SMALL...	0.89	1.1	0.39	1.2	0.00	1.9	1.00	1.0	0.99	1.0	0.59	1.1	0.80	1.2	0.98	1.3	0.94	1.0
AK041146	AK041146	Mus musculus adult male aorta and vein cDNA, RIKEN full-length enriched library, clone:A530085L05 product:FMS-like tyrosine kinase 3 ligand, full insert sequence. [AK041146]	0.90	-1.2	0.47	-1.3	0.00	-1.8	1.00	-1.1	0.91	-1.2	0.20	-1.3	0.90	-1.1	1.00	-1.0	0.98	1.0
AK054424	AK054424	Mus musculus 2 days pregnant adult female ovary cDNA, RIKEN full-length enriched library, clone:E330024G11 product:unclassifiable, full insert sequence. [AK054424]	0.72	1.5	0.47	1.4	0.53	1.2	1.00	1.2	0.91	1.2	0.07	1.6	0.98	-1.0	0.99	-1.1	0.60	-1.3
Akp2	NM_007431	Mus musculus alkaline phosphatase 2, liver (Akp2), mRNA [NM_007431]	0.90	1.2	0.23	1.6	0.01	1.9	1.00	1.1	0.90	1.3	0.31	1.4	0.99	1.0	0.98	1.1	0.36	1.5
Akr1b8	NM_008012	Mus musculus aldo-keto reductase family 1, member B8 (Akr1b8), mRNA [NM_008012]	1.00	1.0	0.31	1.4	0.00	1.7	1.00	1.2	0.91	1.1	0.09	1.4	0.81	1.2	0.98	1.1	0.51	1.2
Akr1c19	NM_001013785	Mus musculus aldo-keto reductase family 1, member C19 (Akr1c19), mRNA [NM_001013785]	0.92	1.1	0.54	1.2	0.01	1.5	1.00	1.0	0.96	1.1	0.70	1.1	0.80	1.2	0.98	1.3	0.03	1.5
Aldh1a3	NM_053080	Mus musculus aldehyde dehydrogenase family 1, subfamily A3 (Aldh1a3), mRNA [NM_053080]	0.99	-1.0	0.69	1.2	0.00	3.0	1.00	1.1	1.00	-1.0	0.72	1.2	0.88	1.2	0.98	1.1	0.95	1.1
Angptl4	NM_020581	Mus musculus angiopoietin-like 4 (Angptl4), mRNA [NM_020581]	0.89	1.5	0.37	2.3	0.07	2.8	1.00	-1.1	0.91	1.5	0.47	1.6	0.91	-1.2	0.98	-1.2	0.62	1.6
Ankrd1	NM_013468	Mus musculus ankyrin repeat domain 1 (cardiac muscle) (Ankrd1), mRNA [NM_013468]	0.96	-1.1	0.85	1.1	0.00	2.4	1.00	1.2	0.96	1.1	0.89	1.1	0.80	1.4	0.99	1.1	0.93	1.1

Aox3	NM_023617	Mus musculus aldehyde oxidase 3 (Aox3), mRNA [NM_023617]	0.99	-1.0	0.82	-1.1	0.01	-1.8	1.00	-1.2	0.98	-1.0	0.35	-1.3	0.93	1.1	0.98	1.2	0.79	-1.1
Areg	NM_009704	Mus musculus amphiregulin (Areg), mRNA [NM_009704]	0.99	1.0	0.80	1.2	0.33	1.5	1.00	1.5	0.90	1.7	0.01	2.1	0.94	-1.1	0.98	-1.2	0.85	-1.1
Arg1	NM_007482	Mus musculus arginase 1, liver (Arg1), mRNA [NM_007482]	0.96	1.1	0.41	1.4	0.01	1.8	1.00	1.2	0.92	1.2	0.12	1.5	0.88	1.1	0.98	1.2	0.78	1.1
Arg2	NM_009705	Mus musculus arginase type II (Arg2), mRNA [NM_009705]	0.87	1.3	0.28	1.7	0.04	1.8	1.00	1.2	0.90	1.6	0.10	1.7	0.84	1.2	0.98	1.4	0.08	2.0
Asf1b	NM_024184	Mus musculus ASF1 anti-silencing function 1 homolog B (S. cerevisiae) (Asf1b), mRNA [NM_024184]	0.98	-1.0	0.59	1.2	0.39	1.3	1.00	1.3	0.90	1.4	0.03	1.6	0.99	-1.0	0.98	-1.2	0.69	1.2
Atf3	NM_007498	Mus musculus activating transcription factor 3 (Atf3), mRNA [NM_007498]	0.95	1.1	0.60	1.2	0.67	1.2	1.00	1.3	0.90	1.5	0.04	1.7	0.86	1.1	1.00	1.0	0.89	1.1
Atp11a	NM_015804	Mus musculus ATPase, class VI, type 11A (Atp11a), mRNA [NM_015804]	0.87	1.2	0.48	1.2	0.01	1.5	1.00	-1.0	0.98	1.0	0.33	1.2	0.86	1.1	0.98	1.2	0.44	1.3
AU020206	AK049415	Mus musculus 7 days embryo whole body cDNA, RIKEN full-length enriched library, clone:C430005K08 product:unclassifiable, full insert sequence [AK049415]	0.93	-1.1	0.37	-1.3	0.00	-1.8	1.00	-1.1	0.91	-1.2	0.05	-1.5	0.93	-1.1	0.98	-1.1	0.71	-1.1
Aurka	NM_011497	Mus musculus aurora kinase A (Aurka), mRNA [NM_011497]	0.98	-1.0	0.83	1.1	0.34	1.4	1.00	1.3	0.90	1.5	0.04	1.8	0.99	1.0	0.98	-1.1	0.77	1.2
Axud1	NM_153287	Mus musculus AXIN1 up-regulated 1 (Axud1), mRNA [NM_153287]	0.18	3.5	0.13	2.9	0.02	3.0	1.00	1.3	0.90	1.8	0.11	2.3	0.97	1.1	1.00	-1.1	0.91	1.1
Aytl1	NM_173014	Mus musculus acyltransferase like 1 (Aytl1), mRNA [NM_173014]	0.86	1.2	0.21	1.3	0.33	1.2	1.00	1.1	0.92	1.1	0.60	1.1	0.92	1.1	0.98	1.1	0.00	1.5
B130024G19Rik	BC070425	Mus musculus RIKEN cDNA B130024G19 gene (B130024G19Rik), mRNA [NM_001004183]	0.90	-1.1	0.48	-1.3	0.11	-1.4	1.00	-1.1	0.90	-1.2	0.04	-1.5	0.81	1.2	0.98	1.1	0.84	1.1
Bbc3	NM_133234	Mus musculus Bcl-2 binding component 3 (Bbc3), mRNA [NM_133234]	0.87	-1.2	0.15	-1.5	0.00	-1.7	1.00	-1.2	0.90	-1.2	0.20	-1.3	0.81	-1.2	0.99	-1.0	0.99	1.0
BC010335	BC010335	Mus musculus cDNA clone IMAGE:3156499, **** WARNING: chimeric clone ****. [BC010335]	0.89	1.2	0.43	1.4	0.02	1.7	1.00	1.1	0.90	1.3	0.04	1.6	0.88	1.1	0.98	1.2	0.62	1.2
BC013672	NM_001081215	ENSMUST00000093485 [BC013672]	0.89	1.1	0.37	1.3	0.97	1.0	1.00	-1.1	0.99	1.0	0.67	1.1	0.80	1.2	0.98	1.2	0.01	1.5
BC021381	NM_145382	Mus musculus cDNA sequence BC021381 (BC021381), mRNA [NM_145382]	0.83	-1.3	0.18	-1.5	0.01	-1.6	1.00	-1.2	0.90	-1.3	0.01	-1.5	0.99	-1.0	0.98	1.1	0.96	-1.0
BC025462	NM_145946	Mus musculus cDNA sequence BC025462 (BC025462), mRNA [NM_145946]	0.95	1.1	0.51	1.3	0.21	1.4	1.00	1.2	0.90	1.2	0.05	1.6	0.98	-1.0	0.98	-1.2	0.81	-1.1
BC031498	BC031498	Mus musculus cDNA clone MGC:27817 IMAGE:3482714, complete cds. [BC031498]	0.94	-1.2	0.88	1.1	0.95	1.1	1.00	-1.0	0.98	1.1	0.86	-1.1	0.87	1.2	0.98	1.2	0.06	2.5
BC089618	NM_001081957	Mus musculus cDNA clone MGC:107680 IMAGE:6766535, complete cds. [BC089618]	0.99	1.0	0.05	2.3	0.01	2.4	1.00	1.8	0.65	2.1	0.02	2.4	0.80	1.5	0.98	1.3	0.00	3.9
Bcan	NM_007529	Mus musculus brevican (Bcan), mRNA [NM_007529]	0.97	-1.0	0.48	-1.3	0.00	-2.0	1.00	-1.0	1.00	1.0	0.68	-1.1	0.97	-1.0	0.99	-1.1	0.36	-1.5

Bcl2a1b	NM_007534	Mus musculus B-cell leukemia/lymphoma 2 related protein A1b (Bcl2a1b), mRNA [NM_007534]	0.92	1.1	0.48	1.4	0.19	1.5	1.00	1.1	0.90	1.4	0.24	1.4	0.89	1.1	0.99	1.1	0.04	1.8
Bcl2a1c	NM_007535	Mus musculus B-cell leukemia/lymphoma 2 related protein A1c (Bcl2a1c), mRNA [NM_007535]	0.90	1.2	0.37	1.5	0.21	1.5	1.00	1.1	0.79	1.6	0.18	1.5	0.80	1.3	0.98	1.2	0.00	2.0
Bcl3	NM_033601	Mus musculus B-cell leukemia/lymphoma 3 (Bcl3), mRNA [NM_033601]	0.98	-1.0	0.71	1.1	0.03	1.6	1.00	1.1	0.91	1.2	0.11	1.5	0.94	1.1	0.99	1.1	0.63	1.2
Bcl6	NM_009744	Mus musculus B-cell leukemia/lymphoma 6 (Bcl6), mRNA [NM_009744]	0.85	-1.3	0.31	-1.4	0.03	-1.5	1.00	-1.2	0.90	-1.2	0.18	-1.4	0.90	-1.1	1.00	1.0	0.88	-1.1
Bex2	NM_009749	Mus musculus brain expressed X-linked 2 (Bex2), mRNA [NM_009749]	1.00	-1.0	0.70	-1.2	0.03	-1.8	1.00	-1.1	0.99	-1.0	0.47	-1.3	0.96	1.1	0.98	1.3	0.14	-1.7
Bhlhb8	NM_010800	Mus musculus basic helix-loop-helix domain containing, class B, 8 (Bhlhb8), mRNA [NM_010800]	0.85	-1.3	0.66	-1.1	0.00	1.7	1.00	1.0	0.99	1.0	0.77	1.1	0.97	1.0	0.98	1.1	0.80	1.1
Birc3	NM_007464	Mus musculus baculoviral IAP repeat-containing 3 (Birc3), mRNA [NM_007464]	0.72	1.3	0.20	1.4	0.00	1.5	1.00	-1.0	0.90	1.2	0.40	1.2	0.98	1.0	0.98	1.1	0.04	1.5
Birc5	NM_009689	Mus musculus baculoviral IAP repeat-containing 5 (Birc5), transcript variant 1, mRNA [NM_009689]	0.99	-1.0	0.59	1.3	0.32	1.5	1.00	1.4	0.90	1.6	0.01	2.2	1.00	-1.0	0.98	-1.2	0.65	1.3
Bmper	NM_028472	Mus musculus BMP-binding endothelial regulator (Bmper), mRNA [NM_028472]	0.87	1.3	0.43	1.3	0.04	1.5	1.00	1.1	0.91	1.2	0.78	1.1	0.81	1.2	0.98	1.1	0.63	1.2
C3	NM_009778	Mus musculus complement component 3 (C3), mRNA [NM_009778]	0.86	1.3	0.00	2.3	0.00	2.0	1.00	1.1	0.89	1.5	0.26	1.4	0.94	1.1	0.98	0.9	0.45	1.5
Calr	NM_007591	Mus musculus calreticulin (Calr), mRNA [NM_007591]	0.87	1.3	0.18	1.6	0.03	1.7	1.00	-1.1	0.96	1.1	0.63	1.2	0.88	-1.1	0.98	-1.2	0.94	-1.0
Capg	NM_007599	Mus musculus capping protein (actin filament), gelsolin-like (Capg), transcript variant 1, mRNA [NM_007599]	0.96	-1.1	0.54	1.2	0.79	1.1	1.00	1.1	0.89	1.3	0.22	1.3	0.80	1.2	0.98	1.1	0.04	1.5
Car13	NM_024495	Mus musculus carbonic anhydrase 13 (Car13), mRNA [NM_024495]	0.98	-1.0	0.62	1.2	0.03	1.6	1.00	1.1	0.93	1.1	0.38	1.3	0.96	1.0	0.99	-1.1	0.79	1.1
Casc5	NM_029617	Mus musculus cancer susceptibility candidate 5, mRNA (cDNA clone MGC:91208 IMAGE:30104270), complete cds. [BC080815]	0.94	1.1	0.70	1.2	0.46	1.4	1.00	1.3	0.90	1.4	0.02	1.9	1.00	-1.0	0.98	-1.3	0.71	-1.2
Casp4	NM_007609	Mus musculus caspase 4, apoptosis-related cysteine peptidase (Casp4), mRNA [NM_007609]	0.87	1.2	0.09	1.6	0.02	1.6	1.00	1.2	0.90	1.3	0.05	1.5	0.81	1.2	0.98	1.1	0.45	1.3
Cat	NM_009804	Mus musculus catalase (Cat), mRNA [NM_009804]	0.87	-1.2	0.36	-1.3	0.01	-1.5	1.00	-1.3	0.90	-1.2	0.19	-1.3	0.81	-1.1	1.00	1.0	0.77	-1.1
Cav1	NM_007616	Mus musculus caveolin, caveolae protein 1 (Cav1), mRNA [NM_007616]	0.99	1.0	0.48	-1.3	0.05	-1.5	1.00	-1.2	0.92	-1.1	0.07	-1.5	0.82	-1.2	0.98	-1.1	0.33	-1.4
Cbx7	NM_144811	Mus musculus chromobox homolog 7 (Cbx7), mRNA [NM_144811]	0.87	-1.2	0.17	-1.4	0.01	-1.6	1.00	-1.1	0.90	-1.3	0.08	-1.4	0.87	1.1	0.98	1.2	0.84	1.1
Ccdc67	NM_181816	Mus musculus coiled-coil domain containing 67 (Ccdc67), mRNA [NM_181816]	0.99	-1.0	0.96	1.0	0.92	1.0	1.00	1.2	0.18	1.5	0.00	1.6	0.94	1.0	1.00	1.0	0.82	1.1
Ccl11	NM_011330	Mus musculus small chemokine (C-C motif) ligand 11 (Ccl11), mRNA [NM_011330]	0.94	-1.1	0.52	1.4	0.04	1.8	1.00	-1.0	0.96	1.1	0.70	1.2	0.80	1.3	0.98	1.3	0.43	1.6

Ccl12	NM_011331	Mus musculus chemokine (C-C motif) ligand 12 (Ccl12), mRNA [NM_011331]	0.97	1.1	0.31	1.7	0.01	2.2	1.00	-1.0	0.94	1.2	0.09	1.7	0.89	1.1	1.00	-1.0	0.08	2.0
Ccl17	NM_011332	Mus musculus chemokine (C-C motif) ligand 17 (Ccl17), mRNA [NM_011332]	0.92	1.2	0.28	1.8	0.01	2.2	1.00	1.2	0.55	2.0	0.03	2.2	0.84	1.2	0.98	1.8	0.41	1.7
Ccl2	NM_011333	Mus musculus chemokine (C-C motif) ligand 2 (Ccl2), mRNA [NM_011333]	0.97	1.1	0.38	2.0	0.00	5.0	1.00	1.5	0.90	1.8	0.01	3.2	0.84	1.3	1.00	1.1	0.02	3.4
Ccl24	NM_019577	Mus musculus chemokine (C-C motif) ligand 24 (Ccl24), mRNA [NM_019577]	0.93	-1.2	0.74	1.3	0.00	3.3	1.00	0.0	1.00	1.0	0.87	1.1	0.92	1.1	0.99	0.1	0.85	-0.1
Ccl3	NM_011337	Mus musculus chemokine (C-C motif) ligand 3 (Ccl3), mRNA [NM_011337]	0.93	1.1	0.47	1.4	0.02	1.8	1.00	1.1	0.90	1.5	0.19	1.5	0.86	1.2	0.98	1.1	0.01	2.1
Ccl4	NM_013652	Mus musculus chemokine (C-C motif) ligand 4 (Ccl4), mRNA [NM_013652]	0.87	1.3	0.21	1.8	0.01	2.3	1.00	1.1	0.96	1.1	0.54	1.3	0.84	1.2	0.98	1.1	0.17	1.8
Ccl7	NM_013654	Mus musculus chemokine (C-C motif) ligand 7 (Ccl7), mRNA [NM_013654]	0.98	0.0	0.44	1.9	0.00	4.2	1.00	1.3	0.90	1.5	0.05	2.5	0.92	1.2	1.00	0.0	0.21	2.4
Ccl8	NM_021443	Mus musculus chemokine (C-C motif) ligand 8 (Ccl8), mRNA [NM_021443]	0.91	1.3	0.00	2.9	0.04	2.3	1.00	1.7	0.65	2.2	0.03	2.3	0.92	1.1	0.98	1.2	0.08	2.5
Ccl9	NM_011338	Mus musculus chemokine (C-C motif) ligand 9 (Ccl9), mRNA [NM_011338]	0.88	1.3	0.15	2.0	0.04	1.9	1.00	1.4	0.46	2.0	0.01	2.2	0.85	1.2	0.98	1.2	0.00	2.6
Ccna1	NM_007628	Mus musculus cyclin A1 (Ccna1), mRNA [NM_007628]	0.95	1.1	0.97	-1.0	0.90	1.1	1.00	1.5	0.00	2.6	0.00	2.3	0.91	1.1	1.00	1.0	0.88	1.1
Ccna2	NM_009828	Mus musculus cyclin A2 (Ccna2), mRNA [NM_009828]	0.96	1.1	0.68	1.2	0.25	1.6	1.00	1.3	0.90	1.5	0.05	1.9	0.97	-1.1	0.98	-1.2	0.89	1.1
Ccnb1	NM_172301	Mus musculus cyclin B1 (Ccnb1), mRNA [NM_172301]	0.91	-1.2	0.71	-1.2	0.85	1.1	1.00	1.2	0.90	1.4	0.07	1.7	0.92	-1.1	0.98	-1.3	0.99	-1.0
Ccnb2	NM_007630	Mus musculus cyclin B2 (Ccnb2), mRNA [NM_007630]	0.98	-1.0	0.82	1.1	0.43	1.3	1.00	1.3	0.86	1.5	0.00	1.9	0.99	1.0	0.98	-1.2	0.64	1.2
Ccng2	NM_007635	Mus musculus cyclin G2 (Ccng2), mRNA [NM_007635]	0.91	-1.1	0.28	-1.4	0.01	-1.7	1.00	-1.1	0.90	-1.3	0.23	-1.3	0.86	-1.1	0.98	-1.2	0.78	-1.1
Ccr5	NM_009917	Mus musculus chemokine (C-C motif) receptor 5 (Ccr5), mRNA [NM_009917]	1.00	1.0	0.40	1.4	0.19	1.4	1.00	1.1	0.90	1.3	0.45	1.2	0.80	1.3	0.98	1.2	0.02	1.8
Ccrn4l	NM_009834	Mus musculus CCR4 carbon catabolite repression 4-like (S. cerevisiae) (Ccrn4l), mRNA [NM_009834]	0.87	1.2	0.59	1.2	0.01	1.6	1.00	1.1	0.92	1.1	0.09	1.3	0.95	-1.0	0.99	1.0	0.74	1.1
Cd14	NM_009841	Mus musculus CD14 antigen (Cd14), mRNA [NM_009841]	0.87	1.3	0.03	2.2	0.00	3.2	1.00	1.6	0.00	2.5	0.00	3.1	0.81	1.3	0.98	1.1	0.04	2.2
Cd177	NM_026862	Mus musculus CD177 antigen (Cd177), mRNA [NM_026862]	0.91	1.2	0.05	1.9	0.03	1.8	1.00	1.1	0.90	1.3	0.57	1.2	0.82	1.2	0.99	1.1	0.60	1.3
Cd200r1	NM_021325	Mus musculus CD200 receptor 1 (Cd200r1), mRNA [NM_021325]	0.92	1.1	0.48	1.3	0.69	1.1	1.00	1.2	0.90	1.3	0.31	1.2	0.80	1.2	0.98	1.1	0.06	1.6
Cd300d	NM_134158	Mus musculus Cd300D antigen (Cd300d), mRNA [NM_134158]	0.94	1.1	0.75	1.1	0.81	-1.1	1.00	1.1	0.91	1.2	0.74	1.1	0.82	1.2	0.98	1.1	0.04	1.7
Cd300lf	NM_145634	Mus musculus CD300 antigen like family member F (Cd300lf), mRNA [NM_145634]	0.87	1.3	0.23	1.6	0.02	1.7	1.00	1.1	0.92	1.2	0.28	1.4	0.83	1.2	0.98	1.3	0.01	1.9

Cd302	NM_025422	Mus musculus CD302 antigen (Cd302), mRNA [NM_025422]	0.87	1.2	0.15	1.4	0.00	1.8	1.00	1.1	0.90	1.2	0.12	1.3	0.97	-1.0	0.98	-1.2	0.51	1.2
Cd33	NM_021293	Mus musculus CD33 antigen (Cd33), mRNA [NM_021293]	0.93	1.1	0.39	1.3	0.33	1.2	1.00	1.0	0.90	1.1	0.39	1.2	0.83	1.1	0.98	1.1	0.00	1.5
Cd44	NM_009851	Mus musculus CD44 antigen (Cd44), transcript variant 1, mRNA [NM_009851]	0.93	1.1	0.59	1.2	0.65	1.1	1.00	1.1	0.90	1.2	0.11	1.3	0.90	1.1	0.98	1.1	0.02	1.5
Cd68	NM_009853	Mus musculus CD68 antigen (Cd68), mRNA [NM_009853]	0.97	-1.1	0.55	1.3	0.29	1.3	1.00	1.3	0.73	1.5	0.03	1.6	0.88	1.1	0.98	-1.1	0.00	2.0
Cd84	NM_013489	Mus musculus CD84 antigen (Cd84), mRNA [NM_013489]	0.99	1.0	0.76	1.1	0.93	1.0	1.00	1.1	0.90	1.3	0.15	1.3	0.80	1.1	0.98	1.1	0.00	1.7
Cdc20	NM_023223	Mus musculus cell division cycle 20 homolog (S. cerevisiae) (Cdc20), mRNA [NM_023223]	0.97	-1.1	0.84	1.1	0.50	1.4	1.00	1.5	0.90	1.8	0.02	2.3	0.97	1.1	0.98	-1.2	0.99	1.0
Cdc42ep3	NM_026514	Mus musculus CDC42 effector protein (Rho GTPase binding) 3 (Cdc42ep3), mRNA [NM_026514]	0.96	-1.1	0.61	-1.2	0.03	-1.6	1.00	-1.1	0.98	1.0	0.78	-1.1	0.90	1.1	0.98	1.1	0.72	1.1
Cdca1	NM_023284	Mus musculus cell division cycle associated 1 (Cdca1), mRNA [NM_023284]	0.98	-1.0	0.95	1.0	0.61	1.2	1.00	1.3	0.90	1.3	0.05	1.7	0.97	-1.0	0.98	-1.2	1.00	-1.0
Cdca3	NM_013538	Mus musculus cell division cycle associated 3 (Cdca3), mRNA [NM_013538]	0.95	-1.1	0.75	1.2	0.46	1.3	1.00	1.3	0.90	1.4	0.04	1.8	0.92	1.1	0.98	-1.1	0.61	1.3
Cdca5	NM_026410	Mus musculus cell division cycle associated 5 (Cdca5), mRNA [NM_026410]	0.98	-1.1	0.61	1.3	0.22	1.5	1.00	1.2	0.90	1.4	0.09	1.7	0.97	1.0	1.00	-1.0	0.67	1.2
Cdca8	NM_026560	Mus musculus cell division cycle associated 8 (Cdca8), mRNA [NM_026560]	1.00	-1.0	0.56	1.3	0.29	1.4	1.00	1.4	0.67	1.7	0.00	2.2	0.97	1.0	0.98	-1.1	0.69	1.2
Cdkn3	BC049694	Mus musculus cyclin-dependent kinase inhibitor 3, mRNA (cDNA clone MGC:58593 IMAGE:6705916), complete cds. [BC049694]	0.96	-1.1	0.81	0.0	0.54	1.3	1.00	1.3	0.90	1.3	0.03	1.9	0.90	-1.1	0.98	-1.2	0.91	0.0
Cebpd	NM_007679	Mus musculus CCAAT/enhancer binding protein (C/EBP), delta (Cebpd), mRNA [NM_007679]	0.49	2.6	0.18	2.5	0.03	2.6	1.00	1.2	0.90	1.7	0.15	2.1	1.00	1.0	1.00	-1.0	0.88	1.2
Cenpe	NM_173762	Mus musculus centromere protein E, mRNA (cDNA clone IMAGE:6811557), partial cds. [BC059032]	0.98	-1.1	0.73	1.2	0.43	1.4	1.00	1.3	0.90	1.6	0.01	2.1	0.97	1.1	0.98	-1.2	0.60	1.3
Cenpf	NM_001081363	PREDICTED: Mus musculus centromere autoantigen F, transcript variant 2 (Cenpf), mRNA [XM_899897]	0.97	-1.1	1.00	-1.0	0.63	1.3	1.00	1.3	0.90	1.6	0.02	2.0	0.99	-1.0	0.98	-1.2	0.95	-1.0
Cfb	NM_008198	Mus musculus complement factor B (Cfb), mRNA [NM_008198]	0.94	1.1	0.15	1.7	0.07	1.6	1.00	1.2	0.89	1.5	0.24	1.4	0.99	1.0	0.98	1.1	0.51	1.3
Cftr	NM_021050	Mus musculus cystic fibrosis transmembrane conductance regulator homolog (Cftr), mRNA [NM_021050]	0.92	1.2	0.63	1.2	0.66	-1.2	1.00	1.3	0.90	1.5	0.08	1.7	0.82	1.2	0.98	1.3	0.01	2.0
Ch25h	NM_009890	Mus musculus cholesterol 25-hydroxylase (Ch25h), mRNA [NM_009890]	0.50	2.0	0.00	2.8	0.00	4.8	1.00	1.7	0.00	3.0	0.00	3.3	0.83	1.3	0.98	1.5	0.00	2.8
Chl1	NM_007697	Mus musculus cell adhesion molecule with homology to L1CAM (Chl1), mRNA [NM_007697]	0.97	0.1	0.21	1.6	0.00	2.7	1.00	1.2	0.92	1.2	0.09	1.7	0.82	1.2	1.00	1.0	0.41	1.4
Chst3	NM_016803	Mus musculus carbohydrate (chondroitin 6/keratan) sulfotransferase 3 (Chst3), mRNA [NM_016803]	0.97	-1.1	0.67	-1.2	0.22	-1.4	1.00	-1.2	0.95	-1.1	0.04	-1.5	0.94	1.1	0.98	1.2	0.97	-1.0

CJ042244	CJ042244	CJ042244 RIKEN full-length enriched mouse cDNA library, C57BL [CJ042244]	0.92	-1.1	0.74	1.1	0.22	1.3	1.00	1.3	0.90	1.3	0.00	1.6	0.83	1.2	0.98	1.1	0.49	1.3
Ckap4	NM_175451	Mus musculus cytoskeleton-associated protein 4 (Ckap4), mRNA [NM_175451]	0.87	1.4	0.23	1.8	0.08	1.8	1.00	1.2	0.92	1.2	0.00	2.1	0.93	1.1	0.98	-1.2	0.98	-1.0
Cks1b	NM_016904	Mus musculus CDC28 protein kinase 1b (Cks1b), mRNA [NM_016904]	0.99	-1.0	0.60	1.2	0.09	1.5	1.00	1.2	0.90	1.3	0.02	1.7	0.96	1.0	1.00	-1.0	0.65	1.2
Cks2	NM_025415	Mus musculus CDC28 protein kinase regulatory subunit 2 (Cks2), mRNA [NM_025415]	0.99	0.0	0.78	1.1	0.50	1.3	1.00	1.2	0.78	1.5	0.01	1.8	0.87	-1.1	0.98	-1.2	0.99	1.0
Clca1	NM_009899	Mus musculus chloride channel calcium activated 1 (Clca1), mRNA [NM_009899]	0.87	1.2	0.53	1.2	0.00	1.6	1.00	1.0	0.96	1.1	0.53	1.2	1.00	-1.0	0.98	1.1	0.88	1.1
Clec4d	NM_010819	Mus musculus C-type lectin domain family 4, member d (Clec4d), mRNA [NM_010819]	0.92	1.2	0.29	1.7	0.19	1.6	1.00	1.3	0.94	1.2	0.29	1.5	0.86	1.2	0.98	1.4	0.08	2.0
Clec4e	NM_019948	Mus musculus C-type lectin domain family 4, member e (Clec4e), mRNA [NM_019948]	0.94	1.1	0.29	1.4	0.02	1.6	1.00	1.1	0.96	1.1	0.52	1.2	0.98	-1.0	1.00	1.0	0.45	1.3
Clec4n	NM_020001	Mus musculus C-type lectin domain family 4, member n (Clec4n), mRNA [NM_020001]	0.93	1.2	0.52	1.4	0.09	1.8	1.00	1.3	0.67	1.8	0.03	1.9	0.83	1.3	0.98	1.2	0.00	3.0
Clec5a	NM_001038604	Mus musculus C-type lectin domain family 5, member a (Clec5a), transcript variant 1, mRNA [NM_001038604]	0.87	1.3	0.19	1.6	0.00	2.0	1.00	1.2	0.90	1.5	0.00	1.7	0.93	1.1	0.98	1.1	0.00	2.4
Clec7a	NM_020008	Mus musculus C-type lectin domain family 7, member a (Clec7a), mRNA [NM_020008]	0.94	1.2	0.62	1.3	0.33	1.5	1.00	1.4	0.86	1.8	0.78	1.2	0.92	1.1	0.98	1.2	0.03	2.5
Clk1	NM_009905	Mus musculus CDC-like kinase 1 (Clk1), mRNA [NM_009905]	0.49	-1.7	0.16	-1.7	0.06	-1.6	1.00	0.0	0.97	-1.1	0.32	-1.3	0.93	-1.1	0.98	-1.1	0.71	-1.2
Clu	NM_013492	Mus musculus clusterin (Clu), mRNA [NM_013492]	0.91	1.2	0.19	1.6	0.01	1.7	1.00	1.3	0.90	1.3	0.00	1.7	0.82	1.2	0.98	1.1	0.65	1.2
Col4a6	BC004800	Mus musculus procollagen, type IV, alpha 6, mRNA (cDNA clone IMAGE:3589442), partial cds. [BC004800]	0.87	-1.3	0.47	-1.3	0.08	-1.5	1.00	-1.1	0.96	-1.1	0.21	-1.4	0.94	1.1	0.98	1.1	0.71	-1.2
Cp	NM_007752	Mus musculus ceruloplasmin (Cp), mRNA [NM_007752]	0.83	1.8	0.00	3.0	0.00	3.5	1.00	1.3	0.90	1.9	0.05	2.2	0.95	1.1	1.00	-1.0	0.87	1.1
Cpne5	NM_153166	Mus musculus copine V (Cpne5), mRNA [NM_153166]	0.96	-1.1	0.52	-1.4	0.11	-1.7	1.00	-1.3	0.90	-1.3	0.08	-1.7	0.96	-1.1	0.99	1.0	0.81	-1.1
Csf2	NM_009969	Mus musculus colony stimulating factor 2 (granulocyte-macrophage) (Csf2), mRNA [NM_009969]	0.95	-1.1	0.59	1.3	0.63	1.3	1.00	1.1	0.86	1.7	0.15	1.7	0.86	1.2	0.98	1.3	0.02	2.5
Csf2rb1	AK154286	Mus musculus NOD-derived CD11c +ve dendritic cells cDNA, RIKEN full-length enriched library, clone:F630014N20 product:colony stimulating factor 2 receptor, beta 1, low-affinity (granulocyte-macrophage), full insert sequence. [AK154286]	0.94	1.1	0.18	1.4	0.00	1.6	1.00	1.2	0.46	1.5	0.02	1.5	0.94	1.1	0.98	-1.1	0.06	1.6
Csf2rb2	NM_007781	Mus musculus colony stimulating factor 2 receptor, beta 2, low-affinity (granulocyte-macrophage) (Csf2rb2), mRNA [NM_007781]	0.91	1.1	0.23	1.5	0.05	1.5	1.00	1.2	0.36	1.5	0.00	1.6	0.95	1.0	0.98	-1.1	0.01	1.7

Cstb	NM_007793	Mus musculus cystatin B (Cstb), mRNA [NM_007793]	0.91	1.1	0.23	1.4	0.00	1.7	1.00	1.2	0.90	1.3	0.03	1.5	0.89	1.1	0.98	1.1	0.26	1.4
Ctps	NM_016748	Mus musculus cytidine 5'-triphosphate synthase (Ctps), mRNA [NM_016748]	0.95	1.1	0.54	1.3	0.00	2.3	1.00	1.1	0.90	1.2	0.02	1.7	0.93	-1.1	0.99	1.1	0.49	1.4
Ctsd	NM_009983	Mus musculus cathepsin D (Ctsd), mRNA [NM_009983]	0.97	-1.0	0.92	-1.0	0.32	-1.3	1.00	1.2	0.90	1.3	0.43	1.2	0.97	1.0	1.00	-1.0	0.04	1.6
Ctsk	NM_007802	Mus musculus cathepsin K (Ctsk), mRNA [NM_007802]	0.95	1.1	0.56	1.4	0.24	1.6	1.00	1.5	0.24	2.5	0.00	2.7	0.81	1.3	0.98	1.4	0.00	2.7
Ctss	NM_021281	Mus musculus cathepsin S (Ctss), mRNA [NM_021281]	0.96	1.1	0.82	1.1	0.94	-1.0	1.00	1.2	0.90	1.4	0.31	1.3	1.00	-1.0	0.99	-1.1	0.00	2.0
Cxcl1	NM_008176	Mus musculus chemokine (C-X-C motif) ligand 1 (Cxcl1), mRNA [NM_008176]	0.98	1.1	0.49	1.6	0.00	2.8	1.00	-1.0	0.90	1.4	0.21	1.8	0.91	-1.1	0.98	-1.2	0.60	1.5
Cxcl10	NM_021274	Mus musculus chemokine (C-X-C motif) ligand 10 (Cxcl10), mRNA [NM_021274]	0.92	1.3	0.13	2.9	0.01	3.5	1.00	1.2	0.92	1.4	0.05	2.7	0.94	1.1	1.00	1.0	0.46	2.0
Cxcl12	NM_021704	Mus musculus chemokine (C-X-C motif) ligand 12 (Cxcl12), transcript variant 1, mRNA [NM_021704]	0.99	1.0	0.23	1.5	0.01	1.6	1.00	1.0	1.00	-1.0	0.40	1.2	0.85	-1.1	0.98	-1.2	0.77	1.1
Cxcl5	NM_009141	Mus musculus chemokine (C-X-C motif) ligand 5 (Cxcl5), mRNA [NM_009141]	0.88	1.6	0.38	2.4	0.07	3.2	1.00	1.4	0.26	4.2	0.01	4.1	0.98	-1.1	0.98	-1.3	0.40	2.6
Cxcl9	NM_008599	Mus musculus chemokine (C-X-C motif) ligand 9 (Cxcl9), mRNA [NM_008599]	0.99	1.0	0.32	1.5	0.09	1.6	1.00	1.1	0.90	1.4	0.14	1.5	0.80	1.3	0.98	1.1	0.04	1.8
Cybb	NM_007807	Mus musculus cytochrome b-245, beta polypeptide (Cybb), mRNA [NM_007807]	0.89	1.2	0.52	1.3	0.99	-1.0	1.00	1.1	0.90	1.2	0.80	1.1	0.81	1.2	0.98	1.1	0.04	1.8
Cyp7b1	NM_007825	Mus musculus cytochrome P450, family 7, subfamily b, polypeptide 1 (Cyp7b1), mRNA [NM_007825]	0.87	1.3	0.11	2.1	0.00	3.2	1.00	1.1	0.92	1.2	0.15	1.7	0.81	1.3	0.98	1.4	0.43	1.6
D11Lgp2e	NM_030150	Mus musculus DNA segment, Chr 11, Lothar Hennighausen 2, expressed (D11Lgp2e), mRNA [NM_030150]	0.99	1.0	0.49	1.3	0.92	-1.0	1.00	-1.1	0.97	1.1	0.62	1.1	0.98	1.0	1.00	-1.0	0.02	1.6
D17H6S56E-5	BI555125	Mus musculus DNA segment, Chr 17, human D6S56E 5 (D17H6S56E-5), mRNA [NM_033075]	0.94	1.2	0.40	1.7	0.03	2.2	1.00	1.5	0.47	2.1	0.00	3.0	0.91	1.1	0.99	0.0	0.15	2.1
D4Wsu53e	NM_023665	Mus musculus DNA segment, Chr 4, Wayne State University 53, expressed (D4Wsu53e), mRNA [NM_023665]	0.85	-1.2	0.22	-1.4	0.00	-1.6	1.00	-1.1	0.92	-1.1	0.25	-1.2	0.80	-1.2	0.98	-1.2	0.28	-1.3
Dhcr24	NM_053272	Mus musculus 24-dehydrocholesterol reductase (Dhcr24), mRNA [NM_053272]	0.97	1.1	0.71	1.2	0.60	1.3	1.00	1.4	0.90	1.4	0.06	1.8	0.81	1.3	1.00	1.0	0.80	1.2
Dleu2	AK084358	Mus musculus 12 days embryo eyeball cDNA, RIKEN full-length enriched library, clone:D230030K09 product:deleted in lymphocytic leukemia, 2, full insert sequence. [AK084358]	0.93	-1.1	0.62	-1.2	0.03	-1.6	1.00	-1.1	0.99	1.0	0.52	-1.2	0.99	-1.0	1.00	1.0	0.99	1.0
Dnajc3	NM_008929	Mus musculus DnaJ (Hsp40) homolog, subfamily C, member 3 (Dnajc3), mRNA [NM_008929]	0.79	1.4	0.17	1.5	0.05	1.5	1.00	1.1	0.90	1.2	0.27	1.3	0.97	-1.0	0.98	-1.1	0.69	-1.2
Dok2	NM_010071	Mus musculus docking protein 2 (Dok2), mRNA [NM_010071]	0.99	1.0	0.23	1.4	0.01	1.6	1.00	1.0	0.90	1.2	0.53	1.1	0.85	1.1	0.98	1.1	0.57	1.2

Dpysl2	NM_009955	Mus musculus dihydropyrimidinase-like 2 (Dpysl2), mRNA [NM_009955]	0.98	1.0	0.57	-1.2	0.02	-1.5	1.00	-1.3	0.90	-1.3	0.13	-1.4	0.83	-1.1	1.00	-1.0	0.63	-1.2
Dusp8	NM_008748	Mus musculus dual specificity phosphatase 8 (Dusp8), mRNA [NM_008748]	0.87	1.3	0.51	1.3	0.76	1.1	1.00	1.1	0.90	1.4	0.06	1.5	0.93	-1.1	0.98	-1.1	0.53	-1.3
E030010N08Rik	XM_355224	PREDICTED: Mus musculus RIKEN cDNA E030010N08 gene (E030010N08Rik), mRNA [XM_355224]	0.96	1.1	0.70	1.2	0.99	1.0	1.00	1.3	0.00	2.2	0.00	2.5	0.80	1.3	0.98	1.2	0.65	1.2
E2f7	NM_178609	Mus musculus E2F transcription factor 7 (E2f7), mRNA [NM_178609]	0.96	-1.1	0.99	1.0	0.58	1.2	1.00	1.1	0.90	1.2	0.08	1.5	0.88	-1.1	0.98	-1.1	0.67	-1.2
E430002G05Rik	NM_173749	Mus musculus RIKEN cDNA E430002G05 gene (E430002G05Rik), mRNA [NM_173749]	0.87	-1.2	0.55	-1.2	0.01	-1.5	1.00	-1.1	0.94	-1.1	0.77	-1.1	0.93	1.1	0.98	1.2	0.68	1.1
Ect2	NM_007900	Mus musculus ect2 oncogene (Ect2), mRNA [NM_007900]	0.98	1.1	0.80	1.1	0.26	1.5	1.00	1.3	0.90	1.5	0.00	2.2	0.86	-1.2	0.98	-1.2	0.75	-1.2
Egr2	NM_010118	Mus musculus early growth response 2 (Egr2), mRNA [NM_010118]	0.87	1.3	0.43	1.5	0.07	1.7	1.00	1.1	0.90	1.4	0.32	1.4	0.92	1.1	0.98	1.1	0.46	1.5
Ehd4	NM_133838	Mus musculus EH-domain containing 4 (Ehd4), mRNA [NM_133838]	0.97	1.0	0.52	-1.2	0.09	-1.4	1.00	-1.2	0.94	-1.1	0.02	-1.5	0.89	-1.1	0.98	1.1	0.42	-1.3
Eif3s8	NM_146200	Mus musculus eukaryotic translation initiation factor 3, subunit 8 (Eif3s8), mRNA [NM_146200]	0.87	1.4	0.52	1.4	0.17	1.7	1.00	1.4	0.90	1.5	0.09	1.8	0.94	1.1	0.98	-1.2	0.80	-1.2
Emilin2	NM_145158	Mus musculus elastin microfibril interfacer 2 (Emilin2), mRNA [NM_145158]	0.95	-1.1	0.22	1.5	0.02	1.5	1.00	1.2	0.91	1.2	0.45	1.2	0.80	1.3	0.98	1.1	0.43	1.3
ENSMUST00000084869	M20831	PREDICTED: Mus musculus similar to Ig heavy chain V-I region V35 precursor (LOC629871), mRNA [XM_894812]	0.92	-1.1	0.95	-1.0	0.95	-1.0	1.00	-1.0	1.00	1.0	0.89	-1.0	0.87	1.1	1.00	1.0	0.06	1.6
Ephx1	NM_010145	Mus musculus epoxide hydrolase 1, microsomal (Ephx1), mRNA [NM_010145]	0.87	-1.2	0.45	-1.2	0.00	-1.5	1.00	-1.1	0.90	-1.1	0.26	-1.2	0.84	-1.1	1.00	-1.0	0.95	-1.0
Ets1	NM_011808	Mus musculus E26 avian leukemia oncogene 1, 5' domain (Ets1), transcript variant 1, mRNA [NM_011808]	1.00	-1.0	0.57	-1.2	0.16	-1.4	1.00	-1.2	0.91	-1.2	0.09	-1.5	0.93	-1.1	0.99	-1.1	0.59	-1.2
F10	NM_007972	Mus musculus coagulation factor X (F10), mRNA [NM_007972]	0.95	1.1	0.35	1.4	0.03	1.6	1.00	1.2	0.90	1.4	0.03	1.6	0.87	1.1	0.98	1.3	0.10	1.6
F3	NM_010171	Mus musculus coagulation factor III (F3), mRNA [NM_010171]	0.97	1.1	0.96	1.0	0.06	1.6	1.00	-1.0	0.93	-1.2	0.69	-1.1	0.87	1.1	0.98	1.2	0.98	0.0
F7	NM_010172	Mus musculus coagulation factor VII (F7), mRNA [NM_010172]	0.95	1.1	0.62	1.2	0.64	1.2	1.00	1.1	0.46	1.7	0.32	1.3	0.90	1.1	0.98	1.3	0.08	1.7
Fabp1	NM_017399	Mus musculus fatty acid binding protein 1, liver (Fabp1), mRNA [NM_017399]	0.93	-1.2	0.66	-1.2	0.01	-2.0	1.00	-1.2	0.97	-1.1	0.67	-1.2	0.99	-1.0	0.99	-1.1	0.95	-1.0
Fbln1	NM_010180	Mus musculus fibulin 1 (Fbln1), mRNA [NM_010180]	0.91	-1.2	0.75	-1.2	0.05	-2.0	1.00	-1.3	0.93	-1.2	0.39	-1.4	0.91	-1.1	0.99	-1.1	0.92	1.1
Fcer1g	NM_010185	Mus musculus Fc receptor, IgE, high affinity I, gamma polypeptide (Fcer1g), mRNA [NM_010185]	0.87	1.2	0.10	1.5	0.04	1.4	1.00	1.2	0.90	1.4	0.18	1.3	0.80	1.2	0.98	1.1	0.05	1.6
Fcgr1	NM_010186	Mus musculus Fc receptor, IgG, high affinity I (Fcgr1), mRNA [NM_010186]	0.99	1.0	0.51	1.3	0.38	1.3	1.00	1.2	0.90	1.2	0.41	1.3	0.88	1.1	1.00	-1.0	0.00	2.1

Fcgr2b	NM_010187	Mus musculus Fc receptor, IgG, low affinity IIb (Fcgr2b), mRNA [NM_010187]	0.98	-0.3	0.59	1.2	0.11	1.4	1.00	1.1	0.90	1.3	0.25	1.3	0.97	0.3	0.98	1.2	0.02	1.6
Fcgr3	NM_010188	Mus musculus Fc receptor, IgG, low affinity III (Fcgr3), mRNA [NM_010188]	0.96	0.0	0.42	1.3	0.27	1.3	1.00	1.2	0.63	1.4	0.12	1.4	0.91	0.0	0.99	1.1	0.04	1.6
Fdps	NM_134469	Mus musculus farnesyl diphosphate synthetase (Fdps), mRNA [NM_134469]	0.97	-1.0	0.81	1.1	0.28	1.3	1.00	1.3	0.90	1.3	0.01	1.6	0.81	1.2	0.98	1.1	0.44	1.3
Ffar2	NM_146187	Mus musculus free fatty acid receptor 2 (Ffar2), mRNA [NM_146187]	0.98	1.0	0.15	1.8	0.00	2.1	1.00	1.1	0.90	1.4	0.21	1.5	0.87	1.1	0.99	1.1	0.18	1.7
Fgg	NM_133862	Mus musculus fibrinogen, gamma polypeptide (Fgg), mRNA [NM_133862]	0.97	1.1	0.74	1.3	0.02	3.0	1.00	1.1	1.00	1.0	0.85	1.2	0.99	1.0	1.00	1.1	0.65	1.5
Fhl1	NM_010211	Mus musculus four and a half LIM domains 1 (Fhl1), mRNA [NM_010211]	0.91	-1.2	0.41	-1.4	0.01	-1.8	1.00	-1.3	0.92	-1.2	0.24	-1.4	0.97	-1.0	0.98	1.2	0.49	-1.4
Fignl1	NM_021891	Mus musculus fidgetin-like 1 (Fignl1), mRNA [NM_021891]	0.96	1.1	0.53	1.3	0.10	1.6	1.00	1.2	0.91	1.2	0.11	1.6	0.82	-1.2	0.98	-1.2	0.98	-1.0
Fkbp11	NM_024169	Mus musculus FK506 binding protein 11 (Fkbp11), mRNA [NM_024169]	0.96	1.1	0.51	1.2	0.01	1.6	1.00	1.1	0.93	1.1	0.32	1.2	0.86	1.1	0.98	1.1	0.87	1.1
Foxf2	NM_010225	Mus musculus forkhead box F2 (Foxf2), mRNA [NM_010225]	1.00	-1.0	0.54	-1.4	0.09	-1.7	1.00	-1.1	0.94	-1.2	0.44	-1.3	0.89	1.1	0.98	1.1	0.98	-1.0
Fpr1	NM_013521	Mus musculus formyl peptide receptor 1 (Fpr1), mRNA [NM_013521]	0.92	-1.2	0.70	-1.2	0.09	-1.7	1.00	-1.2	0.92	1.2	0.65	-1.2	0.96	1.1	1.00	1.0	0.76	1.2
Fst	NM_008046	Mus musculus follistatin (Fst), mRNA [NM_008046]	0.97	-1.1	0.92	1.1	0.05	1.6	1.00	1.1	0.99	-1.0	0.50	1.2	0.96	1.0	0.99	-1.1	0.68	-1.2
Fut4	NM_010242	Mus musculus fucosyltransferase 4 (Fut4), mRNA [NM_010242]	0.87	1.2	0.42	1.3	0.11	1.4	1.00	1.0	0.92	1.1	0.28	1.2	0.80	1.2	0.98	1.3	0.02	1.5
Fxyd4	NM_033648	Mus musculus FXYD domain-containing ion transport regulator 4 (Fxyd4), mRNA [NM_033648]	0.92	1.2	0.06	2.2	0.01	2.3	1.00	1.3	0.90	1.6	0.00	2.7	0.80	1.4	0.98	1.8	0.02	2.3
Gadd45g	NM_011817	Mus musculus growth arrest and DNA-damage-inducible 45 gamma (Gadd45g), mRNA [NM_011817]	0.56	1.7	0.31	1.6	0.00	2.4	1.00	1.1	0.96	1.1	0.18	1.6	0.82	1.2	0.98	1.1	0.54	1.4
Gale	NM_178389	Mus musculus galactose-4-epimerase, UDP (Gale), mRNA [NM_178389]	0.97	-1.0	0.45	1.3	0.03	1.5	1.00	1.3	0.90	1.3	0.04	1.4	0.85	1.1	0.98	1.1	0.67	1.2
Galnt3	NM_015736	Mus musculus UDP-N-acetyl-alpha-D-galactosamine:polypeptide N-acetylgalactosaminyltransferase 3 (Galnt3), mRNA [NM_015736]	0.85	1.3	0.36	1.3	0.13	1.3	1.00	1.2	0.67	1.4	0.02	1.5	0.80	1.2	0.98	1.2	0.05	1.5
Galntl2	NM_030166	Mus musculus UDP-N-acetyl-alpha-D-galactosamine:polypeptide N-acetylgalactosaminyltransferase-like 2 (Galntl2), mRNA [NM_030166]	0.87	-1.3	0.40	-1.5	0.07	-1.7	1.00	-1.1	0.90	-1.3	0.17	-1.5	0.86	1.2	0.98	1.2	1.00	-1.0
Gch1	NM_008102	Mus musculus GTP cyclohydrolase 1 (Gch1), mRNA [NM_008102]	0.99	1.0	0.46	1.2	0.00	1.6	1.00	1.1	0.90	1.3	0.00	1.5	0.96	1.0	0.98	-1.1	0.46	1.3
Gclc	NM_010295	Mus musculus glutamate-cysteine ligase, catalytic subunit (Gclc), mRNA [NM_010295]	0.87	1.3	0.46	1.5	0.02	2.2	1.00	1.4	0.90	1.4	0.00	2.3	0.91	1.1	0.99	1.1	0.78	1.2

Gene Name	Genbank	Gene Description	FDR	Fold	FDR	Fold	FDR	Fold	FDR	Fold	FDR	Fold	FDR	Fold	FDR	Fold	FDR	Fold	FDR	Fold
Gins1	AK013116	Mus musculus 10, 11 days embryo whole body cDNA, RIKEN full-length enriched library, clone:2810418N01 product:HYPOTHETICAL PROTEIN KIAA0186 homolog [Homo sapiens], full insert sequence. [AK013116]	0.96	1.0	0.21	1.4	0.01	1.6	1.00	1.1	0.92	1.1	0.03	1.5	0.96	-1.0	0.98	-1.1	0.79	1.1
Gja7	NM_008122	Mus musculus gap junction membrane channel protein alpha 7 (Gja7), mRNA [NM_008122]	0.90	-1.2	0.28	-1.4	0.02	-1.6	1.00	-1.2	0.92	-1.1	0.36	-1.2	0.94	-1.1	0.99	1.1	0.92	-1.0
Gm1960	NM_203320	Mus musculus gene model 1960, (NCBI) (Gm1960), mRNA [NM_203320]	0.87	1.2	0.03	1.6	0.02	1.6	1.00	1.2	0.76	1.4	0.00	1.6	0.96	-1.0	0.98	-1.1	0.70	1.2
Gpnmb	NM_053110	Mus musculus glycoprotein (transmembrane) nmb (Gpnmb), mRNA [NM_053110]	0.97	1.1	0.67	1.2	0.52	1.3	1.00	1.4	0.81	1.6	0.01	1.9	0.81	1.2	0.98	1.1	0.00	3.6
Gpr109a	NM_030701	Mus musculus G protein-coupled receptor 109A (Gpr109a), mRNA [NM_030701]	0.98	-1.0	0.23	1.6	0.04	1.7	1.00	1.1	0.90	1.3	0.40	1.3	0.80	1.4	0.98	1.3	0.00	2.1
Gpr171	NM_173398	Mus musculus G protein-coupled receptor 171 (Gpr171), mRNA [NM_173398]	0.72	1.4	0.27	1.4	0.21	1.3	1.00	1.3	0.67	1.5	0.05	1.5	0.93	1.1	1.00	-1.0	0.78	1.1
Gpr65	NM_008152	Mus musculus G-protein coupled receptor 65 (Gpr65), mRNA [NM_008152]	0.85	1.2	0.35	1.3	0.58	1.1	1.00	1.1	0.96	1.1	0.78	1.1	0.89	1.1	0.98	1.1	0.01	1.5
Gprasp1	NM_026081	Mus musculus G protein-coupled receptor associated sorting protein 1 (Gprasp1), transcript variant 1, mRNA [NM_026081]	0.87	-1.2	0.20	-1.4	0.00	-1.7	1.00	-1.2	0.67	-1.4	0.03	-1.4	0.91	-1.1	0.99	1.0	0.99	-1.0
Grb7	NM_010346	Mus musculus growth factor receptor bound protein 7 (Grb7), mRNA [NM_010346]	0.86	-1.2	0.23	-1.4	0.00	-1.7	1.00	-1.1	0.90	-1.2	0.21	-1.3	0.95	1.0	0.98	1.2	0.87	1.1
Gsn	NM_146120	Mus musculus gelsolin (Gsn), mRNA [NM_146120]	0.92	-1.1	0.53	-1.3	0.09	-1.6	1.00	-1.2	0.92	-1.2	0.16	-1.5	0.96	-1.1	0.99	1.0	0.46	-1.4
Gsta1	NM_008181	Mus musculus glutathione S-transferase, alpha 1 (Ya) (Gsta1), mRNA [NM_008181]	0.89	-1.2	0.18	-1.6	0.07	-1.5	1.00	-1.1	0.90	-1.4	0.36	-1.3	0.82	-1.2	1.00	1.0	0.43	-1.4
Gstm1	NM_010358	Mus musculus glutathione S-transferase, mu 1 (Gstm1), mRNA [NM_010358]	0.98	-1.1	0.63	-1.3	0.05	-1.8	1.00	-1.1	0.93	-1.2	0.19	-1.5	1.00	1.0	0.98	1.2	0.72	-1.2
Gstm3	NM_010359	Mus musculus glutathione S-transferase, mu 3 (Gstm3), mRNA [NM_010359]	0.92	-1.1	0.45	-1.2	0.01	-1.5	1.00	-1.1	0.90	-1.2	0.02	-1.4	0.84	-1.1	0.99	-1.0	0.26	-1.3
H2afx	NM_010436	Mus musculus H2A histone family, member X (H2afx), mRNA [NM_010436]	0.98	-1.0	0.93	1.0	0.65	1.1	1.00	1.2	0.65	1.4	0.00	1.6	0.88	-1.1	0.98	-1.2	0.93	-1.0
H2afz	NM_016750	Mus musculus H2A histone family, member Z (H2afz), mRNA [NM_016750]	0.99	1.0	0.74	1.1	0.32	1.2	1.00	1.2	0.46	1.4	0.00	1.5	0.91	-1.1	0.99	-1.0	0.51	1.2
H2-Q1	U96752	Mus musculus major histocompability complex Q1b mRNA, complete cds. [U96752]	0.93	1.1	0.74	1.2	0.98	1.0	1.00	1.1	0.94	1.1	0.67	1.2	0.80	1.3	0.98	1.4	0.02	1.9
Havcr2	NM_134250	Mus musculus hepatitis A virus cellular receptor 2 (Havcr2), mRNA [NM_134250]	0.91	-1.1	0.81	1.1	0.64	1.1	1.00	-1.1	0.90	1.2	0.56	1.1	0.88	1.1	0.98	1.2	0.06	1.6
Hbegf	NM_010415	Mus musculus heparin-binding EGF-like growth factor (Hbegf), mRNA [NM_010415]	0.92	1.1	0.91	1.0	0.02	1.6	1.00	1.2	0.93	1.1	0.39	1.2	0.95	-1.0	0.99	1.0	0.96	1.0

Hes2	NM_008236	Mus musculus hairy and enhancer of split 2 (Drosophila) (Hes2), mRNA [NM_008236]	0.87	-1.3	0.26	-1.5	0.00	-1.8	1.00	-1.1	0.90	-1.2	0.36	-1.3	0.85	1.1	0.98	1.1	0.77	-1.1
Hist1h1b	NM_020034	Mus musculus histone 1, H1b (Hist1h1b), mRNA [NM_020034]	0.99	1.0	0.82	1.2	0.60	1.4	1.00	1.5	0.91	1.4	0.07	2.2	0.93	-1.1	0.98	-1.3	0.95	-1.1
Hist1h2aa	NM_175658	Mus musculus histone 1, H2aa (Hist1h2aa), mRNA [NM_175658]	0.97	1.1	0.59	1.2	0.64	1.2	1.00	1.3	0.90	1.4	0.00	1.7	0.90	1.1	0.99	1.0	0.74	1.2
Hist1h2ab	NM_175660	Mus musculus histone 1, H2ab (Hist1h2ab), mRNA [NM_175660]	0.93	-1.2	0.73	1.2	0.51	1.3	1.00	1.3	0.90	1.3	0.05	1.8	0.88	1.2	0.99	-1.1	0.89	1.1
Hist1h2af	NM_175661	Mus musculus histone 1, H2af (Hist1h2af), mRNA [NM_175661]	0.97	0.0	0.50	1.3	0.15	1.4	1.00	1.3	0.90	1.4	0.00	1.8	0.97	0.0	0.99	-1.1	0.79	1.1
Hist1h2ai	NM_178182	Mus musculus histone 1, H2ai (Hist1h2ai), mRNA [NM_178182]	0.99	1.0	0.56	1.2	0.27	1.3	1.00	1.4	0.90	1.4	0.00	1.8	0.99	-1.0	0.98	-1.2	0.94	1.0
Hist1h2ak	NM_178183	Mus musculus histone 1, H2ak (Hist1h2ak), mRNA [NM_178183]	0.99	1.0	0.47	1.4	0.22	1.5	1.00	1.4	0.90	1.5	0.01	2.0	0.98	-1.0	0.98	-1.2	0.91	1.1
Hist1h4f	NM_175655	Mus musculus histone 1, H4f (Hist1h4f), mRNA [NM_175655]	0.99	-1.0	0.65	1.2	0.88	1.1	1.00	1.2	0.90	1.3	0.09	1.6	0.83	1.2	1.00	-1.0	0.92	-1.1
Hist4h4	NM_175652	Mus musculus histone 4, H4 (Hist4h4), mRNA [NM_175652]	0.98	1.0	0.60	1.2	0.98	1.0	1.00	1.3	0.90	1.3	0.05	1.6	0.81	1.2	1.00	-1.0	0.97	-1.0
Hivep3	AK038070	Mus musculus 16 days neonate thymus cDNA, RIKEN full-length enriched library, clone:A130075N07 product:unclassifiable, full insert sequence [AK038070]	0.74	1.3	0.27	1.3	0.00	1.6	1.00	-1.0	0.97	-1.1	0.24	1.2	0.83	1.1	1.00	1.0	0.79	1.1
Hkdc1	NM_145419	Mus musculus hexokinase domain containing 1 (Hkdc1), mRNA [NM_145419]	0.93	-1.1	0.95	-1.0	0.80	1.1	1.00	1.1	0.92	1.2	0.16	1.4	0.80	1.3	0.98	1.5	0.06	1.7
Hmgcs1	NM_145942	Mus musculus 3-hydroxy-3-methylglutaryl-Coenzyme A synthase 1 (Hmgcs1), mRNA [NM_145942]	0.88	1.2	0.48	1.4	0.66	1.2	1.00	1.4	0.90	1.3	0.03	1.7	0.80	1.3	0.98	1.3	0.53	1.3
Hpxn	NM_017371	Mus musculus hemopexin (Hpxn), mRNA [NM_017371]	0.91	1.2	0.31	1.5	0.00	2.5	1.00	-1.0	0.94	1.1	1.00	1.0	0.83	-1.2	0.99	-1.1	0.98	1.0
Hsd17b7	NM_010476	Mus musculus hydroxysteroid (17-beta) dehydrogenase 7 (Hsd17b7), mRNA [NM_010476]	0.87	1.2	0.36	1.4	0.05	1.6	1.00	1.1	0.90	1.2	0.05	1.6	0.80	1.2	0.98	1.1	0.95	1.0
Hspa8	NM_031165	Mus musculus heat shock protein 8 (Hspa8), mRNA [NM_031165]	0.93	-1.1	0.95	-1.0	0.81	1.1	1.00	1.2	0.90	1.4	0.06	1.7	0.82	-1.2	0.98	-1.2	0.93	-1.1
Icos	AK030827	Mus musculus adult male thymus cDNA, RIKEN full-length enriched library, clone:5830414M16 product:inducible T-cell co-stimulator, full insert sequence [AK030827]	0.99	1.0	0.66	1.2	0.81	1.1	1.00	1.0	0.94	1.1	0.97	1.0	0.86	1.1	0.98	1.2	0.00	1.9
Idi1	NM_177960	Mus musculus isopentenyl-diphosphate delta isomerase (Idi1), transcript variant 2, mRNA [NM_177960]	1.00	-1.0	0.63	1.2	0.08	1.4	1.00	1.3	0.91	1.2	0.00	1.7	0.80	1.2	0.98	1.2	0.61	1.2
Ifi204	NM_008329	Mus musculus interferon activated gene 204 (Ifi204), mRNA [NM_008329]	0.99	0.0	0.47	1.3	0.65	1.2	1.00	1.1	0.97	0.0	0.58	1.2	0.91	1.1	0.99	-1.1	0.04	1.7

Ifit1	NM_008331	Mus musculus interferon-induced protein with tetratricopeptide repeats 1 (Ifit1), mRNA [NM_008331]	0.94	1.1	0.33	1.7	0.42	1.4	1.00	1.1	0.92	1.2	0.01	2.1	0.98	1.0	0.98	-1.2	0.46	1.6
Igfbp3	NM_008343	Mus musculus insulin-like growth factor binding protein 3, mRNA (cDNA clone MGC:65287 IMAGE:6487655), complete cds [BC058261]	0.92	-1.2	0.50	-1.4	0.00	-2.2	1.00	-1.1	0.99	-1.0	0.20	-1.5	0.84	1.2	1.00	-1.0	0.89	-1.1
Ighg	BC092269	Mus musculus Immunoglobulin heavy chain (gamma polypeptide), mRNA (cDNA clone MGC:102659 IMAGE:4015795), complete cds. [BC092269]	0.89	-1.3	0.83	-1.2	0.69	-1.3	1.00	1.1	0.97	1.1	0.94	1.1	0.80	1.5	0.99	-1.1	0.07	2.4
Igkv1-132	XM_144770	PREDICTED: Mus musculus similar to Ig kappa chain V-II region RPMI 6410 precursor (LOC243423), mRNA [XM_144770]	0.96	-1.1	0.87	1.1	0.97	1.0	1.00	1.0	0.96	1.1	0.93	-1.0	0.89	1.1	0.98	1.1	0.08	2.0
Igkv1-133	ENSMUST00000103304	PREDICTED: Mus musculus similar to Ig kappa chain V-II region RPMI 6410 precursor (LOC628027), mRNA [XM_892753]	0.95	-1.2	0.86	1.1	0.95	1.1	1.00	1.0	0.97	1.1	0.79	-1.2	0.84	1.3	0.98	1.2	0.07	2.6
Igsf10	XM_887155	PREDICTED: Mus musculus immunoglobulin superfamily, member 10, transcript variant 2 (Igsf10), mRNA [XM_887155]	1.00	1.0	0.87	-1.1	0.05	-1.5	1.00	-1.0	1.00	1.0	0.87	-1.1	0.83	-1.2	0.98	-1.2	0.97	-1.0
Il18bp	NM_010531	Mus musculus interleukin 18 binding protein (Il18bp), mRNA [NM_010531]	0.85	1.2	0.00	1.5	0.01	1.5	1.00	-1.0	0.91	1.1	0.82	1.1	0.82	1.1	0.99	1.0	0.47	1.2
Il1b	NM_008361	Mus musculus interleukin 1 beta (Il1b), mRNA [NM_008361]	0.91	1.3	0.28	2.0	0.04	2.4	1.00	1.7	0.90	1.4	0.23	1.8	0.83	1.3	0.98	1.2	0.47	1.7
Il1r2	NM_010555	Mus musculus interleukin 1 receptor, type II (Il1r2), mRNA [NM_010555]	0.87	1.4	0.03	2.2	0.00	2.5	1.00	1.1	0.95	1.2	0.46	1.3	0.89	1.1	0.98	1.2	0.39	1.6
Il1rn	NM_031167	Mus musculus interleukin 1 receptor antagonist (Il1rn), transcript variant 1, mRNA [NM_031167]	0.89	1.2	0.23	1.5	0.01	1.7	1.00	1.1	0.90	1.3	0.05	1.5	0.97	1.0	0.99	1.0	0.00	1.8
Il4i1	NM_010215	Mus musculus interleukin 4 induced 1 (Il4i1), mRNA [NM_010215]	0.90	1.2	0.23	1.5	0.02	1.6	1.00	1.2	0.90	1.5	0.11	1.5	0.81	1.2	0.98	1.2	0.04	1.7
Il6	NM_031168	Mus musculus interleukin 6 (Il6), mRNA [NM_031168]	0.98	0.3	0.79	1.1	0.01	1.9	1.00	1.1	0.99	0.8	0.26	1.4	0.88	-1.1	0.98	-1.2	0.81	-0.9
Il7r	NM_008372	Mus musculus interleukin 7 receptor (Il7r), mRNA [NM_008372]	0.91	1.2	0.68	1.2	0.95	-1.0	1.00	1.1	0.95	1.2	0.58	1.2	0.81	1.3	0.98	1.3	0.04	2.2
Il8rb	NM_009909	Mus musculus interleukin 8 receptor, beta (Il8rb), mRNA [NM_009909]	0.89	1.1	0.06	1.6	0.13	1.4	1.00	1.0	0.96	1.1	0.81	1.1	0.90	1.1	0.98	1.1	0.67	1.1
Irg1	AK152177	Mus musculus bone marrow macrophage cDNA, RIKEN full-length enriched library, clone:I830053P18 product:immunoresponsive gene 1, full insert sequence. [AK152177]	0.93	1.2	0.08	2.1	0.00	2.5	1.00	1.1	0.93	1.2	0.31	1.5	0.96	1.1	0.99	0.0	0.15	2.0
Irs1	AK141842	Mus musculus adult male diencephalon cDNA, RIKEN full-length enriched library, clone:9330161E08 product:insulin receptor substrate 1, full insert sequence [AK136875]	0.87	-1.4	0.34	-1.5	0.06	-1.7	1.00	-1.1	0.90	-1.3	0.09	-1.6	0.99	1.0	0.98	1.1	0.82	-1.1

Irx1	NM_010573	Mus musculus 8 days embryo whole body cDNA, RIKEN full-length enriched library, clone:5730541C20 product:Iroquois related homeobox 1 (Drosophila), full insert sequence. [AK133937]	0.87	1.2	0.54	1.3	0.37	1.3	1.00	1.1	0.85	1.5	0.08	1.5	0.93	-1.1	0.99	1.1	0.78	1.1
Isyna1	NM_023627	Mus musculus myo-inositol 1-phosphate synthase A1 (Isyna1), mRNA [NM_023627]	0.96	-1.1	0.60	1.2	0.00	1.6	1.00	1.1	0.91	1.1	0.36	1.2	0.99	1.0	0.99	1.0	0.87	1.1
Itga7	L23423	Mus musculus integrin alpha 7 (Itga7), mRNA [NM_008398]	0.96	-1.1	0.55	1.2	0.00	1.6	1.00	1.1	0.93	1.1	0.13	1.3	0.90	1.1	0.99	0.0	0.43	1.3
Itgb6	NM_021359	Mus musculus integrin beta 6 (Itgb6), mRNA [NM_021359]	0.72	1.4	0.08	1.6	0.08	1.4	1.00	1.2	0.89	1.4	0.07	1.4	0.92	1.1	1.00	-1.0	0.91	1.1
Itih4	NM_018746	Mus musculus inter alpha-trypsin inhibitor, heavy chain 4 (Itih4), mRNA [NM_018746]	0.89	1.2	0.28	1.6	0.03	1.8	1.00	1.3	0.90	1.5	0.15	1.6	0.86	1.2	0.98	1.2	0.12	1.8
Jag1	NM_013822	Mus musculus jagged 1 (Jag1), mRNA [NM_013822]	0.88	-1.2	0.64	-1.2	0.06	-1.6	1.00	-1.1	0.96	1.1	0.84	-1.1	0.89	-1.1	0.98	1.1	0.89	-1.1
Junb	NM_008416	Mus musculus Jun-B oncogene (Junb), mRNA [NM_008416]	0.94	1.1	0.57	1.2	0.06	1.5	1.00	-1.0	0.96	-1.1	0.49	1.2	0.89	1.1	0.99	0.0	0.81	1.1
Kctd12b	NM_175429	Mus musculus potassium channel tetramerisation domain containing 12b (Kctd12b), mRNA [NM_175429]	0.89	-1.2	0.47	-1.3	0.04	-1.5	1.00	1.1	0.97	1.1	0.54	-1.2	1.00	1.0	0.98	-1.2	0.97	-1.0
Kif20a	NM_009004	Mus musculus kinesin family member 20A (Kif20a), mRNA [NM_009004]	0.99	1.0	0.71	1.2	0.39	1.4	1.00	1.4	0.89	1.6	0.01	2.2	0.92	-1.1	0.98	-1.3	0.87	1.1
Kif22	NM_145588	Mus musculus kinesin family member 22 (Kif22), mRNA [NM_145588]	0.97	-1.1	0.68	1.2	0.55	1.3	1.00	1.3	0.90	1.4	0.05	1.7	0.95	1.1	0.99	-1.1	0.63	1.3
Kif23	NM_024245	Mus musculus kinesin family member 23 (Kif23), mRNA [NM_024245]	1.00	1.0	0.81	1.1	0.59	1.2	1.00	1.3	0.90	1.4	0.04	1.5	0.92	-1.1	0.98	-1.2	0.99	1.0
Kif4	NM_008446	Mus musculus kinesin family member 4 (Kif4), mRNA [NM_008446]	0.99	1.0	0.81	1.1	0.48	1.2	1.00	1.2	0.90	1.2	0.04	1.5	0.89	-1.1	0.98	-1.2	0.94	-1.0
Klf4	NM_010637	Mus musculus Kruppel-like factor 4 (gut) (Klf4), mRNA [NM_010637]	0.59	2.2	0.37	1.9	0.37	1.6	1.00	1.2	0.90	2.0	0.07	2.2	0.86	-1.3	0.98	-1.5	0.54	-1.6
Lair1	NM_178611	Mus musculus leukocyte-associated Ig-like receptor 1 (Lair1), mRNA [NM_178611]	0.92	1.1	0.28	1.3	0.31	1.2	1.00	-1.0	0.96	1.1	0.67	1.1	0.83	1.1	0.99	1.0	0.00	1.6
Lcn2	NM_008491	Mus musculus lipocalin 2 (Lcn2), mRNA [NM_008491]	0.86	2.0	0.00	4.4	0.00	6.3	1.00	2.2	0.10	3.8	0.00	5.2	0.80	1.6	0.98	1.4	0.00	5.1
Lef1	AK083328	Mus musculus 2 days neonate thymus thymic cells cDNA, RIKEN full-length enriched library, clone:C920006H21 product:lymphoid enhancer binding factor 1, full insert sequence. [AK083328]	0.98	1.0	0.45	-1.3	0.10	-1.5	1.00	-1.2	0.90	-1.4	0.04	-1.6	1.00	1.0	1.00	1.0	0.85	-1.1
Lgals1	NM_008495	Mus musculus lectin, galactose binding, soluble 1 (Lgals1), mRNA [NM_008495]	0.94	-1.1	0.36	1.5	0.06	1.6	1.00	1.1	0.92	1.2	0.31	1.3	0.80	1.2	0.98	1.1	0.49	1.4
Lgals3	NM_010705	Mus musculus lectin, galactose binding, soluble 3 (Lgals3), mRNA [NM_010705]	0.95	-1.1	0.58	1.2	0.05	1.5	1.00	1.3	0.67	1.4	0.03	1.5	0.80	1.4	0.98	1.2	0.02	1.6

Lgi2	AK122570	Mus musculus mRNA for mKIAA1916 protein. [AK122570]	0.90	1.2	0.17	1.7	0.03	1.8	1.00	1.1	0.90	1.4	0.10	1.6	0.86	1.2	0.98	1.2	0.06	1.9
Lilrb4	NM_013532	Mus musculus leukocyte immunoglobulin-like receptor, subfamily B, member 4 (Lilrb4), mRNA [NM_013532]	0.97	-1.0	0.74	1.1	0.05	1.4	1.00	1.2	0.67	1.4	0.00	1.6	0.98	-1.0	0.99	-1.0	0.00	1.8
LOC665500	ENSMUST00000103291	PREDICTED: Mus musculus similar to T-cell receptor beta-1 chain C region (LOC665500), mRNA [XM_977330]	0.89	-1.2	0.37	-1.3	0.12	-1.4	1.00	-1.3	0.89	-1.4	0.00	-1.6	0.91	-1.1	0.98	-1.1	0.92	-1.0
Lrp2	NM_001081088	PREDICTED: Mus musculus low density lipoprotein receptor-related protein 2, transcript variant 1 (Lrp2), mRNA [XM_130308]	0.97	1.1	0.60	1.2	0.02	1.7	1.00	1.1	0.91	1.2	0.24	1.4	0.82	1.2	0.98	1.3	0.60	1.3
Luzp5	NM_133762	Mus musculus leucine zipper protein 5 (Luzp5), mRNA [NM_133762]	0.96	1.1	0.65	1.2	0.30	1.3	1.00	1.3	0.90	1.3	0.04	1.6	0.91	-1.1	0.98	-1.1	0.95	1.0
Ly6f	NM_008530	Mus musculus lymphocyte antigen 6 complex, locus F (Ly6f), mRNA [NM_008530]	0.87	1.7	0.11	3.1	0.21	2.1	1.00	1.4	0.33	3.4	0.02	3.3	0.82	1.4	0.99	1.1	0.00	6.3
Lyl1	NM_008535	Mus musculus lymphoblastomic leukemia (Lyl1), mRNA [NM_008535]	0.51	-1.5	0.33	-1.4	0.66	-1.1	1.00	-1.2	0.90	-1.3	0.03	-1.5	0.98	-1.0	1.00	-1.0	0.87	-1.1
M20632	M20632	Mouse LLRep3 protein mRNA from a repetitive element, complete cds. [M20632]	0.86	1.2	0.03	1.5	0.00	1.8	1.00	1.1	0.90	1.2	0.16	1.3	0.84	1.1	0.98	1.1	0.10	1.4
Macf1	AF150755	Mus musculus microtubule-actin crosslinking factor (Macf) mRNA, complete cds. [AF150755]	0.97	-1.0	0.33	-1.3	0.02	-1.5	1.00	-1.3	0.90	-1.3	0.12	-1.4	0.88	-1.1	0.98	-1.1	0.46	-1.3
Mafb	NM_010658	Mus musculus v-maf musculoaponeurotic fibrosarcoma oncogene family, protein B (avian) (Mafb), mRNA [NM_010658]	0.98	-1.0	0.89	1.1	0.46	1.2	1.00	1.1	0.98	1.0	0.81	1.1	0.88	1.1	0.99	-1.0	0.10	1.5
Malt1	NM_172833	Mus musculus mucosa associated lymphoid tissue lymphoma translocation gene 1 (Malt1), mRNA [NM_172833]	0.96	1.1	0.58	1.2	0.05	1.6	1.00	1.1	0.92	1.2	0.07	1.5	0.90	1.1	0.99	1.1	0.08	1.6
Mamdc2	NM_174857	Mus musculus MAM domain containing 2 (Mamdc2), mRNA [NM_174857]	0.92	-1.1	0.68	-1.2	0.00	-1.9	1.00	-1.2	0.94	1.1	0.61	-1.2	0.94	1.1	0.98	1.1	0.99	1.0
Mapt	NM_001038609	Mus musculus microtubule-associated protein tau (Mapt), transcript variant 1, mRNA [NM_001038609]	0.97	-1.1	0.65	-1.2	0.23	-1.4	1.00	-1.3	0.90	-1.2	0.10	-1.5	0.87	-1.1	0.98	1.1	0.55	-1.3
Mat1a	NM_133653	Mus musculus methionine adenosyltransferase I, alpha (Mat1a), mRNA [NM_133653]	0.94	1.1	0.34	1.4	0.09	1.5	1.00	1.1	0.90	1.3	0.11	1.4	0.90	1.1	0.98	1.1	0.13	1.5
Mbd1	AK007371	Mus musculus 10 day old male pancreas cDNA, RIKEN full-length enriched library, clone:1810008C20 product:methyl-CpG binding domain protein 1, full insert sequence. [AK007371]	0.18	2.4	0.05	2.4	0.00	2.6	1.00	-1.1	0.90	1.6	0.19	1.8	0.80	1.5	0.98	1.5	0.60	1.4
Mcm10	NM_027290	Mus musculus minichromosome maintenance deficient 10 (S. cerevisiae) (Mcm10), mRNA [NM_027290]	0.99	1.0	0.44	1.3	0.16	1.4	1.00	1.2	0.90	1.3	0.04	1.5	0.94	1.1	0.99	-1.0	0.60	1.2

Mcm2	NM_008564	Mus musculus minichromosome maintenance deficient 2 mitotin (S. cerevisiae) (Mcm2), mRNA [NM_008564]	0.94	1.1	0.36	1.4	0.06	1.6	1.00	1.0	0.98	1.0	0.27	1.3	0.96	-1.1	0.98	-1.2	1.00	1.0
Mefv	NM_019453	Mus musculus Mediterranean fever (Mefv), mRNA [NM_019453]	0.92	1.2	0.20	1.8	0.06	1.8	1.00	1.2	0.92	1.2	0.78	1.1	0.89	1.1	0.98	1.1	0.59	1.4
Melk	NM_010790	Mus musculus maternal embryonic leucine zipper kinase (Melk), mRNA [NM_010790]	0.99	-1.0	0.72	1.2	0.33	1.4	1.00	1.4	0.90	1.4	0.07	1.7	0.94	1.1	0.98	-1.2	0.83	1.1
Mettl7a	NM_027334	Mus musculus methyltransferase like 7A (Mettl7a), mRNA [NM_027334]	0.91	-1.1	0.37	-1.4	0.04	-1.5	1.00	-1.0	0.97	-1.1	0.33	-1.3	0.83	-1.1	0.99	-1.0	0.60	-1.2
Mfsd2	NM_029662	Mus musculus major facilitator superfamily domain containing 2 (Mfsd2), mRNA [NM_029662]	0.95	1.2	0.80	1.2	0.05	2.3	1.00	1.6	0.90	1.6	0.04	2.4	0.80	1.8	0.98	1.7	0.53	1.6
MGC73635	BC090402	Mus musculus similar to histone 2a, mRNA (cDNA clone MGC:103288 IMAGE:5150365), complete cds. [BC090402]	1.00	1.0	0.49	1.4	0.26	1.4	1.00	1.2	0.90	1.5	0.00	2.0	0.99	1.0	0.98	-1.1	0.69	1.2
Mki67	X82786	M.musculus mRNA for Ki-67. [X82786]	1.00	1.0	0.55	1.4	0.25	1.6	1.00	1.4	0.90	1.5	0.01	2.2	0.97	-1.0	0.98	-1.3	0.81	1.2
Mmp12	NM_008605	Mus musculus matrix metallopeptidase 12 (Mmp12), mRNA [NM_008605]	0.97	1.0	0.77	1.1	0.68	1.1	1.00	1.1	0.85	1.3	0.02	1.4	1.00	1.0	0.99	1.0	0.00	1.8
Mmp14	NM_008608	Mus musculus matrix metallopeptidase 14 (membrane-inserted) (Mmp14), mRNA [NM_008608]	0.87	1.2	0.30	1.3	0.13	1.3	1.00	1.3	0.90	1.2	0.00	1.6	0.92	1.1	0.98	-1.1	0.63	1.2
Mmp3	NM_010809	Mus musculus matrix metallopeptidase 3 (Mmp3), mRNA [NM_010809]	0.54	1.6	0.00	1.8	0.00	2.0	1.00	1.0	0.96	-1.1	0.88	1.1	0.80	-1.5	0.98	-1.3	0.12	-1.7
Mmp8	NM_008611	Mus musculus matrix metallopeptidase 8 (Mmp8), mRNA [NM_008611]	0.87	1.4	0.05	2.1	0.23	1.5	1.00	1.4	0.90	1.4	0.08	1.7	0.80	1.3	0.98	1.5	0.00	2.4
Mpeg1	NM_010821	PREDICTED: Mus musculus macrophage expressed gene 1, transcript variant 1 (Mpeg1), mRNA [XM_129176]	1.00	-1.0	0.81	-1.1	0.26	-1.3	1.00	1.1	0.90	1.2	0.98	-1.0	0.82	1.1	0.98	1.1	0.06	1.6
Mrc1	NM_008625	Mus musculus mannose receptor, C type 1 (Mrc1), mRNA [NM_008625]	0.99	-1.0	0.70	1.2	0.83	1.1	1.00	1.1	0.90	1.3	0.47	1.3	0.81	1.3	0.98	1.2	0.03	2.1
Ms4a11	AB026047	Mus musculus membrane-spanning 4-domains, subfamily A, member 11 (Ms4a11), mRNA [NM_022431]	0.93	1.1	0.13	1.6	0.00	1.8	1.00	1.3	0.30	1.6	0.00	1.7	0.88	1.1	0.98	1.1	0.00	2.1
Ms4a6c	NM_028595	Mus musculus membrane-spanning 4-domains, subfamily A, member 6C (Ms4a6c), mRNA [NM_028595]	0.95	1.1	0.24	1.5	0.51	1.2	1.00	-1.0	0.90	1.2	0.94	1.0	0.83	1.2	0.98	1.1	0.03	1.7
Ms4a6d	NM_026835	Mus musculus membrane-spanning 4-domains, subfamily A, member 6D (Ms4a6d), mRNA [NM_026835]	0.97	1.1	0.22	1.5	0.00	1.7	1.00	1.3	0.24	1.7	0.00	1.9	0.96	1.0	0.98	1.1	0.00	2.1
Ms4a7	NM_027836	Mus musculus membrane-spanning 4-domains, subfamily A, member 7 (Ms4a7), transcript variant 1, mRNA [NM_027836]	0.95	-1.1	0.95	0.0	0.98	1.0	1.00	1.2	0.76	1.6	0.18	1.5	0.99	0.0	0.98	-1.1	0.00	2.3
Msr1	NM_031195	Mus musculus macrophage scavenger receptor 1 (Msr1), mRNA [NM_031195]	0.97	-1.1	0.54	1.3	0.03	1.7	1.00	1.2	0.90	1.3	0.26	1.4	0.97	1.0	1.00	1.0	0.07	1.8

Mt1	BC027262	Mus musculus metallothionein 1, mRNA (cDNA clone MGC:27821 IMAGE:3483861), complete cds. [BC027262]	0.95	1.1	0.56	1.3	0.00	2.1	1.00	1.3	0.90	1.3	0.04	1.7	0.83	1.2	0.99	0.5	0.65	1.2
Mt2	NM_008630	Mus musculus metallothionein 2 (Mt2), mRNA [NM_008630]	0.90	1.3	0.29	1.9	0.00	5.7	1.00	1.2	0.93	1.2	0.05	2.1	0.90	1.2	1.00	1.0	0.75	1.3
Muc1	NM_013605	Mus musculus mucin 1, transmembrane (Muc1), mRNA [NM_013605]	0.98	1.0	0.56	1.2	0.09	1.5	1.00	1.3	0.90	1.3	0.02	1.7	0.81	1.2	0.98	1.2	0.43	1.4
Muc4	NM_080457	Mus musculus mucin 4 (Muc4), mRNA [NM_080457]	0.95	1.1	0.29	1.6	0.08	1.8	1.00	1.2	0.86	1.6	0.06	1.7	0.80	1.5	0.98	1.2	0.26	1.7
Mvd	NM_138656	Mus musculus mevalonate (diphospho) decarboxylase (Mvd), mRNA [NM_138656]	0.99	-1.0	0.51	1.3	0.21	1.4	1.00	1.5	0.90	1.3	0.05	1.5	0.80	1.2	0.98	1.2	0.50	1.3
Mybpc2	NM_146189	Mus musculus myosin binding protein C, fast-type (Mybpc2), mRNA [NM_146189]	0.85	1.4	0.00	1.8	0.00	2.0	1.00	1.3	0.90	1.4	0.09	1.5	0.86	1.1	0.98	1.1	0.51	1.3
Myd88	NM_010851	Mus musculus myeloid differentiation primary response gene 88 (Myd88), mRNA [NM_010851]	0.96	-0.4	0.35	1.2	0.00	1.5	1.00	1.1	0.78	1.2	0.04	1.3	0.89	1.1	0.99	1.0	0.54	1.2
Myh7	NM_080728	Mus musculus myosin, heavy polypeptide 7, cardiac muscle, beta (Myh7), mRNA [NM_080728]	0.99	1.0	0.62	-1.2	0.03	-1.8	1.00	-1.1	1.00	1.0	0.44	-1.3	0.97	1.0	0.98	1.2	0.75	-1.2
Mylc2b	NM_023402	Mus musculus myosin light chain, regulatory B (Mylc2b), mRNA [NM_023402]	0.97	-1.0	0.58	-1.2	0.03	-1.6	1.00	-1.1	0.92	-1.1	0.50	-1.2	0.92	-1.1	1.00	-1.0	0.72	-1.1
Mylip	NM_153789	Mus musculus myosin regulatory light chain interacting protein (Mylip), mRNA [NM_153789]	0.96	-1.1	0.48	-1.3	0.43	-1.3	1.00	-1.2	0.90	-1.3	0.02	-1.7	0.97	-1.0	1.00	1.0	0.74	-1.2
NAP043130-1	NAP043130-1	Unknown	0.57	-1.5	0.28	-1.4	0.03	-1.6	1.00	-1.1	0.90	-1.2	0.20	-1.3	0.82	1.2	0.98	1.3	0.87	1.1
NAP066348-1	NAP066348-1	Unknown	0.85	1.7	0.23	2.0	0.09	2.0	1.00	1.2	0.90	1.4	0.16	1.8	0.90	1.2	1.00	-1.0	0.94	-1.1
NAP114245-1	NAP114245-1	Unknown	0.91	-1.1	0.38	-1.4	0.06	-1.6	1.00	1.1	0.96	1.1	0.81	-1.1	0.94	1.1	0.98	1.1	0.86	1.1
Nat5	AK046153	Mus musculus adult male corpora quadrigemina cDNA, RIKEN full-length enriched library, clone:B230345H17 product:unclassifiable, full insert sequence [AK046153]	0.00	1.5	0.24	1.3	0.27	1.2	1.00	-1.0	0.96	1.1	0.28	1.2	0.96	1.0	0.98	-1.1	0.99	-1.0
Nek6	NM_021606	Mus musculus NIMA (never in mitosis gene a)-related expressed kinase 6 (Nek6), mRNA [NM_021606]	0.91	1.1	0.36	1.3	0.00	1.6	1.00	1.2	0.46	1.4	0.00	1.7	0.85	1.1	0.99	1.0	0.08	1.4
Nfil3	NM_017373	Mus musculus nuclear factor, interleukin 3, regulated (Nfil3), mRNA [NM_017373]	0.87	1.3	0.44	1.4	0.03	1.8	1.00	1.2	0.91	1.2	0.18	1.5	0.92	-1.1	0.98	-1.5	0.85	-1.1
Nfkbia	NM_010907	Mus musculus nuclear factor of kappa light chain gene enhancer in B-cells inhibitor, alpha (Nfkbia), mRNA [NM_010907]	0.31	2.3	0.12	2.1	0.05	2.0	1.00	1.1	0.90	1.4	0.18	1.7	0.93	1.1	0.99	1.1	0.70	1.3
NM_001012326	AK040896	Mus musculus similar to Retrovirus-related POL polyprotein (Endonuclease) (LOC433762), mRNA [NM_001012326]	0.94	1.2	0.15	2.2	0.00	2.6	1.00	1.0	0.95	1.2	0.33	1.5	0.89	1.2	0.98	1.1	0.57	1.5

Nme2	NM_008705	Mus musculus expressed in non-metastatic cells 2, protein (Nme2), mRNA [NM_008705]	0.93	1.1	0.12	1.3	0.00	1.6	1.00	1.0	0.93	1.1	0.22	1.2	0.81	1.1	0.98	-1.0	0.85	1.1
Nnmt	NM_010924	Mus musculus nicotinamide N-methyltransferase (Nnmt), mRNA [NM_010924]	0.97	-1.1	0.48	1.4	0.08	1.6	1.00	-1.0	0.98	1.0	0.66	1.2	0.98	1.0	1.00	1.0	1.00	-1.0
Noxa1	NM_172204	Mus musculus NADPH oxidase activator 1 (Noxa1), mRNA [NM_172204]	0.95	1.1	0.44	1.4	0.92	1.1	1.00	1.1	0.90	1.5	0.10	1.6	1.00	1.0	0.98	1.1	0.06	1.9
Noxo1	NM_027988	Mus musculus NADPH oxidase organizer 1 (Noxo1), mRNA [NM_027988]	0.87	1.5	0.00	3.0	0.00	3.0	1.00	1.5	0.00	3.0	0.00	3.2	0.86	1.2	0.98	1.2	0.00	3.6
Nr2f2	NM_009697	Mus musculus nuclear receptor subfamily 2, group F, member 2 (Nr2f2), transcript variant 1, mRNA [NM_009697]	0.87	-1.2	0.41	-1.3	0.16	-1.4	1.00	-1.2	0.90	-1.3	0.05	-1.5	0.89	-1.1	0.98	-1.1	0.66	-1.2
Nrn1	NM_153529	Mus musculus neuritin 1 (Nrn1), mRNA [NM_153529]	0.95	-1.1	0.51	-1.3	0.02	-1.6	1.00	1.1	0.96	1.1	0.40	-1.3	0.99	1.0	0.99	-1.0	0.89	-1.1
Nuak1	AK020957	Mus musculus adult male corpora quadrigemina cDNA, RIKEN full-length enriched library, clone:B230104P22 product:unclassifiable, full insert sequence. [AK020957]	0.89	-1.2	0.39	-1.4	0.17	-1.5	1.00	-1.3	0.90	-1.3	0.08	-1.6	0.88	1.1	0.98	1.1	0.93	-1.1
Numa1	NM_133947	Mus musculus nuclear mitotic apparatus protein 1 (Numa1), mRNA [NM_133947]	0.90	-1.1	0.49	-1.2	0.01	-1.6	1.00	-1.1	0.90	-1.2	0.12	-1.4	0.94	-1.1	0.98	1.1	0.88	-1.1
Nup155	NM_133227	Mus musculus nucleoporin 155 (Nup155), mRNA [NM_133227]	0.70	1.6	0.21	1.8	0.09	1.7	1.00	1.2	0.90	1.3	0.17	1.6	0.93	1.1	0.98	1.1	0.47	1.5
Nupr1	NM_019738	Mus musculus nuclear protein 1 (Nupr1), mRNA [NM_019738]	0.87	-1.2	0.35	-1.4	0.02	-1.5	1.00	1.1	1.00	-1.0	0.61	-1.1	0.99	-1.0	0.98	-1.1	0.80	-1.1
Oas1a	NM_145211	Mus musculus 2'-5' oligoadenylate synthetase 1A (Oas1a), mRNA [NM_145211]	0.98	-1.1	0.52	1.4	0.90	1.1	1.00	1.1	0.90	1.4	0.26	1.5	0.90	1.1	0.99	1.1	0.07	1.9
Oas1f	NM_145153	Mus musculus 2'-5' oligoadenylate synthetase 1F (Oas1f), mRNA [NM_145153]	0.99	1.0	0.45	1.4	0.73	1.2	1.00	1.1	0.90	1.2	0.34	1.4	0.95	1.1	0.99	1.1	0.00	2.1
Oasl1	NM_145209	Mus musculus 2'-5' oligoadenylate synthetase-like 1 (Oasl1), mRNA [NM_145209]	0.94	-1.1	0.53	1.2	0.90	1.1	1.00	1.1	0.96	1.1	0.41	1.2	0.88	1.1	1.00	1.0	0.04	1.7
Olr1	NM_138648	Mus musculus oxidized low density lipoprotein (lectin-like) receptor 1 (Olr1), mRNA [NM_138648]	0.98	-1.0	0.95	1.0	0.95	1.0	1.00	1.2	0.90	1.4	0.40	1.3	0.84	1.2	0.98	1.1	0.03	1.9
Orm1	NM_008768	Mus musculus orosomucoid 1 (Orm1), mRNA [NM_008768]	0.92	1.2	0.00	2.4	0.00	2.6	1.00	1.0	0.97	1.1	0.77	1.1	0.86	1.2	1.00	1.0	0.64	1.2
Orm2	NM_011016	Mus musculus orosomucoid 2 (Orm2), mRNA [NM_011016]	0.87	1.4	0.00	3.1	0.00	3.6	1.00	1.1	0.91	1.3	0.60	1.3	0.92	1.1	0.99	1.1	0.62	1.4
Osmr	NM_011019	Mus musculus oncostatin M receptor (Osmr), mRNA [NM_011019]	0.94	1.1	0.55	1.2	0.00	1.6	1.00	1.1	0.90	1.1	0.04	1.4	0.98	1.0	0.98	1.1	0.42	1.2
P2ry14	NM_133200	Mus musculus purinergic receptor P2Y, G-protein coupled, 14 (P2ry14), transcript variant 1, mRNA [NM_133200]	0.89	1.1	0.66	1.1	0.57	1.2	1.00	1.0	0.90	1.2	0.28	1.3	0.80	1.2	0.98	1.2	0.00	1.6
P2ry2	NM_008773	Mus musculus purinergic receptor P2Y, G-protein coupled 2 (P2ry2), mRNA [NM_008773]	0.87	1.2	0.37	1.3	0.01	1.6	1.00	1.2	0.90	1.3	0.10	1.4	0.82	1.1	0.98	1.2	0.34	1.4

Pbk	NM_023209	Mus musculus PDZ binding kinase (Pbk), mRNA [NM_023209]	0.97	-1.1	0.93	-1.1	0.52	1.3	1.00	1.3	0.91	1.3	0.04	1.8	0.82	-1.2	0.98	-1.3	0.83	-1.1
Pbp2	NM_029595	Mus musculus phosphatidylethanolamine binding protein 2 (Pbp2), mRNA [NM_029595]	0.87	1.2	0.18	1.5	0.00	3.9	1.00	1.2	0.95	1.1	0.08	1.5	0.91	1.1	0.98	1.1	0.85	1.1
Pdk1	AK165090	Mus musculus 2 days pregnant adult female ovary cDNA, RIKEN full-length enriched library, clone:E330005M21 product:hypothetical protein, full insert sequence. [AK165090]	0.87	-1.2	0.48	-1.2	0.02	-1.5	1.00	-1.1	0.90	-1.2	0.02	-1.5	0.95	-1.0	0.99	-1.0	0.61	-1.2
Pfdn1	NM_026027	Mus musculus prefoldin 1 (Pfdn1), mRNA [NM_026027]	0.87	1.3	0.46	1.4	0.08	1.5	1.00	1.1	0.94	1.1	0.20	1.4	0.90	1.1	0.98	-1.1	0.74	-1.2
Pglyrp1	NM_009402	Mus musculus peptidoglycan recognition protein 1 (Pglyrp1), mRNA [NM_009402]	0.92	1.1	0.23	1.5	0.08	1.5	1.00	1.2	0.91	1.2	0.45	1.2	0.80	1.4	0.98	1.2	0.36	1.4
Pigr	NM_011082	Mus musculus polymeric immunoglobulin receptor (Pigr), mRNA [NM_011082]	0.89	1.5	0.19	2.8	0.02	3.3	1.00	1.7	0.44	3.1	0.05	2.7	0.80	1.6	0.98	1.5	0.13	2.9
Pilrb	NM_133209	Mus musculus paired immunoglobin-like type 2 receptor beta (Pilrb), mRNA [NM_133209]	0.87	1.2	0.12	1.5	0.02	1.6	1.00	1.1	0.95	1.1	0.51	1.2	0.80	1.2	0.98	1.2	0.55	1.2
Pira3	NM_011090	Mus musculus paired-Ig-like receptor A3 (Pira3), mRNA [NM_011090]	0.92	1.1	0.15	1.5	0.10	1.4	1.00	1.1	0.90	1.3	0.39	1.2	0.80	1.4	0.98	1.4	0.08	1.6
Piwil4	AK143022	Mus musculus 0 day neonate lung cDNA, RIKEN full-length enriched library, clone:E030042M20 product:similar to Hypothetical protein FLJ39518 (piwi) [Homo sapiens], full insert sequence. [AK143022]	0.94	1.1	0.56	1.3	0.02	1.8	1.00	1.2	0.90	1.3	0.02	1.9	0.80	1.3	0.98	1.5	0.20	1.7
Pkib	NM_001039050	Mus musculus protein kinase inhibitor beta, cAMP dependent, testis specific (Pkib), transcript variant 2, mRNA [NM_001039050]	0.87	1.2	0.91	1.0	0.89	1.1	1.00	1.1	0.90	1.2	0.45	1.2	0.80	1.2	0.98	1.1	0.04	1.5
Pla1a	NM_134102	Mus musculus phospholipase A1 member A (Pla1a), mRNA [NM_134102]	0.91	1.1	0.53	1.3	0.01	1.7	1.00	-1.0	0.99	-1.0	0.92	-1.0	0.82	-1.2	1.00	-1.0	0.85	-1.1
Plekha6	BC025841	Mus musculus pleckstrin homology domain containing, family A member 6, mRNA (cDNA clone IMAGE:5149318), partial cds. [BC025841]	0.96	-1.1	0.73	-1.1	0.04	-1.6	1.00	-1.1	0.92	-1.2	0.41	-1.2	0.96	1.0	0.98	1.1	0.92	1.0
Pon1	NM_011134	Mus musculus paraoxonase 1 (Pon1), mRNA [NM_011134]	0.97	-1.1	0.71	-1.2	0.24	-1.6	1.00	-1.4	0.90	-1.7	0.07	-1.9	0.96	-1.1	0.98	1.2	0.36	-1.8
Ppa1	NM_026438	Mus musculus pyrophosphatase (inorganic) 1 (Ppa1), mRNA [NM_026438]	0.98	-1.0	0.50	1.3	0.00	1.8	1.00	1.2	0.90	1.2	0.16	1.4	0.94	1.1	0.99	-1.0	0.88	1.1
Ppp1r14d	NM_028104	Mus musculus protein phosphatase 1, regulatory (inhibitor) subunit 14D (Ppp1r14d), mRNA [NM_028104]	0.90	1.2	0.51	1.3	0.13	1.5	1.00	1.2	0.73	1.6	0.08	1.6	0.81	1.3	0.98	1.2	0.56	1.3
Prc1	NM_145150	Mus musculus protein regulator of cytokinesis 1 (Prc1), mRNA [NM_145150]	1.00	1.0	0.84	1.1	0.64	1.3	1.00	1.4	0.90	1.6	0.03	2.1	0.96	-1.1	0.98	-1.2	0.99	1.0
Prelp	NM_054077	Mus musculus proline arginine-rich end leucine-rich repeat (Prelp), mRNA [NM_054077]	0.97	-1.0	0.53	-1.2	0.02	-1.6	1.00	-1.2	0.96	-1.1	0.24	-1.3	0.80	-1.2	0.98	-1.1	0.29	-1.4

Prickle1	NM_001033217	Mus musculus prickle like 1 (Drosophila) (Prickle1), mRNA [NM_001033217]	0.70	-1.6	0.30	-1.6	0.03	-1.8	1.00	-1.2	0.90	-1.5	0.03	-1.8	0.94	1.1	0.98	1.3	0.80	-1.1
Proz	AK005011	Mus musculus adult male liver cDNA, RIKEN full-length enriched library, clone:1300015B06 product:weakly similar to VITAMIN K-DEPENDENT PROTEIN Z PRECURSOR [Homo sapiens], full insert sequence [AK005011]	0.98	1.1	0.37	1.7	0.02	2.4	1.00	1.6	0.26	2.3	0.00	2.9	0.80	1.6	0.98	1.5	0.00	4.7
Psat1	NM_177420	Mus musculus phosphoserine aminotransferase 1 (Psat1), mRNA [NM_177420]	0.96	-1.1	0.90	1.1	0.10	1.5	1.00	1.1	0.92	1.2	0.42	1.3	0.92	1.1	0.99	-1.1	0.64	1.2
Psmd1	NM_027357	Mus musculus proteasome (prosome, macropain) 26S subunit, non-ATPase, 1 (Psmd1), mRNA [NM_027357]	0.90	1.2	0.52	1.3	0.06	1.5	1.00	1.1	0.91	1.2	0.32	1.3	0.95	-1.1	0.98	-1.2	0.80	-1.1
Psrc1	NM_019976	Mus musculus proline/serine-rich coiled-coil 1 (Psrc1), mRNA [NM_019976]	0.95	-1.1	0.96	1.0	0.53	1.2	1.00	1.1	0.93	1.1	0.04	1.6	0.89	-1.1	0.98	-1.2	0.95	1.0
Ptges	NM_022415	Mus musculus prostaglandin E synthase (Ptges), mRNA [NM_022415]	0.97	-1.0	0.62	1.2	0.00	1.9	1.00	1.2	0.91	1.2	0.13	1.4	0.80	1.2	1.00	1.0	0.71	1.2
Ptgs1	NM_008969	Mus musculus prostaglandin-endoperoxide synthase 1 (Ptgs1), mRNA [NM_008969]	0.97	1.1	0.47	1.4	0.00	2.4	1.00	1.3	0.90	1.2	0.02	1.7	0.94	1.1	0.98	1.3	0.13	1.7
Ptrh1	NM_178595	Mus musculus peptidyl-tRNA hydrolase 1 homolog (S. cerevisiae) (Ptrh1), mRNA [NM_178595]	0.99	-1.0	0.54	1.2	0.00	1.5	1.00	1.1	0.94	1.1	0.40	1.2	0.81	1.1	0.98	1.1	0.58	1.2
Rac3	NM_133223	Mus musculus RAS-related C3 botulinum substrate 3 (Rac3), mRNA [NM_133223]	0.70	-1.5	0.23	-1.5	0.07	-1.5	1.00	-1.1	1.00	1.0	0.50	-1.2	0.83	1.2	0.98	1.4	0.69	1.2
Rad51	NM_011234	Mus musculus RAD51 homolog (S. cerevisiae) (Rad51), mRNA [NM_011234]	0.98	1.0	0.51	1.4	0.13	1.6	1.00	1.3	0.90	1.3	0.04	1.8	0.89	-1.1	0.98	-1.2	0.94	-1.0
Rap2a	AK018024	Mus musculus adult male thymus cDNA, RIKEN full-length enriched library, clone:5830461H18 product:hypothetical Ras small GTPase, Rab type/Ras small GTPase, Ras type/Ras small GTPase, Rho type containing protein, full insert sequence. [AK018024]	0.59	-1.6	0.56	-1.3	0.10	-1.6	1.00	-1.2	0.91	-1.2	0.32	-1.3	0.86	-1.1	0.98	1.1	0.98	1.0
Rbm3	BC106176	Mus musculus RNA binding motif protein 3, mRNA (cDNA clone MGC:118410 IMAGE:30146829), complete cds. [BC106176]	1.00	-1.0	0.98	-1.0	0.07	1.5	1.00	1.0	1.00	1.0	0.88	1.1	0.83	1.2	0.98	1.2	0.60	1.2
Rdm1	NM_025654	Mus musculus RAD52 motif 1 (Rdm1), mRNA [NM_025654]	0.94	-1.1	0.57	-1.2	0.01	-1.5	1.00	1.0	0.97	-1.1	0.67	-1.1	0.87	1.1	0.98	1.1	0.95	-1.0
Retnlg	NM_181596	Mus musculus resistin like gamma (Retnlg), mRNA [NM_181596]	0.87	1.5	0.11	2.5	0.09	2.1	1.00	1.4	0.90	1.5	0.27	1.7	0.80	1.7	0.98	2.4	0.29	2.1
Rgs1	NM_015811	Mus musculus regulator of G-protein signaling 1 (Rgs1), mRNA [NM_015811]	0.85	1.3	0.32	1.4	0.00	1.7	1.00	1.3	0.10	1.6	0.00	1.9	0.93	-1.1	0.99	-1.0	0.05	1.6
Rgs16	NM_011267	Mus musculus regulator of G-protein signaling 16 (Rgs16), mRNA [NM_011267]	0.92	-1.2	0.82	1.1	0.04	1.8	1.00	1.2	0.90	1.4	0.13	1.6	0.93	1.1	1.00	-1.0	0.16	1.8

Rgs2	NM_009061	Mus musculus regulator of G-protein signaling 2 (Rgs2), mRNA [NM_009061]	0.78	-1.4	0.22	-1.5	0.02	-1.6	1.00	-1.3	0.00	-1.8	0.00	-2.0	0.80	1.3	0.98	1.4	0.73	1.2
Rgs3	NM_019492	Mus musculus regulator of G-protein signaling 3 (Rgs3), transcript variant 1, mRNA [NM_019492]	0.98	-1.0	0.55	-1.2	0.59	-1.2	1.00	-1.1	0.90	-1.2	0.03	-1.5	0.99	1.0	1.00	1.0	0.74	-1.1
Rhebl1	NM_026967	Mus musculus Ras homolog enriched in brain like 1 (Rhebl1), mRNA [NM_026967]	0.54	-1.3	0.02	-1.5	0.00	-1.6	1.00	-1.1	0.90	-1.2	0.06	-1.4	0.87	1.1	0.99	1.0	0.87	1.1
Rhob	NM_007483	Mus musculus ras homolog gene family, member B (Rhob), mRNA [NM_007483]	0.00	1.8	0.17	1.6	0.45	1.3	1.00	1.0	0.91	1.2	0.21	1.4	0.95	-1.1	0.98	-1.1	1.00	1.0
Rnase6	NM_030098	Mus musculus ribonuclease, RNase A family, 6 (Rnase6), mRNA [NM_030098]	0.93	-1.1	0.74	-1.1	0.09	-1.6	1.00	-1.1	0.97	-1.1	0.26	-1.4	0.81	1.2	0.98	1.2	0.74	1.2
Rpl22	NM_009079	Mus musculus ribosomal protein L22 (Rpl22), mRNA [NM_009079]	0.90	-1.1	0.43	-1.2	0.00	-1.5	1.00	1.1	0.96	1.1	0.59	-1.1	0.99	1.0	0.98	1.1	0.95	-1.0
Rrbp1	NM_133626	Mus musculus ribosome binding protein 1, mRNA (cDNA clone IMAGE:4238895), complete cds. [BC031452]	0.87	1.2	0.17	1.4	0.00	2.0	1.00	1.1	0.90	1.2	0.15	1.3	0.82	1.1	0.98	1.2	0.33	1.3
Rsnl2	NM_030179	Mus musculus restin-like 2 (Rsnl2), mRNA [NM_030179]	0.87	1.3	0.30	1.5	0.00	2.4	1.00	1.3	0.90	1.4	0.05	1.7	0.80	1.3	0.98	1.2	0.40	1.5
S100a14	NM_025393	Mus musculus S100 calcium binding protein A14 (S100a14), mRNA [NM_025393]	0.96	1.1	0.30	1.5	0.00	2.3	1.00	1.2	0.91	1.2	0.33	1.3	0.80	1.4	0.98	1.4	0.67	1.2
S100a4	NM_011311	Mus musculus S100 calcium binding protein A4 (S100a4), mRNA [NM_011311]	0.99	1.0	0.19	1.5	0.02	1.6	1.00	1.2	0.90	1.3	0.13	1.4	0.96	1.0	0.98	1.1	0.51	1.3
S100a6	NM_011313	Mus musculus S100 calcium binding protein A6 (calcyclin) (S100a6), mRNA [NM_011313]	0.97	1.0	0.31	1.2	0.00	1.7	1.00	1.1	0.97	-1.0	0.68	1.1	0.81	1.1	0.98	1.2	0.61	-1.1
Saa1	NM_009117	Mus musculus serum amyloid A 1 (Saa1), mRNA [NM_009117]	0.83	2.0	0.00	5.9	0.00	11.3	1.00	1.2	0.92	1.4	0.47	1.6	0.99	-1.0	1.00	0.0	0.70	1.5
Saa2	NM_011314	Mus musculus serum amyloid A 2 (Saa2), mRNA [NM_011314]	0.85	1.7	0.00	3.6	0.00	6.9	1.00	1.1	0.95	1.2	0.49	1.4	0.99	-1.0	0.99	-1.1	0.70	1.3
Saa3	NM_011315	Mus musculus serum amyloid A 3 (Saa3), mRNA [NM_011315]	0.72	4.2	0.00	24.7	0.00	65.3	1.00	2.5	0.65	5.6	0.01	8.3	0.89	1.4	0.99	1.2	0.13	6.8
Sdf2l1	NM_022324	Mus musculus stromal cell-derived factor 2-like 1 (Sdf2l1), mRNA [NM_022324]	0.90	1.2	0.23	1.6	0.06	1.7	1.00	1.1	0.90	1.2	0.56	1.2	0.97	-1.0	0.99	-1.0	0.66	1.2
Selp	NM_011347	Mus musculus selectin, platelet (Selp), mRNA [NM_011347]	0.87	1.1	0.22	1.2	0.00	1.5	1.00	1.0	0.94	1.1	0.40	1.1	0.89	-1.0	1.00	0.0	0.78	-1.1
Sema3c	AK078589	Mus musculus 11 days embryo gonad cDNA, RIKEN full-length enriched library, clone:7030412F17 product:sema domain, immunoglobulin domain (Ig), short basic domain, secreted, (semaphorin) 3C, full insert sequence. [AK078589]	0.90	-0.1	0.69	-1.2	0.01	-1.8	1.00	0.1	0.95	1.1	0.56	-1.2	0.98	0.0	0.99	0.0	0.74	-0.2
Serpina3f	NM_0010333 35	Mus musculus serine (or cysteine) peptidase inhibitor, clade A, member 3F (Serpina3f), mRNA [NM_001033335]	0.87	1.2	0.05	1.5	0.00	1.5	1.00	1.1	0.90	1.2	0.03	1.4	0.86	1.1	0.98	1.1	0.23	1.3

Serpina3g	NM_009251	Mus musculus serine (or cysteine) peptidase inhibitor, clade A, member 3G (Serpina3g), mRNA [NM_009251]	0.87	1.2	0.00	1.9	0.00	2.2	1.00	1.2	0.90	1.4	0.00	1.9	0.85	1.1	0.98	1.3	0.03	1.8
Serpina3m	NM_009253	Mus musculus serine (or cysteine) peptidase inhibitor, clade A, member 3M (Serpina3m), mRNA [NM_009253]	0.87	1.4	0.15	1.9	0.00	2.8	1.00	-1.0	0.90	1.3	0.92	-1.1	0.93	1.1	0.98	1.2	0.74	1.2
Serpina3n	NM_009252	Mus musculus serine (or cysteine) peptidase inhibitor, clade A, member 3N (Serpina3n), mRNA [NM_009252]	0.85	1.5	0.03	2.3	0.00	3.0	1.00	1.4	0.90	1.3	0.15	1.7	0.98	-1.0	0.99	1.1	0.79	1.2
Serpinb9	NM_009256	Mus musculus serine (or cysteine) peptidase inhibitor, clade B, member 9 (Serpinb9), mRNA [NM_009256]	0.85	1.4	0.31	1.4	0.56	1.2	1.00	1.2	0.90	1.3	0.08	1.5	0.91	1.1	1.00	1.0	0.67	1.2
Serpind1	NM_008223	Mus musculus serine (or cysteine) peptidase inhibitor, clade D, member 1 (Serpind1), mRNA [NM_008223]	0.89	1.2	0.30	1.4	0.54	1.2	1.00	1.1	0.90	1.3	0.32	1.3	0.97	-1.0	0.98	1.1	0.06	1.6
Sfrp1	NM_013834	Mus musculus secreted frizzled-related sequence protein 1 (Sfrp1), mRNA [NM_013834]	0.87	1.3	0.00	1.7	0.00	1.7	1.00	1.2	0.94	1.1	0.03	1.5	1.00	1.0	1.00	1.0	0.67	1.2
Sgol1	NM_028232	Mus musculus shugoshin-like 1 (S. pombe) (Sgol1), mRNA [NM_028232]	0.97	-1.1	0.72	1.1	0.19	1.4	1.00	1.2	0.90	1.3	0.01	1.7	0.87	-1.1	0.98	-1.3	0.98	1.0
Shcbp1	NM_011369	Mus musculus Shc SH2-domain binding protein 1 (Shcbp1), mRNA [NM_011369]	0.97	-1.1	0.78	1.1	0.33	1.4	1.00	1.2	0.90	1.2	0.05	1.7	0.88	-1.1	0.98	-1.3	1.00	1.0
Siglec1	NM_011426	Mus musculus sialic acid binding Ig-like lectin 1, sialoadhesin (Siglec1), mRNA [NM_011426]	0.98	-1.0	0.80	1.1	0.92	-1.0	1.00	1.1	0.90	1.1	0.46	1.2	0.81	1.1	0.98	1.1	0.00	2.0
Sirpb1	AK054545	Mus musculus 2 days pregnant adult female ovary cDNA, RIKEN full-length enriched library, clone:E330039L08 product:weakly similar to SIGNAL-REGULATORY PROTEIN BETA-1 PRECURSOR (SIRP-BETA1) [Homo sapiens], full insert sequence. [AK054545]	0.92	1.2	0.50	1.4	0.34	1.4	1.00	1.2	0.90	1.5	0.40	1.3	0.81	1.4	0.98	1.3	0.00	2.1
Slamf9	NM_029612	Mus musculus SLAM family member 9 (Slamf9), mRNA [NM_029612]	0.96	-1.1	0.90	1.0	0.89	-1.1	1.00	1.1	0.90	1.2	0.81	1.1	0.80	1.2	0.98	1.1	0.04	1.5
Slc11a1	NM_013612	Mus musculus solute carrier family 11 (proton-coupled divalent metal ion transporters), member 1 (Slc11a1), mRNA [NM_013612]	0.88	1.1	0.00	1.5	0.00	1.6	1.00	1.1	0.90	1.1	0.25	1.2	0.80	1.2	0.99	-1.0	0.14	1.4
Slc13a4	NM_172892	Mus musculus solute carrier family 13 (sodium/sulfate symporters), member 4 (Slc13a4), mRNA [NM_172892]	0.99	-1.0	0.57	-1.3	0.07	-1.7	1.00	-1.2	0.98	1.1	0.68	-1.2	0.93	1.1	0.99	1.1	0.61	1.3
Slc16a6	NM_134038	Mus musculus solute carrier family 16 (monocarboxylic acid transporters), member 6 (Slc16a6), transcript variant 2, mRNA [NM_134038]	0.91	1.2	0.39	1.4	0.08	1.5	1.00	1.2	0.94	1.1	0.42	1.2	0.90	1.1	0.99	1.0	0.28	1.5

Slc24a6	NM_133221	Mus musculus solute carrier family 24 (sodium/potassium/calcium exchanger), member 6 (Slc24a6), mRNA [NM_133221]	0.87	-1.3	0.56	-1.2	0.03	-1.6	1.00	-1.2	0.90	-1.2	0.14	-1.4	0.99	-1.0	0.98	1.2	0.84	1.1
Slc26a4	NM_011867	Mus musculus solute carrier family 26, member 4 (Slc26a4), mRNA [NM_011867]	0.99	1.1	0.34	2.5	0.01	4.0	1.00	2.6	0.00	5.5	0.00	6.5	0.80	2.1	0.98	2.3	0.00	6.3
Slc39a14	NM_144808	Mus musculus solute carrier family 39 (zinc transporter), member 14 (Slc39a14), mRNA [NM_144808]	0.92	1.1	0.61	1.1	0.00	1.7	1.00	-1.1	1.00	1.0	0.20	1.3	0.80	-1.2	0.98	-1.2	0.71	-1.1
Slc7a8	NM_016972	Mus musculus solute carrier family 7 (cationic amino acid transporter, y+ system), member 8 (Slc7a8), mRNA [NM_016972]	0.97	-1.0	0.49	1.4	0.45	1.3	1.00	1.1	0.93	1.2	0.52	1.2	0.85	1.2	0.98	1.2	0.01	2.0
Slfn4	NM_011410	Mus musculus schlafen 4 (Slfn4), mRNA [NM_011410]	0.87	1.2	0.06	1.6	0.46	1.2	1.00	1.1	0.93	-1.1	0.81	1.1	0.94	-1.1	0.98	1.1	0.15	1.5
Slpi	NM_011414	Mus musculus secretory leukocyte peptidase inhibitor (Slpi), mRNA [NM_011414]	0.89	1.3	0.03	2.2	0.01	2.3	1.00	1.4	0.90	1.6	0.01	2.1	0.80	1.3	0.98	1.3	0.00	2.6
Smc2	NM_008017	Mus musculus structural maintenance of chromosomes 2 (Smc2), mRNA [NM_008017]	0.92	1.2	0.52	1.4	0.29	1.4	1.00	1.2	0.92	1.2	0.05	1.7	0.94	-1.1	0.98	-1.2	0.65	-1.2
Snca	NM_009221	Mus musculus synuclein, alpha (Snca), transcript variant 2, mRNA [NM_009221]	0.90	-1.2	0.79	-1.1	0.38	-1.4	1.00	-1.5	0.90	-1.3	0.06	-1.7	0.86	-1.2	0.98	-1.1	0.37	-1.6
Snx7	NM_029655	Mus musculus sorting nexin 7, mRNA (cDNA clone MGC:107328 IMAGE:30303462), complete cds. [BC087942]	0.93	1.1	0.53	1.2	0.00	1.8	1.00	1.4	0.90	1.2	0.00	1.7	0.96	1.0	0.98	1.1	0.47	1.3
Socs3	NM_007707	Mus musculus suppressor of cytokine signaling 3 (Socs3), mRNA [NM_007707]	0.92	-1.1	0.81	1.1	0.03	1.6	1.00	1.1	0.90	1.3	0.07	1.5	0.99	-1.0	0.99	-1.0	0.64	1.2
Sod2	NM_013671	Mus musculus superoxide dismutase 2, mitochondrial (Sod2), mRNA [NM_013671]	0.96	1.1	0.34	1.3	0.00	1.9	1.00	1.0	0.90	1.2	0.17	1.3	0.83	1.1	0.98	1.1	0.55	1.2
Sox7	NM_011446	Mus musculus SRY-box containing gene 7 (Sox7), mRNA [NM_011446]	0.89	-1.3	0.36	-1.6	0.03	-1.9	1.00	-1.2	0.98	-1.1	0.67	-1.2	0.95	1.1	0.98	1.1	0.84	-1.1
Sp5	NM_022435	Mus musculus trans-acting transcription factor 5 (Sp5), mRNA [NM_022435]	0.92	-1.2	0.99	-1.0	0.99	1.0	1.00	1.2	0.92	1.2	0.57	1.2	0.81	1.3	0.98	1.2	0.06	2.0
Spag5	NM_017407	Mus musculus sperm associated antigen 5 (Spag5), mRNA [NM_017407]	0.97	-1.1	0.97	1.0	0.60	1.2	1.00	1.2	0.90	1.4	0.07	1.6	0.87	-1.1	0.98	-1.3	0.90	-1.1
Spon1	AK084717	Mus musculus 13 days embryo heart cDNA, RIKEN full-length enriched library, clone:D330035F22 product:unclassifiable, full insert sequence. [AK084717]	0.72	1.7	0.28	1.8	0.08	1.9	1.00	1.0	0.94	1.2	0.73	1.2	0.92	1.1	0.99	1.1	0.75	1.2
Spp1	NM_009263	Mus musculus secreted phosphoprotein 1 (Spp1), mRNA [NM_009263]	0.98	1.1	0.83	1.2	0.22	2.2	1.00	1.9	0.90	1.6	0.02	3.4	0.94	1.2	1.00	0.4	0.00	4.7
Sprr1a	NM_009264	Mus musculus small proline-rich protein 1A (Sprr1a), mRNA [NM_009264]	0.99	-1.0	0.84	-1.1	0.00	2.2	1.00	1.2	0.98	1.1	0.53	1.2	0.88	1.1	0.99	-1.1	1.00	-1.0
Sqle	NM_009270	Mus musculus squalene epoxidase (Sqle), mRNA [NM_009270]	0.89	1.2	0.36	1.4	0.01	1.6	1.00	1.4	0.45	1.5	0.00	1.8	0.80	1.2	0.98	1.2	0.50	1.3

Steap4	NM_054098	Mus musculus STEAP family member 4 (Steap4), mRNA [NM_054098]	0.92	1.2	0.15	1.8	0.02	1.8	1.00	1.1	0.90	1.4	0.11	1.6	0.92	1.1	0.99	1.1	0.06	1.8
Stil	AK041653	Mus musculus 3 days neonate thymus cDNA, RIKEN full-length enriched library, clone:A630028B08 product:unclassifiable, full insert sequence. [AK041653]	0.99	-1.0	0.95	-1.0	0.76	1.1	1.00	1.1	0.90	1.3	0.07	1.5	0.80	-1.3	0.98	-1.2	0.55	-1.3
Swap70	NM_009302	Mus musculus SWA-70 protein (Swap70), mRNA [NM_009302]	0.97	-1.0	0.52	-1.3	0.06	-1.6	1.00	-1.2	0.93	-1.2	0.27	-1.4	0.84	-1.2	0.98	1.1	0.90	-1.1
Tacc3	NM_001040435	Mus musculus transforming, acidic coiled-coil containing protein 3 (Tacc3), transcript variant 2, mRNA [NM_011524]	0.99	1.0	0.70	1.1	0.20	1.4	1.00	1.2	0.90	1.2	0.02	1.6	0.99	1.0	0.98	-1.1	0.75	1.1
TC1447684	TC1643773	A11A_MOUSE (P98197) Potential phospholipid-transporting ATPase IH (ATPase class I type 11A) (ATPase IS) , partial (11%) [TC1447684]	0.89	1.1	0.37	1.3	0.00	1.9	1.00	1.1	0.95	1.1	0.08	1.3	0.97	1.0	0.98	1.1	0.67	1.1
TC1493944	TC1631866	Unknown	0.94	1.1	0.62	1.2	0.06	1.6	1.00	1.1	0.91	1.2	0.18	1.4	1.00	-1.0	1.00	-1.0	0.72	1.2
Tcfap4	NM_031182	Mus musculus transcription factor AP4 (Tcfap4), mRNA [NM_031182]	0.90	-1.2	0.36	-1.4	0.29	-1.3	1.00	-1.2	0.67	-1.5	0.00	-1.7	0.99	1.0	0.98	1.1	0.97	-1.0
Tcfec	NM_031198	Mus musculus transcription factor EC (Tcfec), mRNA [NM_031198]	0.93	-1.1	0.72	-1.1	0.92	1.0	1.00	-1.0	0.92	1.1	0.79	1.1	0.94	1.1	0.98	1.1	0.02	1.7
Tcp11l2	NM_146008	Mus musculus t-complex 11 (mouse) like 2 (Tcp11l2), mRNA [NM_146008]	0.93	-1.1	0.39	-1.3	0.00	-1.6	1.00	-1.1	0.92	-1.1	0.12	-1.3	0.91	1.1	0.98	1.1	0.82	1.1
Tfrc	NM_011638	Mus musculus transferrin receptor (Tfrc), mRNA [NM_011638]	0.90	1.1	0.48	1.2	0.00	1.5	1.00	1.2	0.90	1.2	0.05	1.4	0.96	-0.1	0.98	1.1	0.48	1.2
Tgfbi	NM_009369	Mus musculus transforming growth factor, beta induced (Tgfbi), mRNA [NM_009369]	0.96	1.1	0.26	1.5	0.01	1.8	1.00	1.4	0.67	1.6	0.01	1.8	0.81	1.2	0.98	1.2	0.07	1.7
Tgm1	NM_019984	Mus musculus transglutaminase 1, K polypeptide (Tgm1), mRNA [NM_019984]	0.90	1.2	0.17	1.6	0.00	2.4	1.00	1.2	0.90	1.3	0.01	1.7	0.83	1.2	0.98	1.2	0.11	1.6
Tgoln2	NM_009444	Mus musculus trans-golgi network protein 2 (Tgoln2), mRNA [NM_009444]	0.98	1.0	0.60	1.2	0.01	1.6	1.00	1.2	0.90	1.2	0.04	1.4	0.84	1.1	0.98	1.1	0.49	1.2
Thbd	NM_009378	Mus musculus thrombomodulin (Thbd), mRNA [NM_009378]	0.93	-1.1	0.40	-1.4	0.00	-1.9	1.00	-1.1	0.97	-1.1	0.34	-1.3	0.80	-1.2	0.98	-1.1	0.49	-1.3
Timeless	NM_011589	Mus musculus timeless homolog (Drosophila) (Timeless), mRNA [NM_011589]	0.93	1.1	0.41	1.4	0.09	1.6	1.00	1.2	0.93	1.1	0.09	1.6	0.97	1.0	0.98	-1.2	0.87	-1.1
Timp1	NM_011593	Mus musculus tissue inhibitor of metalloproteinase 1 (Timp1), mRNA [NM_011593]	0.86	1.6	0.00	3.5	0.00	8.3	1.00	1.4	0.93	1.3	0.12	2.1	0.97	-0.4	0.99	0.4	0.74	1.3
Tjp3	NM_013769	Mus musculus tight junction protein 3 (Tjp3), mRNA [NM_013769]	0.89	1.2	0.20	1.4	0.23	1.3	1.00	1.3	0.30	1.6	0.00	1.7	0.83	1.1	0.98	1.2	0.36	1.4
Tk1	NM_009387	Mus musculus thymidine kinase 1 (Tk1), mRNA [NM_009387]	1.00	-1.0	0.51	1.3	0.14	1.4	1.00	1.2	0.90	1.3	0.05	1.6	0.86	1.1	0.99	-1.1	0.58	1.3
Tlr2	NM_011905	Mus musculus toll-like receptor 2 (Tlr2), mRNA [NM_011905]	0.97	-0.8	0.82	0.9	0.63	1.2	1.00	1.2	0.87	1.3	0.30	1.3	0.89	1.1	0.99	0.6	0.01	1.9

Tlr7	NM_133211	Mus musculus toll-like receptor 7 (Tlr7), mRNA [NM_133211]	0.96	1.0	0.78	1.1	0.98	1.0	1.00	1.0	0.98	1.0	0.93	1.0	0.83	1.1	0.99	1.0	0.00	1.6
Tmc4	NM_181820	Mus musculus transmembrane channel-like gene family 4 (Tmc4), mRNA [NM_181820]	0.95	1.1	0.37	1.4	0.24	1.3	1.00	1.1	0.90	1.3	0.05	1.5	0.80	1.2	0.98	1.1	0.65	1.2
Tmem37	NM_019432	Mus musculus transmembrane protein 37 (Tmem37), mRNA [NM_019432]	0.87	1.3	0.58	1.2	0.01	1.8	1.00	1.0	0.97	1.1	0.54	1.2	0.97	1.0	0.98	1.2	0.69	1.2
Tmem49	NM_029478	Mus musculus transmembrane protein 49 (Tmem49), mRNA [NM_029478]	0.89	1.2	0.50	1.3	0.05	1.5	1.00	1.0	0.92	1.1	0.16	1.4	0.99	-1.0	0.99	1.0	0.44	1.4
Tmem54	NM_025452	Mus musculus transmembrane protein 54 (Tmem54), mRNA [NM_025452]	0.92	1.2	0.36	1.6	0.07	1.8	1.00	1.2	0.90	1.5	0.03	1.9	0.84	1.2	0.98	1.2	0.58	1.4
Tnc	NM_011607	Mus musculus tenascin C (Tnc), mRNA [NM_011607]	0.94	1.1	0.81	1.1	0.04	1.8	1.00	1.2	0.97	1.1	0.28	1.4	0.91	-1.1	1.00	1.0	0.99	-1.0
Tnfaip3	NM_009397	Mus musculus tumor necrosis factor, alpha-induced protein 3 (Tnfaip3), mRNA [NM_009397]	0.86	1.3	0.40	1.3	0.05	1.5	1.00	1.1	0.93	1.1	0.36	1.3	0.98	-1.0	0.99	1.0	0.44	1.3
Tnfrsf12a	NM_013749	Mus musculus tumor necrosis factor receptor superfamily, member 12a (Tnfrsf12a), mRNA [NM_013749]	0.96	1.1	0.97	-1.0	0.08	1.6	1.00	1.2	0.90	1.3	0.04	1.7	0.87	1.1	0.99	-1.1	0.68	-1.2
Tnfrsf4	NM_011659	Mus musculus tumor necrosis factor receptor superfamily, member 4 (Tnfrsf4), mRNA [NM_011659]	0.92	1.1	0.64	1.1	0.46	1.2	1.00	-1.0	1.00	-1.0	0.93	1.0	0.84	1.1	0.98	1.2	0.00	1.6
Tnfrsf9	NM_011612	Mus musculus tumor necrosis factor receptor superfamily, member 9 (Tnfrsf9), mRNA [NM_011612]	0.87	1.2	0.00	1.6	0.03	1.5	1.00	1.1	0.90	1.3	0.28	1.3	0.91	-1.1	0.99	-1.0	0.47	1.3
Tom1l1	AK083630	Mus musculus 9 days embryo whole body cDNA, RIKEN full-length enriched library, clone:D030056H14 product:ADAPTOR MOLECULE SRCASM, full insert sequence. [AK083630]	0.95	1.1	0.85	1.1	0.90	-1.1	1.00	-1.1	0.99	-1.0	0.95	1.0	0.89	1.1	0.98	1.1	0.10	1.6
Tpx2	NM_028109	Mus musculus TPX2, microtubule-associated protein homolog (Xenopus laevis) (Tpx2), mRNA [NM_028109]	0.95	-1.1	0.91	-1.1	0.66	1.2	1.00	1.2	0.91	1.2	0.10	1.5	0.99	-1.0	0.98	-1.2	0.91	1.1
Traf1	NM_009421	Mus musculus Tnf receptor-associated factor 1 (Traf1), mRNA [NM_009421]	0.89	-1.2	0.37	-1.4	0.00	-1.8	1.00	-1.1	0.96	-1.1	0.18	-1.4	0.92	-1.1	0.98	1.1	0.97	-1.0
Trem2	NM_031254	Mus musculus triggering receptor expressed on myeloid cells 2 (Trem2), mRNA [NM_031254]	0.98	0.0	0.59	1.3	0.70	1.2	1.00	1.4	0.73	1.6	0.05	1.7	0.84	1.2	0.98	1.1	0.00	2.5
Trim30	NM_009099	Mus musculus tripartite motif protein 30 (Trim30), mRNA [NM_009099]	0.85	1.4	0.08	1.7	0.24	1.4	1.00	1.1	0.90	1.3	0.11	1.5	0.86	1.1	1.00	-1.0	0.57	1.3
Tspan13	NM_025359	Mus musculus tetraspanin 13 (Tspan13), mRNA [NM_025359]	0.86	1.3	0.78	1.1	0.66	-1.1	1.00	-1.1	0.92	-1.1	0.71	-1.1	0.85	-1.1	0.98	-1.2	0.04	-1.6
Tuba6	NM_009448	Mus musculus blastocyst blastocyst cDNA, RIKEN full-length enriched library, clone:I1C0015P17 product:tubulin, alpha 6, full insert sequence. [AK145567]	0.97	1.0	0.55	1.2	0.00	1.9	1.00	1.1	0.90	1.2	0.11	1.4	0.91	1.1	0.98	1.1	0.36	1.4

Tubb6	NM_026473	Mus musculus tubulin, beta 6 (Tubb6), mRNA [NM_026473]	0.87	1.3	0.09	1.6	0.02	1.6	1.00	1.2	0.90	1.4	0.00	1.7	0.80	1.3	0.98	1.3	0.58	1.2
Tyms	NM_021288	Mus musculus thymidylate synthase (Tyms), mRNA [NM_021288]	0.96	1.1	0.45	1.3	0.05	1.5	1.00	1.2	0.90	1.2	0.01	1.6	0.92	-1.1	0.98	-1.1	0.88	1.1
Ube2c	NM_026785	Mus musculus ubiquitin-conjugating enzyme E2C (Ube2c), mRNA [NM_026785]	0.98	-1.0	0.94	1.0	0.62	1.2	1.00	1.4	0.90	1.4	0.05	1.7	0.99	-1.0	0.98	-1.2	0.95	1.0
Ube2t	NM_026024	Mus musculus ubiquitin-conjugating enzyme E2T (putative) (Ube2t), mRNA [NM_026024]	1.00	-1.0	0.85	1.1	0.39	1.3	1.00	1.2	0.90	1.4	0.05	1.6	0.81	-1.2	0.98	-1.4	0.66	-1.2
Uck2	NM_030724	Mus musculus uridine-cytidine kinase 2 (Uck2), mRNA [NM_030724]	0.98	1.0	0.73	1.1	0.02	1.5	1.00	1.1	0.96	1.1	0.38	1.2	0.92	1.1	1.00	-1.0	0.85	1.1
Uhrf1	NM_010931	Mus musculus ubiquitin-like, containing PHD and RING finger domains, 1 (Uhrf1), mRNA [NM_010931]	0.91	1.3	0.24	2.0	0.03	2.2	1.00	1.3	0.90	1.5	0.08	2.0	0.98	-1.0	0.99	-1.1	0.90	1.1
Ung2	NM_001081062	Mus musculus 0 day neonate eyeball cDNA, RIKEN full-length enriched library, clone:E130318K11 product:similar to URACIL-DNA GLYCOSYLASE 2 [Homo sapiens], full insert sequence [AK053890]	0.97	1.1	0.56	1.3	0.50	1.3	1.00	1.4	0.00	2.3	0.00	2.8	0.98	1.0	1.00	1.0	0.71	-1.2
Vnn1	NM_011704	Mus musculus vanin 1 (Vnn1), mRNA [NM_011704]	0.87	1.5	0.15	2.0	0.30	1.5	1.00	1.2	0.46	2.1	0.01	2.2	0.98	-1.0	0.98	1.2	0.00	2.8
Vnn3	NM_011979	Mus musculus vanin 3 (Vnn3), mRNA [NM_011979]	0.87	1.3	0.03	2.2	0.02	2.0	1.00	1.1	0.46	1.9	0.03	2.0	0.81	1.3	0.98	1.3	0.08	2.0
Wfdc1	NM_023395	Mus musculus WAP four-disulfide core domain 1 (Wfdc1), mRNA [NM_023395]	0.95	-1.1	0.71	-1.2	0.09	-1.7	1.00	-1.0	0.90	1.3	0.42	-1.3	0.99	-1.0	0.98	1.1	0.77	-1.2
Xtrp3s1	NM_139142	Mus musculus X transporter protein 3 similar 1 gene (Xtrp3s1), mRNA [NM_139142]	0.99	1.0	0.27	1.7	0.33	1.5	1.00	1.2	0.26	2.0	0.00	2.3	0.81	1.3	0.98	1.4	0.00	3.3
Zfp503	NM_145459	Mus musculus zinc finger protein 503 (Zfp503), mRNA [NM_145459]	0.86	-1.4	0.31	-1.6	0.12	-1.7	1.00	-1.2	0.90	-1.5	0.00	-1.9	0.97	1.1	0.99	1.1	0.91	-1.1
Zfp704	NM_133218	Mus musculus zinc finger protein 704 (Zfp704), mRNA [NM_133218]	0.94	-1.1	0.36	-1.4	0.02	-1.6	1.00	-1.2	0.90	-1.2	0.16	-1.4	0.97	-1.0	0.98	1.1	0.92	-1.0
Zmynd15	NM_001029929	Mus musculus zinc finger, MYND-type containing 15 (Zmynd15), mRNA [NM_001029929]	0.96	1.1	0.62	1.2	0.58	1.2	1.00	-1.0	0.98	1.1	0.92	1.0	0.99	1.0	0.98	1.1	0.06	1.6

SP2. Overall biological functions perturbed in lung (Enrichment scores > 3.0) by intratracheal instillation of C57BL/6 mice with 0.018, 0.054 and 0.162 mg Printex 90 CBNPs relative to controls, using DAVID functional annotation clustering.

Annotation Cluster 1 (Inflammatory and Immune Response)
Enrichment Score: 20.0

Category	Term	Count	%	Fold Enrichment	Benjamini P-Value
GOTERM_BP_FAT	GO:0006955~immune response	59	12.9	4.7	4.21E-20
GOTERM_BP_FAT	GO:0009611~response to wounding	51	11.2	5.6	2.74E-20
GOTERM_BP_FAT	GO:0006954~inflammatory response	41	9.0	6.9	2.23E-19
GOTERM_BP_FAT	GO:0006952~defense response	50	11.0	4.2	5.52E-15
SP_PIR_KEYWORDS	inflammatory response	22	4.8	11.9	1.33E-14

Annotation Cluster 2 (Extracellular Signaling)
Enrichment Score: 13.0

Category	Term	Count	%	Fold Enrichment	Benjamini P-Value
GOTERM_CC_FAT	GO:0044421~extracellular region part	65	14.3	3.3	4.84E-15
GOTERM_CC_FAT	GO:0005615~extracellular space	50	11.0	3.8	8.86E-14
GOTERM_CC_FAT	GO:0005576~extracellular region	95	20.8	2.2	2.99E-12
SP_PIR_KEYWORDS	Secreted	80	17.5	2.4	4.60E-11
SP_PIR_KEYWORDS	cytokine	24	5.3	5.7	2.01E-09
GOTERM_MF_FAT	GO:0005125~cytokine activity	24	5.3	5.3	2.08E-08

Annotation Cluster 3 (Peptide Binding)
Enrichment Score: 11.2

Category	Term	Count	%	Fold Enrichment	Benjamini P-Value
SP_PIR_KEYWORDS	disulfide bond	132	28.9	2.3	6.23E-18
SP_PIR_KEYWORDS	signal	145	31.8	2.1	7.58E-17
UP_SEQ_FEATURE	disulfide bond	131	28.7	2.1	3.44E-15
UP_SEQ_FEATURE	signal peptide	144	31.6	1.9	1.53E-12
GOTERM_CC_FAT	GO:0005576~extracellular region	95	20.8	2.2	2.99E-12
SP_PIR_KEYWORDS	Secreted	80	17.5	2.4	4.60E-11
SP_PIR_KEYWORDS	glycoprotein	147	32.2	1.7	1.34E-10
UP_SEQ_FEATURE	glycosylation site:N-linked (GlcNAc...)	140	30.7	1.6	2.30E-06
UP_SEQ_FEATURE	topological domain:Extracellular	87	19.1	1.5	7.00E-03
UP_SEQ_FEATURE	topological domain:Cytoplasmic	95	20.8	1.3	2.30E-01
GOTERM_CC_FAT	GO:0031224~intrinsic to membrane	132	28.9	0.9	1.00E+00

Annotation Cluster 4 (Chemokine Signaling)
Enrichment Score: 8.9

Category	Term	Count	%	Fold Enrichment	Benjamini P-Value
SP_PIR_KEYWORDS	inflammatory response	22	4.8	11.9	1.33E-14

INTERPRO	IPR001811:Small chemokine, interleukin-8-like	16	3.5	18.4	1.19E-12
GOTERM_MF_FAT	GO:0008009~chemokine activity	16	3.5	16.8	3.13E-12
GOTERM_MF_FAT	GO:0042379~chemokine receptor binding	16	3.5	16.4	2.49E-12
SMART	SM00199:SCY	16	3.5	14.9	4.91E-12
SP_PIR_KEYWORDS	cytokine	24	5.3	5.7	2.01E-09
GOTERM_MF_FAT	GO:0005125~cytokine activity	24	5.3	5.3	2.08E-08
SP_PIR_KEYWORDS	chemotaxis	15	3.3	10.2	7.32E-09
INTERPRO	IPR000827:Small chemokine, C-C group, conserved site	10	2.2	20.2	1.74E-07
GOTERM_BP_FAT	GO:0006935~chemotaxis	19	4.2	6.6	1.85E-07
GOTERM_BP_FAT	GO:0042330~taxis	19	4.2	6.6	1.85E-07
PIR_SUPERFAMILY	PIRSF001950:small inducible chemokine, C/CC types	10	2.2	15.6	1.02E-06
KEGG_PATHWAY	mmu04060:Cytokine-cytokine receptor interaction	28	6.1	3.4	3.31E-06
GOTERM_BP_FAT	GO:0007626~locomotory behavior	23	5.0	3.6	4.81E-05
INTERPRO	IPR018048:Small chemokine, C-X-C, conserved site	6	1.3	18.2	2.98E-03
PIR_SUPERFAMILY	PIRSF002522:CXC chemokine	6	1.3	16.4	2.07E-03
INTERPRO	IPR002473:Small chemokine, C-X-C/Interleukin 8	5	1.1	19.3	8.27E-03
INTERPRO	IPR001089:Small chemokine, C-X-C	5	1.1	19.3	8.27E-03
KEGG_PATHWAY	mmu04062:Chemokine signaling pathway	18	3.9	3.0	4.67E-03
GOTERM_BP_FAT	GO:0007610~behavior	24	5.3	2.2	1.31E-02

Annotation Cluster 5 (Cell Cycle)

Enrichment Score: 6.0

Category	Term	Count	%	Fold Enrichment	Benjamini P-Value
GOTERM_BP_FAT	GO:0000279~M phase	27	5.9	3.6	6.33E-06
SP_PIR_KEYWORDS	mitosis	20	4.4	4.7	2.04E-06
SP_PIR_KEYWORDS	cell division	23	5.0	3.8	7.26E-06
GOTERM_BP_FAT	GO:0007049~cell cycle	40	8.8	2.5	4.02E-05
GOTERM_BP_FAT	GO:0022403~cell cycle phase	27	5.9	3.1	7.30E-05
GOTERM_BP_FAT	GO:0000087~M phase of mitotic cell cycle	20	4.4	3.9	9.95E-05
SP_PIR_KEYWORDS	cell cycle	30	6.6	2.8	2.98E-05
GOTERM_BP_FAT	GO:0022402~cell cycle process	29	6.4	2.8	1.91E-04
GOTERM_BP_FAT	GO:0007067~mitosis	19	4.2	3.8	2.67E-04
GOTERM_BP_FAT	GO:0000280~nuclear division	19	4.2	3.8	2.67E-04
GOTERM_BP_FAT	GO:0048285~organelle fission	19	4.2	3.7	3.75E-04
GOTERM_BP_FAT	GO:0000278~mitotic cell cycle	21	4.6	3.3	5.05E-04
GOTERM_BP_FAT	GO:0051301~cell division	22	4.8	3.0	1.02E-03

Annotation Cluster 6 (Endotoxin Signaling)

Enrichment Score: 4.6

Category	Term	Count	%	Fold Enrichment	Benjamini P-Value
GOTERM_BP_FAT	GO:0002237~response to molecule of bacterial origin	10	2.2	7.7	3.75E-04
GOTERM_BP_FAT	GO:0032496~response to lipopolysaccharide	8	1.8	8.0	2.12E-03

GOTERM_BP_FAT	GO:0009617~response to bacterium	15	3.3	3.6	2.59E-03

Annotation Cluster 7 (Apoptosis)
Enrichment Score: 4.3

Category	Term	Count	%	Fold Enrichment	Benjamini P-Value
GOTERM_BP_FAT	GO:0042981~regulation of apoptosis	35	7.7	2.4	3.57E-04
GOTERM_BP_FAT	GO:0043067~regulation of programmed cell death	35	7.7	2.4	3.97E-04
GOTERM_BP_FAT	GO:0010941~regulation of cell death	35	7.7	2.4	4.31E-04
GOTERM_BP_FAT	GO:0043066~negative regulation of apoptosis	19	4.2	3.0	2.43E-03
GOTERM_BP_FAT	GO:0043069~negative regulation of programmed cell death	19	4.2	2.9	3.00E-03
GOTERM_BP_FAT	GO:0060548~negative regulation of cell death	19	4.2	2.9	3.05E-03
GOTERM_BP_FAT	GO:0006916~anti-apoptosis	8	1.8	3.4	1.31E-01

Annotation Cluster 8 (Sugar Binding)
Enrichment Score: 4.0

Category	Term	Count	%	Fold Enrichment	Benjamini P-Value
GOTERM_MF_FAT	GO:0030246~carbohydrate binding	28	6.1	3.5	3.42E-06
SP_PIR_KEYWORDS	Lectin	17	3.7	4.3	6.35E-05
GOTERM_MF_FAT	GO:0005529~sugar binding	17	3.7	3.7	1.24E-03
INTERPRO	IPR001304:C-type lectin	11	2.4	4.0	2.52E-02
UP_SEQ_FEATURE	domain:C-type lectin	10	2.2	4.3	8.49E-02
INTERPRO	IPR018378:C-type lectin, conserved site	10	2.2	4.1	3.83E-02
INTERPRO	IPR016186:C-type lectin-like	11	2.4	3.7	3.90E-02
SMART	SM00034:CLECT	11	2.4	3.2	6.96E-02
INTERPRO	IPR002353:Type II antifreeze protein	6	1.3	6.2	8.31E-02

Annotation Cluster 9 (Polysaccharide Binding)
Enrichment Score: 3.8

Category	Term	Count	%	Fold Enrichment	Benjamini P-Value
GOTERM_MF_FAT	GO:0030246~carbohydrate binding	28	6.1	3.5	3.42E-06
GOTERM_MF_FAT	GO:0001871~pattern binding	13	2.9	4.1	6.16E-03
GOTERM_MF_FAT	GO:0030247~polysaccharide binding	13	2.9	4.1	6.16E-03
GOTERM_MF_FAT	GO:0005539~glycosaminoglycan binding	12	2.6	4.2	7.26E-03
GOTERM_MF_FAT	GO:0008201~heparin binding	7	1.5	3.4	3.90E-01
SP_PIR_KEYWORDS	heparin-binding	5	1.1	4.0	2.39E-01

Annotation Cluster 10 (Adaptive Immune Response)
Enrichment Score: 3.8

Category	Term	Count	%	Fold Enrichment	Benjamini P-Value
GOTERM_BP_FAT	GO:0050766~positive regulation of phagocytosis	10	2.2	16.5	1.09E-06
GOTERM_BP_FAT	GO:0050764~regulation of phagocytosis	10	2.2	15.1	2.24E-06

GOTERM_BP_FAT	GO:0002822~regulation of adaptive immune response based on somatic recombination of immune receptors built from immunoglobulin superfamily domains	13	2.9	8.8	4.60E-06
GOTERM_BP_FAT	GO:0002819~regulation of adaptive immune response	13	2.9	8.8	4.60E-06
GOTERM_BP_FAT	GO:0045807~positive regulation of endocytosis	10	2.2	11.1	2.96E-05
GOTERM_BP_FAT	GO:0002250~adaptive immune response	14	3.1	6.3	4.24E-05
GOTERM_BP_FAT	GO:0002460~adaptive immune response based on somatic recombination of immune receptors built from immunoglobulin superfamily domains	14	3.1	6.3	4.24E-05
GOTERM_BP_FAT	GO:0002684~positive regulation of immune system process	20	4.4	3.7	2.22E-04
GOTERM_BP_FAT	GO:0051130~positive regulation of cellular component organization	15	3.3	4.7	3.43E-04
GOTERM_BP_FAT	GO:0002706~regulation of lymphocyte mediated immunity	11	2.4	6.4	5.03E-04
GOTERM_BP_FAT	GO:0030100~regulation of endocytosis	10	2.2	7.3	5.01E-04
GOTERM_BP_FAT	GO:0002712~regulation of B cell mediated immunity	8	1.8	10.1	6.50E-04
GOTERM_BP_FAT	GO:0002889~regulation of immunoglobulin mediated immune response	8	1.8	10.1	6.50E-04
GOTERM_BP_FAT	GO:0002883~regulation of hypersensitivity	6	1.3	17.5	8.38E-04
GOTERM_BP_FAT	GO:0002864~regulation of acute inflammatory response to antigenic stimulus	6	1.3	17.5	8.38E-04
GOTERM_BP_FAT	GO:0002703~regulation of leukocyte mediated immunity	11	2.4	5.9	8.16E-04
GOTERM_BP_FAT	GO:0002697~regulation of immune effector process	12	2.6	5.2	1.03E-03
GOTERM_BP_FAT	GO:0002714~positive regulation of B cell mediated immunity	6	1.3	16.2	1.07E-03
GOTERM_BP_FAT	GO:0002891~positive regulation of immunoglobulin mediated immune response	6	1.3	16.2	1.07E-03
GOTERM_BP_FAT	GO:0002821~positive regulation of adaptive immune response	8	1.8	8.9	1.21E-03
GOTERM_BP_FAT	GO:0002824~positive regulation of adaptive immune response based on somatic recombination of immune receptors built from immunoglobulin superfamily domains	8	1.8	8.9	1.21E-03
GOTERM_BP_FAT	GO:0002252~immune effector process	14	3.1	4.2	1.35E-03
GOTERM_BP_FAT	GO:0002449~lymphocyte mediated immunity	11	2.4	5.5	1.38E-03
GOTERM_BP_FAT	GO:0006911~phagocytosis, engulfment	6	1.3	15.1	1.39E-03
GOTERM_BP_FAT	GO:0001796~regulation of type IIa hypersensitivity	5	1.1	23.7	1.39E-03
GOTERM_BP_FAT	GO:0001798~positive regulation of type IIa hypersensitivity	5	1.1	23.7	1.39E-03
GOTERM_BP_FAT	GO:0002894~positive regulation of type II hypersensitivity	5	1.1	23.7	1.39E-03
GOTERM_BP_FAT	GO:0002892~regulation of type II hypersensitivity	5	1.1	23.7	1.39E-03
GOTERM_BP_FAT	GO:0002888~positive regulation of myeloid leukocyte mediated immunity	5	1.1	23.7	1.39E-03
GOTERM_BP_FAT	GO:0016064~immunoglobulin mediated immune response	10	2.2	6.0	1.63E-03
GOTERM_BP_FAT	GO:0051050~positive regulation of transport	14	3.1	4.0	1.93E-03
GOTERM_BP_FAT	GO:0019724~B cell mediated immunity	10	2.2	5.8	2.01E-03
GOTERM_BP_FAT	GO:0050778~positive regulation of immune response	14	3.1	3.9	2.38E-03
GOTERM_BP_FAT	GO:0002673~regulation of acute inflammatory response	6	1.3	12.6	2.91E-03
GOTERM_BP_FAT	GO:0002861~regulation of inflammatory response to antigenic stimulus	6	1.3	12.6	2.91E-03
GOTERM_BP_FAT	GO:0002885~positive regulation of hypersensitivity	5	1.1	18.9	3.09E-03

GOTERM_BP_FAT	GO:0002866~positive regulation of acute inflammatory response to antigenic stimulus	5	1.1	18.9	3.09E-03
GOTERM_MF_FAT	GO:0019865~immunoglobulin binding	5	1.1	18.1	6.89E-03
GOTERM_BP_FAT	GO:0002443~leukocyte mediated immunity	11	2.4	4.7	3.87E-03
GOTERM_BP_FAT	GO:0031349~positive regulation of defense response	9	2.0	6.0	3.84E-03
GOTERM_BP_FAT	GO:0045087~innate immune response	12	2.6	4.2	3.87E-03
GOTERM_BP_FAT	GO:0048584~positive regulation of response to stimulus	16	3.5	3.3	3.88E-03
GOTERM_BP_FAT	GO:0002675~positive regulation of acute inflammatory response	5	1.1	17.2	4.23E-03
GOTERM_MF_FAT	GO:0019864~IgG binding	4	0.9	31.9	6.79E-03
GOTERM_BP_FAT	GO:0048002~antigen processing and presentation of peptide antigen	7	1.5	7.6	8.03E-03
GOTERM_BP_FAT	GO:0002863~positive regulation of inflammatory response to antigenic stimulus	5	1.1	14.6	8.14E-03
GOTERM_BP_FAT	GO:0060627~regulation of vesicle-mediated transport	10	2.2	4.6	9.33E-03
GOTERM_BP_FAT	GO:0002886~regulation of myeloid leukocyte mediated immunity	5	1.1	12.6	1.42E-02
GOTERM_BP_FAT	GO:0002708~positive regulation of lymphocyte mediated immunity	7	1.5	6.6	1.56E-02
GOTERM_BP_FAT	GO:0002705~positive regulation of leukocyte mediated immunity	7	1.5	6.6	1.56E-02
GOTERM_MF_FAT	GO:0032403~protein complex binding	9	2.0	4.6	2.73E-02
GOTERM_BP_FAT	GO:0002474~antigen processing and presentation of peptide antigen via MHC class I	5	1.1	11.1	2.16E-02
GOTERM_BP_FAT	GO:0001810~regulation of type I hypersensitivity	4	0.9	18.9	2.29E-02
GOTERM_BP_FAT	GO:0002699~positive regulation of immune effector process	7	1.5	5.8	2.94E-02
GOTERM_BP_FAT	GO:0006909~phagocytosis	7	1.5	5.4	3.91E-02
GOTERM_BP_FAT	GO:0002253~activation of immune response	9	2.0	4.0	4.17E-02
GOTERM_BP_FAT	GO:0001803~regulation of type III hypersensitivity	3	0.7	37.8	4.36E-02
GOTERM_BP_FAT	GO:0001805~positive regulation of type III hypersensitivity	3	0.7	37.8	4.36E-02
GOTERM_BP_FAT	GO:0002274~myeloid leukocyte activation	6	1.3	6.5	4.38E-02
SP_PIR_KEYWORDS	igg-binding protein	3	0.7	31.7	3.71E-02
GOTERM_BP_FAT	GO:0050729~positive regulation of inflammatory response	5	1.1	7.9	6.46E-02
GOTERM_BP_FAT	GO:0032103~positive regulation of response to external stimulus	6	1.3	5.8	6.50E-02
GOTERM_MF_FAT	GO:0019763~immunoglobulin receptor activity	3	0.7	29.9	1.08E-01
GOTERM_BP_FAT	GO:0050727~regulation of inflammatory response	7	1.5	4.6	7.07E-02
GOTERM_BP_FAT	GO:0006897~endocytosis	13	2.9	2.6	7.71E-02
GOTERM_BP_FAT	GO:0010324~membrane invagination	13	2.9	2.6	7.71E-02
GOTERM_BP_FAT	GO:0006910~phagocytosis, recognition	4	0.9	11.6	7.77E-02
GOTERM_BP_FAT	GO:0032101~regulation of response to external stimulus	9	2.0	3.3	9.77E-02
GOTERM_BP_FAT	GO:0042590~antigen processing and presentation of exogenous peptide antigen via MHC class I	3	0.7	22.7	1.08E-01
SP_PIR_KEYWORDS	immunoglobulin receptor	3	0.7	18.1	9.35E-02
GOTERM_BP_FAT	GO:0016044~membrane organization	15	3.3	2.1	1.82E-01
GOTERM_BP_FAT	GO:0001812~positive regulation of type I hypersensitivity	3	0.7	16.2	1.82E-01
GOTERM_BP_FAT	GO:0002478~antigen processing and presentation of exogenous peptide antigen	4	0.9	6.6	2.56E-01

GOTERM_BP_FAT	GO:0019882~antigen processing and presentation	7	1.5	3.0	2.93E-01
GOTERM_BP_FAT	GO:0019884~antigen processing and presentation of exogenous antigen	4	0.9	5.4	3.48E-01
GOTERM_BP_FAT	GO:0045576~mast cell activation	3	0.7	7.6	4.61E-01
GOTERM_BP_FAT	GO:0008037~cell recognition	4	0.9	3.2	6.76E-01
GOTERM_BP_FAT	GO:0016192~vesicle-mediated transport	16	3.5	1.3	8.50E-01
KEGG_PATHWAY	mmu04650:Natural killer cell mediated cytotoxicity	5	1.1	1.2	9.51E-01
KEGG_PATHWAY	mmu04666:Fc gamma R-mediated phagocytosis	4	0.9	1.2	9.62E-01

Annotation Cluster 11 (Conjugation)
Enrichment Score: 3.5

Category	Term	Count	%	Fold Enrichment	Benjamini P-Value
SP_PIR_KEYWORDS	ubl conjugation	31	6.8	2.5	2.08E-04
SP_PIR_KEYWORDS	isopeptide bond	18	3.9	2.7	5.51E-03
UP_SEQ_FEATURE	cross-link:Glycyl lysine isopeptide (Lys-Gly) (interchain with G-Cter in ubiquitin)	11	2.4	2.5	5.27E-01

Annotation Cluster 12 (Extracellular Matrix)
Enrichment Score: 3.5

Category	Term	Count	%	Fold Enrichment	Benjamini P-Value
SP_PIR_KEYWORDS	extracellular matrix	16	3.5	3.2	3.88E-03
GOTERM_CC_FAT	GO:0031012~extracellular matrix	20	4.4	2.5	1.27E-02
GOTERM_CC_FAT	GO:0005578~proteinaceous extracellular matrix	19	4.2	2.5	1.70E-02

Annotation Cluster 13 (Sterol and Terpenoid Biosynthesis)
Enrichment Score: 3.4

Category	Term	Count	%	Fold Enrichment	Benjamini P-Value
GOTERM_BP_FAT	GO:0008203~cholesterol metabolic process	13	2.9	7.0	4.19E-05
GOTERM_BP_FAT	GO:0016125~sterol metabolic process	13	2.9	6.4	8.66E-05
GOTERM_BP_FAT	GO:0016126~sterol biosynthetic process	8	1.8	10.1	6.50E-04
GOTERM_BP_FAT	GO:0006695~cholesterol biosynthetic process	7	1.5	11.5	1.14E-03
SP_PIR_KEYWORDS	sterol biosynthesis	6	1.3	10.6	4.23E-03
SP_PIR_KEYWORDS	Steroid biosynthesis	7	1.5	7.4	5.61E-03
GOTERM_BP_FAT	GO:0006694~steroid biosynthetic process	9	2.0	4.8	1.47E-02
SP_PIR_KEYWORDS	Cholesterol biosynthesis	5	1.1	11.7	1.00E-02
GOTERM_BP_FAT	GO:0008202~steroid metabolic process	13	2.9	3.1	2.78E-02
SP_PIR_KEYWORDS	lipid synthesis	8	1.8	3.4	8.29E-02
KEGG_PATHWAY	mmu00900:Terpenoid backbone biosynthesis	4	0.9	8.5	1.60E-01
GOTERM_BP_FAT	GO:0008299~isoprenoid biosynthetic process	4	0.9	6.9	2.35E-01
GOTERM_BP_FAT	GO:0006720~isoprenoid metabolic process	5	1.1	3.9	3.62E-01
GOTERM_BP_FAT	GO:0008610~lipid biosynthetic process	12	2.6	1.6	6.86E-01

Annotation Cluster 14 (Acute Phase Response)

Enrichment Score: 3.2

Category	Term	Count	%	Fold Enrichment	Benjamini P-Value
GOTERM_BP_FAT	GO:0002526~acute inflammatory response	15	3.3	7.0	4.96E-06
SP_PIR_KEYWORDS	acute phase	8	1.8	14.1	3.15E-05
GOTERM_BP_FAT	GO:0006953~acute-phase response	8	1.8	10.1	6.50E-04
GOTERM_CC_FAT	GO:0032994~protein-lipid complex	5	1.1	7.2	7.92E-02
GOTERM_CC_FAT	GO:0034358~plasma lipoprotein particle	5	1.1	7.2	7.92E-02
INTERPRO	IPR000096:Serum amyloid A protein	3	0.7	25.5	1.49E-01
PIR_SUPERFAMILY	PIRSF002472:amyloid protein, SAA type	3	0.7	24.6	1.74E-01
SP_PIR_KEYWORDS	hdl	4	0.9	9.9	7.15E-02
GOTERM_CC_FAT	GO:0034364~high-density lipoprotein particle	4	0.9	9.7	1.08E-01
SMART	SM00197:SAA	3	0.7	20.7	1.52E-01
PIR_SUPERFAMILY	PIRSF002472:Serum_amyloid_A	3	0.7	19.7	2.16E-01
SP_PIR_KEYWORDS	amyloid	3	0.7	10.6	2.14E-01

Annotation Cluster 15 (Immunoglobin Signaling)

Enrichment Score: 3.1

Category	Term	Count	%	Fold Enrichment	Benjamini P-Value
INTERPRO	IPR003599:Immunoglobulin subtype	21	4.6	2.9	8.33E-03
SP_PIR_KEYWORDS	Immunoglobulin domain	26	5.7	2.5	1.37E-03
UP_SEQ_FEATURE	domain:Ig-like C2-type 1	12	2.6	3.6	8.01E-02
UP_SEQ_FEATURE	domain:Ig-like C2-type 2	12	2.6	3.5	7.70E-02
SMART	SM00409:IG	21	4.6	2.3	4.00E-02
INTERPRO	IPR013783:Immunoglobulin-like fold	29	6.4	1.9	5.30E-02
INTERPRO	IPR007110:Immunoglobulin-like	27	5.9	1.9	7.71E-02
INTERPRO	IPR013151:Immunoglobulin	12	2.6	2.9	9.97E-02
INTERPRO	IPR013106:Immunoglobulin V-set	17	3.7	2.0	2.93E-01

Annotation Cluster 16 (Plasma Membrane)

Enrichment Score: 3.1

Category	Term	Count	%	Fold Enrichment	Benjamini P-Value
GOTERM_CC_FAT	GO:0009986~cell surface	23	5.0	2.9	8.07E-04
GOTERM_CC_FAT	GO:0009897~external side of plasma membrane	17	3.7	3.2	3.53E-03
GOTERM_CC_FAT	GO:0044459~plasma membrane part	43	9.4	1.0	9.74E-01

SP3. PCR array validation of microarray gene expression in lung of C57BL/6 mice, exposed to 0.018, 0.054 and 0.162 mg CBNPs, 1, 3 and 28 days post-exposure. Significant findings ($p < 0.05$) are denoted by *. Down-regulated genes are denoted by negative values, calculated according to the negative of the fold-change inverse.

Gene	Day	Dose	Foldchange
Cxcl1	Day 1	0.018 mg	-1.7
		0.054 mg	8.4
		0.162 mg	*19.9
	Day 3	0.018 mg	1.6
		0.054 mg	*6.2
		0.162 mg	*8.7
	Day 28	0.018 mg	1.2
		0.054 mg	1.1
		0.162 mg	8.1
Ccl2	Day 1	0.018 mg	-1.5
		0.054 mg	4.7
		0.162 mg	18.5
	Day 3	0.018 mg	1.1
		0.054 mg	*4.1
		0.162 mg	*11.6
	Day 28	0.018 mg	1.0
		0.054 mg	1.5
		0.162 mg	*10.2
Cxcl5	Day 1	0.018 mg	-1.3
		0.054 mg	*12.3
		0.162 mg	*17.4
	Day 3	0.018 mg	6.3
		0.054 mg	*62.7
		0.162 mg	*44.2
	Day 28	0.018 mg	-1.3
		0.054 mg	-1.2
		0.162 mg	*30.0
Spp1	Day 1	0.018 mg	-1.4
		0.054 mg	-1.4
		0.162 mg	1.2
	Day 3	0.018 mg	1.4
		0.054 mg	1.9
		0.162 mg	*5.6
	Day 28	0.018 mg	1.0
		0.054 mg	-1.1
		0.162 mg	*4.4
Ccl6	Day 1	0.018 mg	1.4
		0.054 mg	1.1
		0.162 mg	1.1
	Day 3	0.018 mg	1.6
		0.054 mg	*2.7
		0.162 mg	*2.1
	Day 28	0.018 mg	1.2
		0.054 mg	1.2
		0.162 mg	*3.2
Ccl22	Day 1	0.018 mg	-1.1

		0.054 mg	1.4
		0.162 mg	1.9
	Day 3	0.018 mg	-1.1
		0.054 mg	1.7
		0.162 mg	2.0
	Day 28	0.018 mg	1.2
		0.054 mg	1.6
		0.162 mg	1.6
Ccr4	Day 1	0.018 mg	1.0
		0.054 mg	2.1
		0.162 mg	1.3
	Day 3	0.018 mg	1.3
		0.054 mg	1.5
		0.162 mg	1.5
	Day 28	0.018 mg	-1.1
		0.054 mg	1.1
		0.162 mg	1.9
Ccl3	Day 1	0.018 mg	1.3
		0.054 mg	2.0
		0.162 mg	*6.2
	Day 3	0.018 mg	1.5
		0.054 mg	*3.9
		0.162 mg	*3.5
	Day 28	0.018 mg	-1.0
		0.054 mg	1.5
		0.162 mg	*4.3
Ccl12	Day 1	0.018 mg	*-1.6
		0.054 mg	1.8
		0.162 mg	1.9
	Day 3	0.018 mg	-1.5
		0.054 mg	1.3
		0.162 mg	*2.6
	Day 28	0.018 mg	-1.6
		0.054 mg	1.3
		0.162 mg	2.6
Ccl9	Day 1	0.018 mg	1.3
		0.054 mg	*2.4
		0.162 mg	*2.0
	Day 3	0.018 mg	1.2
		0.054 mg	1.4
		0.162 mg	1.4
	Day 28	0.018 mg	1.0
		0.054 mg	-1.0
		0.162 mg	1.9
Tnf	Day 1	0.018 mg	-1.8
		0.054 mg	1.1
		0.162 mg	1.7
	Day 3	0.018 mg	-1.0
		0.054 mg	*1.8
		0.162 mg	1.5
	Day 28	0.018 mg	-1.1
		0.054 mg	*1.4

		0.162 mg	*2.8
Ccl7	Day 1	0.018 mg	*-1.8
		0.054 mg	6.8
		0.162 mg	*13.2
	Day 3	0.018 mg	-1.1
		0.054 mg	*3.1
		0.162 mg	*11.0
	Day 28	0.018 mg	-1.2
		0.054 mg	1.8
		0.162 mg	*9.8
Ccl11	Day 1	0.018 mg	*-2.5
		0.054 mg	1.9
		0.162 mg	2.4
	Day 3	0.018 mg	1.1
		0.054 mg	1.3
		0.162 mg	*1.8
	Day 28	0.018 mg	1.6
		0.054 mg	*3.1
		0.162 mg	2.1
Ccl17	Day 1	0.018 mg	-1.2
		0.054 mg	1.8
		0.162 mg	3.1
	Day 3	0.018 mg	1.2
		0.054 mg	*2.3
		0.162 mg	*3.0
	Day 28	0.018 mg	1.0
		0.054 mg	2.0
		0.162 mg	*1.8
Ccl24	Day 1	0.018 mg	-2.0
		0.054 mg	1.2
		0.162 mg	*3.7
	Day 3	0.018 mg	*-1.6
		0.054 mg	-1.5
		0.162 mg	-1.3
	Day 28	0.018 mg	1.3
		0.054 mg	1.2
		0.162 mg	-1.9
Ccl4	Day 1	0.018 mg	1.1
		0.054 mg	2.3
		0.162 mg	*3.8
	Day 3	0.018 mg	-1.1
		0.054 mg	1.1
		0.162 mg	1.3
	Day 28	0.018 mg	-1.0
		0.054 mg	1.1
		0.162 mg	*2.4
Ccl8	Day 1	0.018 mg	-1.5
		0.054 mg	2.2
		0.162 mg	1.6
	Day 3	0.018 mg	1.9
		0.054 mg	1.8
		0.162 mg	*2.9

	Day 28	0.018 mg	-1.9
		0.054 mg	1.4
		0.162 mg	2.3
Ccr5	Day 1	0.018 mg	-1.2
		0.054 mg	-2.3
		0.162 mg	1.2
	Day 3	0.018 mg	1.0
		0.054 mg	1.3
		0.162 mg	1.3
	Day 28	0.018 mg	1.1
		0.054 mg	1.3
		0.162 mg	1.7
Cxcl10	Day 1	0.018 mg	1.2
		0.054 mg	3.8
		0.162 mg	5.2
	Day 3	0.018 mg	1.0
		0.054 mg	*1.7
		0.162 mg	*4.7
	Day 28	0.018 mg	1.7
		0.054 mg	2.2
		0.162 mg	7.0
Cxcl12	Day 1	0.018 mg	-1.2
		0.054 mg	1.2
		0.162 mg	-1.1
	Day 3	0.018 mg	1.0
		0.054 mg	-1.0
		0.162 mg	1.2
	Day 28	0.018 mg	1.1
		0.054 mg	-1.8
		0.162 mg	1.3
Cxcl9	Day 1	0.018 mg	*-1.5
		0.054 mg	2.5
		0.162 mg	2.2
	Day 3	0.018 mg	1.3
		0.054 mg	3.1
		0.162 mg	2.8
	Day 28	0.018 mg	-1.0
		0.054 mg	-1.0
		0.162 mg	*4.1
Il13ra1	Day 1	0.018 mg	-1.1
		0.054 mg	1.2
		0.162 mg	1.4
	Day 3	0.018 mg	-1.0
		0.054 mg	1.0
		0.162 mg	1.1
	Day 28	0.018 mg	1.0
		0.054 mg	1.1
		0.162 mg	1.2
Il1b	Day 1	0.018 mg	2.0
		0.054 mg	2.2
		0.162 mg	4.3
	Day 3	0.018 mg	1.4

		0.054 mg	1.4
		0.162 mg	1.5
	Day 28	0.018 mg	1.1
		0.054 mg	-1.1
		0.162 mg	1.1
Il1r2	Day 1	0.018 mg	2.0
		0.054 mg	*8.5
		0.162 mg	*13.0
	Day 3	0.018 mg	1.3
		0.054 mg	2.0
		0.162 mg	*3.2
	Day 28	0.018 mg	1.2
		0.054 mg	1.6
		0.162 mg	*3.0
Il6	Day 1	0.018 mg	-1.2
		0.054 mg	*4.1
		0.162 mg	*13.2
	Day 3	0.018 mg	1.5
		0.054 mg	*2.8
		0.162 mg	*6.5
	Day 28	0.018 mg	-1.1
		0.054 mg	-1.3
		0.162 mg	1.2
Ccl5	Day 1	0.018 mg	1.2
		0.054 mg	-1.6
		0.162 mg	-1.1
	Day 3	0.018 mg	-1.2
		0.054 mg	*-1.2
		0.162 mg	*-1.9
	Day 28	0.018 mg	-1.2
		0.054 mg	*-1.3
		0.162 mg	-1.5
Ccl20	Day 1	0.018 mg	1.0
		0.054 mg	*5.8
		0.162 mg	*9.8
	Day 3	0.018 mg	4.1
		0.054 mg	*20.8
		0.162 mg	*10.2
	Day 28	0.018 mg	-1.2
		0.054 mg	1.4
		0.162 mg	4.2
Crp	Day 1	0.018 mg	1.8
		0.054 mg	3.5
		0.162 mg	*12.5
	Day 3	0.018 mg	1.1
		0.054 mg	1.3
		0.162 mg	-1.1
	Day 28	0.018 mg	*-4.6
		0.054 mg	-2.3
		0.162 mg	-1.0
Vnn1	Day 1	0.018 mg	1.0
		0.054 mg	*2.1

		0.162 mg	1.5
	Day 3	0.018 mg	1.3
		0.054 mg	*2.6
		0.162 mg	2.7
	Day 28	0.018 mg	-1.2
		0.054 mg	1.1
		0.162 mg	*3.6
Noxo1	Day 1	0.018 mg	1.2
		0.054 mg	6.2
		0.162 mg	*4.2
	Day 3	0.018 mg	1.5
		0.054 mg	*3.4
		0.162 mg	*3.9
	Day 28	0.018 mg	1.1
		0.054 mg	1.2
		0.162 mg	*6.7
Noxa1	Day 1	0.018 mg	-1.1
		0.054 mg	1.3
		0.162 mg	1.5
	Day 3	0.018 mg	-1.1
		0.054 mg	*1.6
		0.162 mg	1.4
	Day 28	0.018 mg	-1.2
		0.054 mg	-1.1
		0.162 mg	*1.8
Sod1	Day 1	0.018 mg	-1.2
		0.054 mg	-1.6
		0.162 mg	-1.6
	Day 3	0.018 mg	-1.1
		0.054 mg	-1.1
		0.162 mg	-1.2
	Day 28	0.018 mg	-1.2
		0.054 mg	-1.1
		0.162 mg	-1.2
Sod2	Day 1	0.018 mg	1.1
		0.054 mg	-1.5
		0.162 mg	1.5
	Day 3	0.018 mg	-1.1
		0.054 mg	1.1
		0.162 mg	1.0
	Day 28	0.018 mg	-1.1
		0.054 mg	1.2
		0.162 mg	-1.3
Gstm1	Day 1	0.018 mg	1.1
		0.054 mg	-1.4
		0.162 mg	-1.3
	Day 3	0.018 mg	-1.1
		0.054 mg	-1.3
		0.162 mg	*-2
	Day 28	0.018 mg	1.0
		0.054 mg	1.1
		0.162 mg	-1.2

Gstm2	Day 1	0.018 mg	1.1
		0.054 mg	-1.5
		0.162 mg	-1.3
	Day 3	0.018 mg	1.0
		0.054 mg	1.0
		0.162 mg	-1.2
	Day 28	0.018 mg	-1.1
		0.054 mg	-1.0
		0.162 mg	-1.3
Gstm3	Day 1	0.018 mg	-1.1
		0.054 mg	-1.1
		0.162 mg	1.3
	Day 3	0.018 mg	-1.2
		0.054 mg	-1.1
		0.162 mg	-1.3
	Day 28	0.018 mg	-1.1
		0.054 mg	-1.2
		0.162 mg	-1.4
Ogg1	Day 1	0.018 mg	1.0
		0.054 mg	1.3
		0.162 mg	1.1
	Day 3	0.018 mg	-1.0
		0.054 mg	1.0
		0.162 mg	1.0
	Day 28	0.018 mg	1.1
		0.054 mg	-1.0
		0.162 mg	1.2
Abcg1	Day 1	0.018 mg	1.2
		0.054 mg	-1.8
		0.162 mg	*-2.3
	Day 3	0.018 mg	-1.0
		0.054 mg	-1.0
		0.162 mg	*-1.4
	Day 28	0.018 mg	1.0
		0.054 mg	-1.0
		0.162 mg	1.5
Abca1	Day 1	0.018 mg	-1.1
		0.054 mg	-3.4
		0.162 mg	*-2.6
	Day 3	0.018 mg	-1.1
		0.054 mg	-1.2
		0.162 mg	*-1.8
	Day 28	0.018 mg	-1.0
		0.054 mg	1.1
		0.162 mg	1.0
Ldlr	Day 1	0.018 mg	-1.1
		0.054 mg	1.0
		0.162 mg	1.5
	Day 3	0.018 mg	1.1
		0.054 mg	1.0
		0.162 mg	1.4
	Day 28	0.018 mg	1.1

		0.054 mg	1.2
		0.162 mg	1.1
Pten	Day 1	0.018 mg	-1.0
		0.054 mg	-1.9
		0.162 mg	-1.3
	Day 3	0.018 mg	-1.1
		0.054 mg	1.0
		0.162 mg	1.0
	Day 28	0.018 mg	-1.1
		0.054 mg	1.0
		0.162 mg	-1.2
Pdcd4	Day 1	0.018 mg	-1.0
		0.054 mg	-1.1
		0.162 mg	-1.4
	Day 3	0.018 mg	-1.1
		0.054 mg	-1.2
		0.162 mg	*-1.5
	Day 28	0.018 mg	1.2
		0.054 mg	1.2
		0.162 mg	1.1
Hprt1	Day 1	0.018 mg	-1.1
		0.054 mg	-1.1
		0.162 mg	-1.1
	Day 3	0.018 mg	-1.1
		0.054 mg	-1.1
		0.162 mg	-1.1
	Day 28	0.018 mg	-1.1
		0.054 mg	1.0
		0.162 mg	-1.0
Actb	Day 1	0.018 mg	1.0
		0.054 mg	-1.1
		0.162 mg	-1.0
	Day 3	0.018 mg	1.0
		0.054 mg	1.2
		0.162 mg	1.2
	Day 28	0.018 mg	1.1
		0.054 mg	1.1
		0.162 mg	1.1
Nono	Day 1	0.018 mg	1.1
		0.054 mg	1.2
		0.162 mg	1.1
	Day 3	0.018 mg	1.0
		0.054 mg	-1.0
		0.162 mg	-1.1
	Day 28	0.018 mg	1.0
		0.054 mg	-1.1
		0.162 mg	-1.1

SP4. Differentially expressed genes (fold-change > 1.5 and FDR p-value < 0.1) for at least one condition in C57/BL6 mouse liver following intratracheal instillation with Printex 90 CBNPs, relative to controls.

			Day 1		Day 3		Day 28	
Gene Name	**Genbank**	**Gene Description**	**FDR p-value**	**Foldchange**	**FDR p-value**	**Foldchange**	**FDR p-value**	**Foldchange**
1500041J02Rik	NM_026424	Mus musculus RIKEN cDNA 1500041J02 gene (1500041J02Rik), transcript variant 2, mRNA [NM_026424]	0.65	1.3	0.97	1.1	0.05	2.1
1700003O08Rik	AK005653	Mus musculus adult male testis cDNA, RIKEN full-length enriched library, clone:1700003O08 product:unclassifiable, full insert sequence. [AK005653]	0.85	1.1	0.99	1.0	0.07	1.7
1810021J13Rik	NM_025464	Mus musculus RIKEN cDNA 1810021J13 gene (1810021J13Rik), mRNA [NM_025464]	0.00	-1.6	0.99	-1.0	0.82	-1.1
2810474O19Rik	NM_026054	Mus musculus RIKEN cDNA 2810474O19 gene (2810474O19Rik), mRNA [NM_026054]	0.02	1.6	0.92	1.1	0.98	1.0
3300001A09Rik	NM_0010813	Mus musculus RIKEN cDNA 3300001A09 gene, mRNA (cDNA clone MGC:48200 IMAGE:1515262), complete cds. [BC039571]	0.97	-1.0	0.99	1.0	0.05	-2.0
4633401B06Rik	AK014609	Mus musculus 0 day neonate skin cDNA, RIKEN full-length enriched library, clone:4633401B06 product:unclassifiable, full insert sequence. [AK014609]	0.04	1.7	0.93	1.1	0.54	1.3
4833442J19Rik	NM_177101	Mus musculus RIKEN cDNA 4833442J19 gene (4833442J19Rik), mRNA [NM_177101]	0.00	2.2	0.97	-1.1	0.65	1.3
4931406C07Rik	NM_133732	Mus musculus RIKEN cDNA 4931406C07 gene (4931406C07Rik), mRNA [NM_133732]	0.08	1.6	1.00	-1.0	0.49	1.3
Abcg8	NM_026180	Mus musculus ATP-binding cassette, sub-family G (WHITE), member 8 (Abcg8), mRNA [NM_026180]	0.98	-1.0	0.92	1.4	0.07	2.3
Adora1	NM_0010085	Mus musculus adenosine A1 receptor (Adora1), transcript variant 1, mRNA [NM_001008533]	0.82	1.1	0.99	1.0	0.05	1.7
AK051522	AK051522	Mus musculus 12 days embryo spinal ganglion cDNA, RIKEN full-length enriched library, clone:D130054J23 product:unclassifiable, full insert sequence. [AK051522]	0.87	1.2	0.00	3.2	0.90	-1.2
Aldh1a1	NM_013467	Mus musculus aldehyde dehydrogenase family 1, subfamily A1 (Aldh1a1), mRNA [NM_013467]	0.00	1.8	0.96	-1.1	1.00	-1.0
Aldoc	NM_009657	Mus musculus aldolase 3, C isoform (Aldoc), mRNA [NM_009657]	0.02	1.5	0.96	1.1	0.85	1.1
Bmper	NM_028472	Mus musculus BMP-binding endothelial regulator (Bmper), mRNA [NM_028472]	0.00	1.5	0.97	1.1	0.99	-1.0
CJ042244	CJ042244	CJ042244 RIKEN full-length enriched mouse cDNA library, C57BL [CJ042244]	0.00	2.0	0.96	1.1	0.78	1.2
Cyp39a1	NM_018887	Mus musculus cytochrome P450, family 39, subfamily a, polypeptide 1 (Cyp39a1), mRNA [NM_018887]	0.72	1.2	0.97	-1.1	0.07	1.6
Cyp4a12	NM_177406	Mus musculus cytochrome P450, family 4, subfamily a, polypeptide 12 (Cyp4a12), mRNA [NM_177406]	0.03	1.6	0.97	1.1	0.98	1.0
Cyp51	NM_020010	Mus musculus cytochrome P450, family 51 (Cyp51), mRNA [NM_020010]	0.00	2.0	0.97	1.1	0.62	1.3
Daam1	NM_026102	Mus musculus dishevelled associated activator of morphogenesis 1 (Daam1), transcript variant 1, mRNA [NM_026102]	0.05	1.5	0.96	1.1	0.63	1.2

Dbp	NM_016974	Mus musculus D site albumin promoter binding protein (Dbp), mRNA [NM_016974]	0.80	1.5	0.96	1.3	0.00	4.9
Dhcr7	NM_007856	Mus musculus 7-dehydrocholesterol reductase (Dhcr7), mRNA [NM_007856]	0.08	1.6	0.96	1.1	0.86	1.1
Egfr	AK049452	Mus musculus 7 days embryo whole body cDNA, RIKEN full-length enriched library, clone:C430014G08 product:unclassifiable, full insert sequence. [AK049452]	0.87	1.2	0.00	2.9	0.98	-1.1
Eif4ebp3	NM_201256	Mus musculus eukaryotic translation initiation factor 4E binding protein 3 (Eif4ebp3), mRNA [NM_201256]	0.05	1.8	0.87	1.5	0.43	1.5
ENSMUST0 0000065861	ENSMUST00(	GB|M60359.1|AAA03650.1 testosterone 16a-hydroxylase type c [NP065022]	0.07	1.8	0.99	1.0	0.94	1.1
Erf	NM_010155	Mus musculus Ets2 repressor factor (Erf), mRNA [NM_010155]	0.70	1.2	0.99	-1.0	0.05	1.6
Fdft1	NM_010191	Mus musculus farnesyl diphosphate farnesyl transferase 1 (Fdft1), mRNA [NM_010191]	0.02	1.7	0.96	1.1	0.83	1.2
Fdps	NM_134469	Mus musculus farnesyl diphosphate synthetase (Fdps), mRNA [NM_134469]	0.00	1.8	0.94	1.1	0.73	1.2
Gbp4	NM_018734	Mus musculus guanylate nucleotide binding protein 4 (Gbp4), mRNA [NM_018734]	0.09	-1.6	0.99	1.0	0.61	-1.3
Gm129	NM_0010333(	Mus musculus gene model 129, (NCBI) (Gm129), mRNA [NM_001033302]	0.59	1.6	0.95	-1.2	0.09	2.4
Gne	AK033507	Mus musculus adult male colon cDNA, RIKEN full-length enriched library, clone:9030414E18 product:UDP-N-acetylglucosamine-2-epimerase [AK033507]	0.53	-1.3	0.90	1.3	0.07	1.7
Gsta4	NM_010357	Mus musculus glutathione S-transferase, alpha 4 (Gsta4), mRNA [NM_010357]	0.03	-1.5	0.98	-1.0	0.98	-1.0
Hmgcr	NM_008255	Mus musculus 3-hydroxy-3-methylglutaryl-Coenzyme A reductase (Hmgcr), mRNA [NM_008255]	0.01	2.4	0.99	-1.1	0.16	2.0
Hmgcs1	NM_145942	Mus musculus 3-hydroxy-3-methylglutaryl-Coenzyme A synthase 1 (Hmgcs1), mRNA [NM_145942]	0.06	2.0	0.94	1.2	0.70	1.4
Idi1	NM_177960	Mus musculus isopentenyl-diphosphate delta isomerase (Idi1), transcript variant 2, mRNA [NM_177960]	0.00	2.3	0.94	1.2	0.55	1.5
Ifi27	AK010014	Mus musculus adult male tongue cDNA, RIKEN full-length enriched library, clone:2310061N23 product:similar to ALPHA-INTERFERON INDUCIBLE PROTEIN (FRAGMENT) [Mesocricetus auratus], full insert sequence. [AK010014]	0.02	-1.9	0.98	-1.1	0.71	-1.3
Klf13	NM_021366	Mus musculus Kruppel-like factor 13 (Klf13), mRNA [NM_021366]	0.94	1.1	1.00	1.0	0.07	1.7
Klhl21	NM_0010333	Mus musculus kelch-like 21 (Drosophila) (Klhl21), mRNA [NM_001033352]	0.84	1.1	0.99	-1.0	0.07	1.5
Kras	NM_021284	Mus musculus v-Ki-ras2 Kirsten rat sarcoma viral oncogene homolog (Kras), mRNA [NM_021284]	0.98	1.0	0.94	-1.1	0.05	-1.5
Lcn2	NM_008491	Mus musculus lipocalin 2 (Lcn2), mRNA [NM_008491]	0.00	4.8	0.96	1.2	0.98	1.1
LOC433520	NM_0010248	Mus musculus similar to zinc finger protein 97 (LOC433520), mRNA [NM_001024825]	0.00	1.7	0.97	-1.1	0.95	1.1
LOC638251	XM_914209	PREDICTED: Mus musculus similar to Bile-salt sulfotransferase 1 (Hydroxysteroid sulfotransferase) (ST) (LOC638251), mRNA [XM_914209]	0.00	5.0	0.98	1.1	0.48	2.4

LOC667984	XR_002113	PREDICTED: Mus musculus similar to serine (or cysteine) peptidase inhibitor, clade A, member 3B (LOC667984), mRNA [XR_002113]	0.06	1.9	0.92	1.2	0.60	1.4
Lpin1	NM_015763	Mus musculus lipin 1 (Lpin1), transcript variant 2, mRNA [NM_015763]	0.69	1.6	0.93	1.4	0.07	3.1
Lpin2	AK012110	Mus musculus 10 days embryo whole body cDNA, RIKEN full-length enriched library, clone:2610511G02 product:unclassifiable, full insert sequence. [AK012110]	0.45	1.4	0.96	1.1	0.05	1.9
Lpin2	NM_022882	Mus musculus lipin 2 (Lpin2), mRNA [NM_022882]	0.35	1.4	0.91	1.2	0.00	1.8
Lss	NM_146006	Mus musculus lanosterol synthase (Lss), mRNA [NM_146006]	0.00	2.6	0.93	1.2	0.72	1.3
Lss	AK147680	Mus musculus adult male brain UNDEFINED_CELL_LINE cDNA, RIKEN full-length enriched library, clone:M5C1106O04 product:lanosterol synthase, full insert sequence [AK147680]	0.00	2.2	0.94	-1.2	0.64	1.4
Miox	AF197127	Mus musculus unknown mRNA. [AF197127]	0.08	1.7	0.97	-1.1	0.98	1.0
Mvk	NM_023556	Mus musculus mevalonate kinase (Mvk), mRNA [NM_023556]	0.00	1.9	0.92	1.2	0.72	1.2
Myc	NM_010849	Mus musculus myelocytomatosis oncogene (Myc), mRNA [NM_010849]	0.03	2.0	0.85	1.6	0.64	-1.4
Myom3	XM_144099	PREDICTED: Mus musculus myomesin family, member 3 (Myom3), mRNA [XM_144099]	0.07	2.0	0.98	1.1	0.90	1.2
Nr1d2	NM_011584	Mus musculus nuclear receptor subfamily 1, group D, member 2 (Nr1d2), mRNA [NM_011584]	0.69	1.4	0.95	1.2	0.10	2.2
Onecut1	BC023444	Mus musculus one cut domain, family member 1, mRNA (cDNA clone MGC:32491 IMAGE:5053834), complete cds. [BC023444]	0.27	1.9	0.91	1.5	0.10	-2.4
Pes1	NM_022889	Mus musculus pescadillo homolog 1, containing BRCT domain (zebrafish) (Pes1), mRNA [NM_022889]	0.03	-1.5	1.00	-1.0	0.27	-1.4
Prss23	NM_029614	Mus musculus protease, serine, 23 (Prss23), mRNA [NM_029614]	0.09	-1.6	0.97	-1.1	0.93	-1.1
Ptp4a1	NM_011200	Mus musculus adult male medulla oblongata cDNA, RIKEN full-length enriched library, clone:6330521E18 product:protein tyrosine phosphatase 4a1, full insert sequence. [AK078120]	0.65	1.2	0.97	1.1	0.07	1.6
Rbm3	BC106176	Mus musculus RNA binding motif protein 3, mRNA (cDNA clone MGC:118410 IMAGE:30146829), complete cds. [BC106176]	0.00	1.9	0.95	-1.1	0.94	1.1
Saa3	NM_011315	Mus musculus serum amyloid A 3 (Saa3), mRNA [NM_011315]	0.00	4.2	1.00	1.0	1.00	-1.0
Sc4mol	NM_025436	Mus musculus sterol-C4-methyl oxidase-like (Sc4mol), mRNA [NM_025436]	0.00	2.1	0.99	1.0	0.55	1.5
Slc16a6	NM_134038	Mus musculus solute carrier family 16 (monocarboxylic acid transporters), member 6 (Slc16a6), transcript variant 2, mRNA [NM_134038]	0.58	-1.3	0.97	1.1	0.00	-2.0
Slc34a2	NM_011402	Mus musculus solute carrier family 34 (sodium phosphate), member 2 (Slc34a2), mRNA [NM_011402]	0.84	-1.2	0.95	1.1	0.05	-1.9
Slc7a2	NM_007514	Mus musculus solute carrier family 7 (cationic amino acid transporter, y+ system), member 2 (Slc7a2), mRNA [NM_007514]	0.06	-1.7	0.92	1.2	0.21	1.5
Snf1lk	NM_010831	Mus musculus SNF1-like kinase (Snf1lk), mRNA [NM_010831]	0.07	1.7	1.00	-1.0	0.80	-1.2
Sqle	NM_009270	Mus musculus squalene epoxidase (Sqle), mRNA [NM_009270]	0.00	1.9	0.94	1.2	0.87	1.2

Srebf2	NM_033218	Mus musculus sterol regulatory element binding factor 2 (Srebf2), mRNA [NM_033218]	0.05	1.5	0.98	-1.0	0.68	1.2
Stard4	NM_133774	Mus musculus StAR-related lipid transfer (START) domain containing 4 (Stard4), mRNA [NM_133774]	0.00	1.6	0.98	1.0	0.55	1.3
Stmn1	NM_019641	Mus musculus stathmin 1 (Stmn1), mRNA [NM_019641]	0.00	-1.9	1.00	-1.0	0.77	-1.2
Sult1e1	NM_023135	Mus musculus sulfotransferase family 1E, member 1 (Sult1e1), mRNA [NM_023135]	0.05	5.9	0.97	1.2	0.41	3.1
Tbc1d10a	NM_134023	Mus musculus TBC1 domain family, member 10a (Tbc1d10a), mRNA [NM_134023]	0.93	-1.0	0.99	-1.0	0.00	1.5
Tef	NM_153484	Mus musculus thyrotroph embryonic factor (Tef), transcript variant 2, mRNA [NM_153484]	0.49	1.7	0.97	1.1	0.00	2.9
Tef	AK045575	Mus musculus adult male corpora quadrigemina cDNA, RIKEN full-length enriched library, clone:B230212L19 product:thyrotroph embryonic factor, full insert sequence. [AK045575]	0.95	1.1	0.98	1.1	0.07	2.0
Them4	NM_029431	Mus musculus adult male hypothalamus cDNA, RIKEN full-length enriched library, clone:A230091K24 product:hypothetical Thioesterase superfamily containing protein, full insert sequence. [AK138397]	0.85	1.1	0.92	1.2	0.07	1.6
Treh	NM_021481	Mus musculus trehalase (brush-border membrane glycoprotein) (Treh), mRNA [NM_021481]	0.00	1.9	0.75	1.4	0.90	1.1
Trib1	NM_144549	Mus musculus tribbles homolog 1 (Drosophila) (Trib1), mRNA [NM_144549]	0.99	1.0	0.99	1.0	0.05	1.8
Tuba1	NM_011653	Mus musculus tubulin, alpha 1 (Tuba1), mRNA [NM_011653]	0.07	-1.6	0.97	1.1	1.00	-1.0
Txndc11	NM_029582	Mus musculus thioredoxin domain containing 11 (Txndc11), transcript variant 1, mRNA [NM_029582]	0.00	1.5	1.00	-1.0	0.99	-1.0
Ugdh	NM_009466	Mus musculus UDP-glucose dehydrogenase (Ugdh), mRNA [NM_009466]	0.02	1.6	0.92	-1.1	0.91	1.1
Usp18	NM_011909	Mus musculus ubiquitin specific peptidase 18 (Usp18), mRNA [NM_011909]	0.03	-1.7	0.98	1.0	0.70	-1.2
Vim	NM_011701	Mus musculus vimentin (Vim), mRNA [NM_011701]	0.00	-1.7	0.99	1.0	0.97	-1.0
Wnt5b	NM_009525	Mus musculus wingless-related MMTV integration site 5B (Wnt5b), mRNA [NM_009525]	0.09	1.6	0.96	-1.1	0.92	-1.1
Zfp259	NM_011752	Mus musculus CRL-1722 L5178Y-R cDNA, RIKEN full-length enriched library, clone:I730052A17 product:zinc finger protein 259, full insert sequence [AK168061]	0.08	2.3	0.91	1.4	0.63	1.5

SP5. Overall biological functions perturbed in liver (Enrichment scores > 3.0) by intratracheal instillation of C57BL/6 mice with 0.018, 0.054 and 0.162 mg Printex 90 CBNPs relative to controls, using DAVID functional annotation clustering.

Annotation Cluster 1 (Sterol and Terpenoid Biosynthesis)
Enrichment Score: 7.7

Category	Term	Count	%	Fold Enrichment	Benjamini
SP_PIR_KEYWORDS	sterol biosynthesis	9	12.2	101.4	1.83E-12
SP_PIR_KEYWORDS	Steroid biosynthesis	10	13.5	67.6	1.04E-12
SP_PIR_KEYWORDS	Cholesterol biosynthesis	8	10.8	120.2	8.25E-12
GOTERM_BP_FAT	GO:0006694~steroid biosynthetic process	11	14.9	36.3	1.83E-10
GOTERM_BP_FAT	GO:0016126~sterol biosynthetic process	9	12.2	70.3	1.03E-10
GOTERM_BP_FAT	GO:0016125~sterol metabolic process	11	14.9	33.5	1.42E-10
GOTERM_BP_FAT	GO:0008202~steroid metabolic process	13	17.6	18.9	3.70E-10
GOTERM_BP_FAT	GO:0006695~cholesterol biosynthetic process	8	10.8	81.5	4.76E-10
GOTERM_BP_FAT	GO:0008203~cholesterol metabolic process	10	13.5	33.5	1.21E-09
SP_PIR_KEYWORDS	lipid synthesis	10	13.5	27.3	2.79E-09
GOTERM_BP_FAT	GO:0008299~isoprenoid biosynthetic process	7	9.5	74.5	2.76E-08
GOTERM_BP_FAT	GO:0008610~lipid biosynthetic process	13	17.6	10.7	1.44E-07
KEGG_PATHWAY	mmu00100:Steroid biosynthesis	6	8.1	65.3	1.21E-06
GOTERM_BP_FAT	GO:0006720~isoprenoid metabolic process	7	9.5	33.5	3.68E-06
KEGG_PATHWAY	mmu00900:Terpenoid backbone biosynthesis	5	6.8	66.1	2.17E-05
GOTERM_CC_FAT	GO:0005783~endoplasmic reticulum	12	16.2	4.7	1.81E-03
SP_PIR_KEYWORDS	oxidoreductase	11	14.9	5.2	8.49E-04
SP_PIR_KEYWORDS	Isoprene biosynthesis	3	4.1	115.9	5.10E-03
GOTERM_BP_FAT	GO:0055114~oxidation reduction	11	14.9	3.8	2.77E-02
SP_PIR_KEYWORDS	nadp	5	6.8	9.5	2.90E-02
GOTERM_CC_FAT	GO:0005777~peroxisome	3	4.1	9.5	4.01E-01
GOTERM_CC_FAT	GO:0042579~microbody	3	4.1	9.5	4.01E-01
SP_PIR_KEYWORDS	peroxisome	3	4.1	8.5	3.92E-01
SP_PIR_KEYWORDS	magnesium	4	5.4	2.7	6.82E-01

Annotation Cluster 2 (Cytochrome p450)
Enrichment Score: 2.1

Category	Term	Count	%	Fold Enrichment	Benjamini
SP_PIR_KEYWORDS	endoplasmic reticulum	13	17.6	5.2	1.37E-04
GOTERM_CC_FAT	GO:0005783~endoplasmic reticulum	12	16.2	4.7	1.81E-03
SP_PIR_KEYWORDS	oxidoreductase	11	14.9	5.2	8.49E-04
GOTERM_BP_FAT	GO:0055114~oxidation reduction	11	14.9	3.8	2.77E-02
GOTERM_CC_FAT	GO:0005792~microsome	5	6.8	9.3	7.79E-02
SP_PIR_KEYWORDS	nadp	5	6.8	9.5	2.90E-02
GOTERM_CC_FAT	GO:0042598~vesicular fraction	5	6.8	9.0	5.93E-02
SP_PIR_KEYWORDS	microsome	4	5.4	10.8	8.17E-02

GOTERM_CC_FAT	GO:0005624~membrane fraction	6	8.1	3.9	3.19E-01
GOTERM_CC_FAT	GO:0005626~insoluble fraction	6	8.1	3.7	2.98E-01
SP_PIR_KEYWORDS	iron	5	6.8	4.2	3.26E-01
GOTERM_CC_FAT	GO:0000267~cell fraction	6	8.1	3.3	3.75E-01
INTERPRO	IPR001128:Cytochrome P450	3	4.1	9.1	1.00E+00
INTERPRO	IPR017972:Cytochrome P450, conserved site	3	4.1	8.9	9.87E-01
COG_ONTOLOGY	Secondary metabolites biosynthesis, transport, and catabolism	3	4.1	7.0	1.85E-01
GOTERM_MF_FAT	GO:0005506~iron ion binding	5	6.8	3.5	9.48E-01
SP_PIR_KEYWORDS	Monooxygenase	3	4.1	7.5	4.36E-01
UP_SEQ_FEATURE	metal ion-binding site:Iron (heme axial ligand)	3	4.1	7.2	9.93E-01
SP_PIR_KEYWORDS	heme	3	4.1	5.7	5.37E-01
GOTERM_MF_FAT	GO:0020037~heme binding	3	4.1	5.0	9.71E-01
GOTERM_MF_FAT	GO:0046906~tetrapyrrole binding	3	4.1	4.8	9.63E-01
GOTERM_MF_FAT	GO:0009055~electron carrier activity	3	4.1	3.6	9.68E-01

Annotation Cluster 3 (Cell Movement)

Enrichment Score: 1.4

Category	Term	Count	%	Fold Enrichment	Benjamini
GOTERM_BP_FAT	GO:0051270~regulation of cell motion	4	5.4	8.8	4.57E-01
GOTERM_BP_FAT	GO:0030334~regulation of cell migration	3	4.1	7.6	9.36E-01
GOTERM_BP_FAT	GO:0040012~regulation of locomotion	3	4.1	6.4	9.64E-01

Annotation Cluster 4 (Membrane-Related Signaling)

Enrichment Score: 1.3

Category	Term	Count	%	Fold Enrichment	Benjamini
SP_PIR_KEYWORDS	endoplasmic reticulum	13	17.6	5.2	1.37E-04
GOTERM_CC_FAT	GO:0005783~endoplasmic reticulum	12	16.2	4.7	1.81E-03
SP_PIR_KEYWORDS	membrane	23	31.1	1.1	8.72E-01
UP_SEQ_FEATURE	transmembrane region	14	18.9	0.8	1.00E+00
GOTERM_CC_FAT	GO:0031224~intrinsic to membrane	15	20.3	0.8	1.00E+00
GOTERM_CC_FAT	GO:0016021~integral to membrane	14	18.9	0.8	1.00E+00
SP_PIR_KEYWORDS	transmembrane	14	18.9	0.7	1.00E+00
UP_SEQ_FEATURE	topological domain:Cytoplasmic	6	8.1	0.5	1.00E+00

SP6. Real-time PCR validation of microarray gene expression in lung and liver of C57BL/6 mice, exposed to 0.018, 0.054 and 0.162 mg CBNPs, 1, 3 and 28 days post-exposure. Significant findings ($p < 0.05$) are are denoted by *. Down-regulated genes are denoted by negative values, calculated according to the negative of the fold-change inverse.

Gene	Day	Dose	Foldchange
Saa3	Day 1	0.018 mg	*4.7
Lung		0.054 mg	*37.9
		0.162 mg	*115.9
	Day 3	0.018 mg	*6.9
		0.054 mg	*14.2
		0.162 mg	*32.5
	Day 28	0.018 mg	1.0
		0.054 mg	2.3
		0.162 mg	*38.8
Saa1	Day 1	0.018 mg	1.6
Lung		0.054 mg	*8.4
		0.162 mg	*34.6
	Day 3	0.018 mg	*1.8
		0.054 mg	*2.5
		0.162 mg	*6.1
	Day 28	0.018 mg	-1.1
		0.054 mg	1.0
		0.162 mg	*3.8
Sqle	Day 1	0.018 mg	-1.1
Lung		0.054 mg	*1.4
		0.162 mg	*2.2
	Day 3	0.018 mg	1.3
		0.054 mg	1.4
		0.162 mg	*1.5
	Day 28	0.018 mg	1.3
		0.054 mg	*1.6
		0.162 mg	1.7
Fdps	Day 1	0.018 mg	-1.1
Lung		0.054 mg	-1.1
		0.162 mg	*1.3
	Day 3	0.018 mg	1.2
		0.054 mg	*1.5
		0.162 mg	*1.6
	Day 28	0.018 mg	1.1
		0.054 mg	1.0
		0.162 mg	1.1
Hmgcr	Day 1	0.018 mg	1.0
Liver		0.054 mg	*-1.4
		0.162 mg	*3.2
	Day 3	0.018 mg	-1.4
		0.054 mg	-1.4
		0.162 mg	1.9
	Day 28	0.018 mg	*2.7
		0.054 mg	2.4
		0.162 mg	*3.5

Fdps	Day 1	0.018 mg	-1.1
Liver		0.054 mg	*-1.4
		0.162 mg	*1.8
	Day 3	0.018 mg	-1.3
		0.054 mg	-1.1
		0.162 mg	1.3
	Day 28	0.018 mg	*1.8
		0.054 mg	1.2
		0.162 mg	1.5
Mvd	Day 1	0.018 mg	-1.4
Liver		0.054 mg	-1.7
		0.162 mg	*1.7
	Day 3	0.018 mg	n/a
		0.054 mg	n/a
		0.162 mg	n/a
	Day 28	0.018 mg	1.4
		0.054 mg	*1.6
		0.162 mg	1.5
Sqle	Day 1	0.018 mg	-1.1
Liver		0.054 mg	-1.3
		0.162 mg	*1.7
	Day 3	0.018 mg	n/a
		0.054 mg	n/a
		0.162 mg	n/a
	Day 28	0.018 mg	*1.8
		0.054 mg	1.4
		0.162 mg	*3.2
Dhcr7	Day 1	0.018 mg	-1.1
Liver		0.054 mg	*-1.4
		0.162 mg	*1.6
	Day 3	0.018 mg	-1.3
		0.054 mg	-1.1
		0.162 mg	1.2
	Day 28	0.018 mg	*1.6
		0.054 mg	1.1
		0.162 mg	1.5

SP7. Significant pathways were established using a rank-based approach. Significant KEGG pathways ($p < 0.05$) for C57BL/6 mice exposed to 18, 54 and 162 µg Printex 90 and sacrificed 1, 3 and 28 days post-exposure relative to controls are presented. Percentage of significant probes, p-value and FDR-adjusted p-value are also presented.

Pathway Name	Pathway ID	# Probes	p-value	FDR p-value	% of Significant Probes within Pathway
Day 1, 18 µg					
Porphyrin and chlorophyll metabolism	860	48	0.0087	0.5407	4.2%
RIG-I-like receptor signaling pathway	4622	115	0.0238	0.5407	10.4%
Small cell lung cancer	5222	179	0.0260	0.5407	15.1%
Bile acid biosynthesis	120	18	0.0303	0.5407	5.6%
Limonene and pinene degradation	903	21	0.0390	0.5407	4.8%
Retinol metabolism	830	92	0.0411	0.5407	13.0%
Glycerophospholipid metabolism	564	112	0.0433	0.5407	11.6%
Apoptosis	4210	167	0.0433	0.5407	10.2%
NOD-like receptor signaling pathway	4621	100	0.0455	0.5407	11.0%
SNARE interactions in vesicular transport	4130	78	0.0476	0.5407	12.8%
mTOR signaling pathway	4150	125	0.0498	0.5407	15.2%
Adipocytokine signaling pathway	4920	117	0.0498	0.5407	13.7%
Day 1, 54 µg					
Renin-angiotensin system	4621	100	0.0108	0.2624	19.0%
NOD-like receptor signaling pathway	4623	84	0.0108	0.2624	17.9%
Bile acid biosynthesis	120	18	0.0108	0.2624	11.1%
Type II diabetes mellitus	4950	39	0.0108	0.2624	10.3%
Toll-like receptor signaling pathway	4622	115	0.0130	0.2624	15.7%
Cytokine-cytokine receptor interaction	4062	330	0.0173	0.2624	14.8%
Methane metabolism	680	15	0.0173	0.2624	13.3%
Synthesis and degradation of ketone bodies	72	16	0.0195	0.2624	31.3%
Calcium signaling pathway	4060	355	0.0195	0.2624	13.5%
ABC transporters	3010	147	0.0216	0.2624	23.1%
Gap junction	4612	129	0.0260	0.2624	10.1%
Basal transcription factors	3030	55	0.0281	0.2624	16.4%
Antigen processing and presentation	4620	161	0.0281	0.2624	11.8%
mTOR signaling pathway	4210	167	0.0281	0.2624	7.8%
Tight junction	4610	116	0.0303	0.2624	14.7%
Chronic myeloid leukemia	5222	179	0.0303	0.2624	9.5%
Nucleotide excision repair	3430	35	0.0303	0.2624	8.6%
Heparan sulfate biosynthesis	534	41	0.0368	0.2624	14.6%
Terpenoid biosynthesis	900	28	0.0368	0.2624	14.3%
Regulation of autophagy	4142	217	0.0368	0.2624	11.1%
PPAR signaling pathway	3410	63	0.0368	0.2624	9.5%
Porphyrin and chlorophyll metabolism	860	48	0.0390	0.2624	10.4%
Glutathione metabolism	480	74	0.0455	0.2624	14.9%
Huntington's disease	5200	619	0.0455	0.2624	9.5%
Asthma	5322	151	0.0476	0.2624	13.2%

RIG-I-like receptor signaling pathway	4630	246	0.0476	0.2624	10.6%
Ubiquinone biosynthesis	130	10	0.0476	0.2624	10.0%
Small cell lung cancer	5310	41	0.0476	0.2624	7.3%
Parkinson's disease - Reference pathway	5016	284	0.0498	0.2624	9.5%
Hedgehog signaling pathway	4360	279	0.0498	0.2624	9.3%
Day 1, 162 µg					
Folate biosynthesis	790	15	0.0022	0.0095	33.3%
Phenylalanine metabolism	360	29	0.0022	0.0095	31.0%
Renin-angiotensin system	4621	100	0.0022	0.0095	29.0%
Bile acid biosynthesis	120	18	0.0022	0.0095	27.8%
Pentose and glucuronate interconversions	40	32	0.0022	0.0095	25.0%
NOD-like receptor signaling pathway	4623	84	0.0022	0.0095	23.8%
Cysteine and methionine metabolism	270	51	0.0022	0.0095	23.5%
Oocyte meiosis	4115	129	0.0022	0.0095	23.3%
Pyrimidine metabolism	240	165	0.0022	0.0095	23.0%
Glutathione metabolism	480	74	0.0022	0.0095	23.0%
Antigen processing and presentation	4620	161	0.0022	0.0095	22.4%
Regulation of autophagy	4142	217	0.0022	0.0095	22.1%
Mismatch repair	3440	50	0.0022	0.0095	22.0%
Nucleotide sugars metabolism	520	72	0.0022	0.0095	20.8%
One carbon pool by folate	670	29	0.0022	0.0095	20.7%
Chronic myeloid leukemia	5222	179	0.0022	0.0095	20.7%
Progesterone-mediated oocyte maturation	4920	117	0.0022	0.0095	19.7%
Tyrosine metabolism	350	46	0.0022	0.0095	19.6%
Glioma	5216	62	0.0022	0.0095	19.4%
Glycosphingolipid biosynthesis - ganglio series	604	26	0.0022	0.0095	19.2%
Cytokine-cytokine receptor interaction	4062	330	0.0022	0.0095	19.1%
Cytosolic DNA-sensing pathway	4640	144	0.0022	0.0095	18.8%
VEGF signaling pathway	4512	169	0.0022	0.0095	18.3%
Calcium signaling pathway	4060	355	0.0022	0.0095	18.3%
Asthma	5322	151	0.0022	0.0095	17.9%
Terpenoid biosynthesis	900	28	0.0022	0.0095	17.9%
Metabolism of xenobiotics by cytochrome P450	980	94	0.0022	0.0095	17.0%
mTOR signaling pathway	4210	167	0.0022	0.0095	16.8%
Galactose metabolism	52	43	0.0022	0.0095	16.3%
Peroxisome	4150	125	0.0022	0.0095	16.0%
Type I diabetes mellitus	4960	75	0.0022	0.0095	16.0%
Huntington's disease	5200	619	0.0022	0.0095	16.0%
Adherens junction	4540	177	0.0022	0.0095	15.3%
Glycolysis / Gluconeogenesis	10	92	0.0022	0.0095	15.2%
Viral myocarditis	4320	46	0.0022	0.0095	15.2%
Dilated cardiomyopathy	1100	1743	0.0022	0.0095	15.0%
Amyotrophic lateral sclerosis (ALS) - Reference pathwa	5020	54	0.0022	0.0095	14.8%
Focal adhesion	4514	270	0.0022	0.0095	14.4%
Bladder cancer	5221	124	0.0022	0.0095	13.7%
Primary immunodeficiency	5412	167	0.0022	0.0095	13.2%
C21-Steroid hormone metabolism	140	61	0.0022	0.0095	13.1%
Toll-like receptor signaling pathway	4622	115	0.0022	0.0095	13.0%
RIG-I-like receptor signaling pathway	4630	246	0.0022	0.0095	13.0%
Pyruvate metabolism	620	67	0.0022	0.0095	11.9%
Porphyrin and chlorophyll metabolism	860	48	0.0022	0.0095	8.3%

Basal transcription factors	3030	55	0.0043	0.0145	34.5%
Biosynthesis of steroids	100	34	0.0043	0.0145	29.4%
Glycosphingolipid biosynthesis - globo series	603	23	0.0043	0.0145	21.7%
Glycosaminoglycan degradation	531	34	0.0043	0.0145	20.6%
Cell cycle	4114	221	0.0043	0.0145	17.6%
Basal cell carcinoma	5219	85	0.0043	0.0145	17.6%
Tight junction	4610	116	0.0043	0.0145	15.5%
N-Glycan degradation	511	26	0.0043	0.0145	15.4%
Fructose and mannose metabolism	51	63	0.0043	0.0145	14.3%
Purine metabolism	230	289	0.0043	0.0145	14.2%
Tryptophan metabolism	380	59	0.0043	0.0145	13.6%
Axon guidance	4510	413	0.0043	0.0145	13.6%
Melanogenesis	4930	101	0.0043	0.0145	12.9%
Type II diabetes mellitus	4950	39	0.0043	0.0145	10.3%
Nucleotide excision repair	3430	35	0.0065	0.0175	31.4%
PPAR signaling pathway	3410	63	0.0065	0.0175	25.4%
Maturity onset diabetes of the young	5010	261	0.0065	0.0175	18.4%
alpha-Linolenic acid metabolism	592	22	0.0065	0.0175	18.2%
Aldosterone-regulated sodium reabsorption	5012	172	0.0065	0.0175	17.4%
Homologous recombination	3450	23	0.0065	0.0175	17.4%
Arrhythmogenic right ventricular cardiomyopathy (ARV	5416	161	0.0065	0.0175	16.1%
Notch signaling pathway	4350	156	0.0065	0.0175	15.4%
T cell receptor signaling pathway	4664	146	0.0065	0.0175	15.1%
Alzheimer's disease	5014	107	0.0065	0.0175	15.0%
Gap junction	4612	129	0.0065	0.0175	14.7%
Regulation of actin cytoskeleton	4912	196	0.0065	0.0175	13.8%
Drug metabolism - cytochrome P450	982	110	0.0065	0.0175	13.6%
Methane metabolism	680	15	0.0065	0.0175	13.3%
Drug metabolism - other enzymes	983	73	0.0087	0.0211	17.8%
Oxidative phosphorylation	190	164	0.0087	0.0211	16.5%
Acute myeloid leukemia	5223	115	0.0087	0.0211	15.7%
Small cell lung cancer	5310	41	0.0087	0.0211	14.6%
Endometrial cancer	5215	202	0.0087	0.0211	12.9%
Hematopoietic cell lineage	4660	229	0.0087	0.0211	12.7%
Non-homologous end-joining	4010	514	0.0087	0.0211	10.7%
Jak-STAT signaling pathway	4650	226	0.0087	0.0211	10.6%
Ubiquinone biosynthesis	130	10	0.0108	0.0237	30.0%
Chondroitin sulfate biosynthesis	532	33	0.0108	0.0237	21.2%
Neuroactive ligand-receptor interaction	4110	241	0.0108	0.0237	15.8%
Alanine, aspartate and glutamate metabolism	250	52	0.0108	0.0237	15.4%
Melanoma	5220	163	0.0108	0.0237	15.3%
Prion diseases	5210	184	0.0108	0.0237	15.2%
Allograft rejection	5340	67	0.0108	0.0237	14.9%
Arginine and proline metabolism	330	76	0.0108	0.0237	14.5%
Vitamin B6 metabolism	750	9	0.0108	0.0237	11.1%
Base excision repair	3420	81	0.0130	0.0267	22.2%
O-Glycan biosynthesis	512	48	0.0130	0.0267	16.7%
Ubiquitin mediated proteolysis	4130	78	0.0130	0.0267	16.7%
Thyroid cancer	5218	153	0.0130	0.0267	12.4%
Cardiac muscle contraction	4270	224	0.0130	0.0267	12.1%
Hedgehog signaling pathway	4360	279	0.0130	0.0267	11.8%
Lysine biosynthesis	300	2	0.0152	0.0293	50.0%

ABC transporters	3010	147	0.0152	0.0293	17.0%
Renal cell carcinoma	5213	121	0.0152	0.0293	14.9%
Olfactory transduction	4810	411	0.0152	0.0293	12.2%
Insulin signaling pathway	4914	177	0.0152	0.0293	11.9%
Natural killer cell mediated cytotoxicity	4662	166	0.0152	0.0293	10.8%
Inositol phosphate metabolism	562	108	0.0173	0.0322	17.6%
Parkinson's disease - Reference pathway	5016	284	0.0173	0.0322	17.3%
MAPK signaling pathway	4012	200	0.0173	0.0322	11.5%
Prostate cancer	5217	94	0.0173	0.0322	10.6%
Glycerophospholipid metabolism	564	112	0.0195	0.0349	19.6%
GnRH signaling pathway	4916	188	0.0195	0.0349	12.2%
ECM-receptor interaction	4520	174	0.0195	0.0349	11.5%
Phosphatidylinositol signaling system	4080	396	0.0195	0.0349	8.1%
Vascular smooth muscle contraction	4310	293	0.0216	0.0377	15.0%
Pancreatic cancer	5214	145	0.0216	0.0377	13.1%
Cell adhesion molecules (CAMs)	4530	267	0.0216	0.0377	12.0%
Histidine metabolism	340	33	0.0238	0.0394	21.2%
Proteasome	3060	51	0.0238	0.0394	17.6%
Chemokine signaling pathway	4070	158	0.0238	0.0394	17.1%
Long-term potentiation	4730	155	0.0238	0.0394	13.5%
B cell receptor signaling pathway	4666	187	0.0238	0.0394	11.8%
SNARE interactions in vesicular transport	4140	52	0.0238	0.0394	7.7%
Riboflavin metabolism	740	28	0.0260	0.0406	14.3%
Fc epsilon RI signaling pathway	4670	212	0.0260	0.0406	13.2%
Propanoate metabolism	640	48	0.0260	0.0406	12.5%
Lysosome	4144	413	0.0260	0.0406	12.1%
Taste transduction	4910	278	0.0260	0.0406	10.8%
Lysine degradation	310	77	0.0260	0.0406	9.1%
Dorso-ventral axis formation	4340	90	0.0260	0.0406	7.8%
Colorectal cancer	5212	163	0.0281	0.0426	14.7%
Circadian rhythm	4722	258	0.0281	0.0426	13.6%
RNA degradation	3020	48	0.0281	0.0426	10.4%
Glycine, serine and threonine metabolism	260	44	0.0281	0.0426	9.1%
Pathways in cancer	5211	150	0.0303	0.0449	14.0%
Selenoamino acid metabolism	450	41	0.0303	0.0449	12.2%
Biosynthesis of secondary metabolites	2010	87	0.0303	0.0449	8.0%
Long-term depression	4742	60	0.0325	0.0477	13.3%
Ribosome	3018	112	0.0346	0.0498	13.4%
TGF-beta signaling pathway	4370	150	0.0346	0.0498	10.0%
Aminoacyl-tRNA biosynthesis	970	83	0.0346	0.0498	9.6%
p53 signaling pathway	4120	315	0.0368	0.0525	11.4%
Heparan sulfate biosynthesis	534	41	0.0390	0.0548	12.2%
ErbB signaling pathway	4020	351	0.0390	0.0548	11.7%
Arachidonic acid metabolism	590	106	0.0433	0.0605	8.5%
Spliceosome	3050	71	0.0455	0.0626	21.1%
Hypertrophic cardiomyopathy (HCM)	5414	202	0.0455	0.0626	11.9%
Intestinal immune network for IgA production	4720	148	0.0476	0.0647	14.2%
Glycosphingolipid biosynthesis - lacto and neolacto ser	601	45	0.0476	0.0647	11.1%
Nicotinate and nicotinamide metabolism	760	43	0.0498	0.0672	7.0%
Day 3, 18 µg					
Synthesis and degradation of ketone bodies	72	16	0.0173	0.9017	12.5%

Glioma	5216	62	0.0216	0.9017	11.3%
Keratan sulfate biosynthesis	533	25	0.0368	0.9017	12.0%
Terpenoid biosynthesis	900	28	0.0411	0.9017	10.7%
O-Mannosyl glycan biosynthesis	514	6	0.0476	0.9017	16.7%
Day 3, 54 µg					
Homologous recombination	3450	23	0.0022	0.0581	26.1%
Glioma	5216	62	0.0022	0.0581	14.5%
Galactose metabolism	52	43	0.0022	0.0581	14.0%
Bladder cancer	5221	124	0.0022	0.0581	10.5%
Primary immunodeficiency	5412	167	0.0022	0.0581	9.0%
Terpenoid biosynthesis	900	28	0.0043	0.0581	17.9%
Glutathione metabolism	480	74	0.0043	0.0581	17.6%
Regulation of autophagy	4142	217	0.0043	0.0581	14.3%
Endometrial cancer	5215	202	0.0043	0.0581	12.9%
Nucleotide sugars metabolism	520	72	0.0043	0.0581	11.1%
Cytosolic DNA-sensing pathway	4640	144	0.0043	0.0581	11.1%
Biosynthesis of steroids	100	34	0.0065	0.0581	32.4%
Folate biosynthesis	790	15	0.0065	0.0581	26.7%
Asthma	5322	151	0.0065	0.0581	19.9%
O-Glycan biosynthesis	512	48	0.0065	0.0581	18.8%
Renin-angiotensin system	4621	100	0.0065	0.0581	18.0%
Pyruvate metabolism	620	67	0.0065	0.0581	17.9%
Calcium signaling pathway	4060	355	0.0065	0.0581	13.8%
Renal cell carcinoma	5213	121	0.0065	0.0581	12.4%
ECM-receptor interaction	4520	174	0.0065	0.0581	11.5%
Adherens junction	4540	177	0.0065	0.0581	10.7%
Parkinson's disease - Reference pathway	5016	284	0.0065	0.0581	10.2%
Porphyrin and chlorophyll metabolism	860	48	0.0087	0.0588	18.8%
Biosynthesis of unsaturated fatty acids	1040	39	0.0087	0.0588	15.4%
One carbon pool by folate	670	29	0.0087	0.0588	13.8%
Bile acid biosynthesis	120	18	0.0087	0.0588	11.1%
Dilated cardiomyopathy	1100	1743	0.0087	0.0588	10.5%
Peroxisome	4150	125	0.0087	0.0588	9.6%
Thyroid cancer	5218	153	0.0087	0.0588	8.5%
Basal transcription factors	3030	55	0.0108	0.0627	18.2%
Viral myocarditis	4320	46	0.0108	0.0627	15.2%
Pancreatic cancer	5214	145	0.0108	0.0627	11.0%
Type I diabetes mellitus	4960	75	0.0108	0.0627	10.7%
Nicotinate and nicotinamide metabolism	760	43	0.0108	0.0627	9.3%
Cysteine and methionine metabolism	270	51	0.0130	0.0646	13.7%
Butanoate metabolism	650	57	0.0130	0.0646	10.5%
Prion diseases	5210	184	0.0130	0.0646	10.3%
Huntington's disease	5200	619	0.0130	0.0646	8.1%
PPAR signaling pathway	3410	63	0.0152	0.0646	17.5%
Riboflavin metabolism	740	28	0.0152	0.0646	14.3%
Phenylalanine metabolism	360	29	0.0152	0.0646	13.8%
Aldosterone-regulated sodium reabsorption	5012	172	0.0152	0.0646	8.7%
RIG-I-like receptor signaling pathway	4630	246	0.0152	0.0646	8.5%
Pantothenate and CoA biosynthesis	770	26	0.0152	0.0646	7.7%
T cell receptor signaling pathway	4664	146	0.0173	0.0646	10.3%
Oocyte meiosis	4115	129	0.0173	0.0646	10.1%

Melanogenesis	4930	101	0.0173	0.0646	9.9%
Cytokine-cytokine receptor interaction	4062	330	0.0173	0.0646	9.4%
Alzheimer's disease	5014	107	0.0173	0.0646	9.3%
Neuroactive ligand-receptor interaction	4110	241	0.0173	0.0646	8.7%
Prostate cancer	5217	94	0.0173	0.0646	8.5%
Pentose and glucuronate interconversions	40	32	0.0195	0.0646	15.6%
Lysine degradation	310	77	0.0195	0.0646	11.7%
Base excision repair	3420	81	0.0195	0.0646	11.1%
Hematopoietic cell lineage	4660	229	0.0195	0.0646	9.6%
MAPK signaling pathway	4012	200	0.0195	0.0646	9.0%
Cell cycle	4114	221	0.0195	0.0646	7.7%
Ubiquitin mediated proteolysis	4130	78	0.0195	0.0646	6.4%
Glycosaminoglycan degradation	531	34	0.0216	0.0646	17.6%
C21-Steroid hormone metabolism	140	61	0.0216	0.0646	13.1%
Tyrosine metabolism	350	46	0.0216	0.0646	13.0%
Propanoate metabolism	640	48	0.0216	0.0646	10.4%
Antigen processing and presentation	4620	161	0.0216	0.0646	9.9%
Insulin signaling pathway	4914	177	0.0216	0.0646	9.0%
Toll-like receptor signaling pathway	4622	115	0.0216	0.0646	7.8%
Tryptophan metabolism	380	59	0.0216	0.0646	6.8%
Glycosphingolipid biosynthesis - globo series	603	23	0.0238	0.0651	17.4%
Arginine and proline metabolism	330	76	0.0238	0.0651	11.8%
mTOR signaling pathway	4210	167	0.0238	0.0651	9.6%
Acute myeloid leukemia	5223	115	0.0238	0.0651	9.6%
Intestinal immune network for IgA production	4720	148	0.0238	0.0651	8.8%
Vascular smooth muscle contraction	4310	293	0.0238	0.0651	8.2%
Progesterone-mediated oocyte maturation	4920	117	0.0260	0.0682	10.3%
Hedgehog signaling pathway	4360	279	0.0260	0.0682	9.0%
RNA polymerase	3022	62	0.0260	0.0682	8.1%
Phenylalanine, tyrosine and tryptophan biosynthesis	400	5	0.0303	0.0702	40.0%
Glyoxylate and dicarboxylate metabolism	630	25	0.0303	0.0702	16.0%
Oxidative phosphorylation	190	164	0.0303	0.0702	11.6%
NOD-like receptor signaling pathway	4623	84	0.0303	0.0702	10.7%
Glycerophospholipid metabolism	564	112	0.0303	0.0702	9.8%
Pentose phosphate pathway	30	45	0.0303	0.0702	8.9%
p53 signaling pathway	4120	315	0.0303	0.0702	8.9%
Regulation of actin cytoskeleton	4912	196	0.0303	0.0702	8.7%
Cell adhesion molecules (CAMs)	4530	267	0.0303	0.0702	8.6%
Olfactory transduction	4810	411	0.0303	0.0702	8.3%
Jak-STAT signaling pathway	4650	226	0.0325	0.0735	9.3%
Ribosome	3018	112	0.0325	0.0735	8.9%
Glycosphingolipid biosynthesis - ganglio series	604	26	0.0346	0.0758	11.5%
Axon guidance	4510	413	0.0346	0.0758	7.7%
Chronic myeloid leukemia	5222	179	0.0346	0.0758	6.7%
Spliceosome	3050	71	0.0368	0.0788	12.7%
Nucleotide excision repair	3430	35	0.0368	0.0788	8.6%
Fructose and mannose metabolism	51	63	0.0390	0.0817	11.1%
Maturity onset diabetes of the young	5010	261	0.0390	0.0817	7.7%
Fatty acid biosynthesis	61	10	0.0411	0.0818	20.0%
Purine metabolism	230	289	0.0411	0.0818	10.7%
Circadian rhythm	4722	258	0.0411	0.0818	9.7%
Lysosome	4144	413	0.0411	0.0818	9.2%

Metabolism of xenobiotics by cytochrome P450	980	94	0.0411	0.0818	8.5%
B cell receptor signaling pathway	4666	187	0.0455	0.0895	6.4%
Fc epsilon RI signaling pathway	4670	212	0.0476	0.0902	9.4%
Natural killer cell mediated cytotoxicity	4662	166	0.0476	0.0902	8.4%
Non-homologous end-joining	4010	514	0.0476	0.0902	7.4%
Keratan sulfate biosynthesis	533	25	0.0476	0.0902	4.0%
GnRH signaling pathway	4916	188	0.0498	0.0925	8.5%
Glycolysis / Gluconeogenesis	10	92	0.0498	0.0925	6.5%
Day 3, 162 µg					
Biosynthesis of steroids	100	34	0.0022	0.0222	47.1%
Terpenoid biosynthesis	900	28	0.0022	0.0222	35.7%
Homologous recombination	3450	23	0.0022	0.0222	30.4%
Ubiquinone biosynthesis	130	10	0.0022	0.0222	30.0%
Asthma	5322	151	0.0022	0.0222	29.1%
Cytosolic DNA-sensing pathway	4640	144	0.0022	0.0222	22.2%
Amyotrophic lateral sclerosis (ALS) - Reference pathwa	5020	54	0.0022	0.0222	20.4%
Folate biosynthesis	790	15	0.0022	0.0222	20.0%
Antigen processing and presentation	4620	161	0.0022	0.0222	17.4%
Regulation of autophagy	4142	217	0.0022	0.0222	17.1%
Primary immunodeficiency	5412	167	0.0022	0.0222	16.8%
Glioma	5216	62	0.0022	0.0222	16.1%
Insulin signaling pathway	4914	177	0.0022	0.0222	12.4%
Peroxisome	4150	125	0.0022	0.0222	12.0%
C21-Steroid hormone metabolism	140	61	0.0022	0.0222	9.8%
Basal transcription factors	3030	55	0.0043	0.0222	21.8%
Glutathione metabolism	480	74	0.0043	0.0222	21.6%
Renin-angiotensin system	4621	100	0.0043	0.0222	21.0%
NOD-like receptor signaling pathway	4623	84	0.0043	0.0222	19.0%
Synthesis and degradation of ketone bodies	72	16	0.0043	0.0222	18.8%
alpha-Linolenic acid metabolism	592	22	0.0043	0.0222	18.2%
Oocyte meiosis	4115	129	0.0043	0.0222	17.8%
Calcium signaling pathway	4060	355	0.0043	0.0222	16.6%
Maturity onset diabetes of the young	5010	261	0.0043	0.0222	16.1%
Type I diabetes mellitus	4960	75	0.0043	0.0222	16.0%
PPAR signaling pathway	3410	63	0.0043	0.0222	14.3%
Neuroactive ligand-receptor interaction	4110	241	0.0043	0.0222	14.1%
Hematopoietic cell lineage	4660	229	0.0043	0.0222	14.0%
Galactose metabolism	52	43	0.0043	0.0222	14.0%
Bladder cancer	5221	124	0.0043	0.0222	13.7%
Cytokine-cytokine receptor interaction	4062	330	0.0043	0.0222	13.0%
B cell receptor signaling pathway	4666	187	0.0043	0.0222	12.8%
Cell cycle	4114	221	0.0043	0.0222	11.8%
Jak-STAT signaling pathway	4650	226	0.0043	0.0222	11.5%
Bile acid biosynthesis	120	18	0.0043	0.0222	11.1%
Butanoate metabolism	650	57	0.0043	0.0222	8.8%
Pantothenate and CoA biosynthesis	770	26	0.0043	0.0222	3.8%
O-Mannosyl glycan biosynthesis	514	6	0.0065	0.0222	33.3%
Pentose and glucuronate interconversions	40	32	0.0065	0.0222	21.9%
Glycosphingolipid biosynthesis - globo series	603	23	0.0065	0.0222	21.7%
Oxidative phosphorylation	190	164	0.0065	0.0222	20.1%
Mismatch repair	3440	50	0.0065	0.0222	18.0%

Cysteine and methionine metabolism	270	51	0.0065	0.0222	17.6%
Parkinson's disease - Reference pathway	5016	284	0.0065	0.0222	17.6%
Aldosterone-regulated sodium reabsorption	5012	172	0.0065	0.0222	17.4%
Toll-like receptor signaling pathway	4622	115	0.0065	0.0222	16.5%
Pyruvate metabolism	620	67	0.0065	0.0222	16.4%
Viral myocarditis	4320	46	0.0065	0.0222	15.2%
Nucleotide excision repair	3430	35	0.0065	0.0222	14.3%
Adherens junction	4540	177	0.0065	0.0222	13.6%
Nucleotide sugars metabolism	520	72	0.0065	0.0222	12.5%
Dilated cardiomyopathy	1100	1743	0.0065	0.0222	12.4%
Valine, leucine and isoleucine degradation	280	74	0.0065	0.0222	12.2%
Progesterone-mediated oocyte maturation	4920	117	0.0065	0.0222	12.0%
Chronic myeloid leukemia	5222	179	0.0065	0.0222	11.7%
Purine metabolism	230	289	0.0065	0.0222	10.4%
Pyrimidine metabolism	240	165	0.0065	0.0222	10.3%
Fatty acid biosynthesis	61	10	0.0087	0.0222	30.0%
O-Glycan biosynthesis	512	48	0.0087	0.0222	16.7%
Fructose and mannose metabolism	51	63	0.0087	0.0222	14.3%
Riboflavin metabolism	740	28	0.0087	0.0222	14.3%
VEGF signaling pathway	4512	169	0.0087	0.0222	14.2%
Endometrial cancer	5215	202	0.0087	0.0222	13.4%
Pancreatic cancer	5214	145	0.0087	0.0222	13.1%
Basal cell carcinoma	5219	85	0.0087	0.0222	12.9%
RIG-I-like receptor signaling pathway	4630	246	0.0087	0.0222	12.6%
Base excision repair	3420	81	0.0087	0.0222	12.3%
Tryptophan metabolism	380	59	0.0087	0.0222	11.9%
Prostate cancer	5217	94	0.0087	0.0222	11.7%
Huntington's disease	5200	619	0.0087	0.0222	11.5%
Thyroid cancer	5218	153	0.0087	0.0222	11.1%
Lysine degradation	310	77	0.0087	0.0222	10.4%
One carbon pool by folate	670	29	0.0087	0.0222	10.3%
Biosynthesis of secondary metabolites	2010	87	0.0087	0.0222	10.3%
MAPK signaling pathway	4012	200	0.0087	0.0222	10.0%
Nicotinate and nicotinamide metabolism	760	43	0.0087	0.0222	9.3%
Propanoate metabolism	640	48	0.0087	0.0222	8.3%
Porphyrin and chlorophyll metabolism	860	48	0.0108	0.0245	16.7%
Biosynthesis of unsaturated fatty acids	1040	39	0.0108	0.0245	15.4%
Prion diseases	5210	184	0.0108	0.0245	14.1%
Renal cell carcinoma	5213	121	0.0108	0.0245	14.0%
Natural killer cell mediated cytotoxicity	4662	166	0.0108	0.0245	13.3%
Fc epsilon RI signaling pathway	4670	212	0.0108	0.0245	13.2%
Arginine and proline metabolism	330	76	0.0108	0.0245	13.2%
Olfactory transduction	4810	411	0.0108	0.0245	12.7%
Alzheimer's disease	5014	107	0.0108	0.0245	12.1%
Non-homologous end-joining	4010	514	0.0108	0.0245	10.7%
Vitamin B6 metabolism	750	9	0.0130	0.0275	22.2%
Glyoxylate and dicarboxylate metabolism	630	25	0.0130	0.0275	20.0%
Tight junction	4610	116	0.0130	0.0275	12.9%
Chemokine signaling pathway	4070	158	0.0130	0.0275	12.7%
Circadian rhythm	4722	258	0.0130	0.0275	10.1%
Tyrosine metabolism	350	46	0.0130	0.0275	8.7%
Allograft rejection	5340	67	0.0152	0.0284	17.9%

Glycerophospholipid metabolism	564	112	0.0152	0.0284	14.3%
Graft-versus-host disease	5410	176	0.0152	0.0284	14.2%
Focal adhesion	4514	270	0.0152	0.0284	13.7%
Hypertrophic cardiomyopathy (HCM)	5414	202	0.0152	0.0284	13.4%
Melanogenesis	4930	101	0.0152	0.0284	11.9%
Glycosphingolipid biosynthesis - lacto and neolacto ser	601	45	0.0152	0.0284	11.1%
mTOR signaling pathway	4210	167	0.0152	0.0284	10.8%
Phenylalanine metabolism	360	29	0.0152	0.0284	10.3%
Axon guidance	4510	413	0.0152	0.0284	10.2%
Wnt signaling pathway	4330	73	0.0152	0.0284	9.6%
Pentose phosphate pathway	30	45	0.0152	0.0284	6.7%
Metabolism of xenobiotics by cytochrome P450	980	94	0.0173	0.0302	14.9%
T cell receptor signaling pathway	4664	146	0.0173	0.0302	14.4%
Ether lipid metabolism	565	52	0.0173	0.0302	13.5%
Notch signaling pathway	4350	156	0.0173	0.0302	11.5%
Leukocyte transendothelial migration	4710	26	0.0173	0.0302	11.5%
Taste transduction	4910	278	0.0173	0.0302	11.5%
Protein export	3320	115	0.0173	0.0302	10.4%
Regulation of actin cytoskeleton	4912	196	0.0173	0.0302	9.7%
Cell adhesion molecules (CAMs)	4530	267	0.0195	0.0331	12.0%
Vascular smooth muscle contraction	4310	293	0.0195	0.0331	10.2%
ECM-receptor interaction	4520	174	0.0195	0.0331	8.6%
Acute myeloid leukemia	5223	115	0.0216	0.0358	13.0%
Hedgehog signaling pathway	4360	279	0.0216	0.0358	9.0%
Ribosome	3018	112	0.0216	0.0358	6.3%
Complement and coagulation cascades	4614	31	0.0238	0.0388	12.9%
Glycolysis / Gluconeogenesis	10	92	0.0238	0.0388	6.5%
Lysosome	4144	413	0.0260	0.0409	11.6%
Phosphatidylinositol signaling system	4080	396	0.0260	0.0409	9.8%
Long-term potentiation	4730	155	0.0260	0.0409	9.0%
Keratan sulfate biosynthesis	533	25	0.0260	0.0409	4.0%
Melanoma	5220	163	0.0281	0.0436	10.4%
Arachidonic acid metabolism	590	106	0.0281	0.0436	7.5%
Thiamine metabolism	730	13	0.0303	0.0463	15.4%
ErbB signaling pathway	4020	351	0.0303	0.0463	10.8%
Phenylalanine, tyrosine and tryptophan biosynthesis	400	5	0.0325	0.0488	20.0%
TGF-beta signaling pathway	4370	150	0.0325	0.0488	10.0%
Gap junction	4612	129	0.0346	0.0502	16.3%
Fc gamma R-mediated phagocytosis	4672	75	0.0346	0.0502	13.3%
Arrhythmogenic right ventricular cardiomyopathy (ARV	5416	161	0.0346	0.0502	12.4%
Inositol phosphate metabolism	562	108	0.0346	0.0502	12.0%
Cardiac muscle contraction	4270	224	0.0346	0.0502	9.4%
GnRH signaling pathway	4916	188	0.0411	0.0591	8.0%
Glycerolipid metabolism	561	79	0.0433	0.0614	11.4%
Endocytosis	4146	131	0.0433	0.0614	9.2%
Small cell lung cancer	5310	41	0.0455	0.0631	14.6%
Dorso-ventral axis formation	4340	90	0.0455	0.0631	8.9%
Intestinal immune network for IgA production	4720	148	0.0455	0.0631	8.1%
Colorectal cancer	5212	163	0.0498	0.0676	10.4%
p53 signaling pathway	4120	315	0.0498	0.0676	8.9%
Starch and sucrose metabolism	500	59	0.0498	0.0676	6.8%

Day 28, 18 µg					
Biosynthesis of unsaturated fatty acids	1040	39	0.0043	0.4797	7.7%
Apoptosis	4260	117	0.0108	0.4797	21.4%
Graft-versus-host disease	5410	176	0.0216	0.4797	12.5%
Protein export	3320	115	0.0238	0.4797	12.2%
Hypertrophic cardiomyopathy (HCM)	5414	202	0.0238	0.4797	10.4%
Pentose phosphate pathway	30	45	0.0260	0.4797	15.6%
Phenylalanine, tyrosine and tryptophan biosynthesis	400	5	0.0281	0.4797	0.0%
Fructose and mannose metabolism	51	63	0.0325	0.4797	14.3%
Riboflavin metabolism	740	28	0.0346	0.4797	14.3%
C21-Steroid hormone metabolism	140	61	0.0368	0.4797	9.8%
Biosynthesis of secondary metabolites	2010	87	0.0411	0.4797	10.3%
Day 28, 54 µg					
Apoptosis	4260	117	0.0079	0.5508	15.4%
Cyanoamino acid metabolism	460	9	0.0159	0.5508	22.2%
Histidine metabolism	340	33	0.0159	0.5508	15.2%
Riboflavin metabolism	740	28	0.0317	0.5508	14.3%
Type I diabetes mellitus	4960	75	0.0397	0.5508	12.0%
Arginine and proline metabolism	330	76	0.0397	0.5508	9.2%
Hypertrophic cardiomyopathy (HCM)	5414	202	0.0397	0.5508	8.4%
Bile acid biosynthesis	120	18	0.0476	0.5508	16.7%
Taurine and hypotaurine metabolism	430	16	0.0476	0.5508	12.5%
Nucleotide sugars metabolism	520	72	0.0476	0.5508	12.5%
Day 28, 162 µg					
Riboflavin metabolism	740	28	0.0079	0.0411	25.0%
Glycosphingolipid biosynthesis - ganglio series	604	26	0.0079	0.0411	23.1%
Fructose and mannose metabolism	51	63	0.0079	0.0411	20.6%
NOD-like receptor signaling pathway	4623	84	0.0079	0.0411	19.0%
Glutathione metabolism	480	74	0.0079	0.0411	18.9%
Regulation of autophagy	4142	217	0.0079	0.0411	18.0%
Calcium signaling pathway	4060	355	0.0079	0.0411	17.7%
Renin-angiotensin system	4621	100	0.0079	0.0411	17.0%
Cytokine-cytokine receptor interaction	4062	330	0.0079	0.0411	17.0%
Tryptophan metabolism	380	59	0.0079	0.0411	16.9%
Colorectal cancer	5212	163	0.0079	0.0411	16.6%
Natural killer cell mediated cytotoxicity	4662	166	0.0079	0.0411	16.3%
Fc epsilon RI signaling pathway	4670	212	0.0079	0.0411	16.0%
Fc gamma R-mediated phagocytosis	4672	75	0.0079	0.0411	16.0%
Cytosolic DNA-sensing pathway	4640	144	0.0079	0.0411	16.0%
Jak-STAT signaling pathway	4650	226	0.0079	0.0411	15.9%
Asthma	5322	151	0.0079	0.0411	15.9%
Arginine and proline metabolism	330	76	0.0079	0.0411	15.8%
Cysteine and methionine metabolism	270	51	0.0079	0.0411	15.7%
Protein export	3320	115	0.0079	0.0411	15.7%
Chronic myeloid leukemia	5222	179	0.0079	0.0411	15.6%
Antigen processing and presentation	4620	161	0.0079	0.0411	15.5%
ECM-receptor interaction	4520	174	0.0079	0.0411	15.5%
B cell receptor signaling pathway	4666	187	0.0079	0.0411	15.5%
Thiamine metabolism	730	13	0.0079	0.0411	15.4%
Systemic lupus erythematosus	5332	78	0.0079	0.0411	15.4%

Toll-like receptor signaling pathway	4622	115	0.0079	0.0411	14.8%
Nucleotide sugars metabolism	520	72	0.0079	0.0411	13.9%
Arrhythmogenic right ventricular cardiomyopathy (ARV	5416	161	0.0079	0.0411	13.0%
T cell receptor signaling pathway	4664	146	0.0079	0.0411	13.0%
O-Glycan biosynthesis	512	48	0.0079	0.0411	12.5%
Focal adhesion	4514	270	0.0079	0.0411	12.2%
mTOR signaling pathway	4210	167	0.0079	0.0411	12.0%
Melanogenesis	4930	101	0.0079	0.0411	11.9%
RIG-I-like receptor signaling pathway	4630	246	0.0079	0.0411	11.8%
Ether lipid metabolism	565	52	0.0079	0.0411	11.5%
Hematopoietic cell lineage	4660	229	0.0079	0.0411	11.4%
Porphyrin and chlorophyll metabolism	860	48	0.0079	0.0411	8.3%
Vitamin B6 metabolism	750	9	0.0159	0.0579	22.2%
Selenoamino acid metabolism	450	41	0.0159	0.0579	19.5%
Small cell lung cancer	5310	41	0.0159	0.0579	19.5%
Taurine and hypotaurine metabolism	430	16	0.0159	0.0579	18.8%
Pentose phosphate pathway	30	45	0.0159	0.0579	17.8%
Autoimmune thyroid disease	5330	81	0.0159	0.0579	16.0%
Glycosphingolipid biosynthesis - lacto and neolacto ser	601	45	0.0159	0.0579	15.6%
Tight junction	4610	116	0.0159	0.0579	15.5%
Tyrosine metabolism	350	46	0.0159	0.0579	15.2%
Adipocytokine signaling pathway	4940	89	0.0159	0.0579	14.6%
Type I diabetes mellitus	4960	75	0.0159	0.0579	13.3%
Non-small cell lung cancer	5320	94	0.0159	0.0579	12.8%
Pantothenate and CoA biosynthesis	770	26	0.0159	0.0579	11.5%
Taste transduction	4910	278	0.0159	0.0579	10.8%
Phenylalanine metabolism	360	29	0.0159	0.0579	10.3%
Hedgehog signaling pathway	4360	279	0.0159	0.0579	9.7%
Fatty acid biosynthesis	61	10	0.0238	0.0609	20.0%
Oocyte meiosis	4115	129	0.0238	0.0609	19.4%
Glioma	5216	62	0.0238	0.0609	17.7%
Prion diseases	5210	184	0.0238	0.0609	15.2%
Starch and sucrose metabolism	500	59	0.0238	0.0609	13.6%
Huntington's disease	5200	619	0.0238	0.0609	13.2%
Cell adhesion molecules (CAMs)	4530	267	0.0238	0.0609	13.1%
Glycosphingolipid biosynthesis - globo series	603	23	0.0238	0.0609	13.0%
Circadian rhythm	4722	258	0.0238	0.0609	12.8%
Graft-versus-host disease	5410	176	0.0238	0.0609	12.5%
Olfactory transduction	4810	411	0.0238	0.0609	12.4%
Hypertrophic cardiomyopathy (HCM)	5414	202	0.0238	0.0609	12.4%
Arachidonic acid metabolism	590	106	0.0238	0.0609	12.3%
Lysosome	4144	413	0.0238	0.0609	12.1%
Axon guidance	4510	413	0.0238	0.0609	12.1%
Primary immunodeficiency	5412	167	0.0238	0.0609	12.0%
Non-homologous end-joining	4010	514	0.0238	0.0609	11.9%
Glycine, serine and threonine metabolism	260	44	0.0238	0.0609	11.4%
Dilated cardiomyopathy	1100	1743	0.0238	0.0609	10.3%
Heparan sulfate biosynthesis	534	41	0.0238	0.0609	9.8%
TGF-beta signaling pathway	4370	150	0.0238	0.0609	9.3%
Nicotinate and nicotinamide metabolism	760	43	0.0238	0.0609	9.3%
beta-Alanine metabolism	410	34	0.0238	0.0609	8.8%
Keratan sulfate biosynthesis	533	25	0.0317	0.0763	20.0%

Limonene and pinene degradation	903	21	0.0317	0.0763	14.3%
Melanoma	5220	163	0.0317	0.0763	11.7%
Endocytosis	4146	131	0.0317	0.0763	10.7%
Nitrogen metabolism	910	30	0.0317	0.0763	6.7%
Renal cell carcinoma	5213	121	0.0397	0.0878	17.4%
Fatty acid metabolism	71	66	0.0397	0.0878	15.2%
Dorso-ventral axis formation	4340	90	0.0397	0.0878	13.3%
Progesterone-mediated oocyte maturation	4920	117	0.0397	0.0878	12.8%
Phosphatidylinositol signaling system	4080	396	0.0397	0.0878	10.9%
One carbon pool by folate	670	29	0.0397	0.0878	10.3%
Allograft rejection	5340	67	0.0397	0.0878	9.0%
Phenylalanine, tyrosine and tryptophan biosynthesis	400	5	0.0476	0.0938	40.0%
Biosynthesis of unsaturated fatty acids	1040	39	0.0476	0.0938	15.4%
Glycerolipid metabolism	561	79	0.0476	0.0938	12.7%
Sphingolipid metabolism	600	72	0.0476	0.0938	12.5%
Gap junction	4612	129	0.0476	0.0938	10.9%
Maturity onset diabetes of the young	5010	261	0.0476	0.0938	10.3%
Ribosome	3018	112	0.0476	0.0938	8.9%
Valine, leucine and isoleucine biosynthesis	290	24	0.0476	0.0938	8.3%
Valine, leucine and isoleucine degradation	280	74	0.0476	0.0938	8.1%
Notch signaling pathway	4350	156	0.0476	0.0938	7.7%
alpha-Linolenic acid metabolism	592	22	0.0476	0.0938	4.5%

SP8. Number of common genes between each disease model and CBNP exposed mice (18, 54 and 162 µg Printex 90 vs. vehicle control). N represents the total number of significant genes for each disease model or CBNP exposure condition. Cut-off of fold-change of >1.5 and p <0.05 was employed.

Mouse Model and Description	Day 1			Day 3			Day 28		
	0.018 mg n=123	**0.054 mg** n=232	**0.162 mg** n=423	**0.018 mg** n=34	**0.054 mg** n=130	**0.162 mg** n=273	**0.018 mg** n=149	**0.054 mg** n=77	**0.162 mg** n=350
Bacterial Infection									
LPS aerosolized[a] n=818	12	49	79	5	23	42	8	8	60
LPS i.p.[a] n=1446	23	53	101	5	24	46	14	12	70
Mycoplasma pulmonis n=1423	18	61	123	10	42	69	35	10	100
Mycobacterium tuberculosis[a] n=1160	8	37	72	8	25	47	26	6	66
Pseudomonas aeruginosa[b] n=815	15	39	60	4	20	28	6	6	41
Th2 Response									
Aspergillus **Extract**[a] n=152	2	2	5	1	4	4	2	3	5
IL-13 overexpression n=695	9	40	86	9	34	49	24	10	80
Nippostrongylus brasiliensis[b] n=612	3	22	48	6	26	40	9	7	49
Ovalbumin[a] **(C57BL/6)** n=1144	10	41	82	10	30	64	23	11	91
Ovalbumin[b] **(BALB/c)** n=461	8	26	42	7	30	47	11	6	59
Lung Injury and Fibrosis									
Bleomycin-induced acute lung injury[a] n=383	4	16	45	2	11	25	9	5	33
Bleomycin-induced fibrosis[a] n=283	4	16	41	5	15	25	3	3	36
Tumor Necrosis Alpha n=966	14	48	88	11	34	63	35	10	80

[a]–C57BL/6
[b]–BALB/c

SP9. Summary of biological functions perturbed for A) genes that were in common between CBNP exposure and each disease model and B) genes that were unique to CBNP.

A)

Model and Function	Enrichment S
Bleomycin-induced acute lung injury Day 1	
Annotation Cluster 1: Glycoprotein	2.63
Annotation Cluster 2: Tissue morphogenesis	2.21
Annotation Cluster 3: Inflamatory response	2.07
Annotation Cluster 4: Extracellular region	1.64
Annotation Cluster 5: EGF-like	1.34
Bleomycin-induced acute lung injury Day 3	
Annotation Cluster 1: Inflammatory response	9.45
Annotation Cluster 2: Glycoprotein	8.55
Annotation Cluster 3: Acute Phase Response	3.39
Annotation Cluster 4: Toll-like response	3.38
Annotation Cluster 5: Chemokine	3.20
Annotation Cluster 6: Cell death	2.57
Annotation Cluster 7: Oxidative stress	2.28
Annotation Cluster 8: Lipocalin	2.17
Annotation Cluster 9: Immune response	1.99
Annotation Cluster 10: Extracellular matrix	1.65
Annotation Cluster 11: Immune/inflammatory response	1.60
Annotation Cluster 12: Hormone stimulus	1.59
Annotation Cluster 13: EGF-like	1.55
Annotation Cluster 14: Coagulation	1.53
Annotation Cluster 15: Cellular homeostasis	1.52
Annotation Cluster 16: Immune response	1.48
Annotation Cluster 17: Carbohydrate binding	1.45
Bleomycin-induced acute lung injury Day 28	
Annotation Cluster 1: Disulfide bond	5.28
Annotation Cluster 2: Immune/inflammatory response	3.14
Annotation Cluster 3: Adaptive immune response	2.99
Annotation Cluster 4: Cytokine/chemokine response	2.81
Annotation Cluster 5: Lysosome	1.84
Bleomycin-induced fibrosis Day 1	
Annotation Cluster 1: Glycoprotein	4.64
Annotation Cluster 2: Cytokine/chemokine response	3.83
Annotation Cluster 3: Epithelial cell proliferation	2.97
Annotation Cluster 4: Cell differentiation	2.68
Annotation Cluster 5: Tissue morphogenesis	2.66
Annotation Cluster 6: Fibronectin	1.69
Bleomycin-induced fibrosis Day 3	
Annotation Cluster 1: Inflammatory response	3.73
Annotation Cluster 2: Glycoprotein	2.42
Annotation Cluster 3: Cell cycle	1.50

Bleomycin-induced fibrosis Day 28	
Annotation Cluster 1: Inflammatory/immune response	2.86
Annotation Cluster 2: Lysosome	2.06
Annotation Cluster 3: Chemotaxis	1.83
Annotation Cluster 4: Carbohydrate binding	1.82
Annotation Cluster 5: Cytokine activity	1.70
IL-13 overexpression Day 1	
Annotation Cluster 1: Inflammatory response	7.63
Annotation Cluster 2: Acute phase response	2.12
Annotation Cluster 3: Carbohydrate binding	1.89
Annotation Cluster 4: Cell fraction	1.57
Annotation Cluster 5: Fibronectin	1.40
IL-13 overexpression Day 3	
Annotation Cluster 1: Disulfide bond	5.54
Annotation Cluster 2: Inflammatory/immune response	4.79
IL-13 overexpression Day 28	
Annotation Cluster 1: Glycoprotein	8.29
Annotation Cluster 2: Plasma membrane	2.89
Annotation Cluster 3: Innate ummune response	2.87
Annotation Cluster 4: Chemotaxis	2.25
Annotation Cluster 5: Phagocytosis/endocytosis	2.20
Annotation Cluster 6: Lysosome	2.11
Annotation Cluster 7: Carbohydrate binding	2.04
Annotation Cluster 8: Immune response	1.75
Annotation Cluster 9: Cell surface	1.75
Annotation Cluster 10: Cell death	1.52
Annotation Cluster 11: Immunoglobin	1.49
Annotation Cluster 12: Leukocyte/lymphocyte activation	1.33
LPS aerosolized Day 1	
Annotation Cluster 1: Inflammatory/immune response	6.97
Annotation Cluster 2: Acute phase response	3.48
Annotation Cluster 3: Response to bacterium	2.30
Annotation Cluster 4: Cell death	1.67
Annotation Cluster 5: Lectin	1.67
Annotation Cluster 6: Cell migration	1.64
Annotation Cluster 7: EGF-like	1.59
LPS aerosolized Day 3	
Annotation Cluster 1: Cytokine/chemokine response	5.98
Annotation Cluster 2: Extracellular space	4.90
LPS aerosolized Day 28	
Annotation Cluster 1: Immune response	6.69
Annotation Cluster 2: Inflammatory/immune response	5.48
Annotation Cluster 3: Chemotaxis	3.40
Annotation Cluster 4: Cell death	2.29
Annotation Cluster 5: Leukocyte/lymphocyte activation	1.78

Annotation Cluster 6: Signal transduction	1.68
Annotation Cluster 7: Extracellular	1.65
LPS i.p. Day 1	
Annotation Cluster 1: Inflammatory response	6.60
Annotation Cluster 2: Acute phase response	3.60
Annotation Cluster 3: Signal transduction inhibition	2.66
Annotation Cluster 4: Cell migration	1.83
Annotation Cluster 5: EGF-like	1.48
Annotation Cluster 6: Lectin	1.47
Annotation Cluster 7: Response to bacterium	1.28
LPS i.p. Day 3	
Annotation Cluster 1: Inflammatory response	3.94
Annotation Cluster 2: G protein signaling	1.86
LPS i.p. Day 28	
Annotation Cluster 1: Inflammatory response	5.45
Annotation Cluster 2: Plasma membrane	3.21
Annotation Cluster 3: Adaptive immune response	2.65
Annotation Cluster 4: Apoptosis	2.52
Annotation Cluster 5: Immune response	2.32
Annotation Cluster 6: Cytokine/chemokine response	2.20
Annotation Cluster 7: Chemotaxis	1.50
***Mycoplasma pulmonis* Day 1**	
Annotation Cluster 1:Inflammatory response	9.56
Annotation Cluster 2: Glycoprotein	7.84
Annotation Cluster 3: Acute phase response	3.50
Annotation Cluster 4: Fibronectin	1.46
***Mycoplasma pulmonis* Day 3**	
Annotation Cluster 1: Inflammatory response	6.07
Annotation Cluster 2: Glycoprotein	4.97
Annotation Cluster 3: Cell cycle	2.74
***Mycoplasma pulmonis* Day 28**	
Annotation Cluster 1: Disulfide bond	11.22
Annotation Cluster 2: Glycoprotein	9.96
Annotation Cluster 3: Plasma membrane	3.84
Annotation Cluster 4: Inflammatory response	2.94
Annotation Cluster 5: Chemotaxis	2.55
Annotation Cluster 6: Leukocyte/lymphocyte activation	2.44
Annotation Cluster 7: Apoptosis	2.21
Annotation Cluster 8: Carbohydrate binding	1.98
Annotation Cluster 9: Lysosome	1.95
***Mycobacterium tuberculosis* Day 1**	
Annotation Cluster 1: Inflammatory response	7.33
Annotation Cluster 2: Acute phase response	2.26
***Mycobacterium tuberculosis* Day 3**	

Annotation Cluster 1: Cytokine/chemokine response	3.96
Annotation Cluster 2: Cell cycle	3.29
***Mycobacterium tuberculosis* Day 28**	
Annotation Cluster 1: Glycoprotein	7.49
Annotation Cluster 2: Plasma membrane	3.63
Annotation Cluster 3: Phagocytosis and adaptive immunity	3.11
Annotation Cluster 4: Cytokine/chemokine activity	2.21
Annotation Cluster 5: Apoptosis	2.18
Annotation Cluster 6: Chemotaxis	1.40
Annotation Cluster 7: Carbohydrate binding	1.36
Annotation Cluster 8: Lysosome	1.34
***Nippostrongylus brasiliensis* Day 1**	
Annotation Cluster 1: Inflammatory response	5.82
Annotation Cluster 2: Glycoprotein	4.55
Annotation Cluster 3: Tissue morphogenesis	1.32
***Nippostrongylus brasiliensis* Day 3**	
Annotation Cluster 1: Inflammatory response	3.00
Annotation Cluster 2: Glycoprotein	2.56
Annotation Cluster 3: Cell cycle	1.49
***Nippostrongylus brasiliensis* Day 28**	
Annotation Cluster 1: Glycoprotein	5.22
Annotation Cluster 2: Cytokine/chemokine response	3.13
Annotation Cluster 3: Phagocytosis/endocytosis	2.75
Annotation Cluster 4: Transmembrane	2.01
Annotation Cluster 5: Lysosome	1.55
Ovalbumin Day 1	
Annotation Cluster 1: Inflammatory/immune response	8.73
Annotation Cluster 2: Acute phase response	2.33
Annotation Cluster 3: Cell differentiation	1.36
Ovalbumin Day 3	
Annotation Cluster 1: Cytokine/chemokine response	3.70
Annotation Cluster 2: Cell cycle	3.65
Annotation Cluster 3: Glycoprotein	2.62
Annotation Cluster 4: Meiosis	1.66
Ovalbumin Day 28	
Annotation Cluster 1: Disulfide bond	8.23
Annotation Cluster 2: Glycoprotein	7.42
Annotation Cluster 3: Plasma membrane	3.32
Annotation Cluster 4: Carbohydrate binding	3.02
Annotation Cluster 5: Phagocytosis/endocytosis	2.90
Annotation Cluster 6: Inflammatory response	2.85
Annotation Cluster 7: Cell adhesion	1.90
Annotation Cluster 8: Apoptosis	1.54
Annotation Cluster 9: Leukocyte/lymphocyte activation	1.36

Ovalbumin Day 1

Annotation Cluster 1: Cytokine/chemokine response	7.36
Annotation Cluster 2: Acute phase response	2.84

Ovalbumin Day 3

Annotation Cluster 1: Cytokine/chemokine response	3.68
Annotation Cluster 2: Cell cycle	3.21

Ovalbumin Day 28

Annotation Cluster 1: Glycoprotein	6.52
Annotation Cluster 2: Transmembrane	3.75
Annotation Cluster 3: Cytokine/chemokine response	3.06
Annotation Cluster 4: Phagocytosis/endocytosis	2.83
Annotation Cluster 5: Lectin	2.17
Annotation Cluster 6: Lysosome	1.36

***Pseudomonas aeruginosa* Day 1**

Annotation Cluster 1: Cytokine/chemokine response	6.89
Annotation Cluster 2: Acute phase response	3.91
Annotation Cluster 3: Cell migration	1.95
Annotation Cluster 4: Cell death	1.72

***Pseudomonas aeruginosa* Day 3**

Annotation Cluster 1: Inflammatory/immune response	4.12

***Pseudomonas aeruginosa* Day 28**

Annotation Cluster 1: Inflammatory/immune response	5.53
Annotation Cluster 2: Disulfide bond	5.43
Annotation Cluster 3: Cytokine production	3.65
Annotation Cluster 4: Immune response	2.54
Annotation Cluster 5: Cytokine/chemokine response	2.53
Annotation Cluster 6: Chemotaxis	1.72
Annotation Cluster 7: Carbohydrate binding	1.68
Annotation Cluster 8: Transmembrane	1.58
Annotation Cluster 9: Cell death	1.53

TNF Day 1

Annotation Cluster 1: Inflammatory response	9.49
Annotation Cluster 2: Response to bacterium	2.46
Annotation Cluster 3: Carbohydrate binding	2.14
Annotation Cluster 4: EGF-like	1.55
Annotation Cluster 5: Lectin	1.40

TNF Day 3

Annotation Cluster 1: Cytokine/chemokine response	4.25
Annotation Cluster 2: Cell cycle	3.99

TNF Day 28

Annotation Cluster 1: Glycoprotein	8.45
Annotation Cluster 2: Transmembrane	3.47
Annotation Cluster 3: Inflammatory/immune response	3.45
Annotation Cluster 4: Chemotaxis	2.70

Annotation Cluster 5: Phagocytosis/endocytosis	2.07
Annotation Cluster 6: Cell surface	2.04
Annotation Cluster 7: Lectin	1.93
Annotation Cluster 8: Adaptive immune response	1.89
Annotation Cluster 9: Immunoglobulin	1.84
Annotation Cluster 10: Lysosome	1.57
Annotation Cluster 11: Apoptosis	1.43

B)

Model and Function	**Enrichment S**
***Aspergillus* Extract Day 1**	
Annotation Cluster 1: Glycoprotein	11.50
Annotation Cluster 2: Cytokine/chemokine response	11.32
Annotation Cluster 3: Acute phase response	3.52
Annotation Cluster 4: Chemokine signaling	3.04
Annotation Cluster 5: Cell communication	2.86
Annotation Cluster 6: Extracellular matrix	2.83
Annotation Cluster 7: Cell death	2.27
Annotation Cluster 8: Hormone stimulus	2.25
Annotation Cluster 9: EGF-like	2.16
Annotation Cluster 10: Carbohydrate binding	2.14
Annotation Cluster 11: Oxidative stress	2.06
Annotation Cluster 12: Adaptive immune response	2.04
Annotation Cluster 13: Lectin	1.94
Annotation Cluster 14: Toll-like response	1.92
Annotation Cluster 15: Immune response	1.89
Annotation Cluster 16: Cell migration	1.53
Annotation Cluster 17: Lipocalin	1.51
Annotation Cluster 18: Homeostatic process	1.44
Annotation Cluster 19: Repeat	1.44
Annotation Cluster 20: Regulation of immune response	1.42
Annotation Cluster 21: Coagulation	1.38
***Aspergillus* Extract Day 3**	
Annotation Cluster 1: Cell cycle	10.05
Annotation Cluster 2: Nucleosome organization	4.42
Annotation Cluster 3: Cytokine/chemokine response	4.30
Annotation Cluster 4: Steroid and terpenoid biosynthesis	3.51
Annotation Cluster 5: Microtubule	2.92
Annotation Cluster 6: Glycoprotein	2.76
Annotation Cluster 7: Cyclin	2.69
Annotation Cluster 8: Regulation of cell cycle	2.20
Annotation Cluster 9: Chromosome segregation	2.14
Annotation Cluster 10: Carbohydrate binding	1.42
Annotation Cluster 11: Meiosis	1.39
Annotation Cluster 12: Protein locolization	1.33
Annotation Cluster 13: Cytoskeleton organization	1.32
Annotation Cluster 14:Protease inhibition	1.31
***Aspergillus* Extract Day 28**	
Annotation Cluster 1: Glycoprotein	16.62

Annotation Cluster 2: Inflammatory response	9.19
Annotation Cluster 3: Plasma membrane	7.78
Annotation Cluster 4: Cell death	4.03
Annotation Cluster 5: Immunoglobulin	3.98
Annotation Cluster 6: Lectin	3.44
Annotation Cluster 7: Adaptive immune response	3.40
Annotation Cluster 8: Cell adhesion	2.94
Annotation Cluster 9: Immune response	2.82
Annotation Cluster 10: Cytokine/chemokine response	2.63
Annotation Cluster 11: Secretion	2.13
Annotation Cluster 12: Toll-like response	1.85
Annotation Cluster 13: Cytokine production	1.82
Annotation Cluster 14: Plasma membrane binding	1.80

Bleomycin-induced acute lung injury Day 1

Annotation Cluster 1: Cytokine/chemokine response	9.45
Annotation Cluster 2: Glycoprotein	8.55
Annotation Cluster 3: Acute Phase Response	3.39
Annotation Cluster 4: Toll-like response	3.38
Annotation Cluster 5: Chemokine Signaling	3.20
Annotation Cluster 6: Cell death	2.57
Annotation Cluster 7: Oxidative stress	2.28
Annotation Cluster 8: Lipocalin	2.17
Annotation Cluster 9: Adaptive Immune Response	1.99
Annotation Cluster 10: Extracellular matrix	1.65
Annotation Cluster 11: Cytokine production	1.60
Annotation Cluster 12: Hormone stimulus	1.59
Annotation Cluster 13: EGF-like	1.55
Annotation Cluster 14: Coagulation	1.53
Annotation Cluster 15: Cellular homeostasis	1.52
Annotation Cluster 16: Immune Response	1.48
Annotation Cluster 17: Carbohydrate binding	1.45

Bleomycin-induced acute lung injury Day 3

Annotation Cluster 1: Cell cycle	9.97
Annotation Cluster 2: Nucleosome assembly	4.38
Annotation Cluster 3: Chemokine	4.26
Annotation Cluster 4: Steroid and terpenoid biosynthesis	3.49
Annotation Cluster 5: Microtubule	2.87
Annotation Cluster 6: Cyclin	2.67
Annotation Cluster 7: Glycoprotein	2.67
Annotation Cluster 8: Regulation of cell cycle	2.18
Annotation Cluster 9: Chromosome segregation	2.11
Annotation Cluster 10: Carbohydrate binding	1.41
Annotation Cluster 11: Meiotic cell cycle	1.38
Annotation Cluster 12: Cytoskeleton organization	1.32
Annotation Cluster 13: Cell cycle	1.31

Bleomycin-induced acute lung injury Day 28

Annotation Cluster 1: Glycoprotein	12.37
Annotation Cluster 2: Plasma Membrane	6.44

Annotation Cluster 3: Immune response	2.70
Annotation Cluster 4: Lectin	2.69
Annotation Cluster 5: Cell death	2.61
Annotation Cluster 6: Immune/inflammatory response	2.60
Annotation Cluster 7: Immunoglobulin	2.60
Annotation Cluster 8: Adaptive immune response	2.30
Annotation Cluster 9: Phagocytosis	1.91
Annotation Cluster 10: Leukocyte activation	1.89
Annotation Cluster 11: Extracellular region	1.75
Annotation Cluster 12: Secretion	1.53

Bleomycin-induced fibrosis Day 1

Annotation Cluster 1: Glycoprotein	8.53
Annotation Cluster 2: Cytokine/chemokine response	6.64
Annotation Cluster 3: Acute phase response	3.55
Annotation Cluster 4: EGF-like	2.11
Annotation Cluster 5: Extracellular matrix	2.07
Annotation Cluster 6: Oxidative stress	1.98
Annotation Cluster 7: Toll-like response	1.85
Annotation Cluster 8: Hormone stimulus	1.72
Annotation Cluster 9: Lipocalin	1.61
Annotation Cluster 10: Carbohydrate binding	1.59
Annotation Cluster 11: Cholesterol metabolism	1.59
Annotation Cluster 12: Repeat	1.58
Annotation Cluster 13: Cell death	1.56
Annotation Cluster 14: Apoptosis	1.46
Annotation Cluster 15: Coagulation	1.43
Annotation Cluster 16: Blood circulation	1.42
Annotation Cluster 17: Cellular homeostasis	1.42
Annotation Cluster 18: Immune response	1.35
Annotation Cluster 19: Lectin	1.34
Annotation Cluster 20: Leukocyte activation	1.31

Bleomycin-induced fibrosis Day 3

Annotation Cluster 1: Cell cycle	8.65
Annotation Cluster 2: Chromatin assembly	4.61
Annotation Cluster 3: Steroid and terpenoid biosynthesis	3.75
Annotation Cluster 4: Microtubule	2.74
Annotation Cluster 5: Regulation of cell cycle	2.11
Annotation Cluster 6: Cyclin	2.01
Annotation Cluster 7: Inflammatory response	1.93
Annotation Cluster 8: Meiosis	1.55
Annotation Cluster 9: Protease inhibition	1.42
Annotation Cluster 10: Nucleotide binding	1.35
Annotation Cluster 11: Cytoskeleton organization	1.31

Bleomycin-induced fibrosis Day 28

Annotation Cluster 1: Glycoprotein	10.74
Annotation Cluster 2: Plasma membrane	6.32
Annotation Cluster 3: Cell death	2.77
Annotation Cluster 4: Adaptive immune response	2.35

Annotation Cluster 5: Inflammatory response	2.34
Annotation Cluster 6: Carbohydrate binding	2.27
Annotation Cluster 7: Immunoglobulin	2.20
Annotation Cluster 8: Leukocyte and lymphocyte activation	1.84
Annotation Cluster 9: Cytokine activity	1.81
Annotation Cluster 10: Response to bacterium	1.68
Annotation Cluster 11: Cell adhesion	1.42
Annotation Cluster 12: Secretion	1.35

IL-13 overexpression Day 1

Annotation Cluster 1: Glycoprotein	7.33
Annotation Cluster 2: Acute Phase Response	4.79
Annotation Cluster 3: Toll-like response	2.62
Annotation Cluster 4: Inflammatory response	2.58
Annotation Cluster 5: Cell death	2.53
Annotation Cluster 6: Extracellular matrix	2.21
Annotation Cluster 7: Carbohydrate binding	2.03
Annotation Cluster 8: Innate immune response	2.02
Annotation Cluster 9: Lipocalin	1.81
Annotation Cluster 10: Immune response	1.78
Annotation Cluster 11: Chemotaxis	1.72
Annotation Cluster 12: Signal transduction	1.70
Annotation Cluster 13: Adaptive immune response	1.69
Annotation Cluster 14: EGF-like	1.52
Annotation Cluster 15: Hormone stimulus	1.48
Annotation Cluster 16: Cytokine/chemokine response	1.43
Annotation Cluster 17: Oxidative stress	1.33
Annotation Cluster 18: calcium ion binding	1.30

IL-13 overexpression Day 3

Annotation Cluster 1: Cell cycle	10.22
Annotation Cluster 2: Non-membrane bound organelle	5.57
Annotation Cluster 3: Chromatin assembly	4.99
Annotation Cluster 4: Steroid and terpenoid biosynthesis	3.20
Annotation Cluster 5: Cyclin	2.97
Annotation Cluster 6: Cytoskeleton	2.84
Annotation Cluster 7: Regulation of cell cycle	1.99
Annotation Cluster 8: Meiosis	1.64
Annotation Cluster 9: Cytoskeleton organization	1.53
Annotation Cluster 10: Microtubule	1.35
Annotation Cluster 11: Chemotaxis	1.31
Annotation Cluster 12: Nucleotide binding	1.30

IL-13 overexpression Day 28

Annotation Cluster 1: Glycoprotein	6.56
Annotation Cluster 2: Inflammatory response	4.05
Annotation Cluster 3: Immunoglobulin	2.90
Annotation Cluster 4: Adaptive immune response	2.31
Annotation Cluster 5: Lectin	2.31
Annotation Cluster 6: Phagocytosis/endocytosis	2.15
Annotation Cluster 7: Cell death	1.97
Annotation Cluster 8: Response to bacterium	1.95

Annotation Cluster 9: Cell adhesion	1.53
LPS aerosolized Day 1	
Annotation Cluster 1: Extracellular space	7.22
Annotation Cluster 2: Inflammatory/immune response	3.79
Annotation Cluster 3: Acute phase response	2.81
Annotation Cluster 4: Lipocalin	2.41
Annotation Cluster 5: Oxydative stress	2.32
Annotation Cluster 6: Chemotaxis	2.03
Annotation Cluster 7: Repeat	1.71
Annotation Cluster 8: Response to bacterium	1.66
Annotation Cluster 9: Carbohydrate binding	1.60
Annotation Cluster 10: Hormone stimulus	1.56
Annotation Cluster 11: EGF-like	1.41
Annotation Cluster 12: Adaptive immune response	1.35
Annotation Cluster 13: Immunoglobulin	1.35
Annotation Cluster 14: Tissue morphogenesis	1.32
Annotation Cluster 15: Homeostatic process	1.31
LPS aerosolized Day 3	
Annotation Cluster 1: Cell cycle	10.32
Annotation Cluster 2: Nucleosome organization	4.99
Annotation Cluster 3: Microtubule	3.60
Annotation Cluster 4: Steroid and terpenoid biosynthesis	3.18
Annotation Cluster 5: Cyclin	2.96
Annotation Cluster 6: Chromosome condensation	2.31
Annotation Cluster 7: Regulation of cell cycle	1.98
Annotation Cluster 8: Protein localization	1.50
Annotation Cluster 9: Meiosis	1.50
Annotation Cluster 10: Nucleotide binding	1.45
Annotation Cluster 11: Cytoskeleton organization	1.34
LPS aerosolized Day 28	
Annotation Cluster 1: Disulfide bond	12.23
Annotation Cluster 2: Plasma membrane	6.10
Annotation Cluster 3: carbohydrate binding	3.70
Annotation Cluster 4: Immunoglobulin	3.51
Annotation Cluster 5: Innate immune response	2.85
Annotation Cluster 6: Adaptive immune response	2.46
Annotation Cluster 7: Phagocytosis/endocytosis	2.11
Annotation Cluster 8: Lysosome	1.50
Annotation Cluster 9: Cell adhesion	1.47
LPS i.p. Day 1	
Annotation Cluster 1: Glycoprotein	6.85
Annotation Cluster 2: Cytokine/chemokine response	3.88
Annotation Cluster 3: Acute phase response	3.12
Annotation Cluster 4: Oxidative stress	2.74
Annotation Cluster 5: Lipocalin	2.15
Annotation Cluster 6: Chemotaxis	2.09
Annotation Cluster 7: Stimulus response	2.04
Annotation Cluster 8: Carbohydrate binding	1.75

Annotation Cluster 9: Cellular homeostasis	1.72
Annotation Cluster 10: Phagocytosis/endocytosis	1.70
Annotation Cluster 11: Immunoglobulin	1.64
Annotation Cluster 12: Response to external stimulus	1.63
Annotation Cluster 13: Circulation	1.62
Annotation Cluster 14: Immune response	1.47
Annotation Cluster 15: Coenzyme binding	1.41
Annotation Cluster 16: EGF-like	1.37
Annotation Cluster 17: Steroid and terpenoid biosynthesis	1.31

LPS i.p. Day 3

Annotation Cluster 1: Cell cycle	9.90
Annotation Cluster 2: Non-membrane bound organelle	5.86
Annotation Cluster 3: Nucleosome assembly	4.64
Annotation Cluster 4: Steroid and terpenoid biosynthesis	3.15
Annotation Cluster 5: Cyclin	2.91
Annotation Cluster 6: Microtubule	2.74
Annotation Cluster 7: Chromosome condensation	2.11
Annotation Cluster 8: Extracellular region	1.94
Annotation Cluster 9: Regulation of cell cycle	1.81
Annotation Cluster 10: Enzyme inhibition	1.50
Annotation Cluster 11: Protein localization	1.49
Annotation Cluster 12: Cytoskeleton organization	1.33
Annotation Cluster 13: Chemotaxis	1.33

LPS i.p. Day 28

Annotation Cluster 1: Glycoprotein	11.99
Annotation Cluster 2: Transmembrane	4.72
Annotation Cluster 3: Carbohydrate binding	3.79
Annotation Cluster 4: Immunoglobulin	2.98
Annotation Cluster 5: Inflammatory/immune response	2.69
Annotation Cluster 6: Extracellular region	2.05
Annotation Cluster 7: Cytokine production	1.98
Annotation Cluster 8: Phagocytosis/endocytosis	1.82
Annotation Cluster 9: Cell adhesion	1.74
Annotation Cluster 10: Lysosome	1.47
Annotation Cluster 11: Negative regulation of apoptosis	1.37
Annotation Cluster 12: Cell surface	1.36

***Mycoplasma pulmonis* Day 1**

Annotation Cluster 1: Glycoprotein	4.84
Annotation Cluster 2: Acute phase response	3.50
Annotation Cluster 3: Toll-like response	2.02
Annotation Cluster 4: Lipocalin	1.95
Annotation Cluster 5: EGF-like	1.94
Annotation Cluster 6: Chemotaxis	1.94
Annotation Cluster 7: Adaptive immune response	1.80
Annotation Cluster 8: Immune response	1.69
Annotation Cluster 9: Enzyme inhibition	1.66
Annotation Cluster 10: Adaptive immune response	1.57
Annotation Cluster 11: Homeostatic process	1.43

***Mycoplasma pulmonis* Day 3**

Annotation Cluster 1: Chromatin assembly	5.08
Annotation Cluster 2: Cell cycle	5.04
Annotation Cluster 3: Steroid and terpenoid biosynthesis	3.46
Annotation Cluster 4: Microtubule	2.20
Annotation Cluster 5: Meiosis	2.05
Annotation Cluster 6: Regulation of cell cycle	2.00
Annotation Cluster 7: Protein localization	1.96
Annotation Cluster 8: Nucleotide binding	1.41

***Mycoplasma pulmonis* Day 28**

Annotation Cluster 1: Glycoprotein	7.44
Annotation Cluster 2: Transmembrane	4.64
Annotation Cluster 3: Plasma membrane	2.53
Annotation Cluster 4: Immunoglobulin	2.42
Annotation Cluster 5: Inflammatory response	2.18
Annotation Cluster 6: Carbohydrate binding	2.04
Annotation Cluster 7: Cytokine production	1.74
Annotation Cluster 8: Extracellular region	1.38
Annotation Cluster 9: Carbohydrate binding	1.34
Annotation Cluster 10: Regulation of apoptosis	1.05
Annotation Cluster 11: Plasma membrane	0.74

***Mycobacterium tuberculosis* Day 1**

Annotation Cluster 1: Extracellular space	7.32
Annotation Cluster 2: Acute phase response	4.69
Annotation Cluster 3: Cytokine/chemokine response	3.39
Annotation Cluster 4: EGF-like	2.31
Annotation Cluster 5: Toll-like response	2.15
Annotation Cluster 6: Extracellular matrix	1.89
Annotation Cluster 7: Response to stimulus	1.87
Annotation Cluster 8: Adaptive immune response	1.80
Annotation Cluster 9: Lipocalin	1.75
Annotation Cluster 10: Cell death	1.72
Annotation Cluster 11: Immune response	1.71
Annotation Cluster 12: EGF-like	1.69
Annotation Cluster 13: Chemotaxis	1.61
Annotation Cluster 14: Leukocyte/lymphocyte mediated immunity	1.58
Annotation Cluster 15: Carbohydrate binding	1.58
Annotation Cluster 16: Lectin	1.43

***Mycobacterium tuberculosis* Day 3**

Annotation Cluster 1: Chromatin assembly	4.85
Annotation Cluster 2: Steroid and terpenoid biosynthesis	4.06
Annotation Cluster 3: Cell cycle	3.85
Annotation Cluster 4: Microtubule	2.14
Annotation Cluster 5: Meiosis	1.94
Annotation Cluster 6: Protein localization	1.83
Annotation Cluster 7: Microtubule-based movement	1.60
Annotation Cluster 8: Protease inhibition	1.58
Annotation Cluster 9: Regulation of cell cycle	1.54
Annotation Cluster 10: Chemotaxis	1.50

***Mycobacterium tuberculosis* Day 28**

Annotation Cluster 1: Glycoprotein	6.43
Annotation Cluster 2: Immunoglobulin	2.59
Annotation Cluster 3: Carbohydrate binding	2.55
Annotation Cluster 4: Inflammatory response	2.55
Annotation Cluster 5: Immune response	2.21
Annotation Cluster 6: Extracellular region	1.99
Annotation Cluster 7: Leukocyte activation	1.84
Annotation Cluster 8: Cell adhesion	1.82
Annotation Cluster 9: Apoptosis	1.36

***Nippostrongylus brasiliensis* Day 1**

Annotation Cluster 1: Glycoprotein	8.26
Annotation Cluster 2: Inflammatory response	5.31
Annotation Cluster 3: Acute phase response	4.84
Annotation Cluster 4: Toll-like response	2.71
Annotation Cluster 5: EGF-like	2.54
Annotation Cluster 6: Oxidative stress	2.32
Annotation Cluster 7: Extracellular matrix	2.18
Annotation Cluster 8: Carbohydrate binding	2.09
Annotation Cluster 9: Adaptive immune response	1.87
Annotation Cluster 10: Cell death	1.86
Annotation Cluster 11: Apoptosis	1.77
Annotation Cluster 12: Immune response	1.72
Annotation Cluster 13: Cytokine production	1.68
Annotation Cluster 14: Adaptive immune response	1.65
Annotation Cluster 15: Lipocalin	1.65
Annotation Cluster 16: Repeat	1.62
Annotation Cluster 17: Complement	1.58
Annotation Cluster 18: Response to stimulus	1.56
Annotation Cluster 19: Cell migration	1.51
Annotation Cluster 20: Carbohydrate binding	1.39
Annotation Cluster 21: Chemotaxis	1.34
Annotation Cluster 22: T cell activation	1.31

***Nippostrongylus brasiliensis* Day 3**

Annotation Cluster 1: Cell cycle	7.25
Annotation Cluster 2: Chromatin assembly	4.84
Annotation Cluster 3: Steroid and terpenoid biosynthesis	3.17
Annotation Cluster 4: Chromosome condensation	2.58
Annotation Cluster 5: Regulation of cell cycle	2.50
Annotation Cluster 6: Meiosis	2.38
Annotation Cluster 7: Microtubule	2.06
Annotation Cluster 8: Chemotaxis	1.84
Annotation Cluster 9: Protein localization	1.51
Annotation Cluster 10: Protease inhibition	1.49
Annotation Cluster 11: Microtubule-based process	1.42
Annotation Cluster 12: ATP binding	1.35

***Nippostrongylus brasiliensis* Day 28**

Annotation Cluster 1: Glycoprotein	12.26

Annotation Cluster 2: Transmembrane	5.95
Annotation Cluster 3: Immunoglobulin	3.62
Annotation Cluster 4: Immune response	2.85
Annotation Cluster 5: Cytokine production	2.76
Annotation Cluster 6: carbohydrate binding	2.63
Annotation Cluster 7: Leukocyte/lymphocyte activation	2.25
Annotation Cluster 8: Cell adhesion	2.13
Annotation Cluster 9: Inflammatory response	2.11
Annotation Cluster 10: Apoptosis	1.98
Annotation Cluster 11: Response to bacterium	1.79
Annotation Cluster 12: Secretion	1.43
Annotation Cluster 13: Extracellular space	1.40
Ovalbumin Day 1	
Annotation Cluster 1: Glycoprotein	6.55
Annotation Cluster 2: Inflammatory response	4.59
Annotation Cluster 3:Extracellular matrix	2.37
Annotation Cluster 4: Carbohydrate binding	1.92
Annotation Cluster 5: Chemotaxis	1.91
Annotation Cluster 6: Carbohydrate binding	1.85
Annotation Cluster 7: Adaptive immune response	1.85
Annotation Cluster 8: Apoptosis	1.80
Annotation Cluster 9: Cell death	1.77
Annotation Cluster 10: Repeat	1.74
Annotation Cluster 11: Lipocalin	1.74
Annotation Cluster 12: Immune response	1.63
Annotation Cluster 13: Response to stimulus	1.58
Annotation Cluster 14: EGF-like	1.51
Annotation Cluster 15: T cell activation and B cell differentiation	1.41
Annotation Cluster 16: GPI-achor	1.38
Ovalbumin Day 3	
Annotation Cluster 1: Chromatin assembly	4.85
Annotation Cluster 2: Cell cycle	3.49
Annotation Cluster 3: Steroid and terpenoid biosynthesis	3.32
Annotation Cluster 4: Meiosis	1.84
Annotation Cluster 5: Microtubule	1.56
Annotation Cluster 6: Cytokine/chemokine response	1.40
Annotation Cluster 7: Microtubule-based process	1.30
Ovalbumin Day 28	
Annotation Cluster 1: Glycoprotein	9.65
Annotation Cluster 2: Transmembrane	4.48
Annotation Cluster 3: Inflammatory response	3.26
Annotation Cluster 4: Cytokine production	2.81
Annotation Cluster 5: Cell surface	2.43
Annotation Cluster 6: Immunoglobin	2.26
Annotation Cluster 7: Carbohydrate binding	1.89
Annotation Cluster 8: Cell death	1.66
Ovalbumin Day 1	
Annotation Cluster 1: Extracellular space	7.82

Annotation Cluster 2: Inflammatory/immune response	4.37
Annotation Cluster 3: Acute phase response	3.59
Annotation Cluster 4: Extracellular matrix	2.65
Annotation Cluster 5: EGF-like	2.47
Annotation Cluster 6: Oxidative stress	2.26
Annotation Cluster 7: Response to bacterium	2.21
Annotation Cluster 8: Cell death	2.16
Annotation Cluster 9: Lectin	2.03
Annotation Cluster 10: Adaptive immune response	1.93
Annotation Cluster 11: Apoptosis	1.79
Annotation Cluster 12: Phagocytosis/endocytosis	1.78
Annotation Cluster 13: Response to stimulus	1.75
Annotation Cluster 14: Carbohydrate binding	1.62
Annotation Cluster 15: Lipocalin	1.62
Annotation Cluster 16: Repeat	1.58
Annotation Cluster 17: Complement	1.55
Annotation Cluster 18: Tissue morphogenesis	1.48
Annotation Cluster 19: Adaptive immune response	1.45
Annotation Cluster 20: Circulation	1.45
Annotation Cluster 21: Immune response	1.40
Annotation Cluster 22: Homeostatic process	1.37
Annotation Cluster 23: Immunoglobulin	1.35
Annotation Cluster 24: Plasma membrane	1.34

Ovalbumin Day 3

Annotation Cluster 1: Chromatin assembly	4.68
Annotation Cluster 2: Cell cycle	3.83
Annotation Cluster 3: Steroid and terpenoid biosynthesis	3.26
Annotation Cluster 4: Microtubule	2.03
Annotation Cluster 5: Microtubule-based process	1.93
Annotation Cluster 6: Meiosis	1.88
Annotation Cluster 7: Protease inhibition	1.54
Annotation Cluster 8: Chemotaxis	1.47
Annotation Cluster 9: negative regulation of apoptosis	1.33
Annotation Cluster 10: Regulation of cell cycle	1.31

Ovalbumin Day 28

Annotation Cluster 1: Glycoprotein	10.93
Annotation Cluster 2: Transmembrane	4.84
Annotation Cluster 3: Inflammatory/immune response	3.73
Annotation Cluster 4: Immunoglobulin	3.08
Annotation Cluster 5: Cell surface	2.66
Annotation Cluster 6: Carbohydrate binding	2.52
Annotation Cluster 7: Adaptive immune response	2.32
Annotation Cluster 8: Cell adhesion	2.29
Annotation Cluster 9: Toll-like response	1.98
Annotation Cluster 10: Response to bacterium	1.92
Annotation Cluster 11: Apoptosis	1.92
Annotation Cluster 12: Extracellular region	1.56
Annotation Cluster 13: Leukocyte activation	1.42

***Pseudomonas aeruginosa* Day 1**

Annotation Cluster 1: Glycoprotein	7.86
Annotation Cluster 2: Inflammatory/immune response	4.40
Annotation Cluster 3: Acute phase response	2.66
Annotation Cluster 4: Extracellular matrix	2.52
Annotation Cluster 5: Response to bacterium	2.47
Annotation Cluster 6: Oxidative stress	2.43
Annotation Cluster 7: Lipocalin	2.27
Annotation Cluster 8: Chemotaxis	2.09
Annotation Cluster 9: EGF-like	2.01
Annotation Cluster 10: Coagulation	1.70
Annotation Cluster 11: Homeostatic process	1.62
Annotation Cluster 12: Response to stimulus	1.62
Annotation Cluster 13: carbohydrate binding	1.55
Annotation Cluster 14: Repeat	1.55
Annotation Cluster 15: Immune response	1.54
Annotation Cluster 16: Apoptosis	1.52
Annotation Cluster 17: Negative regulation of apoptosis	1.50
Annotation Cluster 18: EGF-like	1.37
Annotation Cluster 19: Circulation	1.35
Annotation Cluster 20: Immunoglobulin	1.34

***Pseudomonas aeruginosa* Day 3**

Annotation Cluster 1: Cell cycle	10.98
Annotation Cluster 2: Chromatin assembly	4.68
Annotation Cluster 3: Microtubule	3.09
Annotation Cluster 4: Steroid and terpenoid biosynthesis	3.07
Annotation Cluster 5: Cyclin	2.86
Annotation Cluster 6: Chromosome condensation	2.48
Annotation Cluster 7: Cell cycle	2.25
Annotation Cluster 8: Cytokine/chemokine response	1.70
Annotation Cluster 9: ATP binding	1.67
Annotation Cluster 10: Meiosis	1.54
Annotation Cluster 11: Microtubule-based process	1.47
Annotation Cluster 12: Protein localization	1.43

***Pseudomonas aeruginosa* Day 28**

Annotation Cluster 1: Glycoprotein	12.94
Annotation Cluster 2: Transmembrane	6.37
Annotation Cluster 3: Inflammatory response	4.06
Annotation Cluster 4: Immunoglobulin	4.01
Annotation Cluster 5: Immune response	2.40
Annotation Cluster 6: Lectin	2.33
Annotation Cluster 7: Immunoglobulin	2.23
Annotation Cluster 8: Extracellular region	1.83
Annotation Cluster 9: Apoptosis	1.64
Annotation Cluster 10: Cell adhesion	1.57
Annotation Cluster 11: Lysosome	1.44

TNF Day 1

Annotation Cluster 1: Glycoprotein	6.69
Annotation Cluster 2: Acute phase response	6.30
Annotation Cluster 3: Extracellular matrix	2.38

Annotation Cluster 4: Response to stiumuls	2.23
Annotation Cluster 5: Oxidative stress	2.20
Annotation Cluster 6: Negative regulation of signal transuction	1.86
Annotation Cluster 7: Adaptive immune response	1.85
Annotation Cluster 8: apoptosis	1.78
Annotation Cluster 9: Repeat	1.74
Annotation Cluster 10: Lipocalin	1.74
Annotation Cluster 11: Chemotaxis	1.70
Annotation Cluster 12: Tissue morphogenesis	1.58
Annotation Cluster 13: Cholesterol metabolism	1.55
Annotation Cluster 14: Immunoglobulin	1.55
Annotation Cluster 15: Immune response	1.52
Annotation Cluster 16: EGF-like	1.45
Annotation Cluster 17: Tcell and B cell differentiation	1.44
Annotation Cluster 18: Blood vessel morphogenesis	1.34
TNF Day 3	
Annotation Cluster 1: Chromatin assembly	5.07
Annotation Cluster 2: Cell cycle	3.60
Annotation Cluster 3: Steroid and terpenoid biosynthesis	3.52
Annotation Cluster 4: Microtubule	2.00
Annotation Cluster 5: Microtubule-based process	1.45
Annotation Cluster 6: Organelle localization	1.32
Annotation Cluster 7: Extracellular region	1.31
TNF Day 28	
Annotation Cluster 1: Glycoprotein	9.03
Annotation Cluster 2: Transmembrane	4.01
Annotation Cluster 3: Inflammatory/immune response	3.48
Annotation Cluster 4: Immunoglobulin	3.01
Annotation Cluster 5: carbohydrate binding	2.94
Annotation Cluster 6: Adaptive immune response	2.21
Annotation Cluster 7: Immunoglobulin	2.17
Annotation Cluster 8: Phagocytosis/endocytosis	2.15
Annotation Cluster 9: Extracellular space	1.80
Annotation Cluster 10: Cell adhesion	1.70
Annotation Cluster 11: Cytokine production	1.63
Annotation Cluster 12: Apoptosis	1.60

SP10. Association of CBNP exposure to disease, using previously currated gene expression studies in Next Bio. The 162 µg dose was employed for analysis.

	Respiratory Disease	Score	Number of Studies
Day 1			
	Severe acute respiratory syndrome	92	3
	Injury of lung	73	20
	Congenital cystic adenomatoid malformation	50	1
	Asthma	50	39
	Hypoxia	46	112
	Pulmonary Embolism	46	4
	Interstitial lung disease	44	10
	Chronic sinusitis	43	1
	Pneumonia	35	8
	Pulmonary Hypertension	34	7
	Chronic obstructive pulmonary disease	34	19
	Pulmonary thromboembolism	32	1
	Respiratory distress syndrome in the newborn	25	1
	Lung transplant rejection	14	1
	Pulmonary lymphangioleimyomatosis	22	3
	Pneumothorax	19	1
	Infectious disease of lung	16	3
	Lower respiratory tract infection	16	3
	Disorder of lung	14	5
	Fibrosis of lung	14	7
Day 3			
	Severe acute respiratory syndrome	94	4
	Injury of lung	72	20
	Congenital cystic adenomatoid malformation	52	1
	Asthma	52	39
	Interstitial lung disease	50	11
	Pulmonary Embolism	48	4
	Hypoxia	48	112
	Pneumonia	47	8
	Pulmonary Hypertension	45	8
	Pulmonary thromboembolism	41	1
	Chronic sinusitis	37	2
	Fibrosis of lung	35	8
	Chronic obstructive pulmonary disease	32	18
	Infectious disease of lung	31	3
	Lower respiratory tract infection	31	3
	Disorder of lung	30	5
	Respiratory distress syndrome in the newborn	27	1
	Pulmonary lymphangioleimyomatosis	25	3
	Lung transplant rejection	23	1
Day 28			
	Severe acute respiratory syndrome	99	3
	Congenital cystic adenomatoid malformation	68	1
	Injury of lung	64	20
	Pulmonary Hypertension	58	7

Asthma	57	40
Chronic sinusitis	54	3
Pulmonary thromboembolism	52	1
Pneumonia	49	8
Hypoxia	49	114
Pulmonary Embolism	49	4
Interstitial lung disease	46	10
Fibrosis of lung	45	9
Disorder of lung	43	5
Chronic obstructive pulmonary disease	40	20
Lung transplant rejection	40	1
Respiratory distress syndrome in the newborn	35	1
Immotile cilia syndrome	33	2
Infectious disease of lung	29	3
Lower respiratory tract infection	29	3
Central alveolar hypoventilation syndrome	21	1
Sleep-related respiratory failure	20	1

SUPPLEMENTARY FIGURES

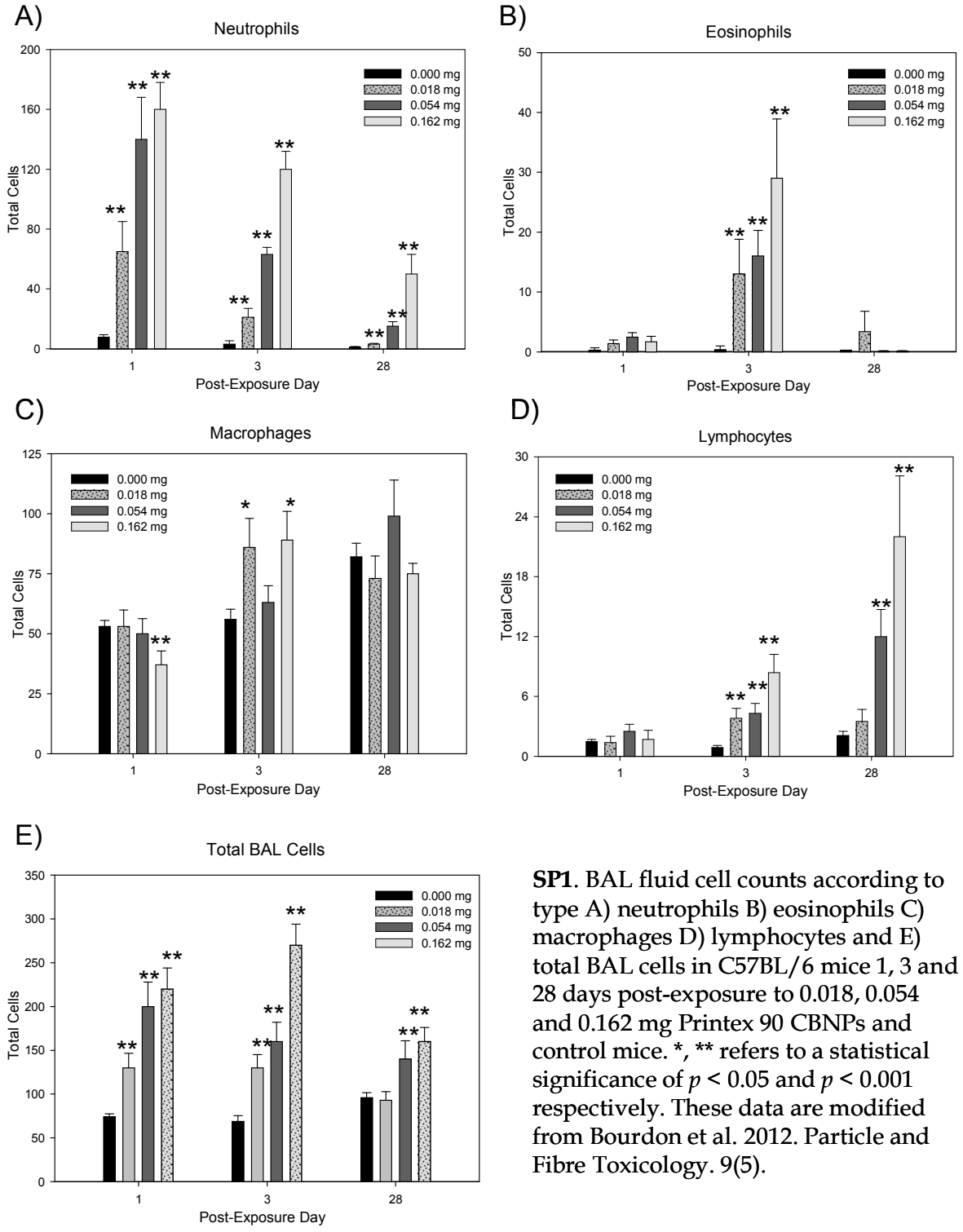

SP1. BAL fluid cell counts according to type A) neutrophils B) eosinophils C) macrophages D) lymphocytes and E) total BAL cells in C57BL/6 mice 1, 3 and 28 days post-exposure to 0.018, 0.054 and 0.162 mg Printex 90 CBNPs and control mice. *, ** refers to a statistical significance of $p < 0.05$ and $p < 0.001$ respectively. These data are modified from Bourdon et al. 2012. Particle and Fibre Toxicology. 9(5).

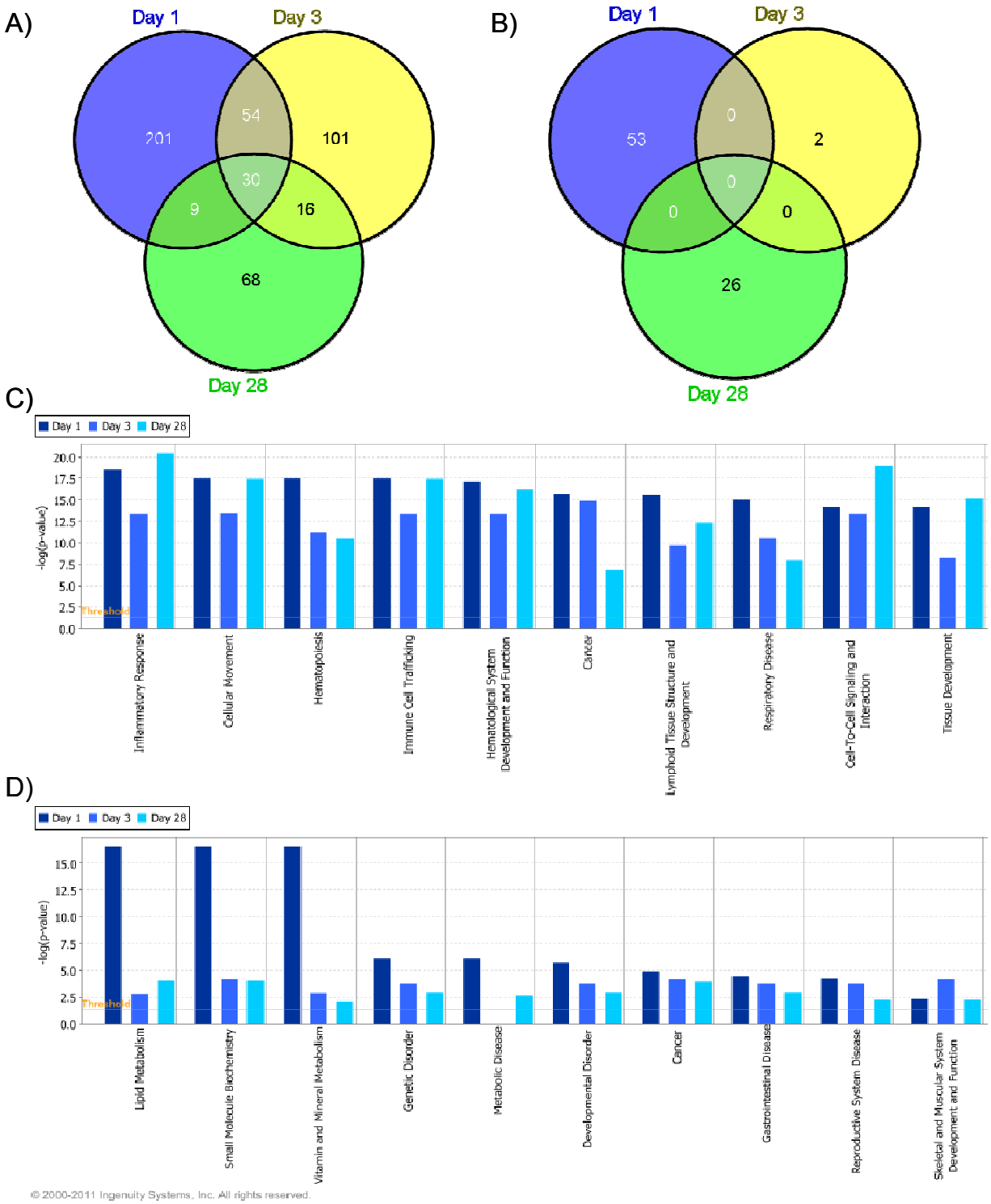

SP2. C57/BL6 mice were intratracheally instilled with 0.162 mg Printex 90 CBNPs and sacrificed 1, 3 and 28 days post-exposure alongside controls. Distribution of differentially expressed genes according to time-point was examined in lung (A) and liver (B). Top ten biological functions were identified in Ingenuity Pathway Analysis, in lung (A) and liver (B).

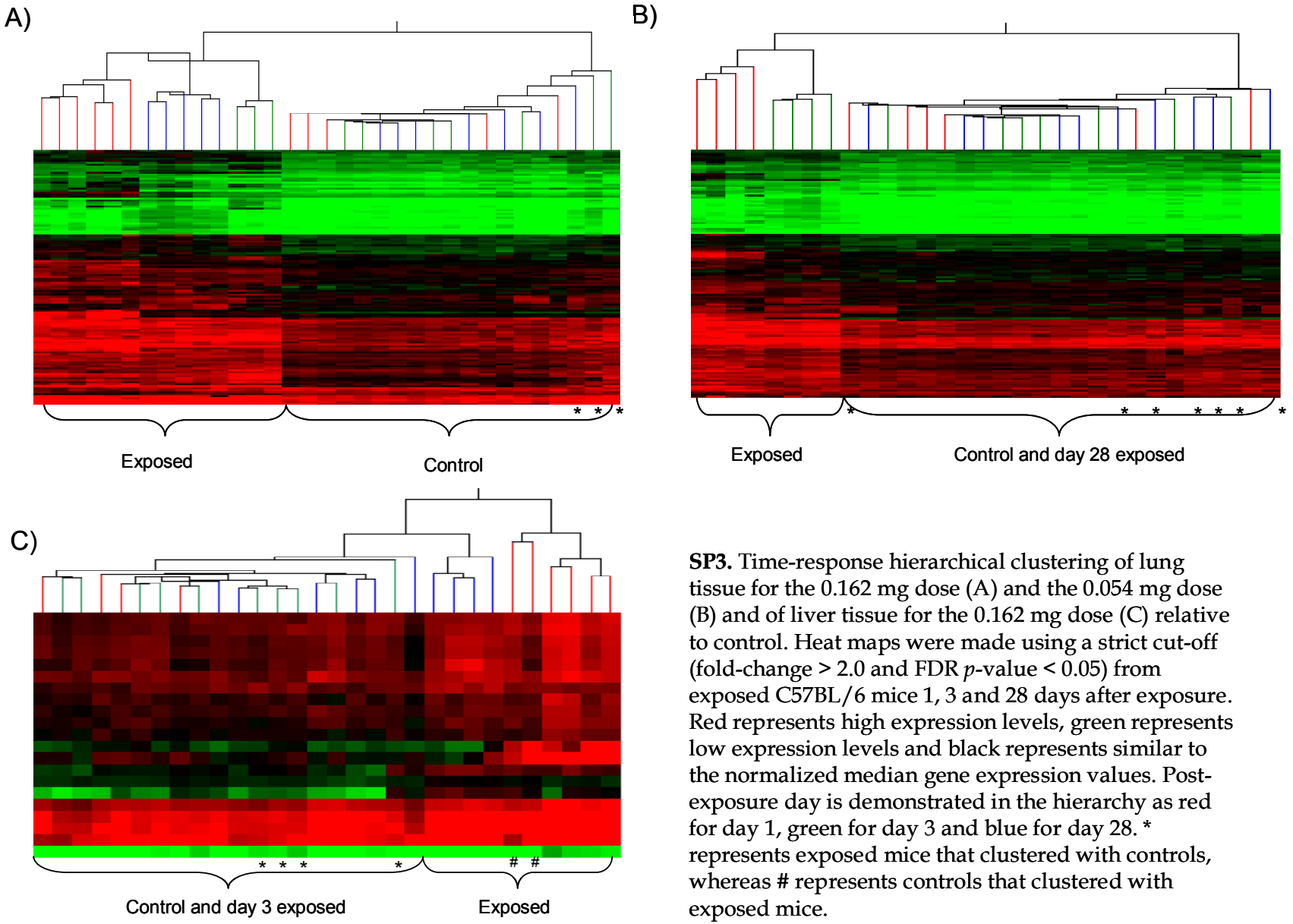

SP3. Time-response hierarchical clustering of lung tissue for the 0.162 mg dose (A) and the 0.054 mg dose (B) and of liver tissue for the 0.162 mg dose (C) relative to control. Heat maps were made using a strict cut-off (fold-change > 2.0 and FDR *p*-value < 0.05) from exposed C57BL/6 mice 1, 3 and 28 days after exposure. Red represents high expression levels, green represents low expression levels and black represents similar to the normalized median gene expression values. Post-exposure day is demonstrated in the hierarchy as red for day 1, green for day 3 and blue for day 28. * represents exposed mice that clustered with controls, whereas # represents controls that clustered with exposed mice.

SP4. Top networks and canononical pathways based on differentially expressed genes (FDR *p*-value < 0.1 and fold-change > 1.5) using IPA. Red shapes represent genes that were significantly up-regulated whereas green shapes represent genes that were down-regulated. Connecting line represent interactions between genes that are described in the Ingenuity Knowledge database. White shapes were added by IPA based on their relationship to deregulated genes.

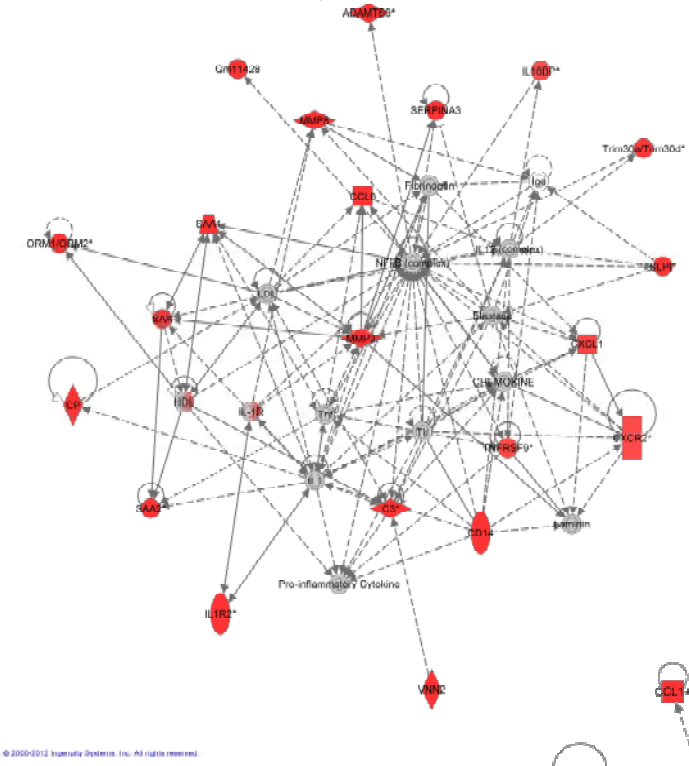

Day 1, 54 µg

Top Network (left):

- Cellular movement and immune cell trafficking

Other Networks:

- Total=3, lipid metabolism, inflammation, DNA repair, proliferation, free radical scavenging

Top Canononical Pathways:

- LXR/RXR activation (p=7.15E-08)
- Acute phase response signalling (p=7.48E-07)
- Role of osteoblasts, osteoclasts and chondrocytes in rheumatoid arthritis (p=8.59E-04)

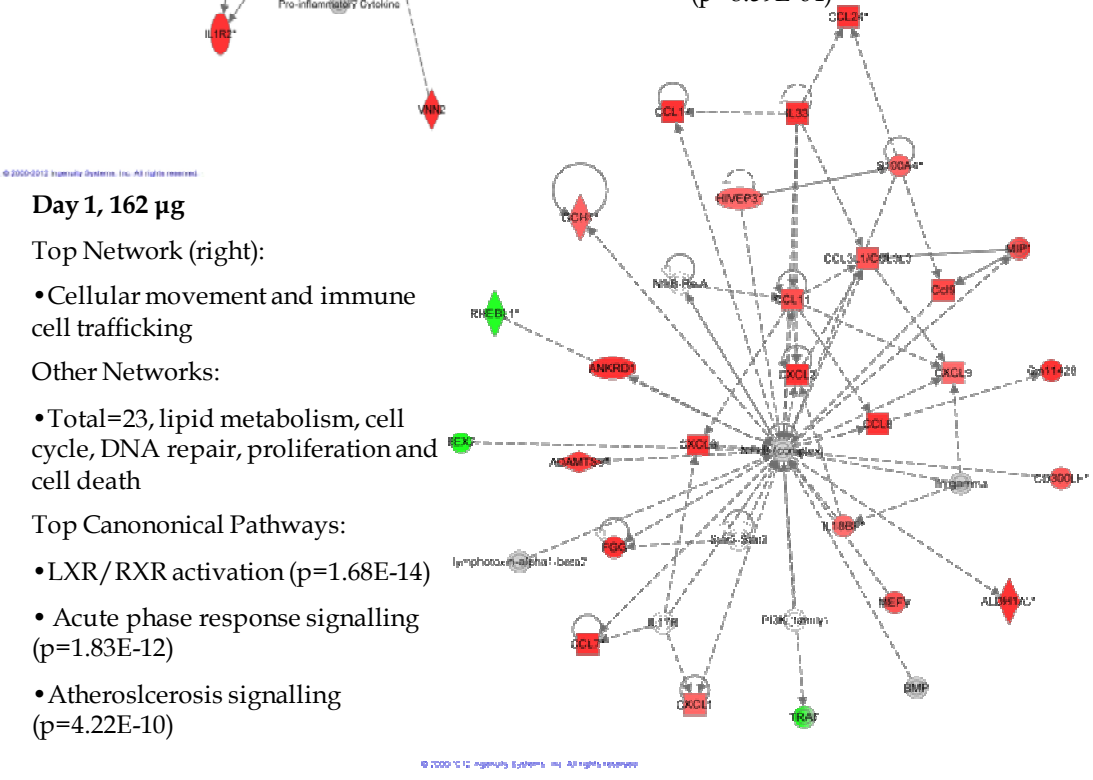

Day 1, 162 µg

Top Network (right):

- Cellular movement and immune cell trafficking

Other Networks:

- Total=23, lipid metabolism, cell cycle, DNA repair, proliferation and cell death

Top Canononical Pathways:

- LXR/RXR activation (p=1.68E-14)
- Acute phase response signalling (p=1.83E-12)
- Atheroslcerosis signalling (p=4.22E-10)

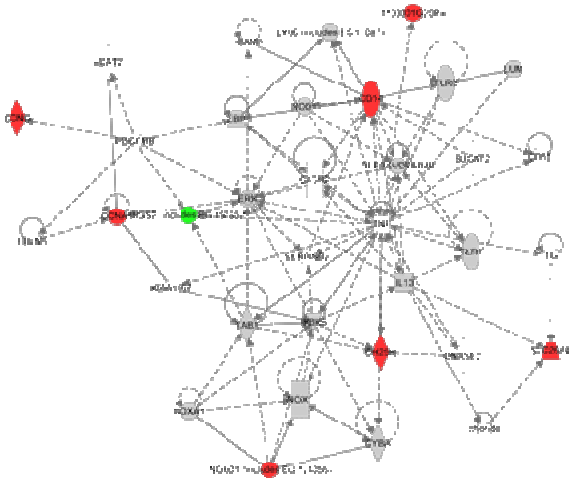

Day 3, 54 µg

Top Network (left):

- Lipid Metabolism

Other Networks:

- None

Top Canononical Pathways:

- Antiproliferative role of TOB in T cell signalling (p=1.13E-02)
- MIF-mediated glucocorticoid regulation (p=1.30E-02)
- MIF regulation of innate immunity (p=1.66E-02)

Day 3, 162 µg

Top Network (right):

- Cell cycle, DNA repair, DNA replication

Other Networks:

- Total=17, cell death, free radical scavenging, inflammation, cellular movement, proliferation

Top Canononical Pathways:

- LXR/RXR activation (p=8.97E-06)
- Role of IL-17F in allergic inflammatory airway diseases (p=2.63E-05)
- Biosynthesis of steroids (p=3.54E-05)

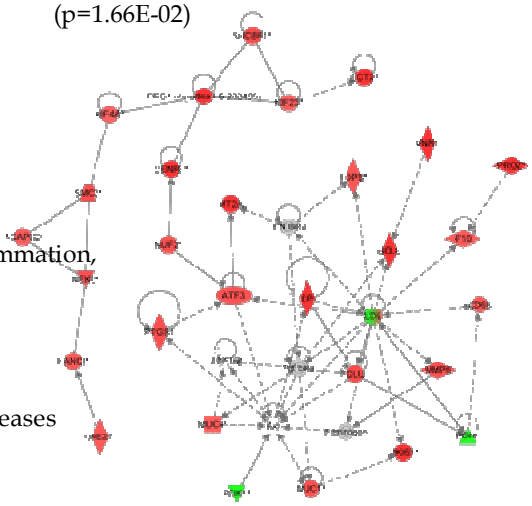

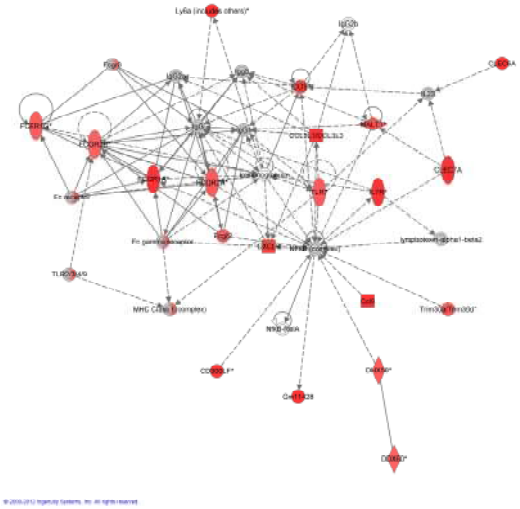

Day 28, 162 µg

Top Network (left):

- Inflammation and cell to cell signalling

Other Networks:

- Total=11, free radical scavenging, cell death, proliferation

Top Canononical Pathways:

- Communication between innate and adaptive immune cells (p=5.04E-09)
- Dendtritic cell maturation (p=1.18E-07)
- IL-10 signalling (p=3.38E-06)

SP5. Potential transcription regulators affected by CBNP exposure were determined in IPA, according to significance of down-stream genes. Significant transcription regulators exhibited a z-score within ± 2.0. Transcription regulators are presented in grey and expression of down-stream genes are coloured red for up-regulated genes and green for down-regulated genes. Solid lines represent direct interactions whereas dashed lines represent indirect effects.

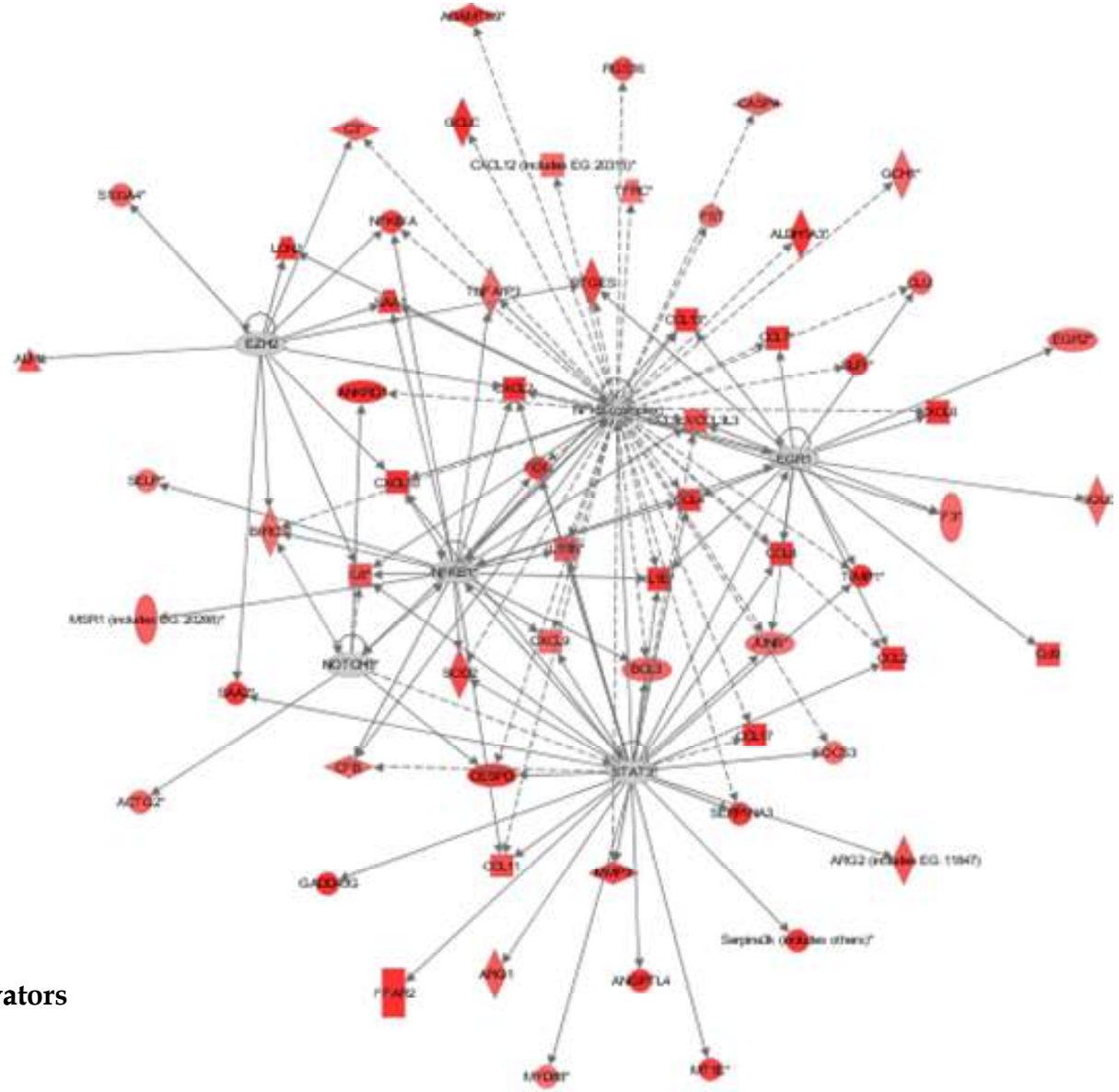

Day 1, 162 µg dose

Transcriptional Activators

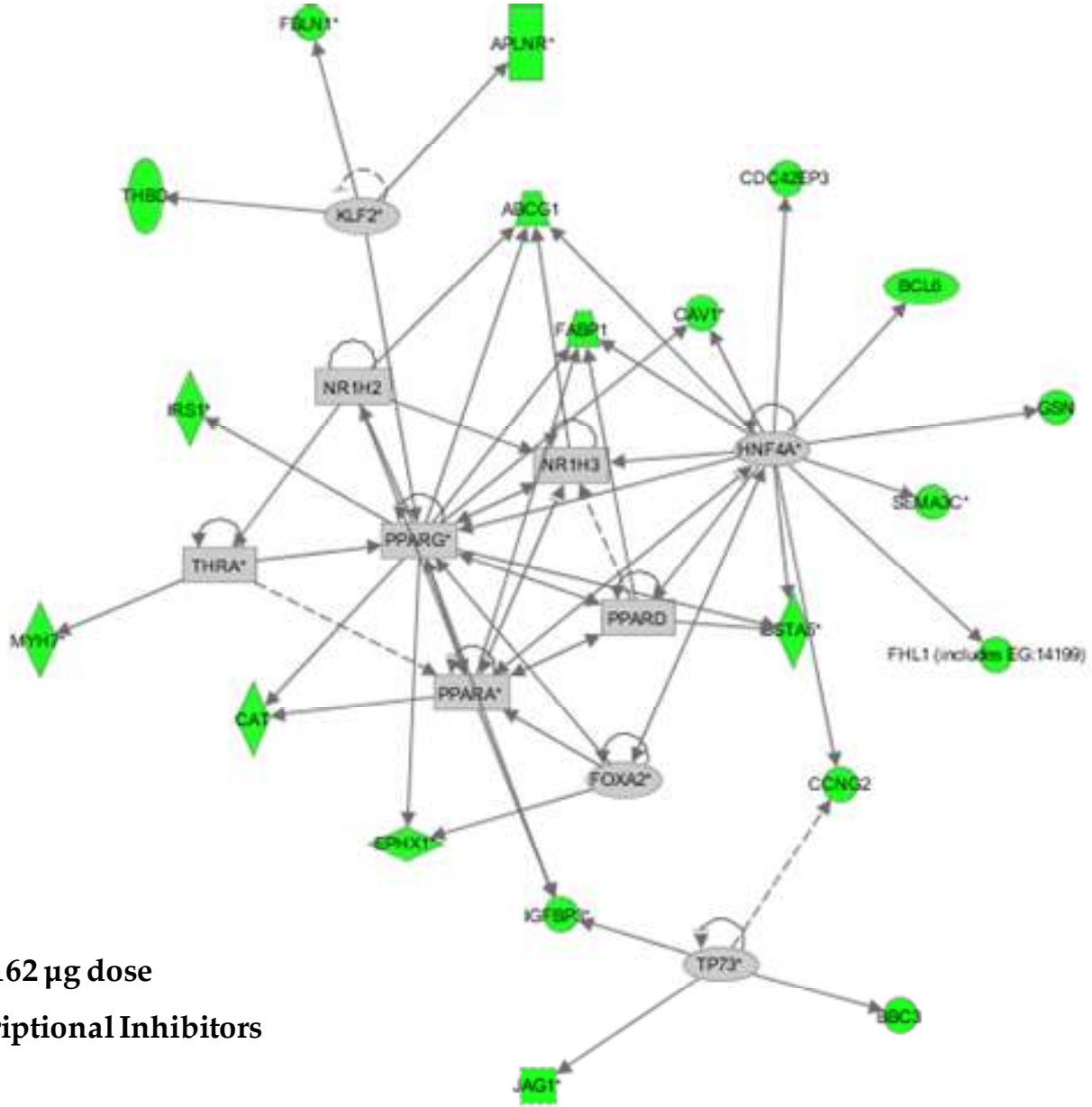

Day 1, 162 µg dose

Transcriptional Inhibitors

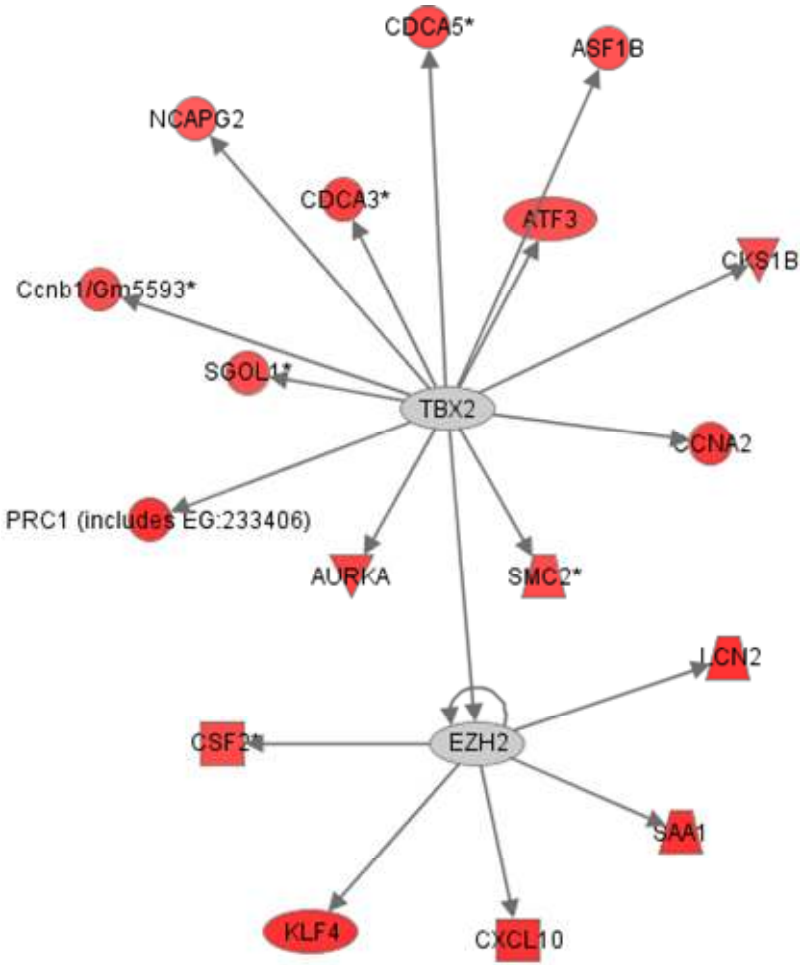

Day 3, 162 µg dose

Transcriptional Activators

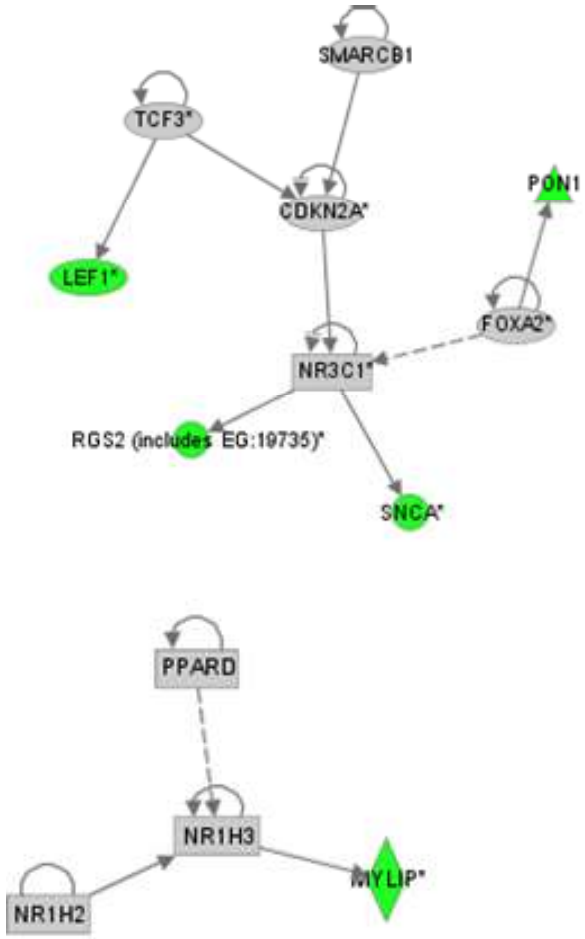

Day 3, 162 µg dose

Transcriptional Inhibitors

SP6. Best fit curves for BMD modelling of pulmonary apical endpoint and RT-PCR validation results. All models were demonstrated to have an appropriate fit for modelling ($p > 0.05$).

Neutrophil Influx Day 1

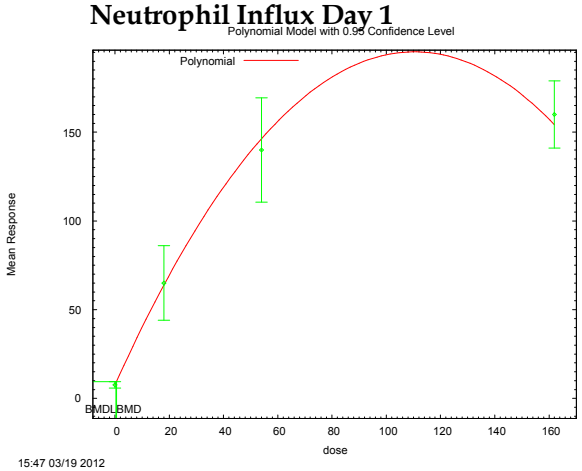

15:47 03/19 2012

Neutrophil Influx Day 3

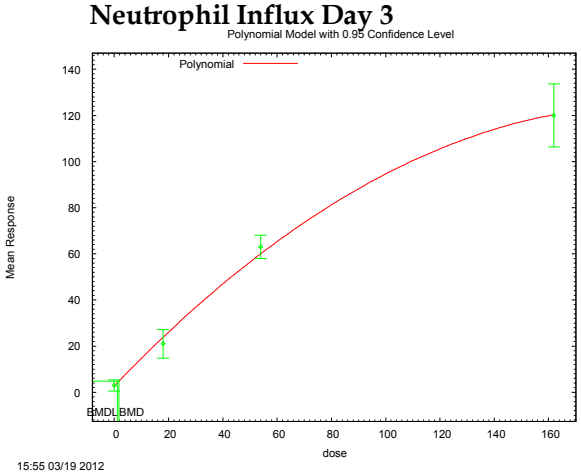

15:55 03/19 2012

Neutrophil Influx Day 28

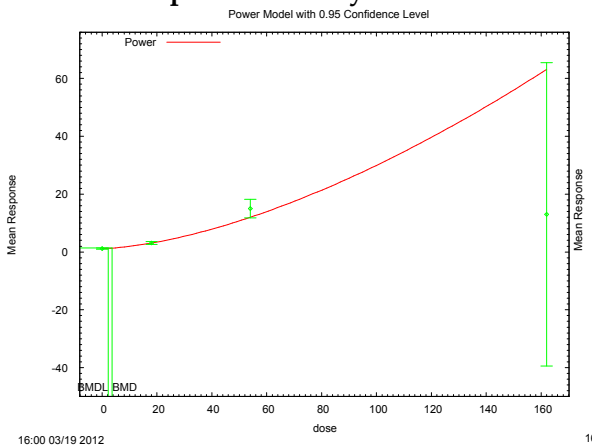

16:00 03/19 2012

DNA Strand Breaks Day 1

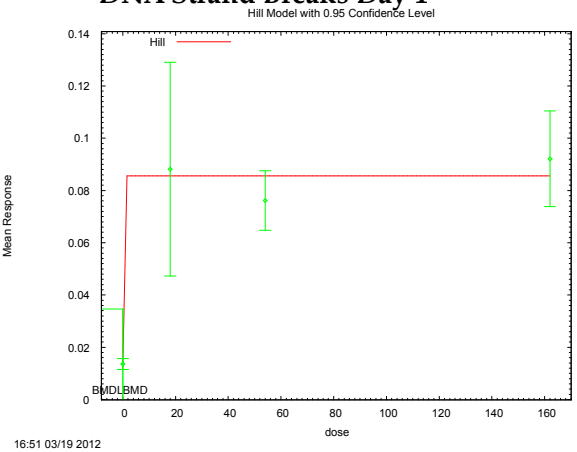

16:51 03/19 2012

DNA Strand Breaks Day 3

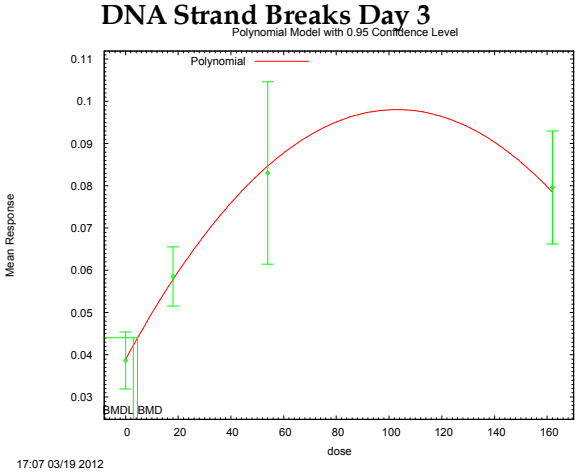

17:07 03/19 2012

DNA Strand Breaks Day 28

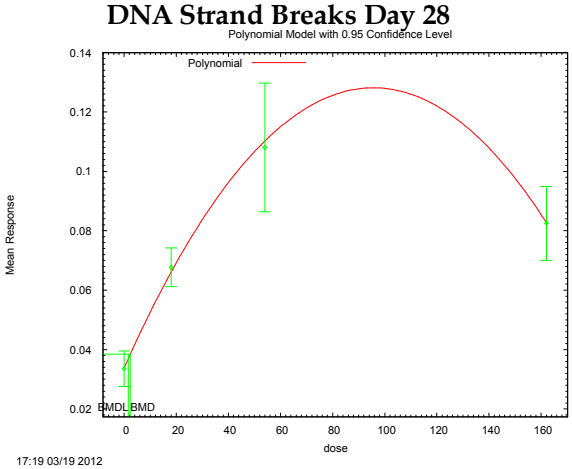

17:19 03/19 2012

Total BAL Cell Influx Day 1

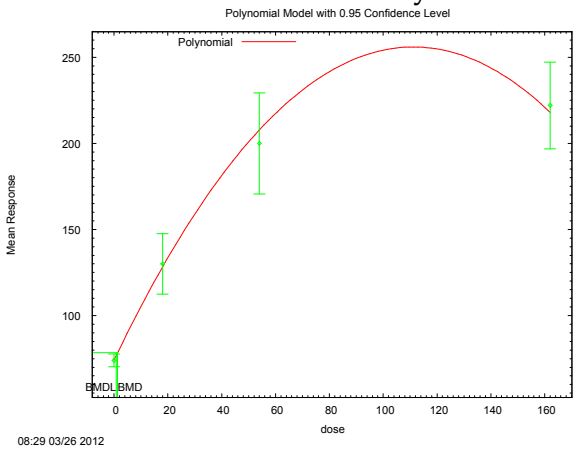

08:29 03/26 2012

Eosinophil Influx Day 3

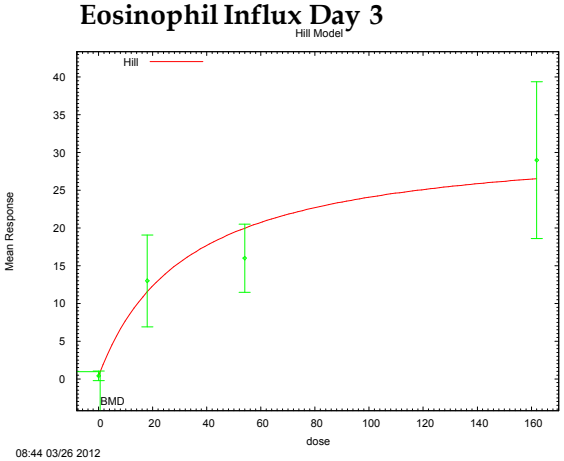

08:44 03/26 2012

Lymphocyte Influx Day 28

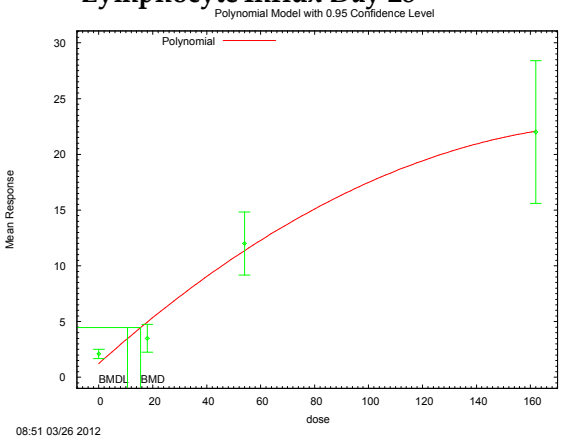

08:51 03/26 2012

Saa3 Day 1

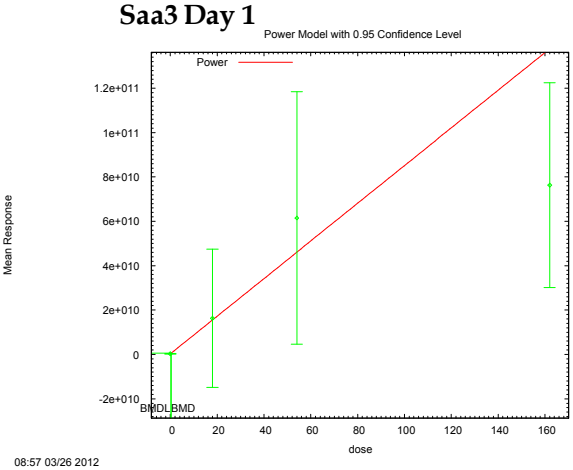

08:57 03/26 2012

Saa3 Day 3

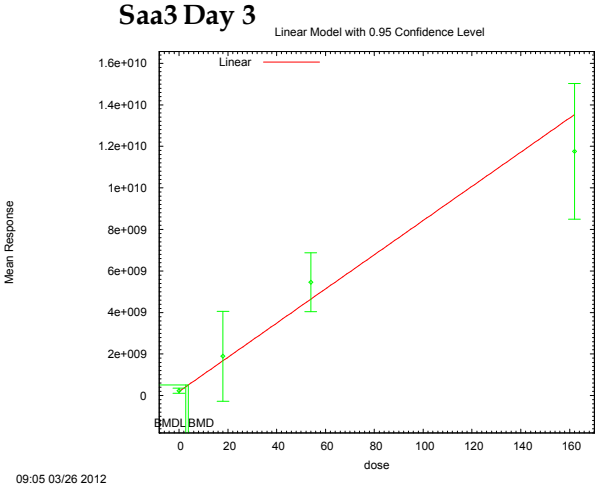

09:05 03/26 2012

Saa3 Day 28

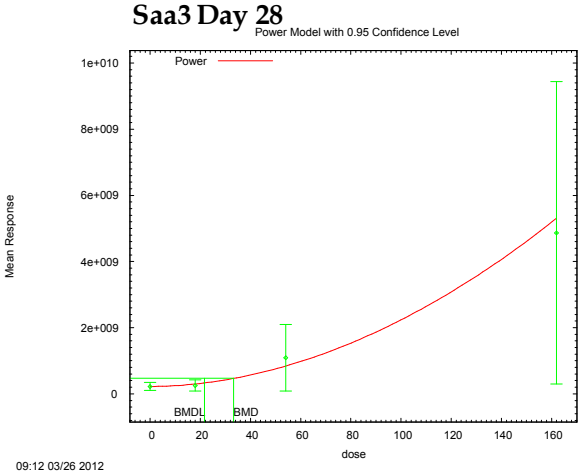

09:12 03/26 2012

Il6 Day 1

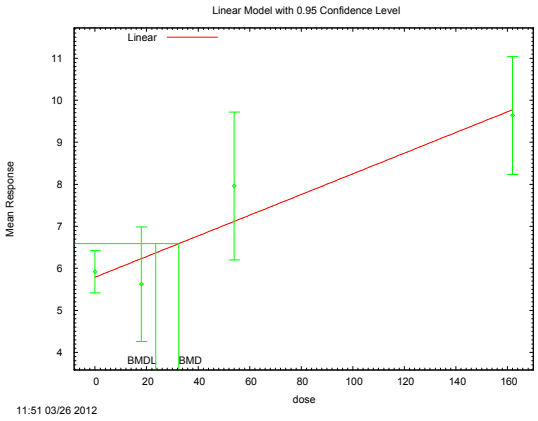

Il6 Day 3

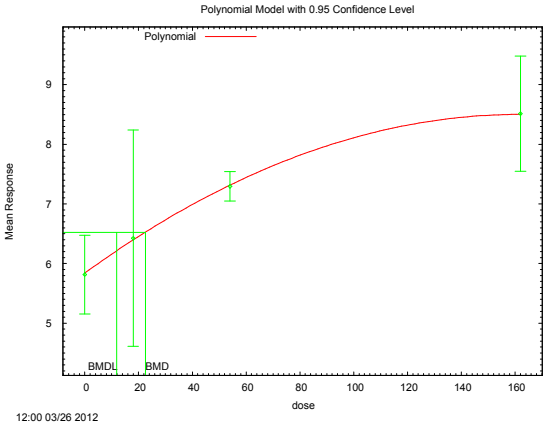

Cxcl5 Day 1

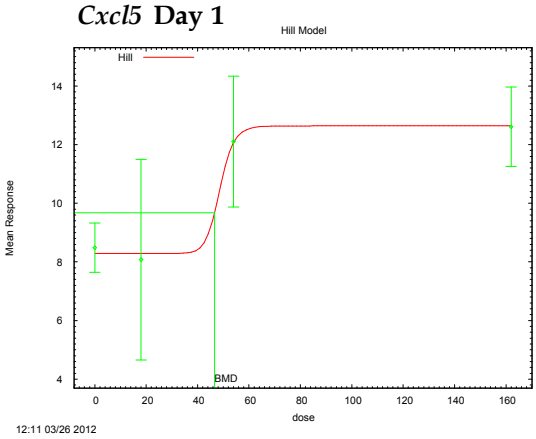

Cxcl5 Day 3

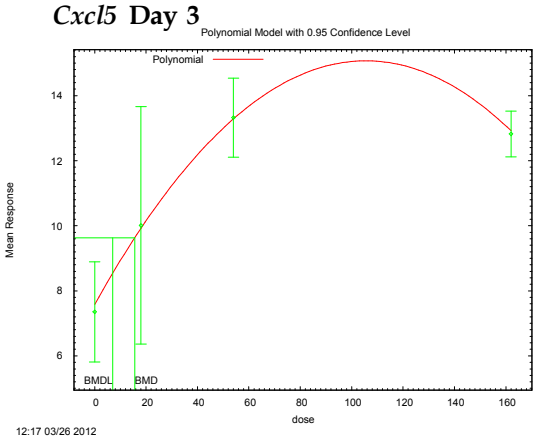

Tnf Day 28

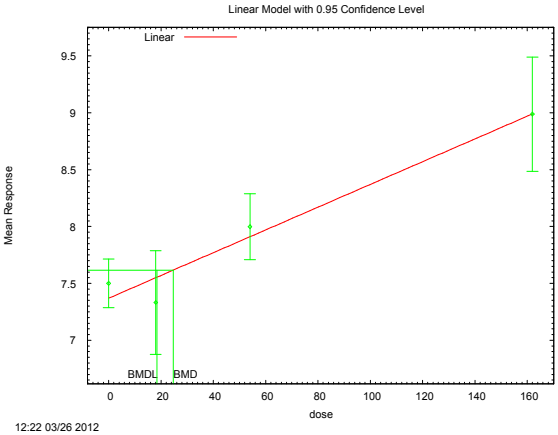

Il1r2 Day 1

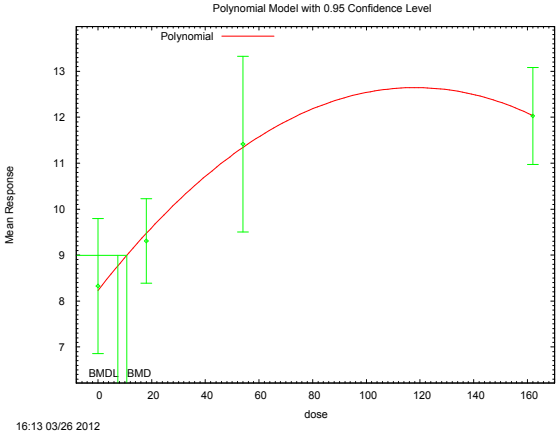

Cxcl1 Day 3

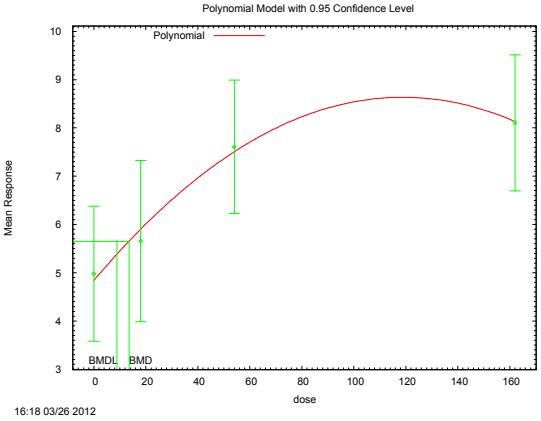

Ccl2 Day 3

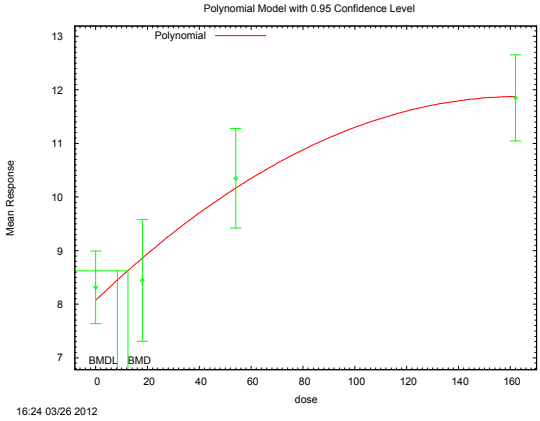

Ccl7 Day 28

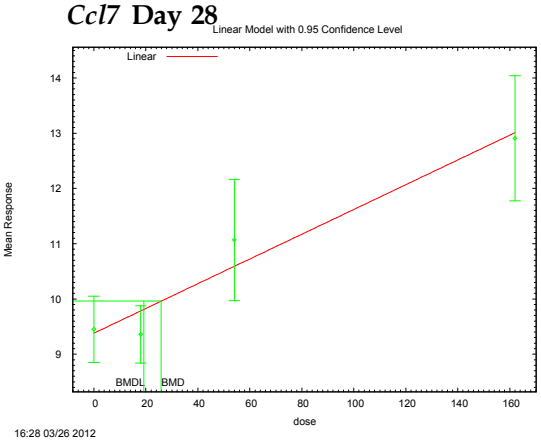

Ccl17 Day 28

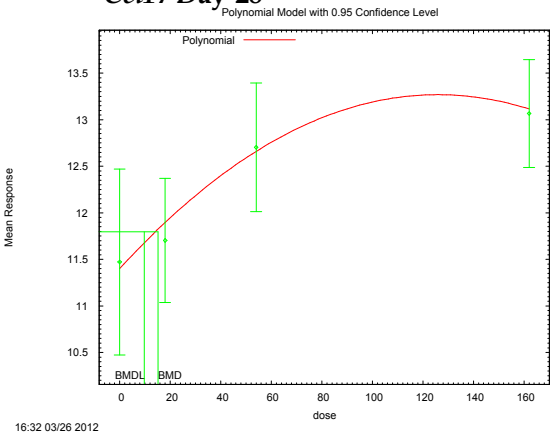

Cxcl10 Day 28